

LANGLEY GRAN

IN-26-CR
124518
2558

A Progress Report

Grant No. NAG-1-745

ENVIRONMENT ASSISTED DEGRADATION MECHANISMS
IN ALUMINUM-LITHIUM ALLOYS

Submitted to:

National Aeronautics and
Space Administration
Langley Research Center
Hampton, VA 23665

Attention: Mr. J. F. Royall, Jr.
Grants Officer, MS 126

For Consideration By:
Mr. D.L. Dicus
M/S 188A, Metallic Materials Branch

Submitted by:

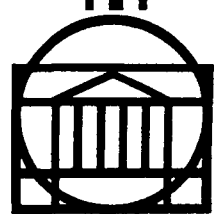
Richard P. Gangloff
Associate Professor

Glenn E. Stoner
Professor

Robert E. Swanson
Assistant Professor
Department of Materials Engineering
Virginia Polytechnic and State University

Report No. UVA/528266/MS88/101

January 1988



SCHOOL OF ENGINEERING AND
APPLIED SCIENCE

DEPARTMENT OF MATERIALS SCIENCE

UNIVERSITY OF VIRGINIA
CHARLOTTESVILLE, VIRGINIA 22901

N88-17782

Unclas
0124518

G3/26

CSSL 11F

(NASA-CR-182462) ENVIRONMENT ASSISTED
DEGRADATION MECHANISMS IN ALUMINUM-LITHIUM
ALLOYS Progress Report (Virginia Univ.)
255 P

A Progress Report
ENVIRONMENT ASSISTED DEGRADATION MECHANISMS
IN ALUMINUM-LITHIUM ALLOYS

Submitted to:

National Aeronautics and
Space Administration
Langley Research Center
Hampton, VA 23665

Attention: Mr. J. F. Royall, Jr.
Grants Officer, MS 126

For Consideration By:

Mr. D. L. Dicus
M/S 188A, Metallic Materials Branch

Submitted by:

Richard P. Gangloff
Associate Professor

Glenn E. Stoner
Professor

Robert E. Swanson
Assistant Professor
Department of Materials Engineering
Virginia Polytechnic and State University

Department of Materials Science
SCHOOL OF ENGINEERING AND APPLIED SCIENCE
UNIVERSITY OF VIRGINIA
CHARLOTTESVILLE, VIRGINIA

Report No. UVA/528266/MS88/101

January 1988

Copy No. _____

TABLE OF CONTENTS

	<u>Page</u>
I. EXECUTIVE SUMMARY	1
II. INTRODUCTION	
ENVIRONMENT ASSISTED DEGRADATION MECHANISMS IN ALUMINUM-LITHIUM ALLOYS	4
A. The Problem	4
B. The NASA Sponsored Research Program	5
C. Complementary Research Programs	7
D. Report Organization	8
III. PROGRAM 1	
DAMAGE LOCALIZATION MECHANISMS IN AQUEOUS CHLORIDE CORROSION FATIGUE OF ALUMINUM-LITHIUM ALLOYS	9
A. Summary	9
B. Objective	9
C. Progress for the Period April 1, 1987, to November 30, 1987	10
1. Literature Review and Approach	10
2. Progress on Experimental Results and Discussions	12
a. Phase 1	12
i. Alloy Chemistry, Microstructure and Mechanical Properties	12
ii. Electrochemical Corrosion Testing	14
iii. Selection of Heat Treatments for Corrosion Fatigue	18
iv. Small Fatigue Crack Experimental Methods	19
1) Electrical Potential Difference (P.D.) Technique	19
2) Qualification of Electrical Potential and Crack Growth Measurements	21
3) Conclusions	23
v. Intrinsic Fatigue Crack Propagation	23
1) L-T Orientation Intrinsic FCG	25
2) L-S Orientation Intrinsic FCG	29

b.	Phase 2	32
i.	Experimental Procedures	32
ii.	Environmental Effects on Intrinsic Fatigue Crack Growth	34
1)	Alloy 7075	34
2)	Alloy 2090: Preliminary Work in Gaseous Environments	36
3)	Alloy 2090 in Purified Gaseous and Aqueous Environments	38
4)	Alloy 2090 in Aqueous Chloride: The Effect of Frequency	39
5)	Alloy 2090 in Aqueous Chloride: The Effect of Electrode Potential .	40
iii.	Summary and Conclusions	42
D.	Future Work for the Period April 1, 1988, to March 31, 1989	44
IV.	PROGRAM 2 MEASUREMENTS AND MECHANISMS OF LOCALIZED AQUEOUS CORROSION IN ALUMINUM-LITHIUM ALLOYS	46
A.	Summary	46
B.	Progress Report	47
1.	Mechanisms of Local Corrosion in Aluminum-Lithium Alloys	47
a.	Introduction	47
b.	Pitting	47
c.	Local Occluded Environments	49
2.	Microreference Electrodes	51
a.	Introduction	51
b.	Construction of Microreference Electrodes	51
c.	Operation of Microreference Electrodes ...	52
d.	Microreference Electrodes for Measuring pH	55
e.	Some Experimental Techniques	55
3.	Report on Research Conducted to Date	57
a.	Microreference Electrodes	57
b.	In Situ Corrosion Observations	59
c.	Simulated Local Environment Tests	60
d.	Scanning Electron Microscopy and Energy Dispersive Spectroscopy	61

C.	Future Work for the Period	
	April 1, 1988 to March 31, 1989	62
	1. Study of Local Corrosion Utilizing	
	Microelectrodes and In Situ Observation	62
	a. In Situ Corrosion Observations	62
	b. pH Microreference Electrodes	63
	c. Simulated Occluded Environments	63
V.	PROGRAM 3	
	ENVIRONMENTAL DEGRADATION OF Al-Li ALLOYS:	
	THE EFFECT OF HYDROGEN (A Proposal for the	
	Period April 1, 1988 - March 31, 1990)	64
	A. Summary	64
	B. Introduction and Background	64
	C. Technical Program	66
	1. Microstructure	66
	2. Charpy Impact Tests	67
	3. Stress State Effects	68
	4. Material Needs	69
	D. Statement of Work	70
	E. Key Personnel	70
	F. Equipment and Facilities	70
	1. Introduction	70
	2. Academic Colleges	71
	3. Academic Support Facilities	73
	4. Academic Departments and Programs	75
	5. Major Research Groups	77
	6. Academic Facilities	78
	7. Materials Engineering Department	80
VI.	PROGRAM 4	
	NEW INITIATIVE ON ENVIRONMENTAL	
	FRACTURE OF ADVANCED LIGHT METALS	86
	A. Elevated Temperature Crack Growth in	
	Advanced PM Aluminum Alloys	87
	1. Introduction	87
	2. Objective	88
	B. Technical Program	88
	1. Tensile Fracture	88
	a. Background	88
	b. Proposed Research	89
	2. Subcritical Creep Crack Propagation	90
	a. Background	90
	b. Proposed Research	91
	C. Closure	92

VII.	REFERENCES	93
VIII.	FIGURES (See Table of Figures, pp. vi)	104

APPENDICES

APPENDIX I: Mechanisms of Intrinsic Damage
Localization During Corrosion Fatigue:
Al-Li-Cu System

APPENDIX II: Curricula Vitae

TABLE OF FIGURES

Figure 1	Program Schedule.	105
Figure 2	Microstructure of Alloy 2090 rolled plate etched with Keller's reagent).	106
Figure 3	Precipitation strengthening characteristics of Alloy 2090 for aging at 190°C, and in terms of hardness and tensile yield strength change.	107
Figure 4	Precipitation strengthening characteristics of Alloy 2090 for aging at 160°C.	108
Figure 5	Variation of the pitting potential of peak aged and over aged Alloy 2090 as a function of NaCl concentration.	109
Figure 6a	Constituent particle composition by EDX analysis.	110
Figure 6b	Matrix composition by EDX analysis.	111
Figure 7	Stringer of constituent particle pits contained in peak aged Alloy 2090. Test conditions; 0.1% NaCl, 5 days at -0.700 V (SCE).	112
Figure 8	Sub-boundary pitting in peak aged Alloy 2090; (a) 1000X - exposed, (b) 1000X - etched sub-boundaries without chloride exposure, (c) 1500X - exposed, (d) 2000X - exposed. Test conditions; 0.1% NaCl, 3.5 days at -1.000 V (SCE).	113
Figure 9	Micronotched, short edge crack specimen design.	114
Figure 10	Computer automated electrical potential difference system for fatigue crack growth control and monitoring.	115
Figure 11	Comparison of the Laplacian analysis and Johnson's equation calibration procedures for relating measured electrical potential to crack length.	116
Figure 12	Crack length predicted by potential measurements and the Laplacian model versus crack length measured by SEM and optical fracture surface examination.	117

Figure 13	Comparison of 4130 steel constant ΔK and decreasing ΔK test results with the FCG characteristics of a comparable steel in moist air.	118
Figure 14	Comparison of two constant ΔK test results with the FCG characteristics of 4340 steel in the high purity helium environment.	119
Figure 15	Test cell configuration for aqueous NaCl corrosion fatigue experiments.	120
Figure 16	Comparison of two 4130 steel constant ΔK test results with the corrosion fatigue crack growth characteristics of API-2H steel in a deaerated NaCl environment with cathodic polarization.	121
Figure 17	Comparison of the FCG characteristics of Alloy 2090 as measured by microstructurally small crack, long crack high R and long crack low R test techniques (after Ritchie et al. (30,31) and Hertzberg et al. (32).)	122
Figure 18	Short crack specimen orientation in rolled aluminum alloy plates.	123
Figure 19	Illustration of short crack orientation for L-T and L-S microstructures.	124
Figure 20	Fatigue crack growth in Alloy 2090 in the L-T direction; (a) short crack specimen fracture surface, (b) constant ΔK -constant R test results, (c) comparison of constant ΔK and decreasing ΔK -constant R test results.	125
Figure 21	Short crack decreasing ΔK -increasing R/constant K_{max} test results for Alloy 2090 in the L-T orientation.	126
Figure 22	A comparison of the constant ΔK -step increased R/constant K_{max} test results with decreasing ΔK -constant R or constant K_{max} results for Alloy 2090 in the L-T orientation.	127
Figure 22a	Crack length versus loading cycles plot of the decreasing ΔK -increasing R/constant K_{max} test results shown in Figure 22.	128

Figure 22b	A detailed crack length versus loading cycles plot of data shown in Figure 22(a).	129
Figure 23	Fatigue crack growth in Alloy 2090 in the L-S direction; (a) short crack specimen fracture surface, (b) constant ΔK -constant R test results, (c) comparison of constant ΔK and decreasing ΔK -constant R test results.	130
Figure 24	A comparison of the constant ΔK -step increased R/constant K_{max} test results with decreasing ΔK -constant R or constant K_{max} results for Alloy 2090 in the L-S orientation.	131
Figure 25	A summary of intrinsic fatigue crack growth in Alloy 2090 for two orientations.	132
Figure 26	Intrinsic fatigue crack propagation in Alloy 2090, characterized by short crack constant stress intensity techniques and by microstructurally small crack replication procedures after Ritchie et al. (31).	133
Figure 27	The effect of highly purified gaseous and aqueous environments on intrinsic corrosion fatigue crack growth in peak aged Alloy 7075 in the L-S orientation.	134
Figure 28	The results of current experiments from Figure 27 compared to literature data for corrosion fatigue at high ΔK (37) and to literature data for near threshold intrinsic fatigue crack growth (32).	135
Figure 29	The effect of impure helium and water vapor + helium environments on fatigue crack growth in Alloy 2090 at constant stress intensity and constant R.	136
Figure 30	The effect of highly purified gaseous and aqueous environments on intrinsic corrosion fatigue crack growth in peak aged Alloy 2090 in the L-T orientation.	137
Figure 31	The effect of cyclic loading frequency on intrinsic corrosion fatigue crack propagation in L-T peak aged Alloy 2090 exposed to aqueous 1% NaCl at constant anodic potential.	138

Figure 32	The effect of frequency on corrosion fatigue crack propagation in Alloy 2090 exposed to aqueous 1% NaCl at constant high applied stress intensity range and applied electrode potential.	139
Figure 33	The effect of frequency on corrosion fatigue crack propagation in Alloy 2090 exposed to aqueous 1% NaCl at constant low applied stress intensity range and applied electrode potential.	140
Figure 34	The effect of cathodic polarization on the intrinsic corrosion fatigue crack growth rate in L-T peak aged Alloy 2090 at a constant ΔK of $2.5 \text{ MPa}\cdot\text{m}^{\frac{1}{2}}$ in deaerated 1% NaCl.	141
Figure 35	The effect of cathodic polarization on the intrinsic corrosion fatigue crack growth rate in L-T peak aged Alloy 2090 at constant ΔK levels of 2.1 and $9.6 \text{ MPa}\cdot\text{m}^{\frac{1}{2}}$ for high and low R conditions, respectively and in deaerated 1% NaCl.	142
Figure 36	The effect of cathodic polarization on the intrinsic corrosion fatigue crack growth rate in L-S peak aged Alloy 2090 at constant ΔK levels of 4.1 and $8.5 \text{ MPa}\cdot\text{m}^{\frac{1}{2}}$ at high low R = 0.6 and in deaerated 1% NaCl.	143
Figure 37	The effect of cathodic polarization on the intrinsic corrosion fatigue crack growth rate in L-S over aged Alloy 2090 at a constant ΔK level of $3.8 \text{ MPa}\cdot\text{m}^{\frac{1}{2}}$ for high R = 0.6 and in deaerated 1% NaCl.	144
Figure 38	Scanning electron photomicrograph of the drawn tip of a glass pipette used in constructing a microreference electrode.	145
Figure 39	Optical photomicrograph of a microreference electrode situated to measure the variation in potential due to the activity of the corroding pit on peak aged 2090 in 3.5 w/o NaCl solution.	146
Figure 40	Plot of applied potential and potential variation measured by microreference electrode over a pit during a polarization scan vs. time. Peak aged 2090, 3.5 w/o NaCl solution.	147

Figure 41	Same plot as in Figure 3. Measure potential represents the difference in potential between a microreference electrode near a pit and one removed from the pit by several hundred micrometers.	148
Figure 42	Optical photomicrograph of the evolution of gas bubbles during an in situ corrosion observation experiment.	149
Figure 43a	No visible activity of E_{CORR} ($-1.0 V_{SCE}$).	150
Figure 43b	Site 1 inactive, site 2 active at $-1.3 V_{SCE}$.	150
Figure 43c	Site 1 active, site 2 inactive at $-0.7 V_{SCE}$.	150
Figure 44	Plot of pH vs. time for 2090 in solutionized and peak aged conditions in an artificial crevice experiment.	151
Figure 45	Plot of pH vs. time for solutionized and peak aged 2090 shavings immersed in 3.5 w/o NaCl solution.	152
Figure 46	Scanning electron photomicrograph of a pitted region. EDS spectra show the signal obtained from the 3 different regions. Note variation in the chlorine and copper signals.	153
Figure 47	Typical time-history plots from Charpy V-notch tests.	154
Figure 48	Charpy V-notch test results.	155
Figure 49	Schematic of disk pressurizing assembly.	156
Figure 50	Graph of cumulative acoustic emission counts vs. gas pressure for mild steel disks tested in a disk pressurization system. Notes indicate the occurrence of various phenomena.	157

SECTION I

EXECUTIVE SUMMARY

This report documents the progress which has been achieved on NASA-LaRC Grant NAG-1-745, entitled "Environment Assisted Degradation Mechanisms in Aluminum-Lithium Alloys," and based on research conducted during the period from April 1 to November 30, 1987. A discussion of proposed work in year 2 (April 1, 1988 to March 31, 1989) is integrated with this progress report. A proposal for grant renewal is being issued under separate cover.

The participants in this sponsored program include three faculty and three PhD candidate graduate students from the Departments of Materials Science at the University of Virginia and Materials Engineering at Virginia Polytechnic Institute and State University. Biographical information is presented in Appendix II. The NASA grant monitor is D. L. Dicus of the Metallic Materials Branch at the Langley Research Center.

SECTION II provides an overview of the need for research on the mechanisms of environmental-mechanical degradation of advanced aerospace alloys based on aluminum and lithium. Three specific research programs are introduced and the common goal of the work is cited. That is, the research is aimed at providing NASA with the fundamental basis which is necessary to enable metallurgical optimization of alloy performance and engineering design with damage tolerance, long term durability and reliability.

SECTION III reports on the progress of work on "Damage Localization Mechanisms in Aqueous Chloride Corrosion Fatigue of Aluminum-Lithium Alloys" conducted by Mr. R. S. Piascik and Prof. R. P. Gangloff at UVa. This work is targeted at characterizing aqueous and gaseous environment corrosion fatigue crack propagation kinetics, microstructural paths and damage mechanisms for Alloy 2090. Three tasks have been accomplished. A detailed literature review and experimental plan, presented in

Appendix I, was completed and approved by the PhD Committee and the grant monitor. Alloys 2090 and 7075, supplied by Alcoa, have been characterized with respect to microstructure, mechanical properties and corrosion behavior. Computer automated, fracture mechanics methods and electrical potential difference monitoring of crack growth, have been successfully adapted to study short cracks in highly purified gaseous and aqueous chloride/controlled electrode potential environments. Emphasis here is on the characterization of intrinsic crack propagation behavior free of complicating extrinsic closure effects. These methods have been applied to characterize the corrosion fatigue behavior of peak aged Alloy 2090 in aqueous 1% NaCl/anodic polarization, purified water vapor, purified helium, moist air, 1% NaCl/cathodic polarization and purified oxygen. Both high stress intensity and near threshold crack growth rates decrease according to the listed order of environments. Oxygen and cathodic polarization/NaCl conditions promote significant reductions in environmental cracking susceptibility. Decreased loading frequency does not exacerbate corrosion fatigue. While each alloy exhibited similar trends, Alloy 2090 is generally more corrosion fatigue resistant compared to Alloy 7075. A plan which emphasizes experimental analysis and mechanistic work is presented to complete the corrosion fatigue research and Mr. Piascik's PhD program during year 2.

SECTION IV reports on the progress of work on "Measurements and Mechanisms of Localized Aqueous Corrosion in Aluminum-Lithium Alloys" conducted by Mr. R. G. Buchheit, Jr., and Prof. G. E. Stoner at UVA. This work is targeted at isolating and measuring localized processes which are hypothesized to control corrosion and embrittlement of aluminum-lithium alloys. A literature review was conducted and Ag/AgCl microreference electrodes were successfully constructed with inner bore diameter tip sizes as small as 5 μm . These probes have been used to measure potential variations as small as 0.6 mV at localized sites on actively corroding surfaces of Alloy 2090. Growing corrosion pits have been emphasized during this reporting period. Measurement of time dependent pH changes have been performed for artificial crevices

and immersed machined shavings in solutionized and peak aged Alloy 2090, with an effect of heat treatment indicated. A proposed plan is presented for work in year 2 and which emphasizes several additional probes of localized chemistry in pits and cracks.

SECTION V provides a detailed technical proposal for research on "Environmental Degradation of Al-Li Alloys: The Effect of Hydrogen" by Prof. R. E. Swanson at VPI. This work was originally proposed by Prof. M. R. Louthan to begin in year 2 and is on schedule as the result of the effort recorded here. The proposal describes a 24-month study to characterize the effects of hydrogen on the mechanical behavior and microstructure of Alloy 2090. The goal of this work is to increase the understanding of the role of microstructure and stress state on the susceptibility to hydrogen damage in Al-Li alloys. Microstructural characterizations will include: optical microscopy, scanning electron microscopy, transmission electron microscopy and differential thermal analysis or scanning calorimetry. Mechanical property characterizations will include uniaxial tension tests, biaxial loading tests, Charpy impact tests, and microhardness indentation tests.

SECTION VI provides a new proposal by Prof. Gangloff for the incorporation of a fourth, PhD level graduate student and a fourth area of research. Five potential research topics are suggested, all with the common features of examining the environmental resistance of advanced, light metals and emphasizing an integrated metallurgical and fracture mechanics approach. A specific example proposal is presented for the particularly important area of "Elevated Temperature Crack Growth in Advanced Powder Metallurgy Aluminum Alloys." Important uncertainties, likely materials, modern fracture mechanics tools and a mechanistic approach are summarized. We propose that NASA provide mainly student support in year 2 to develop a specific topic, literature review and experimental plan, ideally in conjunction with Langley researchers in metals and fracture.

SECTION II

INTRODUCTION

ENVIRONMENT ASSISTED DEGRADATION MECHANISMS IN ALUMINUM-LITHIUM ALLOYS

A. The Problem

Aluminum-lithium based alloys are the object of intense government, industrial and academic research aimed at developing low density, high strength and high stiffness materials. Commercial alloys containing Al-Li-Cu-Zr (eg. 2090) and Al-Li-Cu-Mg-Zr (eg. 8090) are becoming available, particularly for fastened airframe components (1)*. Future aerospace applications will include cryogenic tankage.

Problems of alloy degradation and failure currently impede reliable application of Al-Li alloys in engineered structures and require additional research, as documented at several international conferences (2-5). Unresolved issues include:

- ✕ Low fracture toughness attributed to elastic and plastic strain localization, precipitates and impurities localized at grain boundaries (6-9).
- ✕ Dependence of fatigue crack propagation resistance on extrinsic factors which are beneficial for laboratory specimens, but which are not easily modeled by damage tolerant life prediction methods (10).
- ✕ Environmental stability with regard to properties and mechanisms governing aqueous corrosion and hydrogen embrittlement over a range of cryogenic to elevated temperatures, and specifically including the lack of capabilities to predict component behavior from laboratory data (11-14).
- ✕ Heterogeneous microstructures such as grain boundary phases and precipitate free zones, complex precipitation sequences, anisotropic and textured grain structure, and deformation mechanisms which influence the above properties.

* All references are contained in Section VII.

Microstructural effects on the benign environment mechanical properties of Al-Li alloys have been characterized, behavioral mechanisms have been reported (6-10) and thermal-mechanical processing has lead to Al-Li type alloys with excellent strength and longitudinal toughness, particularly at cryogenic temperatures (15- 19).

Research has focused on the phenomenology of pitting corrosion and short transverse SCC of Al-Li-X alloys in chloride containing environments. Lithium additions alone do not cause unacceptably high chemical reactivity in aqueous environments containing aggressive ions such as chloride. Properties are encouraging; for example, specific metallurgical structures are reported to exhibit excellent stress corrosion cracking resistance. Deficiencies exist, however, including:

- ✕ Speculative models explain portions of data, however, mechanisms have been neither developed quantitatively, nor tested critically.
- ✕ Laboratory measurements have not separated and characterized the localized processes which are relevant to complex failure modes. Data are not scalable to predict performance.
- ✕ Hydrogen contributions to localized corrosion, deformation and brittle fracture have not been studied systematically.
- ✕ Fatigue-environment interactions have not been studied.

B. The NASA Sponsored Research Program

In March of 1987, the NASA-Langley Research Center funded a multi-faceted research program at the University of Virginia and at the Virginia Polytechnic Institute and State University to investigate degradation of Al-Li-X alloy properties due to gaseous and aqueous environmental exposures and to dissolved hydrogen (20).

The goal of the proposed research program is to characterize alloy behavior and to develop mechanisms for environmental failure of commercial type Al-Li-Cu alloys. This work is necessary to enable metallurgical optimization of alloy performance and engineering design with damage tolerance and long term reliability. Current understanding

in these regards is insufficient for safe use of aluminum-lithium alloys in aerospace missions.

As developed in the initial proposal, three specific research projects have been initiated to address the aforementioned uncertainties (20). These projects are interrelated and will be conducted collaboratively, by faculty members of the Materials Science Department at the University of Virginia and the Materials Engineering Department at the Virginia Polytechnic Institute and State University. NASA-LaRC funded research programs at UVa and VPI include:

DAMAGE LOCALIZATION MECHANISMS IN AQUEOUS CHLORIDE
CORROSION FATIGUE OF ALUMINUM-LITHIUM ALLOYS

Investigator: R.P. Gangloff
Proposed Duration: April, 1987 to March, 1989
Graduate Student: Robert S. Piascik, PhD candidate
Support: Original proposal (20).

Status: The program was initiated on schedule; research accomplishments are described in this progress report. The technical direction for project completion in year 2 is proposed herein.

MEASUREMENTS AND MECHANISMS OF LOCALIZED AQUEOUS
CORROSION IN ALUMINUM-LITHIUM ALLOYS

Investigator: G.E. Stoner
Proposed Duration: August, 1987 to March, 1990
Graduate Student: Rudolph G. Buchheit, Jr., PhD candidate
Support: Original proposal (20).

Status: The program was initiated on schedule; four months of research have been accomplished as described in this progress report. The technical direction for years 2 and 3 is proposed.

DEFORMATION AND FRACTURE OF ALUMINUM-LITHIUM ALLOYS:
THE EFFECT OF DISSOLVED HYDROGEN

Investigator: R.E. Swanson (M.R. Louthan, Jr.) (VPI)
Proposed Duration: April, 1988 to March, 1990
Graduate Student: To be recruited (VPI)
Support: Original proposal (20).

Status: M.R. Louthan is no longer affiliated with VPI, and has been replaced on this project by Professor Robert E. Swanson. Preliminary work has been conducted at VPI, as discussed in this progress report and a detailed proposal for hydrogen embrittlement research in years 2 and 3 is presented.

As an addition to the original proposal, a fourth PhD candidate, Mr. William Porr, will begin work on either elevated temperature environmental cracking of advanced PM aluminum alloys or environmental degradation of an aluminum matrix discontinuous fiber composite material. Startup funding for this effort is included in the proposal for renewal in year 2 to March, 1989 and full program funding is proposed for year 3.

In summary the NASA-LaRC sponsored research project is designed as a three year effort by three faculty to train four doctoral level graduate students in the interdisciplinary areas of metallurgy, electrochemistry and solid mechanics. Along with the participating faculty, these students represent a meaningful resource which is relevant to NASA light metals, fracture mechanics, and structures development missions.

C. Complementary Research Programs

Several additional programs have been initiated since the original proposal and are funded by a variety of sources including industry and NASA.

DEFORMATION AND FRACTURE OF ALUMINUM-LITHIUM ALLOYS: THE EFFECT OF CRYOGENIC TEMPERATURES

Investigator: Richard P. Gangloff
Graduate Student: John A. Wagner, PhD candidate
Support: On-site research at NASA-LaRC.

Status: Mr. Wagner, a NASA-Langley employee, has completed all course work and examinations for the PhD degree in Materials Science at the University of Virginia. He will conduct dissertation research on cryogenic fracture and hydrogen embrittlement of superplastically formed Al-Li-Cu-X alloys at LaRC.

The cost of Mr. Wagner's research is not included in this proposal, however the work will follow directly from the hydrogen embrittlement study.

STRESS CORROSION CRACKING
OF ALUMINUM-LITHIUM-COPPER ALLOYS

Investigator: Glenn E. Stoner
Graduate Student: James P. Moran, PhD candidate
Support: Alcoa and Virginia CIT

Status: Mr. Moran's research has been underway for the past two years and is being closely coordinated with Mr. Buchheit's work.

NASA sponsored research further benefits by contacts with ongoing, industrial and government sponsored research within the Light Metals Center at UVA.

D. Report Organization

This report describes the progress achieved on each of the three NASA-LaRC funded research programs between the period April 1st and November 31, 1987 (Sections III, IV and V). Technical descriptions for future research follow the reports of progress in each of the three program sections. The proposed direction of Mr. Porr's research is presented after the discussions of the three original projects and in Section VI.

The program on Environmental Degradation Mechanisms is being integrated into a proposed UVA-NASA/LaRC program on Light Alloy Technology. A specific proposal for grant renewal, including complete budgetary information for year 2, is provided in this regard and under separate cover.

SECTION III

Program 1

DAMAGE LOCALIZATION MECHANISMS IN AQUEOUS CHLORIDE CORROSION FATIGUE OF ALUMINUM-LITHIUM ALLOYS

Robert S. Piascik and Richard P. Gangloff

A. Summary

The objective of this research is to study mechanisms of crack tip damage fundamental to environmentally assisted fatigue crack growth in Al-Li-Cu alloys. Intrinsic mechanisms of fatigue crack growth in alloy 2090 are examined by fracture mechanics methods applied to small cracks. Two regimes of environmental effect, low mean stress-high stress intensity range hydrogen embrittlement and high R-near threshold cracking by hydrogen or film rupture/dissolution are studied by programmed constant stress intensity experimentation. The potential difference monitored crack growth studies are performed in purified helium, oxygen, water vapor and aqueous sodium chloride environments. Fatigue crack growth is first measured as a function of frequency and then for small crack-microstructure orientations giving single or multiple grains along the crack front. Experiments are designed to probe crack tip environmental damage for the two regimes. Crack interactions with grain boundaries will be resolved. Growth in gaseous environments will be compared to environmental effects produced by electrode potential controlled aqueous environments. The results of this work are reported here. Confirming experiments and analyses are progressing in the next reporting period.

B. Objective

The objectives of this research program are to characterize corrosion fatigue crack propagation in Al-Li-Cu alloys exposed to gaseous and aqueous environments at room temperature, and to develop mechanisms of damage localization from crack tip-environment-microstructure interactions. The goal of this work is to identify

beneficial metallurgical conditions and quantitative damage tolerant life prediction models to mitigate environmental cracking.

C. Progress for the Period April 1 to November 30, 1987

1. Literature Review and Approach

Mr. Piascik has conducted an in-depth literature review and developed a detailed technical plan for his doctoral research program. This work, described by the document in Appendix I, was presented to Mr. Dennis Dicus, the NASA-LaRC contract monitor, and to Mr. Piascik's PhD Committee in August of 1987. The committee approved his proposal.

The experimental approach to examining corrosion fatigue damage in Al-Li-Cu Alloy 2090 was designed based on the literature review which identified important parameters and critical uncertainties from prior published work. In summary our fracture mechanics based study is designed to:

- ✕ Emphasize intrinsic corrosion fatigue damage through the use of short crack specimens, and controlled stress intensity range and stress ratio techniques to minimize closure related extrinsic fatigue processes.
- ✕ Examine small crack-environment and small crack-microstructure interactions to reveal details of crack tip damage and to develop characterizations relevant to realistic crack geometries for aerospace applications.
- ✕ Employ high resolution, in situ electrical potential difference monitoring of crack length, computer programmed constant stress intensity techniques and high stress ratio loading to characterize intrinsic, transient and steady state corrosion fatigue damage.
- ✕ Examine two regions of crack tip stress intensity, including near threshold and higher ΔK Paris Law fatigue, where the mechanism for environmental cracking may vary from film formation/rupture to hydrogen embrittlement.
- ✕ Control electrode potential for aqueous environments, and cyclic loading frequency effects for electrolyte and gaseous exposures.

- ✕ Control alloy microstructure to define deleterious phases and morphologies.
- ✕ Employ several techniques; including post environmental exposure fracture toughness, single grain cracking in controlled microstructures, fractography, and frequency or electrode potential change transient experiments; to define localized crack tip damage mechanisms.

Specific details pertaining to material, specimen design and fatigue-fracture mechanics, microstructure-crack orientations, environmental chambers and chemistry control are presented in Appendix I. This material provides the necessary background for the discussion of experimental results.

Research on corrosion fatigue is approached in three phases as follows:

Phase 1: Experiments will develop the foundation necessary for planning and executing the research program. Tasks will: (1) Characterize the microstructure of Alloy 2090 as a function of aging; (2) Characterize free corrosion and electrochemical polarization behavior as a function of microstructure and solution chloride composition; (3) Adapt the electrical potential method for study of small corrosion fatigue cracks in aluminum alloys; and (4) Demonstrate intrinsic, stress intensity similar-fatigue crack propagation for the benign moist air environment.

Phase 2: Experiments and analyses will characterize the growth kinetics and microstructural paths of corrosion fatigue cracks in Alloy 2090 and 7075. Tasks will: (1) Demonstrate intrinsic, stress intensity similar-fatigue crack propagation for embrittling gaseous and aqueous environments, (2) Determine stress intensity-stress ratio, frequency and electrode potential conditions for corrosion fatigue in several gaseous and aqueous environments.

Phase 3: Research will probe mechanisms for intrinsic corrosion fatigue damage.

Specific experiments for each phase are listed in Tables 4, 5 and 6 contained in Appendix I. The research plan and experimental design are entirely consistent with the original proposal to NASA (20).

The schedule for Phases 1, 2 and 3 is presented in Figure 1. Work is progressing according to this schedule; all of the Phase 1 work and about 75% of the Phase 2 characterization experiments have been completed. The results of this research, conducted between April 1 and November 31, 1987, are presented in the following sections.

2. Progress on Experimental Results and Discussions

a. Phase 1: Alloy Characterization, Corrosion Behavior, Short Fatigue Crack Experimental Methods and Intrinsic Fatigue Crack Propagation for Moist Air

i. Alloy Chemistry, Microstructure and Mechanical Properties

Alloy 2090, an Al-Li-Cu-Zr material in rolled plate (38.1 mm thick), has been selected for this study. Alloy 7075-T651 (Al-Zn-Mg-Cu) material, also in rolled plate form (63.5 mm thick), was selected as a reference material. Alloy 2090 was provided in the solution treated and stretched (6%) condition, and Alloy 7075 material was provided in the peak aged T651 condition. Both plates were supplied by Messrs Colvin and Bretz of the Alcoa Technical Center. Chemical analyses, conducted on specific samples of each plate by Alcoa, yielded the compositions given in Table 1.

Table 1:

Chemical Composition (by weight percent)

Alloy 2090

Li	Cu	Zr	Fe	Si	Mn	Mg	Cr	Ni	Ti	Na	Zn	Ca
2.14	2.45	0.09	0.05	0.04	0.00	0.00	0.00	0.00	0.01	0.001	0.01	0.0005

Alloy 7075

Zn	Mg	Cu	Cr	Zr	Fe	Si	Mn	Ni	Ti	Na	Ca	Li
5.74	2.31	1.58	0.20	0.01	0.26	0.10	0.05	0.01	0.05	0.000	0.0001	0.000

The microstructure of Alloy 2090 is shown in Figure 2. Large flattened and elongated grains are oriented with the major dimension along the rolling (longitudinal) direction. Grain size measurements, performed for the transverse and short transverse directions, yielded average values of 3.3 mm and 0.11 mm, respectively. The grain sizes in these directions are of interest because short fatigue crack growth will be characterized for the longitudinal-transverse and longitudinal-short orientation, as discussed below. The structure is generally unrecrystallized, with low angle boundaries forming a cellular structure characterized by a subboundary grain size which is, as yet, undetermined.

The precipitation strengthening characteristics of Alloy 2090 are shown in Figure 3 and 4 for aging temperatures of 190°C and 160°C, respectively. The peak aged condition is employed for all experiments in Phases 1 and 2. Peak aged mechanical properties are given in Table 2 for both Alloy 2090 and 7075.

Table 2:

Mechanical Properties of Peak Aged Material

<u>Alloy 2090</u>					
<u>Aging Temp(°C)</u>	<u>Aging Time(hrs)</u>	<u>Yield (MPa)</u>	<u>Ultimate (MPa)</u>	<u>Elong. (%)</u>	<u>Orientation</u>
190	4	496	517	-----	Long-Trans
160	16(20)	505(500)	530(537)	(6)	Long-Trans
160	(20)	(525)	(551)	(6)	Trans
160	(20)	(437)	(455)	(3.5)	Short-Trans
<u>Alloy 7075</u>					
<u>Aging Temp(°C)</u>	<u>Aging Time(hrs)</u>	<u>Yield (MPa)</u>	<u>Ultimate (MPa)</u>	<u>Elong. (%)</u>	<u>Orientation</u>
T-651 condition		(466)	(540)	(11.8)	Long-Trans
T-651 condition		(432)	(500)	(2.9)	Short-Trans

() - Results supplied by Alcoa

A detailed transmission electron microscopy (TEM) analysis of peak aged Alloy 2090 has been completed. The precipitates that have been identified are δ' (Al_3Li), θ' (Al_2Cu), T_1 (Al_2CuLi), and T_2 (Al_6CuLi_3). δ' , T_1 , and θ' were found to be distributed throughout the matrix. T_2 precipitates are located at high angle grain boundaries. Large δ' precipitate free zones are located adjacent to the high angle grain boundaries. Increased concentrations of T_1 were observed at low angle boundaries. The increased amount of sub boundary T_1 precipitates is associated with a region of decreased δ' , forming a narrow δ' denuded zone along the subboundary. These results are consistent with extensive microscopic studies conducted by at UVa by Cassada, Shiflet and Starke. Detailed micrographs will be presented in the final report for year 1.

Alloy 7075 will be characterized during the next reporting period. Work to date establishes that each of the materials chosen for study are representative of current quality 2090 and 7075.

ii. Electrochemical Corrosion Testing

Potentiodynamic and constant potential electrochemical tests were performed to characterize the general and localized corrosion properties of Alloy 2090 in aqueous NaCl environments. The objective of the potentiodynamic polarization tests was to determine breakaway (pitting) potentials and passive region corrosion-microstructure relations for different precipitation strengthened conditions of the alloy and for various NaCl concentrations. Based on the results of these tests, specific constant polarization potentials and a NaCl concentration were selected for aqueous corrosion fatigue experiments. The constant potential experiments were performed to study the corrosion characteristics of specimens exposed to the aqueous NaCl environment at constant passive region potentials.

Specimens were prepared by heat treating 38.1 mm thick plate material to peak aged (4 hrs at 190°C) and overaged (22 hrs at 190°C) conditions, by machining a 25.4 mm x 25.4 mm x 12.7 mm specimen from the plate midsection and by polishing the rolling plane surface (25.4 mm x 25.4 mm face) as follows:

180, 320, 400, 600, 2400, 4000 grit SiC
15 μm , 5 μm , 1 μm Al_2O_3
0.06 μm Silica

A nickel wire was spot welded to the edge surface of the specimen which was in turn mounted to a plexiglass electrochemical test cell. A teflon ring (1 cm^2 exposed inner area) was placed between the polished surface of the specimen and the aqueous environment. The teflon ring contained a knife edge to minimize contact area and to limit crevice corrosion at the cell-specimen interface. A platinum counter electrode was used to polarize the working electrode (specimen) and a standard saturated calomel electrode (+0.227 V versus the standard hydrogen electrode) was used as the reference.

Extreme care was taken prior to testing to rid the electrochemical test apparatus of oxygen. The electrolyte was stored in a reservoir where the NaCl solution was deaerated (using high purity helium) for a minimum of 4 hours prior to transferring to the helium purged electrochemical cell. Upon the introduction of the electrolyte to the cell, vigorous deaeration with helium was continued for 15 to 24 hours while the specimen was held at a potentiostatically controlled constant potential of -1.00 V (SCE). This value is the approximate free corrosion potential of Alloy 2090 in deaerated NaCl solution.

All potentiodynamic polarization testing was conducted at a sweep rate of 2 mV/sec. The tests were initiated by first scanning in the cathodic direction. The potential was reversed to the anodic direction once a slight cathodic current was detected, typically at a voltage of between -1.20 V and -1.30 V SCE. The specimen was anodically

polarized through the passive region and past the pitting potential. Once a significant anodic (breakaway) current was reached (100 μ a), the specimen was again polarized in the cathodic direction until the repassivation potential was reached, that is at the potential corresponding to the original passive region current. At this point the experiment was terminated, the specimen was removed from the cell, dried and immediately examined using optical microscopy.

The polarization response of specimens exposed to aerated NaCl solution exhibited little passive region. Deaeration was required to limit the oxidation reduction reaction and to shift the open circuit potential cathodically from the pitting potential. The large passive region, produced by deaeration, allowed constant anodic polarization of specimens without entering the pitting regime. The pitting potential was easily obtained for this material. Passive region current increased linearly with increasing potential until the breakaway level was reached. At breakaway, a sudden increase in anodic current established the pitting potential.

Figure 5 reveals a significant difference in the pitting potential of peak aged and overaged Alloy 2090 for different concentrations of deaerated NaCl solutions. The different slopes of the peak aged and overaged pitting potential dependencies suggest altered passive film characteristics. The increased pitting susceptibility of overaged Alloy 2090 may indicate the formation of new or larger electrochemically active precipitates, and/or a general degradation of passive film protection due to altered surface film chemistry. As chloride ion content is increased to 3.5% NaCl, both aging treatments become equally susceptible to pitting. This behavior suggests that the chloride ion content of 3.5% NaCl solution promotes a general degradation of the passive film that could mask important environmental/microstructural interactions.

Constant potential tests were conducted at applied values ranging from -1.000 V to -0.700 V SCE in deaerated NaCl solution (0.1

and 0.7 wt%). Both peak aged and overaged material were exposed for 12 hours; the exposed surfaces were then examined for localized corrosion using optical and scanning electron microscopy. Results show that constituent particles and low angle boundary phases (T_1) are sites of localized corrosion. Constituent particles (Al_7Cu_2Fe phase (21)), refer to EDX analysis shown in Figure 6a and 6b, were observed to freely corrode at potentials 100 mV anodic to the deaerated open circuit potential and well below the macroscopic breakaway potential. Shown in Figure 7 is a typical stringer of pits, formed by localized attack of stringered constituent particles. This peak aged specimen was maintained at a potential of -0.700 V SCE (open circuit of -1.100 V SCE) while exposed to 0.1% NaCl solution for 5 days.

Attack of phases at subboundaries is illustrated in Figures 8a, 8c and 8d, which are successively higher magnification micrographs showing the localized corrosion of the same area. This peak aged specimen was exposed to 0.1% NaCl solution for 3.5 days at a constant potential of -1.000 V SCE. The etched but unexposed surface of the same specimen, Figure 8b, reveals the subboundary structure. A comparison of Figure 8a (exposed) and Figure 8b (etched, unexposed) reveals that localized corrosive attack occurs at sites along low angle grain boundaries. Examination, at higher magnification shows that surface attack occurs at small discrete regions aligned along the sub-boundaries. Based on TEM examination, only T_1 precipitates are localized on sub-boundaries. These results suggest that the aluminum-copper-lithium phases (T_1 and possibly T_2) are susceptible to corrosion. These results will facilitate interpretation of scanning electron fractography of corrosion fatigue crack surfaces.

Based on the polarization data and other considerations, a 1 wt% NaCl environment was chosen for aqueous corrosion fatigue testing. While lower concentrations allow a wider range of anodic polarization before pitting, most literature corrosion fatigue experiments are

conducted with 3.5% NaCl or more complex seawater. Also, because of the corrosion fatigue cell geometry, very low ionic concentrations result in a large solution IR drop which limits the range of polarization and which complicates reference electrode measurements.

iii. Selection of Heat Treatments for Corrosion Fatigue

Since the number of chemical environment and mechanical loading variables which critically influence corrosion fatigue is large, it is necessary to emphasize a single aged microstructure in the current study. Once such variables are systematically characterized and understood, future work can examine microstructural effects based on proper selection and control of the relevant environment and mechanical system parameters.

The peak aged condition (4 hours at 190°C) of Alloy 2090 was selected for Phase 1 and 2 corrosion fatigue experimentation because of the main objective of examining the effects of T_1 and T_2 phases on crack growth. Polarization studies indicate that the Li-Cu containing precipitates are environmentally susceptible. TEM analysis of peak aged material has shown that these phases concentrate at high energy sites such as sub boundaries (T_1) and high angle grain boundaries (T_2). With this microstructure and short crack techniques, it may be possible to isolate the crack front interaction with either the T_1 phase on subboundaries or the T_2 phase on high angle grain boundaries.

Underaged Alloy 2090 contains a more uniform concentration of T_1 phase and little, if any, T_2 precipitation. Based on corrosion studies and preliminary aqueous corrosion fatigue fracture surface examination, over aged material exhibits a high degree of pitting which masks fracture surface detail.

Studies of constant or monotonically increasing environmental cracking of Al-Li alloys show that the degree of aging is a critical variable. Results are conflicting and the precise effect of aging remains uncertain in a general sense. The corrosion fatigue sensitivity of the peak aged microstructure is a reasonable starting issue to

address. Work by Lin and Starke shows that the peak aged condition of Alloy 7075 is most susceptible to corrosion fatigue crack propagation by a presumed hydrogen embrittlement mechanism (22).

Finally, the majority of corrosion fatigue crack propagation studies have been performed on peak aged aluminum alloys in the 2000 and 7000 series. The behavior of peak aged 2090 should be directly comparable to these literature data.

iv. Small Fatigue Crack Experimental Methods

Small crack corrosion fatigue propagation experiments are being conducted with a specimen containing a single edge crack grown from an initiating micronotch. Twenty specimens of the type shown in Figure 9 have been machined successfully from the aluminum alloy plates and including 0.25 mm deep micronotches fabricated by electrospark discharge machining methods. These specimens are provided by the Cincinnati Tool Company at a cost of \$250 to \$300 per piece. The stress intensity equation, the analysis for qualification under the small scale or net section yielding criteria and the method for programmed stress intensity control are described in Appendix I.

1) Electrical Potential Difference (P.D.) Technique

The electrical potential difference technique is being employed for continuous crack length measurement. The experimental setup is shown in Figure 10. A constant direct current of between 8 and 15 amperes is applied to the specimen through the loading fixture. Two 0.127 mm diameter copper potential drop probes are spot welded within a specified distance from the micronotch. The potential difference is amplified by 10^4 , measured, and converted from an analog to digital signal that is input to a computer where all test functions are automatically controlled. Using an analytical calibration procedure (Laplacian analysis), crack length is computed for each measured value of electrical potential. As in previous studies with ferrous and nickel based alloys (23), crack growth resolution of less

than 5 μm has been achieved. Crack growth rates are computed for each crack depth value using standard ASTM E647 methods (24). Associated crack tip stress intensities are calculated using methods described in Appendix I.

During this reporting period, we have successfully demonstrated the application of the electrical potential method to aluminum alloys, representing the first use of this approach for this class of materials. Potential probes were attached to aluminum Alloy 2090 and 7075 specimens; joints did not preferentially corrode and detach during prolonged exposures to aqueous chloride environments. The resistivity of aluminum is about 25% that of steels and nickel based alloys; resulting potential differences for small cracks are proportionately less. None-the-less, potentials on the order of 50 to 80 μV for the aluminum alloy samples were measured with + 0.1 μV sensitivity. The signal is sufficiently stable compared to the several day time frame of corrosion fatigue experiments to render accurate, low frequency crack growth rates.

The analysis used for correlating potential difference to crack length is based on a closed form solution of Laplace's equation derived for infinite plate boundary conditions (25). The Laplacian analysis was used so that accurate crack length measurements could be maintained as the crack initiates and propagates from the micronotch. An alternate approach, Johnson's equation (26), can only be used for crack length measurement after the crack has grown some finite length away from the notch. A comparison of the Laplacian analysis and Johnson's equation is shown in Figure 11 for the short crack specimen. Most experimentation will be performed for $a/W < 0.4$. Figure 11 shows that both analysis techniques yield results within 5% for these short crack lengths. Neither analysis method is rigorously correct for the finite, notched specimen studied; experiments are required to test the calibration procedure.

2) Qualification of Electrical Potential and Crack Growth Measurements

Experiments were performed using 4130 and 4340 steels and aluminum alloys to demonstrate that developed methods accurately monitor fatigue crack growth in the environments of interest (air, helium and aqueous NaCl). Results, compared to referenced data, show that specimen design, electrical potential measurement accuracy, computer control methods and specimen loading apparatus used for aluminum alloy research do not anomalously alter experimental results.

The accuracy of the Laplacian calibration procedure is demonstrated in Figure 12. Plotted are predicted crack lengths, calculated from potential difference measurements of small fatigue cracks, compared to actual crack lengths taken from optical or SEM fracture surface measurements. Each data point represents a single specimen. These results confirm that accuracy is maintained for the range of crack lengths relevant to this study. Specimen to specimen crack length measurement errors for aluminum alloys are less than $\pm 15\%$ and comparable to those obtained for steels and nickel based alloys (23). Since the error is random, the results shown in Figure 12 support the usage of the Laplacian analysis compared to the Johnson approach. From Figure 11, the latter predicts crack lengths which are between 1 and 10% less than values calculated from the Laplacian solution.

All fatigue crack growth rate and stress intensity values are corrected for crack length measurement errors, up to $\pm 15\%$ in magnitude, based on linear apportionment of the difference between final predicted and measured crack length. The magnitude of error shown in Figure 12 does not significantly affect the growth kinetics of interest. In fact the correction procedure will also account for the additional error introduced by the use of Johnson's equation. Some care must be exercised regarding the effect of crack length errors on the accuracy of real time, constant stress intensity control. Such errors are

compounded by crack surface contact and electrical potential shorting phenomena.

Fatigue crack growth rate data, obtained by applying the developed methods to low alloy steels, are in excellent agreement with literature results for moist air, purified helium and aqueous chloride with applied cathodic polarization. The results of three experiments performed in air are shown in Figure 13, and include two constant cyclic stress intensity tests (4130SC1A and 4130SC2A) conducted at high stress ratio ($R=0.6$) and a programmed decreasing ΔK experiment ($C=-0.3/m$) also at constant $R=0.6$. For constant ΔK loading, the linearity of measured crack length versus load cycle data was excellent. Excellent agreement exists between 4130 results and fatigue crack growth data for a comparable API Grade E-75 steel (27).

A metal gasket sealed vacuum chamber, equipped with a 44.5 kN (10 kip) servohydraulic loading frame and capable of an atmosphere of 1 μPa (1×10^{-8} torr), will be used for all high purity gaseous atmosphere testing. Two constant ΔK tests ($R=0.6$) were performed in high purity helium (4340SC1A and 4340SC1B) to demonstrate intrinsic crack growth in inert gaseous environments. Prior to testing, the vacuum chamber was evacuated to 3 μPa (3×10^{-8} torr) and backfilled with high purity helium (99.998%), further purified by passage through an immersed liquid nitrogen cold trap. Crack length increased linearly with load cycles up to a crack depth of 3 mm. Crack growth rates calculated by linear regression analysis are in excellent agreement with the referenced fatigue crack growth characteristics of 4340 steel, shown in Figure 14 (28). Experiments with the vacuum system demonstrated that specimen rotation is impeded for longer cracks and the actual applied stress intensity is less than that given by the equation. Crack growth rates accordingly decrease. All experiments with aluminum alloys will be limited in crack length to avoid this error.

Aqueous environment corrosion fatigue crack propagation experiments will be performed in the plexiglass cell represented

diagrammatically in Figure 15 and described in Appendix I. This cell was employed to characterize corrosion fatigue crack propagation in 4130 steel exposed to deaerated 3.0% NaCl at an applied cathodic potential of -1000 mV (SCE). Two constant ΔK tests (4130SC3A and 4130SC3B) yielded linear cyclic crack length data. Crack growth rates from least squares analysis are in excellent agreement with the corrosion fatigue crack growth characteristics of a comparable steel, API-2H, of equivalent yield strength and microstructure (29). This comparison is shown in Figure 16.

3) Conclusions

The direct current electrical potential method, as implemented at the University of Virginia, accurately monitors fatigue crack propagation in both steels and aluminum alloys exposed to a variety of benign and corrosive environments. These methods, demonstrated for the first time for short cracks in aluminum alloys, are now available for application to the study of microstructural and environmental effects on intrinsic fatigue crack propagation in aluminum Alloys 2090 and 7075.

v. Intrinsic Fatigue Crack Propagation

Investigators have recently shown that the significantly increased fatigue crack growth resistance of Al-Li-Cu alloys is attributed to extrinsic crack tip shielding by crack closure and deflection mechanisms (17,30). The relevance of extrinsic fatigue crack growth resistance to mechanistic studies and to a variety of loading histories and component geometries is unclear. The objective of the current study is to eliminate interfering extrinsic effects in order to study intrinsic environmental fatigue crack propagation, a basic material property. We believe that such data are more easily interpreted from a mechanistic perspective and are perhaps most relevant to general life prediction exercises.

Extrinsic crack closure effects are essentially eliminated by high mean stress loading above about $R(K_{\min}/K_{\max})=0.5$, by short/small crack lengths with reduced wakes and by fine scale microstructures. From these considerations, various test techniques have been used in an attempt to monitor intrinsic fatigue crack growth in high strength Al-Li alloys. Figure 17 illustrates fatigue crack growth characterized by a microstructurally small crack technique (surface replication - *) (31), a long crack - high and increasing stress ratio (R) method (crack mouth opening gage - Δ) (32) and long crack - low R testing (crack mouth opening gage - \square) (30). These data reveal a significant difference in the measured fatigue crack growth characteristics of the Al-Li-Cu alloy. The increased fatigue crack growth behavior measured by high R testing, compared to low R test results, is attributed to reduced extrinsic crack closure effects (33). The small crack growth results are not influenced by retarding crack closure, and also reveal enhanced growth rates at very low stress intensities. This latter effect is attributed to the atypically large crack tip opening plastic strains which occur when a small crack is encased within one or two grains (33). These data suggest that microstructural small cracks (dimensions less than a grain size) exhibit no intrinsic fatigue crack growth threshold.

The results shown in Figure 17 clearly illustrate how extrinsic effects, such as crack tip shielding, can alter the true fatigue crack growth characteristics of Al-Li alloys by reducing crack tip mechanical driving forces. These data provide a starting point for the current experiments.

For the current study, three high stress ratio experimental techniques were used to characterize the fatigue crack growth characteristics of Alloy 2090. These techniques include:

1. Decreasing ΔK - constant K_{\max} and increasing R, using the long crack geometry according to the method recently reviewed by Hertzberg and represented in Figure 17 (32).

2. Decreasing ΔK - constant R, using the short crack geometry and high R, after a general method presented by Donald and represented in Figure 17 (34).
3. Constant ΔK - step increasing R at constant K_{\max} and using the short crack geometry.

Long crack testing was conducted using a single edge notched specimen (B = 5.08 mm, W = 22.35 mm, and notch depth = 5.08 mm).

All short crack geometry testing was performed using the micronotched specimen shown in Figure 9. Intrinsic fatigue crack growth was monitored in both the longitudinal-transverse (L-T) and longitudinal-short (L-S) orientations shown in Figure 18. These two crack path directions have been selected to optimize the difference in crack front microstructural conditions. Figure 19 illustrates how the L-T and L-S orientations will significantly change the high angle grain boundary microstructure sampled by the crack front. As seen in Figure 19a, a flaw propagating normal to the pancake grains in the L-S orientation is completely embedded within one or two grains, with the crack front sampling/impinging the subgrain microstructure. Figure 19b shows a flaw in the L-T orientation which allows a greater number (10 to 30) of high angle grain boundaries to be sampled by the crack front. These crack paths may allow unique Phase 3 experiments to be performed by monitoring crack growth transients as significantly different microstructural features interact with the advancing crack front. The following paragraphs describe the results of experiments to characterize intrinsic fatigue crack growth in the L-T and L-S orientations.

1) L-T Orientation Intrinsic FCG

Shown in Figure 20 are the fatigue crack growth results obtained using the micronotched specimen in the L-T orientation. Figure 20a presents a micrograph of the surface of a short fatigue crack which illustrates regions of constant ΔK and decreasing ΔK -constant R propagation. The constant ΔK test results, represented as a plot of crack length (a) versus cycles (N) in Figure 20b, exhibit a

linear slope which is indicative of intrinsic crack growth over a range of crack lengths from 0.35 to 0.75 mm. A continued decrease in the slope of the a versus N plot is characteristic of interfering extrinsic effects, likely due to closure, as the wake and deflection develop. Shown in Figure 20b is the average growth rate (center region) and rates at the beginning and end of testing, each calculated by least squares analysis. While crack growth just beyond the notch affected zone ($a_n = 0.30 + 0.03$ mm) is perhaps at a slightly (20%) faster growth rate, little variation in da/dN is observed for the majority of the constant stress intensity experiment. (Crack growth within 0.03 mm of the notch is affected by notch tip bluntness, the notch stress concentration effect on stress intensity and the brittle melted layer formed by electrospark discharge machining (23). This growth is not analyzed by fracture mechanics and is ignored in this study).

The results of the decreasing ΔK -constant R test, shown in Figure 20c, predict a threshold cyclic stress intensity range of $2.2 \text{ MPa m}^{\frac{1}{2}}$. Also plotted is the result of the constant ΔK ($4.1 \text{ MPa m}^{\frac{1}{2}}$) test represented as the range of growth, 1.03×10^{-5} to 8.35×10^{-6} mm/cycle, for the crack lengths given in Figure 20b. Comparison of the results for the two tests reveals an increased growth rate for constant ΔK testing at the shorter crack lengths. These results suggest that either cracks of length less than 1 mm exhibit accelerated fatigue crack growth due to a crack tip strain mechanism and/or the decreasing ΔK test results were influenced overload delay retardation. This latter influence is a concern given the high stress intensity shedding rate employed for short crack experimentation. As will be shown in a following section, crack closure does not occur for $R = 0.6$, consistent with published data for Alloy 2090 (30).

To clarify the above results, a constant K_{\max} -decreasing ΔK experiment was performed using the large SEN specimen described earlier. This geometry allowed adequate crack length so that a reduced stress intensity gradient (C) could be chosen to minimize possible overload effects and higher stress ratios were examined. The test was conducted

at a constant $K_{\max} = 16 \text{ MPa m}^{\frac{1}{2}}$, an initial $R = 0.61$ and $C = -0.177 \text{ mm}^{-1}$. Closure loads were monitored during fatigue testing using a crack mouth opening displacement gage. Load versus deflection measurements were periodically obtained as the cyclic stress intensity was reduced with increasing R . A comparison of specimen compliance, measured before and after fatigue testing, with the periodic load-deflection results revealed that closure loads were maintained below 25% of the minimum applied load. These results indicate that extrinsic crack closure effects were eliminated by high R testing.

Crack growth results shown in Figure 21 indicate a threshold cyclic stress intensity of $2.1 \text{ MPa m}^{\frac{1}{2}}$. A comparison of these data with the previously discussed decreasing ΔK -constant R test results is shown by the insert in Figure 21. Good agreement between both ΔK decreasing techniques suggests that overload retardation effects have not been introduced during the constant R load shedding experiment and a true increase in crack growth was observed during the constant ΔK test with the physically short crack.

The constant ΔK -step increased R /constant K_{\max} method was used to ensure the measurement of intrinsic crack growth at different levels of cyclic stress intensity. This constant ΔK technique, results shown in Figure 22, allowed each constant ΔK level to be applied over a substantial crack length interval to ensure a linear a versus N response and thus steady state intrinsic growth. Figure 22a is the crack length versus loading cycles plot showing the seven ΔK levels of linear crack growth. To determine intrinsic growth characteristics, each region was plotted separately and evaluated for linear response. The fatigue crack growth at each ΔK was determined by least squares analysis. No overload effects were observed when the cyclic stress intensity was reduced from $15.98 \text{ MPa m}^{\frac{1}{2}}$ to $1.68 \text{ MPa m}^{\frac{1}{2}}$. The linear crack growth shown in the low ΔK region ($1.68/0.90$) reveals a constant growth for 2 million cycles with no evidence of crack growth retardation. Figure 22b is a more detailed region of the a - N curve showing linear growth at constant ΔK levels of 2.20, 2.75, 3.29 and $6.58 \text{ MPa m}^{\frac{1}{2}}$. It is significant to note

that these data demonstrate intrinsic growth at a relatively low ΔK and at maximum crack lengths where closure effects would dominate. Furthermore, there is no evidence of delayed crack growth just after a stress intensity range increase, demonstrating that load shedding at constant K_{\max} does not induce delay retardation presumably because the maximum or forward loading plastic zone size is constant. The results of these tests are shown in Figure 22, with the R and K_{\max} value noted for each constant ΔK experiment.

Also plotted in Figure 22 are the results for the two load shedding experiments discussed above. Above the near threshold regime, good agreement is observed between the three test techniques. The constant ΔK -step increased R technique resulted in the measurement of accelerated crack growth below the threshold stress intensities indicated by the continuous load shedding techniques, and yielding a ΔK_{th} level of less than $1.5 \text{ MPa m}^{\frac{1}{2}}$. In the Paris regime, the faster growth rates associated with the load shedding experiments are possibly due to the fact that the high stress intensity, constant ΔK experiments were conducted at low R values and may have been influenced by closure. These points in Figure 22 are accordingly marked with arrows which point in the direction of assumed intrinsic crack growth behavior.

From Figures 20 to 22, it is interesting to note that the intrinsic crack growth characteristics of Alloy 2090 do not follow typical Paris or power-law behavior. A region of crack growth exists which is weakly dependent on ΔK , forming an S-shaped intrinsic fatigue crack growth curve. This behavior in 2000 and 7000 series aluminum alloys has been related to the regime where the cyclic plastic zone size is less than one or two grain sizes. That explanation does not explain the results shown in Figures 20 to 22.

The data shown in Figure 22 establish that each of the three programmed stress intensity procedures yield intrinsic fatigue crack propagation kinetics. The constant ΔK -step increasing R/constant K_{\max} method is preferred for the current study of corrosion fatigue because

both transient and steady state crack growth kinetics can be characterized. Load shedding effects are evident in nonlinear cyclic crack length data. This technique may also yield lower values of the threshold compared to the continuous load shedding methods.

2) L-S Orientation Intrinsic FCG

The L-S orientation introduces a significantly different microstructural crack path compared to L-T, as illustrated in Figures 18 and 19. Because of the large, pancake shaped grains, the crack front produced by the micronotched specimen is embedded within one or two grains at any given instant. The potential for "single crystal type" high crack opening strains exists. A strong crystallographic texture could further promote differences between L-T and L-S crack orientations.

Initial fatigue experiments indicated that this orientation promotes significant crack path deflection. To account for deflected crack growth, modifications were made to the applied stress intensity and crack growth rates using current fracture mechanics models reported by Suresh (35). These corrections were small in magnitude and did not affect experimental trends.

Figure 23 shows the results of constant ΔK and decreasing ΔK -constant R experiments. Figure 23a is a micrograph showing the fatigue crack surface for the single specimen employed during both experiments. Figure 23b is a plot of the initial constant ΔK test results which exhibit a significant decrease in slope and thus in crack growth rate at a crack length of 0.51 mm. Careful examination of the fracture surface revealed that a portion of the crack had deflected at a different angle at this point. This resulted in a decrease in crack tip cyclic stress intensity range and an associated reduction in fatigue crack growth. These results demonstrate how the constant ΔK technique is sensitive to deflection, even at high mean stresses. Work to date has not shown large changes in crack growth rate as high angle grain

boundaries are crossed by the short/small crack at constant ΔK and in the L-S orientation. Additional experiments and analysis are needed to clarify this issue.

Within the region noted in Figure 23b (0.33 mm to 0.51 mm), fatigue crack path deflection was uniform and appropriate correction factors could be applied to the constant cyclic stress intensity and crack growth rate. These corrected results are compared to the load shed data in Figure 23c. The constant ΔK results exhibited an increased growth rate, similar to the L-T orientation when compared to the decreasing ΔK experimental results.

The constant ΔK -step increased R/constant K_{\max} test results are shown in Figure 24 along with the decreasing ΔK test results. As described for the L-T orientation, each segment of constant ΔK crack growth was evaluated for intrinsic growth; specific data will be presented during the next reporting period. Somewhat higher fatigue crack growth rates were observed for the constant ΔK -step increased R technique, particularly for crack growth near threshold and analogous to the trend observed for the L-T orientation. Also note the intermediate stress intensity range "plateau" behavior which yields to more conventional Paris-Law kinetics at higher ΔK . As discussed earlier, arrows are shown pointing in the direction of assumed intrinsic crack growth for the low R experimental results.

We conclude that rates of intrinsic fatigue crack growth in the L-T and L-S orientations are equivalent. Intrinsic fatigue crack growth in Alloy 2090 is not dependent on high angle grain boundary morphology and crystallographic orientation associated with rolled plate. This conclusion is at odds with data reported by Ritchie and obtained by correction of long crack data through opening load measurement and $K_{\max} - K_{\text{OPEN}}$ (30). Figure 25 provides a summary comparison of fatigue crack growth rate results for both the L-T and L-S orientations. The dashed lines envelop all results of the load shedding experiments performed for both the L-T and L-S orientations. Specific data points

represent constant ΔK -increasing R/constant K_{\max} experiments. The two high ΔK tests of the L-S orientation exhibited crack path deflection. Because of possible crack tip shielding due to closure at the low stress ratios characteristic of the high ΔK experiments, arrows have been drawn to note possible growth retardation associated with these data. (Note that, while deflection effects on applied stress intensity and crack growth rate are approximated by fracture mechanics models, deflected cracks exhibit increased crack wake closure if Mode II displacements are operative. Opening load measurements, not performed here, are required to develop intrinsic rates of crack growth.)

The intrinsic fatigue crack growth in Alloy 2090, developed from short crack geometry techniques in this study, is compared in Figure 26 to the propagation kinetics of microstructurally small cracks reported by Ritchie and coworkers (31). Although the comparison could be affected by possible heat-to-heat material differences, the intrinsic growth rates revealed by both techniques are comparable for stress intensities above the threshold regime. The growth of microstructurally small cracks below the threshold evidenced by the current short crack data is most probably due to high crack tip opening strains associated with single grain plasticity, and is expected based on literature results (33,36). The results of constant ΔK testing of short cracks of a ' 1.0 mm are also shown in Figure 26. The accelerated growth rates exhibited by these tests suggests a regime where the crack geometry studied here is acting as a microstructurally small crack. The growth of such cracks is characterized by a high degree of variability and microstructural sensitivity.

At this juncture in the research, the main point to be gleaned from the data contained in Figure 26 is that intrinsic fatigue crack propagation rates in Alloy 2090 are produced and monitored by the short crack, constant ΔK -increasing R/constant K_{\max} and electrical potential technique developed here. Such rates are on the same order as the disturbingly high values measured for so-called microstructurally small cracks. This information is relevant to mechanistic studies and to life

prediction models for components. The current research is now positioned to examine the potentially important effects of environment on the intrinsic growth of fatigue cracks in an advanced Al-Li-Cu alloy.

b. Phase 2: Characterization of Intrinsic Corrosion Fatigue Crack Propagation in Embrittling Environments

Using the techniques developed during Phase 1, experiments have been performed to investigate the effects of gaseous and aqueous NaCl environments on aluminum-lithium Alloy 2090. Identical experiments have also been performed using Alloy 7075 so that chemically short crack propagation trends could be compared between the two alloys.

i. Experimental Procedures

Fatigue crack propagation experiments in gaseous environments; including oxygen, helium and water vapor; were performed in a vacuum chamber using the procedures described previously and in Appendix I. To simulate the level of moisture and oxygen found in air, 2 kPa (15 torr) of water vapor and 20 kPa (150 torr) of oxygen gas were selected as static test environments. A constant static pressure of 2 kPa (15 torr) of helium was used for the inert reference environment. While high vacuum is an interesting and reasonable inert environment for study of mechanical fatigue, helium at the selected pressure was required to maintain specimen temperature to within 5°C of ambient. Experiments demonstrated that the vacuum environment could not be used because of specimen heating, to as high as 50°C, caused by the applied current required for the P.D measurement. We recognize that the purified helium and oxygen environments may be contaminated by trace (≤ 1 ppm) amounts of water vapor. Petit and coworkers have in fact claimed that such contamination dominates environmental cracking, at least in 7000 series alloys. The impact of this issue on the results which follow will be examined during the next reporting period.

Aqueous NaCl corrosion fatigue experiments were performed in the plexiglass cell, Figure 15, containing deaerated 1% NaCl solution under constant electrode potential maintained by a Wenking potentiostat.

Previous electrochemical measurements showed that the free corrosion potential of Al-Li-Cu alloys varies significantly with exposure time. Such changes are caused by small differences in solution oxygen concentration and by changes in the surface composition of the corroding alloys. The literature review presented in Appendix I further establishes that electrode potential is a critical variable which affects environmental fracture of aluminum alloys. It was therefore concluded that all corrosion fatigue tests must be conducted at a constant, known applied potential. This approach will enable comparisons with literature data and modeling of crack tip chemical driving forces. Monitoring of transient crack growth responses as the result of varying controlled electrode potential may provide mechanistic insight, as envisaged for Phase 3 research.

All corrosion fatigue testing was performed using either the constant ΔK -step increased R/constant K_{\max} or the constant ΔK -constant R methods described earlier. The constant ΔK -step increased R technique was used to investigate environmental effects on intrinsic fatigue crack growth within the high and near-threshold ΔK regimes. Constant ΔK -constant, R-constant tests were used to investigate frequency and electrode potential effects on intrinsic crack growth for constant stress intensity.

Crack surfaces are often maintained clean and electrically conducting during environmental exposure; as such, crack surface contact during loading and unloading results in a load dependence of the electrical potential signal known as "crack surface shorting" (23). Preliminary experiments showed this effect for Alloy 2090 in purified helium. Work will be conducted in Phase 3 to systematically characterize crack shorting for a variety of gaseous and aqueous environment exposures to gain mechanistic insight. Crack shorting can lead to potential drop predicted crack lengths which are erroneously less than true values. To minimize this error, Phase 2 corrosion fatigue experiments were conducted at high R ratio where K_{\min} is hopefully above the point of electrical crack separation. The computer

was programmed to acquire all electrical potential measurements at maximum load. Comparisons of predicted and measured crack lengths established that these procedures eliminated errors due to crack shorting.

ii. Environmental Effects on Intrinsic Fatigue Crack Growth

1) Alloy 7075.

Shown in Figure 27 are the results of environmental fatigue testing of Alloy 7075 at high and low stress intensity ranges, and a relatively fast loading frequency of 5 Hz. (For these experiments, the R values are 0.05, 0.05, and 0.87 for the three stress intensity ranges of 16, 10, and 2 MPa m^{1/2}, respectively. These tests were initiated at a ΔK of 10 MPa m^{1/2} ($K_{max} = 11.0$ MPa m^{1/2}), to ensure that small scale yielding and plane strain criteria were not violated. Once the crack was grown to a sufficient length, K_{max} was increased to 16.8 MPa m^{1/2} and then maintained constant for the high and low ΔK levels. A linear response for the lower level constant ΔK tests ensured that interfering overload effects were not present and intrinsic crack growth was monitored.

Compared to intrinsic fatigue crack growth in helium, both 1% NaCl (-760 mV SCE) and water vapor cause accelerated crack growth, with the maximum difference approaching a factor of six. Most interestingly, exposure to the high purity oxygen environment produced a retardation in fatigue crack growth. In all likelihood corrosion fatigue represented in Figure 27 is occurring at maximum stress intensity values below K_{ISCC} for the two lowest stress intensity ranges. Some static load cracking may contribute to the behavior observed for the highest ΔK for the water vapor and salt solution environments.

Figure 28 demonstrates that the corrosion fatigue results at high stress intensity correlate well with the findings of other investigators (37,38). The increased growth rates obtained in water vapor and aqueous NaCl have been interpreted in terms of a hydrogen embrittlement

mechanism operative at high ΔK . One expects that crack growth rates in this regime will increase with decreasing cyclic loading frequency and with increasing hydrogen environment activity. The decrease in high stress intensity range growth rates due to oxygen exposure is most interesting and consistent with the argon-oxygen data comparison reported by Wei, Figure 28 (37). Many researchers believe that surface films, formed by gaseous environmental exposure, promote fatigue damage by causing crack tip slip irreversibility compared to the inert environment clean surface case where glide dislocations can freely reverse in response to load/unload cycles. The data shown in Figure 28 are not consistent with this view. One is tempted to speculate that oxide films can reduce irreversible plastic strain at crack tips by perhaps retarding dislocation nucleation. Obviously, slip related arguments can be tailored to explain any effect of surface film and our observations are not yet complete. The mechanism for the oxygen effect will be probed in Phase 3 research.

Since the high ΔK tests were performed at low stress ratio, $R = 0.05$, it is possible that the observed crack growth response in oxygen compared to helium is caused by a reduction in crack tip stress intensity caused by oxide induced closure. The retarding effect of purified oxygen on fatigue crack growth is also observed at the low stress intensity range, Figure 27. Since crack growth in this regime was conducted at high R , it is unlikely that the oxygen effect is explained by a simple closure mechanism.

In general, environmental effects on intrinsic fatigue crack growth rate at low stress intensities are poorly understood. The data in Figure 27 show that the high ΔK trends are also observed for low ΔK -high R loading. For hydrogen embrittlement, this suggests that the maximum stress intensity plays an important role in the embrittlement process. If real, the convergence of the helium and water vapor growth rates may indicate a reduced hydrogen effect. The beneficial effect of gaseous oxygen persists to the low ΔK condition despite the fact that the cyclic stress intensity range and hence the crack tip cyclic plastic strain range is decreased significantly.

Figure 28 also contains the "upper bound" curve for all microstructurally small crack experiments (32,39) and a single specimen trend line for decreasing ΔK -increasing R test results (32). The three types of measurement shown in Figure 28 provide growth rates for Alloy 7075 which are consistent with the results obtained for Alloy 2090. Assuming that short crack, high R experiments in moist air produce growth kinetics between pure helium and water vapor environments, then a comparison of our low ΔK results with these sub-mm, microstructurally small crack data reveals comparable fatigue crack growth rates for short cracks (a '3 mm) oriented in the L-S direction. The short cracks studied here intersect many high angle grain boundaries compared to the microstructurally small crack growth data. This comparison suggests that, as shown for Alloy 2090 (Figure 26), the closure-free, intrinsic crack growth rates of cracks significantly larger than microstructural small cracks approach high levels previously ascribed to the "single crystal" crack tip opening strain effect. Microstructurally small cracks can, however, grow below the intrinsic short crack threshold, as discussed for alloy 2090, Figure 26. The short crack constant ΔK -increasing R results are at somewhat higher rates than the single specimen, long crack, decreasing ΔK -decreasing R data.

2) Alloy 2090: Preliminary Work in Gaseous Environments.

Corrosion fatigue crack growth rate results for the aluminum-lithium alloy are generally similar to the data presented for Alloy 7075. Notably, however, environmental effects on Alloy 2090 are not severe and intrinsic fatigue crack growth rates are generally less than those exhibited by Alloy 7075. Fatigue crack propagation is impeded by exposure to either gaseous oxygen or cathodically polarized aqueous chloride conditions. Decreasing frequency generally produces a reduction in corrosion fatigue crack propagation rates, contradicting the general concept of reaction rate or hydrogen transport control of the cracking kinetics.

The results of an initial gaseous environmental experiment using Alloy 2090 is shown in Figure 29. Here the micronotched specimen was fatigued in a plexiglass chamber at constant ΔK and $R = 0.6$. Prior to starting the test, the chamber was helium purged for 2 hours, with the exit gas bubbled through high purity diffusion pump oil to prevent back diffusion of air into the chamber. The chamber was maintained at a positive pressure during the test to limit the ingress of air. When desired, helium was bubbled through distilled and deaerated water to produce a moist environment. (These environments are probably contaminated by trace amounts of nitrogen and oxygen, the concentration of which varies with test time. Resulting data may not be quantitatively comparable to results obtained with gases in the high vacuum chamber, however, trends are likely to be similar.)

Fatigue crack growth was initiated at constant ΔK in helium, as shown in Figure 29 by the linear crack growth rate for a 0.70 mm. Moisture was then introduced into the chamber; a corresponding reduction in crack growth rate is shown in Figure 29. (The discontinuous, apparent increase in crack length at the point of water vapor introduction is caused by an instability in the electrical potential signal due to the environmental change or, less probably, by a change from a shorted crack surface to an oxide coated and insulated surface.) When dry helium was reintroduced into the chamber, the fatigue crack growth rate increased with very little transient incubation time. At crack lengths of 0.90 mm and 0.95 mm, crack arrest occurred reproducibly when the specimen was again exposed to wet helium. While water vapor retarded crack growth relative to helium in Alloy 2090 after each of three exposures, the latter two caused full arrest, while the first exposure caused a mild decrease in rate. Since applied ΔK is constant for each exposure, this history dependence suggests either varying oxygen contamination, a buildup of voluminous and load bearing corrosion products, or a chemical mechanism as yet not understood. Given the behavior of Alloy 7075 and the likelihood of hydrogen embrittlement from

water vapor, these results were unexpected. Further experimentation in purified environments was conducted.

3) Alloy 2090: Purified Gaseous and Aqueous Environments.

To understand environmental effects on fatigue crack growth in Alloy 2090, a series of experiments, similar to those performed for Alloy 7075, were conducted with the high vacuum system and the constant ΔK -step increased R method. (Gaseous environment testing was performed with the identical R, K_{\max} , and ΔK scheme described for gaseous environment testing of alloy 7075. The data shown for aqueous NaCl are from three separate specimen constant ΔK -constant R experiments.) Results are presented in Figure 30. Because of the complex shape of the fatigue crack growth rate-stress intensity response for moist air exposure, lines have only been drawn for the two regimes of interest at high and low ΔK .

At high ΔK , differences in crack growth rate were less than two-fold for aqueous NaCl, water vapor, helium and air. The chloride and water vapor environments produced the highest growth rates. Notably, however, these corrosion fatigue speeds are measurably less than the values presented in Figure 28 for Alloy 7075. The rate for moist air was reduced and unexpectedly equal to that recorded for purified helium. Testing in the oxygen environment resulted in a significant reduction in fatigue crack growth. These trends are identical to those presented for Alloy 7075.

At low ΔK , considerable differences in fatigue crack growth were observed for the different environments. Cracking in helium and aqueous NaCl continued to exhibit similar and high growth rates, while crack growth in water vapor decreased to that observed in air. Considerable reduction in fatigue crack growth rate was observed for the oxygen environment. These results are consistent with those observed for the impure helium/water vapor experiment, Figure 29. That is, the environmental ingredients (water vapor and oxygen) which are possibly

introduced by bubbling helium through distilled water retard fatigue crack growth relative to pure helium and at low cyclic stress intensity. The mechanism for this result will be pursued in Phase 3. Analogous to high ΔK conditions, Alloy 2090 is less sensitive to near threshold, chloride or water vapor corrosion fatigue compared to Alloy 7075.

4) Alloy 2090 in Aqueous Chloride: The Effect of Frequency.

The corrosion fatigue crack growth rate of Alloy 2090 was measured as a function of loading frequency for the 1% aqueous NaCl environment. The objective of these tests was to determine if the intrinsic crack growth rate was dependent on frequency within the high and low cyclic stress intensity regimes. Shown in Figure 31 is the fatigue crack growth of Alloy 2090 at a frequency of 5 Hz and 0.1 Hz for anodic polarization in chloride. Tests conducted at 5 Hz exhibited slightly higher fatigue crack growth at high and low cyclic stress intensities. No crossover in frequency response was observed for Alloy 2090. (Recall from Appendix I that slow frequencies generally exacerbate high ΔK corrosion fatigue due to hydrogen embrittlement, while high frequencies promote near threshold cracking by film rupture processes.) Results for Alloy 2090 may indicate that rapid crack tip reaction and film formation prevents any change in the frequency dependence of fatigue crack growth in aqueous NaCl environment. The kinetics of passive film formation may play an important role in protection of lithium containing aluminum alloys.

The results shown in Figure 31 are confirmed by the constant ΔK results shown in Figures 32 and 33. Figure 32 shows the different crack growth rates for three frequency levels at high constant ΔK . The changes in slope of the a versus N curve highlight a significant change in da/dN for the three frequency levels. A factor of five increase in fatigue crack growth rate is observed for experiments performed at 5 Hz and 0.1 Hz. Figure 33 reveals little change in fatigue crack growth rate at low cyclic stress intensity. Specifically note little

difference in crack growth rate for increasing frequency by a factor of 285 (0.07 Hz to 20 Hz).

5) Alloy 2090 in Aqueous Chloride: The Effect of Electrode Potential.

To further understand crack tip mechanisms in the aqueous NaCl environment, a series of four experiments were performed to determine the FCG response of Alloy 2090 at different electrode potentials. The constant ΔK tests were also conducted at different levels of cyclic stress intensity to qualitatively assess the relationship of crack tip mechanical driving force (ΔK level) and crack tip chemical driving force (electrochemical potential). The results of these experiments are shown in Figures 34 to 37.

The fatigue crack growth response at a constant ΔK of $2.5 \text{ MPa m}^{\frac{1}{2}}$ is shown in Figure 34. An initial, constant crack growth rate was established at an applied anodic potential of -0.76 V (SCE) . At a crack length of 2.05 mm , the specimen potential was changed to a mildly cathodic potential of -1.16 V (SCE) . As noted by the horizontal dotted line, crack arrest occurred at this cathodic potential. At a cycle count of 1×10^6 cycles, the potential was changed to an anodic value of -0.76 V . Approximately 76 hours of cyclic loading elapsed before crack growth resumed. The same fatigue crack growth rate, as initially monitored at -0.76 V (SCE) , was eventually reached. Crack arrest was again noted when a cathodic potential of -1.16 V (SCE) was applied to the specimen. This dramatic effect of cathodic polarization is consistent with the general, beneficial trends for environmental cracking of 2000 and 7000 series aluminum alloys summarized in the literature review, Appendix I.

Cathodic potential reduced rates of corrosion fatigue at higher stress intensity ranges. Results of high constant ΔK testing ($9.6 \text{ MPa m}^{\frac{1}{2}}$) at a low stress ratio ($R = 0.1$) are shown in Figure 35. After initial cracking at an anodic potential of -0.76 V (SCE) , a mild reduction in crack speed was produced by cathodic polarization to

-1.16 V (SCE), and a significant and time dependent retardation in crack growth was observed at a cathodic potential of -1.26 V (SCE). Given the low mean stress intensity for this experiment, retardation may have been caused by a closure effect due to increased surface film formation. The applied stress intensity range was then decreased to a ΔK of 2.1 MPa m^{1/2} at R = 0.9 with K_{max} maintained constant. A slow recovery to a steady state growth rate was observed at an anodic potential of -0.76 V (SCE). Crack growth arrest was subsequently produced by cathodic polarization at -1.16 V (SCE), reproducing the results shown in Figure 33.

A variety of frequency changes were effected during the constant stress intensity tests represented in Figures 34 and 35. Specifically in Figure 34, frequency was varied from 0.07 to 20 Hz during the initial anodic polarization. In Figure 35 frequency was varied over a similar range during the first cathodic and the second anodic polarizations. Frequency levels are noted on Figures 36 and 37 where significant changes in crack growth rate were due to changes in frequency. In general decreasing frequency results in a mild decrease in corrosion fatigue crack growth rate for each of the stress intensity and electrode potential conditions examined. These changes were small, but clearly demonstrated by the constant ΔK procedure. Occasionally, variability in the electrical potential signal and crack deflection obscured the effect of frequency. At this point the clear conclusion is that corrosion fatigue crack propagation in the Alloy 2090 is not exacerbated by very slow loading frequencies for the chemical conditions examined.

The beneficial effect of cathodic polarization was also demonstrated for the L-S orientation, including both peak and over aged microstructures. Peak aged L-S material is represented in Figure 36 for intermediate constant stress intensity loading. The crack was grown to a length of 1.59 mm at a constant ΔK of 4.1 MPa m^{1/2} (R = 0.6). The stress intensity was then increased to a ΔK of 8.45 MPa m^{1/2} (R = 0.6), resulting in a significant increase in crack growth rate. For each ΔK level, cathodic polarization below -1.2 V (SCE) mildly retarded the growth of

the corrosion fatigue crack relative to the anodic potentials of - 0.86 and -0.96 V (SCE). Anodic to cathodic and cathodic to anodic potential changes caused immediately resolvable changes in crack growth rate without evidence of long transient incubation periods. Notably, the high levels of cathodic polarization did not cause enhanced corrosion fatigue, as expected should hydrogen embrittlement be operative.

The corrosion fatigue crack growth response of over aged L-S Alloy 2090 is shown in Figure 37 for intermediate stress intensity loading. At a cathodic potential of -1.16 V (SCE), where crack arrest was achieved in peak aged L-T materials at $\Delta K = 2.5 \text{ MPa m}^{\frac{1}{2}}$ (Figure 34), significant crack growth was obtained for the current conditions. A more cathodic potential of -1.26 V (SCE) was required before crack growth retardation was observed. Anodic polarization caused increased fatigue crack growth rates.

Based on the results of these experiments, we speculate that mild cathodic polarization produces a crack tip chemistry that promotes crack tip film formation. Increased cyclic stress intensity is required to cause fatigue damage of the filmed surface relative to more anodic conditions. This effect may be related to the retarding effect of oxygen exposure on fatigue crack growth in Alloys 2090 and 7075. Work during the next reporting period will explore the possible common effect of film forming environments on fatigue.

iii. Summary and Conclusions

Based on an in-depth literature review, an experimental plan was developed to identify mechanisms of intrinsic damage localization during corrosion fatigue of Al-Li-Cu alloys.

Using the potential difference technique, short crack specimen geometry and decreasing ΔK -step increased R test scheme, an excellent method has been developed for the continuous monitoring of intrinsic fatigue crack growth in aluminum alloys exposed to aggressive environments.

The true (intrinsic) transgranular fatigue crack growth characteristics of Al-Li-Cu-Zr rolled plate material are independent of crack path direction and are not strongly affected by interactions with microstructural boundaries.

Short fatigue cracks of length less than 1 mm exhibit crack growth rates that are significantly greater than cracks of longer length.

The environmental effects on transgranular, intrinsic fatigue crack propagation in Alloy 2090 depend on the level of applied stress intensity. At high ΔK , small differences in crack growth rate occur, with the order of ranking from fastest to slowest growth rate being: aqueous chloride, water vapor, moist air, purified helium and oxygen. Oxygen particularly retards crack growth. At near threshold ΔK levels, chloride and helium promote rapid cracking, with water vapor, moist air and oxygen causing progressively decreasing corrosion fatigue. The purity of the gaseous environments will be confirmed in future experiments.

Cathodic polarization significantly reduces aqueous chloride corrosion fatigue in Alloy 2090, while anodic polarization exacerbates the environmental effect.

Decreased frequency mildly reduces rates of corrosion fatigue crack growth in Alloy 2090 exposed to aqueous chloride.

Alloy 7075 is, in general, more environmentally susceptible compared to Alloy 2090. The aggressive character of each environment increases from oxygen to helium to water vapor to aqueous chloride, analogous to the behavior of Alloy 2090.

Environmental results suggest (speculatively) that crack tip surface films play an important role in crack tip damage mechanisms during corrosion fatigue of Al-Li-Cu alloys. This is evidenced by:

- ✕ retarded growth in oxide and hydroxide forming environments including purified oxygen gas and cathodically polarized aqueous NaCl;

- ✕ additional mechanical driving force required to overcome environmental effects;
- ✕ increased corrosion fatigue crack growth with increased frequency.

D. Future Work for the Period April 1, 1988 to March 31, 1989

The program plan for the study of Damage Localization Mechanisms in Aqueous Chloride Corrosion Fatigue of Al-Li Alloys was developed in the original proposal (20) and was amplified in further detail in Appendix I. The timing of specific tasks is presented in Figure 1.

As presented in the preceding sections, work during the first reporting period has accomplished all Phase 1 tasks and about 75% of the Phase 2 tasks. All Phase 2 tasks will be completed by the end of year 1, that is by March 31, 1988.

At this point we envision no major departures from the original plan. The work to be conducted in year 2 will follow the original proposal, Appendix I and Figure 1. Specifically, emphasis will be placed on the following tasks:

- ✕ Systematically analyze the crack growth rate data obtained in year 1. This work will include verification of important trends, analyses of potential environment contamination effects, detailed fractographic analyses of critical specimens; and will result in two publications on intrinsic fatigue crack propagation in Alloy 2090 for moist air exposure and on environmental effects on intrinsic fatigue crack propagation in alloy 2090.
- ✕ Design and execute Phase 3 experiments which follow from the analyses of Phase 2 work and which are aimed at elucidating mechanisms of environmental fracture. Interests here include explaining the dramatic, inhibiting effects of gaseous oxygen and cathodic polarization on fatigue crack growth; probing the possibility for a hydrogen contribution to corrosion fatigue; and explaining the mild and inverse frequency dependency reported herein.

✕ Mr. Piascik will begin to draft his doctoral dissertation in the summer of 1988 with a graduation goal of December, 1988. This effort will lead to one or two additional publications and selected experiments through the last three months of year 2 to March 31, 1989.

The completion of the corrosion fatigue program at the end of year 2 will coincide with Mr. Piascik's graduation. Corrosion fatigue work on monolithic Alloy 2090 will most likely not be included in the renewal proposal for year 3. We expect that work in year 3 will emphasize environmental fracture of a metal matrix composite-ambient temperature gaseous/aqueous system and of a powder metallurgy aluminum alloy-elevated temperature system. Work on Alloys 2090 and 7075 will provide the necessary foundations for studies of stress corrosion cracking/corrosion fatigue of the composite. The direction of elevated temperature work is presented in Section VI.

SECTION IV

Program 2

MEASUREMENTS AND MECHANISMS OF LOCALIZED AQUEOUS CORROSION IN ALUMINUM-LITHIUM ALLOYS

G. E. Stoner and R. G. Buchheit, Jr.

The goals of this phase of the program, as stated in the original proposal, are to isolate and measure local processes hypothesized to control corrosion and embrittlement of aluminum-lithium alloys. This progress report and continuation proposal represents six months effort towards achieving the above objectives.

A. Summary

Based on a review of the literature, microreference Ag/AgCl electrodes have been constructed and tested. Microreference electrode tips have been made as small as 5 μm (inner bore diameter). Electrodes constructed show excellent reference potential stability and have been used to measure potential variations as small as 0.6 mV on an actively corroding metal surface. Microreference electrodes have been used to measure the variation in potential in the vicinity of corrosion pits on peak aged 2090 (Al-2.7Cu-2.2Li-0.12Zr) during potentiodynamic polarization scans.

Measurements of the change in pH versus time have been performed for artificial crevices and immersed machine shavings in solutionized and peak aged 2090. Preliminary results suggest that pH versus time behavior is dependent on alloy heat treatment.

B. Progress Report

1. Mechanisms of Local Corrosion in Aluminum-Lithium Alloys

a. Introduction

Many heat treatable high strength aluminum alloys are susceptible to local corrosion in aqueous environments. Local corrosion is a result of galvanic activity which is related to microstructural heterogeneity. This type of environmental attack manifests itself in pitting, crevice corrosion, stress corrosion cracking, and in some cases hydrogen embrittlement.

Local corrosion differs from general or uniform corrosion in that areas of anodic and cathodic activity are well defined. Active anodic sites are usually small areas of intense metallic dissolution. As a result of this metallic dissolution pits form and grow and pre-existing crevices may deepen. As the pit or crevice grows, the environment becomes isolated from outside and is said to be 'occluded'. Diffusional transport of chemical species from outside of the occluded environment is severely inhibited which facilitates dramatic changes in the occluded environment chemistry.

Aluminum-lithium alloys are susceptible to local corrosion but in some cases show a marked decrease in susceptibility to stress corrosion cracking when compared to conventional high strength aluminum alloys (40-42). The discussion below outlines the important aspects of pitting, crevice and stress corrosion cracking in Al-Li alloys and compares the behavior of these alloys to the local corrosion behavior of conventional high strength aluminum alloys.

b. Pitting

Pitting in high strength aluminum alloys immersed in aqueous chloride environments is initiated near second phase strengthening particles or constituents. Local differences in composition due to solute enrichment of the particle or solute depletion in the supersaturated matrix in the vicinity of the particle

create local anodes and cathodes. When these are established galvanic, corrosion activity can occur. Dissolution of the more anodic region can result in the formation of a pit.

Grain boundaries and sub-grain boundaries are favorable sites for the nucleation of second phase particles and as such are regions of increased dissolution and pitting (43-46). In Al-Li-Cu alloys the presence of active lithium bearing phases is thought to promote local corrosion by pitting (47). However, lithium is not the sole contributor to pitting activity. Some experimental evidence suggests that copper-lithium rich phases which populate subgrain boundaries in Al-Li-Cu alloys are active phases. In particular, T_1 (Al_2LiCu) appears to increase the dissolution of sub-grain boundaries (48,49).

In even the most pure high strength aluminum alloys, iron and silicon constituent particles are present. It has been shown that iron acts as a cathode when brought in contact with pure aluminum and accelerates aluminum dissolution in aerated 0.1M NaCl solution (50). Research performed at the University of Virginia on Alloy 2090 shows that Fe-Si constituent particles are sites for the initiation of gross pitting (51). Another type of constituent, oxide particles, are often included in the processing of powder metallurgy alloys. These oxide inclusions usually grouped in stringers may also serve as sites for preferential pit formation (52).

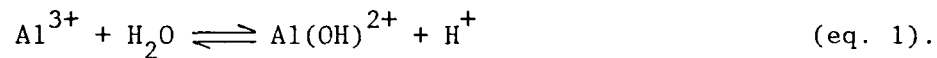
Microstructural heterogeneity is an important aspect in the pitting of high strength aluminum alloys, but for appreciable local corrosion the environment must be sufficiently damaging. In general, the passive film on aluminum alloys is unstable in aqueous chloride environments for pH values greater than about 10 and less than about 4 (53). Pitting will occur in aqueous environments of extreme pH. Pitting is artificially stimulated by anodic polarization, although a definite critical potential marking the onset of pitting is often difficult to establish with a high degree of precision (54).

Pits that form as the result of local anodic dissolution will often follow grain boundaries and tend to grow in depth faster than they grow in width. These pits grow into fissures which become effective stress concentrators when an external load is applied.

c. Local Occluded Environments

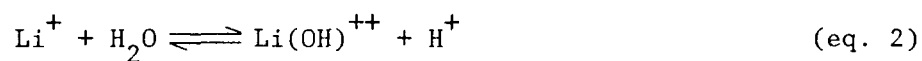
The occluded crack chemistry that develops in a lithium bearing aluminum alloy differs substantially from that found in other conventional high strength aluminum alloys. In Al-Li-X alloys the solution within a long crack under proper conditions is alkaline at least initially while a long crack in a non-lithium bearing aluminum alloy will be acidic (49,55,56,57).

Solution pH values measured at the tips of mechanically induced cracks in 7475 immersed in 3 w/o NaCl solution are consistent with the equilibrium reaction (58):



Measured pH values stabilized at values between 2.5 and 3 after 2 days under constant immersion conditions. Concentrations of ionic species in occluded cracks were measured far in excess of the bulk species concentration. Anionic species concentration, primarily Cl^- , was measured in the range of 2-3 M. The total concentration of cationic species was estimated at 0.7 M. Cationic species included ions of Na, Zn, Cu and Mg with copper plating on the crack walls. The amount of Cl^- constituting the difference in the concentration of anions and cations was presumed to be tied up in cationic complexes and solids depositing in the crack.

The reaction:



occurs at a pH of about 11 for a lithium concentration of 0.002 M (49). The pH of a solution measured in natural and artificially created

cracks in Al-Li-Cu-Mg alloy 8090 immersed in 3.5 w/o NaCl solution suggests that this reaction rather than the aluminum dissolution reaction controls the critical solution chemistry in occluded environments (56).

It has been suggested that environments that are at the extremes of pH (too acidic or too alkaline) will not support stress corrosion crack growth in aluminum alloys (49). However, it has been demonstrated that crack environments in Al-Li-Cu-Mg alloys can be modified by alternate immersion testing so that the crack growth can be supported (49,59).

Stressed specimens of 8090 Al-Li-Cu-Mg alloy showed no evidence of stress corrosion cracking after 30 days of constant immersion in 3.5 w/o NaCl solution (56). Blunt intergranular fissures were observed however. All of the stressed specimens failed within two days after removal from the solution and exposure to laboratory air. Specimens immersed in NaCl solution and then exposed to air of 100% relative humidity without CO₂ did not fail.

The following sequence of events was proposed to explain the phenomenon (56):

- 1) Immersion in the NaCl solution caused local attack to occur forming fissures, but the environment was too aggressive for sharp cracks to form.

- 2) When the specimens were removed from the bulk solution, access to surface cathodes was no longer available and lithium dissolution reaction controlled the crack chemistry driving it alkaline.

- 3) Upon exposure to air, CO₂ was absorbed into the fissure causing a concentrated chloride/carbonate/bicarbonate solution to form and causing a reduction in pH.

- 4) The reduction in pH and the interaction of these species with the passive layer established an environment that allowed sharp cracks to initiate and propagate to failure.

These results have been duplicated for alloy 2090 at the University of Virginia (60).

2. Microreference Electrodes

a. Introduction

Local corrosion occurs when anodic dissolution is confined to very small areas while larger areas behave as cathodes. The particularly damaging aspect of localized corrosion is that the penetration rate of the metal in localized areas is much greater than that found in general corrosion (61).

Since anodic dissolution is well separated from regions of cathodic activity, the two different areas can be investigated independently. Anodic activity occurs in a concentrated area and is quite intense while cathodic activity is usually spread over a larger area and is less intense. As a result, measurements of local corrosion are usually aimed at detecting anodic activity. Different types of microprobes can be used to investigate a localized area. These include microreference electrodes for measuring potential (61-68), pH microreference electrodes for measuring pH in local regions (69) and scanning vibrating microelectrodes used for measuring local currents (70-74).

Microreference electrodes used for measuring potential and pH are inexpensive and relatively easy to make in the laboratory. Scanning vibrating electrodes used to measure corrosion currents are more complicated to operate since they require complicated mechanical drives to achieve scanning and vibrating action. The following discussion will focus on the construction and operation of microreference electrodes.

b. Construction of Microreference Electrodes

Microreference electrodes can be as simple as a single platinum wire coated with an insulating lacquer (68). However, metallic wires less than 25 μm are difficult to obtain and more difficult to work with. Typically, microreference electrodes are constructed from a metallic wire immersed in an ionic solution contained within a glass pipette. The tip of the pipette is drawn down in a flame to the desired diameter.

A typical glass microreference electrode constructed by Doig and Edington (63) in the above way used a 25 μm silver wire chlorodized in 0.1 M hydrochloric acid. The chlorodized wire had a silver chloride surface and was suitable for use as a reference electrode. The wire was immersed in a glass capillary containing 1 M NaCl solution. The tip of the electrode was drawn down so that the inner diameter of the glass capillary was 0.2 μm .

A primary requirement for microreference electrodes is that they be small. That is that the tip of the electrode should be as small or preferably smaller than the region of from which the measurement is to be taken. The region of interest can be as large as the heat affected zone in a welded structure (millimeters) or as small as microstructural features in metals like larger second phase particles (tens of microns or less).

In general, the smaller the electrode tip, the greater the sensitivity and utility of the electrode. The disadvantage is that small tipped electrodes generally have very high impedances leading to electrical noise which may become a problem.

Another requirement for a microreference electrode is that it must remain stable over the course of the experiment. Silver-silver chloride electrodes fashioned from chlorodized silver wire exhibit excellent stability when properly prepared and aged (75).

c. Operation of Microreference Electrodes

The ability of microreference electrodes to measure potential variations associated with local anodic areas depends on several factors. These include: the diameter of tip of the microelectrode, the distance between the the tip of the electrode and the metal surface, the conductivity of the electrolyte and the corrosion cell geometry (shape, anode to cathode area) on the surface of the working electrode. Presently, there is some debate over the relative importance among these factors.

Microreference electrodes do not measure the potential of the metal surface but rather the potential of the metal solution interface in the vicinity of the the microelectrode tip. When examining anodic regions associated with structural features in metals it is important that the electrode tip be close enough to the area of interest so that measurable potentials can be detected, but not so close that the presence of the microelectrode tip interferes with the distribution of the potential field (hence current density distribution) in solution.

The effect of corrosion cell geometry and solution conductivity on the performance of microreference electrodes can be examined with the following equation (76):

$$L_i = K |dE_i/dJ_i| \quad (\text{eq. 1})$$

where K is the solution conductivity and the quantity dE_i/dJ_i is simply the polarization resistance in the electrolyte of the ith redox couple. The quantity L_i or 'polarization parameter' has units of length and is a quantity that has been used to classify corrosion cells since the 1940's. Waber determined that L usually falls in the range of 0.25 to 25 mm (77).

Another parameter, defined by Stern, is used to describe galvanic cells by a critical or characteristic cell dimension (78). This characteristic dimension, λ , is usually taken as the smallest dimension of the anode area. Typically, the smallest dimension of an electrode exerts the greatest influence on the distribution of the potential and current density fields.

When the polarization parameter, L, is less than the characteristic cell dimension, λ , there is significant potential and current density variation in the solution in the vicinity of the electrode. When $L \gg \lambda$, the potential and current density field variations in the vicinity of the electrode are negligible.

Starke and Marek (64) used the arguments presented above in an attempt to verify results obtained in microelectrode studies of grain boundaries in an aged Al-7.2Mg-4.4Cu alloy immersed in 3.5 w/o NaCl solution by Doig and Edington (63). Starke and Marek did not measure any potential variation in the vicinity of grain boundaries using Ag/AgCl microreference electrodes in contrast to results presented by Doig and Edington. Starke and Marek claimed that the characteristic cell dimension of a grain boundary in the aged Al-7.2Mg-4.4Cu alloy was the half width of the solute depleted zone around the grain boundary. Since the polarization parameters, L , for likely redox couples were much greater than the half width of the solute depleted zone, negligible variation in the potential in the electrolyte in the vicinity of a grain boundary would be expected. Therefore micro electrodes could not be used for measuring local potential in this situation.

O'Halloran et al. (66) used Ag/AgCl microreference electrodes to study local potential variations around corrosion pits in mild steel immersed in NaCl solution of varying concentration. They were able to resolve corrosion pits as small as 50 μm in diameter with an electrode tip that was 38 μm in diameter. They also noted that the signal from the microreference electrode decreased significantly for an order of magnitude increase in the electrolyte concentration.

Kackley and Latanision (68) mechanically scanned a lacquered 100 μm platinum wire over the surface of a 5052 aluminum alloy immersed in slightly diluted ASTM substitute ocean water. Corrosion pits as small as 2 μm in width and 15 μm in length were resolved in their experiments. The location of the pits on the scanning plot were then correlated with photomicrographs obtained with a scanning electron microscope.

d. Microreference Electrodes for Measuring pH

The construction and use of pH microreference electrodes has been described by Davis (69). Microreference electrodes were used to measure the pH in mechanically induced cracks in single edge notched (SEN) 7075-T651 sheet immersed in 4.46 w/o KCl solution.

The configuration of the pH microreference electrodes used in this experiment was similar to that of the Ag/AgCl microreference electrodes described above. The pH microreference electrodes were made for pH glass pipettes (Corning 0150 pH glass) mechanically drawn by pipette puller to a tip diameter of 1 to 5 μm . In this case the tip of the electrode was sealed. The pipette was filled with double distilled water, and a 125 μm diameter platinum wire was inserted and the pipette was sealed. The electrode was calibrated by measuring the potential of the pH microelectrode with respect to an Ag/AgCl microelectrode in solutions buffered to pH solutions in the range of interest.

The pH in the crack in the SEN specimen was measured in a fashion similar to that in the calibration process. Both the pH reference and the Ag/AgCl reference electrodes were inserted into the crack and the potential difference was recorded. The pH was then determined from the calibration curve. Values of pH ranging from 2 to 10 were measured in cracks using this technique.

e. Some Experimental Techniques

Microreference electrodes can be used for corrosion measurements in a variety of arrangements. Three of these arrangements are described below.

The first commonly used arrangement utilizes a microreference electrode and another standard reference electrode in an electrochemical test cell. The microreference electrode is positioned in the vicinity of the area of interest on the working electrode. The microreference electrode can be positioned manually or by micromanipulators. Another standard reference electrode is then positioned further away from the surface of the working electrode.

The microreference electrode measures a potential which is largely determined by reactions occurring on the local surface of the working electrode. The standard electrode further away from the working electrode measures a potential which is determined, for the most part, by the reactions occurring on the majority of the surface of the working electrode. The potential difference between the two reference electrodes can then be plotted as a function of other quantities like time or net corrosion current. Another option for data presentation is to measure the potential difference between the microreference electrode and the working electrode itself as a function of time or net current or position.

A second experimental arrangement uses a single microreference electrode that is scanned over some prescribed area of the working electrode. Using this type of technique, isopotential contour maps can be developed which are usually used to highlight areas of significant anodic activity associated with pitting (65,66,68).

There are two important drawbacks to the scanning microreference electrode methods. The first disadvantage is that the scanning of the electrode agitates the solution. The second disadvantage is that a single area scan can take up to several minutes. In a potentiodynamic polarization experiment changes in the position and intensity of corrosion activity might be missed.

The problems associated with the scanning electrode methods can be eliminated by using an array of microreference electrodes. The array of electrodes is held stationary and eliminates agitation. The electrodes can be monitored continuously or can be scanned electronically. A complete area scan performed electronically can be completed much more quickly than a mechanical scan thereby increasing the chances of detecting transient behavior during an experiment performed under potentiodynamic conditions.

3. Report on Research Conducted to Date

a. Microreference Electrodes

As discussed in the original research proposal (20), microreference electrodes were constructed and tested to determine the practicality of utilizing them for measuring potentials and pH values in the vicinity of corroding grain boundaries, reactive precipitates and occluded geometries. Techniques for constructing Ag/AgCl microreference electrodes and glass pH microreference electrodes in the laboratory have been developed with some assistance from concepts reported in the literature. The method used here follows closely to that used by Doig and Edington (63), Davis (69) and Ives and Janz (75). Ag/AgCl microreference electrodes have been constructed and tested for stability of potential and ability to detect variations in potential on a corroding metal surface. Potential variations as small as 0.25 mV have been detected in solution near actively corroding pits on the surface of alloy 2090 (Al-2.7Cu-2.2Li-0.12Zr).

The technique developed for constructing Ag/AgCl microreference electrodes (hereafter called microelectrodes) is relatively simple and has been repeatedly carried out in our laboratory. The microelectrode is a 250 μm diameter pure Ag wire that has been anodically polarized, or chlorodized, in hydrochloric acid. Up to ten 2.5 cm Ag wires were chlorodized at a time. The wires were immersed in 1.0 M HCl as working electrodes. A platinum counter electrode and reference electrode were used in this arrangement. The cell was potentiostatically controlled to maintain a current density of 7 to 10 ma/cm^2 for 10 minutes. The silver wires developed a brown to purple coating as the chlorodizing proceeded. After the process was completed the chlorodized wires were stored in 3.5 w/o NaCl solution for aging. Potentials measured versus a calomel electrode showed that potential variation with time did occur and stable potentials were reached after about 3 days. For most potentiodynamic polarization experiments (lasting less than 10 minutes) the

variation in Ag/AgCl potential was negligible, hence aging was unnecessary prior to use of the microelectrode for experiments of short duration.

For use in experiments, the chlorodized Ag wire was placed in a glass pipette filled with 3.5 w/o NaCl solution (the test solution for most experiments). The end of the pipette was drawn down to an inner bore diameter of less than 5 μm (Fig. 38). To introduce solution into the small end of the pipette, the pipettes were boiled in the solution for 30 minutes. Boiling served to drive all of the gas out of the narrow end of the pipette. After the wire was inserted into the pipette, the large end of the glass pipette was sealed with wax or rubber cement.

Aged microelectrodes showed excellent stability, in that the measured potential drift between a calomel electrode and microreference electrode in 3.5 w/o NaCl solution was less than 3 mV.

The microelectrode's ability to detect variations in potential was tested in potentiodynamic polarization scans performed on Alloy 2090 in aerated 3.5 w/o NaCl solution. The cell was set up on the stage of an upright Olympus BHMJ-N optical microscope equipped with extended working distance objective lenses (about 7 mm for a 20 X lens). The microscope allowed for accurate placement of the microelectrode tip and also allowed for observation of corrosion activity in situ.

The microelectrode tip was manually positioned near a site likely to initiate a pit. In these experiments Fe-rich constituent particles were known to be such sites (Fig. 39). A calomel electrode was positioned several millimeters away from the surface of the working electrode in the cell. The electrical leads of the microelectrode and the calomel electrode were connected directly to a strip chart recorder and the difference between the two was measured during polarization scans.

The lower limit of the polarization scans were -1000 mV SCE or -1300 mV SCE and upper limits were -450 mV SCE. The scan rate was

5 mV/sec. Open circuit corrosion potentials in air were determined to be in the range of -780 to -740 mV. Potential spikes representing the difference in potential between the microelectrode over an active pit and a calomel electrode removed from the surface of the working electrode were recorded. The magnitude of the spikes was between 17 and 20 mV (Fig. 40). The onset of the potential spikes occurred when the working electrode was polarized to about -585 mV and ended at a polarization potential of about -690 mV. The onset of the potential spike corresponded to onset of copious gas (e.g. H₂) evolution from the mouth of the pit.

A second type of experiment was performed to measure the difference in potential between a region that was actively pitting and a region that was apparently quiescent. Again a microelectrode was positioned over a site likely to initiate a pit. Another microelectrode was positioned a few microns away but not near a site favorable for pitting. A polarization scan identical to the one described above was performed. The beginning and end of the potential spike and the onset of gas evolution from the mouth of the pit were the same as described for the first experiment. However, the magnitude of the spike was 0.6 mV for the first scan and 0.25 mV for a second scan (Fig. 41).

b. In Situ Corrosion Observations

Use of the long working distance optical microscope described above allows for the observation of corrosion of a working electrode in an aqueous environment while it takes place. The maximum magnification that can be achieved with the microscope is 500 X and features as small as a few micrometers can be easily resolved.

The evolution of gas from sites of intense activity is the most easily distinguishable event that is observed (Fig. 42). Gas bubbles are often observed coming out of pits over a large range of potentials during a polarization scan. Gas evolution is the most intense at potentials more anodic than the breakaway potential (-600 mV) and at extreme cathodic potentials (-1200 mV).

Preliminary observations indicate that there are sites which evolve gas when the working electrode is anodically polarized with respect to the open circuit corrosion potential, but are not visibly active when the working electrode is polarized cathodically (Fig. 43a,b,c). Other sites appear to be active at both large anodic and cathodic polarizations.

c. Simulated Local Environment Tests

Local environment tests have been used extensively by Holroyd et al. in categorizing the corrosion and stress corrosion behavior of an Al-Li-Cu-Mg alloy, 8090 (49,55,56). Two primary types of experiments described by Holroyd et al. were used in this study of alloy 2090. In the first type of experiment an artificial crevice was machined in two specimens. The first specimen was solutionized and cold water quenched. The second was solutionized, cold water quenched and aged at 160°C for 14 hours corresponding to a peak to slightly over aged condition for 2090. A round hole, 1 cm in diameter and 3.5 cm deep, was drilled in the specimen. The hole was filled with 3.5 w/o NaCl solution and a glass pH electrode was inserted. The hole was then sealed with wax to reduce the amount of oxygen that could diffuse into the solution. The pH was measured as a function of time for 104 minutes (Fig. 44).

The initial pH was measured at 6.5 and steadily increased to a pH of 8.75 for the peak aged alloy and 8.25 for the solutionized alloy after about 100 minutes. Measured pH values for the solutionized alloy then fell to 6.5 before stabilizing at pH 8.0. The pH for the aged alloy fell to a value of about 7.5 after 2000 minutes, but did not exhibit the same degree of stability as the solutionized alloy.

In the second experiment, 15 grams of machine shavings of solutionized and aged 2090 were immersed in a volume of NaCl solution (about 30 ml) which just covered the shavings. The object of this experiment was to determine the effect of a large (crevice) surface area

to solution volume ratio on the solution chemistry. Solution pH was continuously monitored with glass pH electrodes for 8000 minutes (Fig. 45).

Initial solution pH values were 7.25. Measured pH values for both the solutionized and aged shavings steadily increased. Both pH values stabilized at 10.5.

It should be noted that the results for simulated local environments are based on one set of tests. While these trends agree with data reported for Al-Li-Cu alloys, the results should be regarded as preliminary.

d. Scanning Electron Microscopy and Energy Dispersive Spectroscopy

Scanning Electron Microscopy (SEM) has been used in examining pitted surfaces and pit morphology because of the large depth of focus that can be attained. Energy Dispersive Spectroscopy (EDS) was used in determining the presence and distribution of elements like iron, copper, magnesium, chlorine, etc. in and around pits.

Scanning electron microscopy was performed on a JEOL JSM-35 scanning electron microscope. EDS was performed with a Tracor-Northern 5500 EDS/Image Analysis System attached to the JSM-35. The TN 5500 system has the ability to quantitatively assess the composition of a selected region of a specimen surface scanned by the JSM-35. The data can be displayed numerically, graphically or pictorially by way of X-ray mapping.

EDS spectrum analysis of a pitted region suggests that variation in the distribution of elements like chlorine and copper can be associated in different parts of a pit (Fig. 46). X-ray mapping of a pit also indicates that pitting is associated with higher than average concentrations of copper.

C. Future Work

1. Study of Local Corrosion Utilizing Microelectrodes and In Situ Observation

The potential field variation in the vicinity of a pit will be measured by using an array of a small number of microelectrodes. This information can then be correlated to pit morphology and corrosion product composition obtained by SEM and EDS analysis. Of particular interest is the phenomenon of copper plating on the walls of crevices and pits which has previously been reported to occur in Al-Li-Cu-Mg alloys (55).

Microelectrodes will also be employed to isolate and identify sites that are susceptible to pitting. Presently, it is known that Fe rich constituents are such sites but experimental observations show that pitting is occurring at other sites as well. Differences in the pitting potentials for these sites might be determined by using microelectrodes to detect the onset of potential variation during an anodic polarization scan. The effects of aging and environment chemistry on pitting potentials might then be determined. Results will be compared to similar tests performed on alloy 2024.

In research performed at the University of Virginia, Piascik has found that pitting of 2090 occurs at potentials more cathodic than the pitting potential. By measuring the variation in the potential near a site likely to initiate a pit with a microelectrode the time and environmental conditions required for pit initiation may be identified. Again, data will be compared to that obtained in similar results performed on Alloy 2024.

a. In Situ Corrosion Observations

Using the Olympus BHMJ optical microscope and a video camera attachment, a video recording of the changes occurring on a working electrode surface during a potentiodynamic polarization scan

will be recorded. Images will be referenced to the applied potential and the measured net corrosion current.

b. pH Microreference Electrodes

The method for constructing microreference pH electrodes derived from literature will be applied. Calibration and testing of the electrodes will be performed. Calibration will include the derivation of calibration curves relating measured potential and solution pH. Basic experiments including the measurement of the variation of pH within actively corroding pits and artificial crevices will be performed. A comparison of data obtained in experiments for Alloy 2090 and conventional high strength aluminum alloys like 2024 and 7075 will be made. A comparison to experimental and theoretical results reported by Holroyd et al. for Al-Li-Cu-Mg will also be possible (49,55,56).

c. Simulated Occluded Environments

Artificial crevices of varying geometry will be machined in 2090 and 2024. pH will then be measured by commercial glass pH electrodes and pH microreference electrodes as a function of time. The effect of varying aging treatment and availability of oxygen to the crevice solution will be examined. Experiments will be performed in which the specimen will be coupled to external cathode and immersed in a large volume of solution. pH versus time behavior and crevice mouth potential versus time behavior will be examined. Scanning electron microscopy and energy dispersive spectroscopy will be used to examine the local corrosion of these specimens.

Shavings experiments will be performed on 2090 and 2024 to determine the effect of the variation of metal surface area to solution volume on the pH versus time behavior of the system. The effect of oxygen availability and aging treatment will also be examined.

SECTION V

Program 3

ENVIRONMENTAL DEGRADATION OF Al-Li ALLOYS: THE EFFECT OF HYDROGEN

Robert E. Swanson
Virginia Polytechnic Institute
and State University

A. Summary

This proposal describes a 24-month study to characterize the effects of hydrogen on the mechanical behavior and microstructure of AA 2090, an Al-Li alloy intended for use as tank material for the cryogenic storage of hydrogen. Microstructural characterizations will include: optical microscopy, scanning electron microscopy (SEM), transmission electron microscopy (TEM), and differential thermal analysis (DTA) or differential scanning calorimetry (DSC). Mechanical property characterizations will include uniaxial tension tests, biaxial loading tests, Charpy impact tests, and microhardness indentation tests.

The goal of the project is to increase the understanding of the role of microstructure and stress state on the susceptibility to hydrogen damage in Al-Li alloys. The coupling of the University of Virginia and the Virginia Tech programs, and the interaction between investigators, will greatly assist in meeting this goal.

B. Introduction and Background

The design and manufacture of the next generation of aerospace structures will require materials of high specific strength and specific stiffness to achieve major weight savings. Fatigue behavior and environmental degradation must also be evaluated to assure durability. Stress corrosion cracking (SCC) of a structural component

made of high-strength aluminum alloys has led to many failures in the aircraft industry. More specifically, the exposure of these alloys to hydrogen from gaseous or aqueous sources is a major concern.

The Al-Cu base alloy, AA 2024, and the Al-Zn-Mg-Cu alloy, AA 7075, are two of the most widely used aluminum alloys in aerospace applications. A modification of the 7xxx-series includes the addition of cobalt to reduce SCC susceptibility. These alloys, AA 7090 and AA 7091, have been used but are rapidly being displaced by Al-Li base alloys, largely due to increases in strength-to-weight and stiffness-to-weight ratios. A fundamental problem with the use of Al-Li base alloys is the propensity for localized corrosion at lithium-rich phases along grain boundaries (79-82). A comprehensive SCC study of 2090 (Al-2.7Cu-2.2Li-0.12Zr) found that overaging reduced SCC resistance, likely due to increased amounts of δ (AlLi) at grain boundaries (82). This is in contrast to 7075 and 7090, where overaging tends to reduce SCC susceptibility compared with the peak age condition (83,84).

Although extensive studies have been conducted on the specific mechanisms of SCC in high-strength alloys such as 7075 (85-94), no such study has been conducted on 2090. Additionally, the effect of hydrogen alone on mechanical property degradation has not been evaluated.

Although the rate of diffusion of hydrogen in aluminum alloys is low (about $10^{-14} \text{ cm}^2 \text{ sec}^{-1}$) (95), the accumulation of hydrogen at second-phase particles and precipitates is generally considered to promote microvoid initiation via the fracture of particles or the weakening of particle-matrix interfaces. Strain field interaction then leads to void growth and coalescence. An understanding of the role of hydrogen in these processes will aid in the establishment of design guidelines for current alloys and will suggest modifications for the design of new, resistant alloys.

Although the formation of an aluminum hydride has been proposed as causing SCC in moist air, its stability is uncertain (96). However,

the formation of lithium hydride must be considered in alloys such as 2090 (97). The formation and stability of lithium hydride must be evaluated.

Since several design uses of 2090 include cryogenic storage of liquid hydrogen in tanks, the effects of hydrogen on the low temperature mechanical behavior of 2090 must be investigated. In addition, biaxial loading studies must be incorporated.

C. Technical Program

This program includes the characterization of 2090 aluminum, and possibly other Al-Li alloys, supplied by either Alcoa or NASA. The Virginia Tech program will include evaluation of the same commercial and model alloys used in the University of Virginia studies. This will assure that the various characterizations can be combined for a comprehensive understanding of the environmental degradation of 2090. In addition this will help minimize duplication of some characterizations.

1. Microstructure

The microstructural characterization of 2090 in the UA, PA, and OA conditions will include optical microscopy and SEM for grain structure and degree of recrystallization. TEM/STEM examinations of thin film as well as bulk specimens will provide general information about dispersoid and precipitate type, size, and distribution; solute depletion; and slip character. Because the electron microscopy could become an extensive investigation itself, the Virginia Tech study will utilize results from the University of Virginia study as well as literature results.

Virginia Tech will perform DTA and/or DSC analysis to follow coarsening and precipitation reactions. In addition, DSC analysis of specimens cathodically charged with hydrogen will provide information on the effect of hydrogen on these reactions, as well as on the possible formation of hydrides.

Microhardness tests of both uncharged and cathodically precharged specimens will provide a simple mechanical property for correlations with the above results. Previous studies with 7075 and 2024 have shown that hydrogen may promote overaging (98).

2. Charpy Impact Tests

Charpy impact tests will be conducted on the instrumented impact tester with a microcomputer data acquisition system. Tests will be conducted from -196°C to 100°C , using uncharged and cathodically charged notched bars of all three tempers. This test system allows for separation of initiation from propagation. Representative CVN energy versus time results are shown in Figure 47 for a high-strength steel. Figure 48 shows that the initiation energy is essentially constant over the range of test temperatures, while the total energy curve tends to follow the propagation energy curve. Such tests will be conducted on 2090 to evaluate the effect of hydrogen charging on initiation and propagation events. Correlations of these results will be made with fractography.

In order to evaluate the effect of orientation on hydrogen embrittlement, two orientations of the PA temper will be evaluated, ST and LT. These samples will be coated with a barrier lacquer to minimize hydrogen pickup except at the notch. Because of the disk-shaped grains, the ST orientation is expected to have lower values of CVN energy than the LT orientation. It is not known which orientation is more affected by internal hydrogen.

Some Charpy bars of the PA temper will be machined to give a range of notch root radius. The PA temper is selected because of the low fracture toughness of the OA temper. Some bars will be fatigue precracked, using the machine purchased in the first year of the work. These bars, having a range of root radius, from a crack to the standard value of 0.25 mm, will be tested at two strain rates.

Some specimens will be tested in slow 3-point bending, while others will be tested with the standard Charpy impact method. Apparent fracture

toughness and CVN values will be plotted against notch root radius as well as against the square root of notch root radius. These tests will permit us to determine if a stress singularity exists for the V-notch at two strain rates.

3. Stress State Effects

Because balanced biaxial loading more closely simulates the stress state for the storage of pressurized hydrogen than does uniaxial tensile testing, it is essential that this study include biaxial loading of 2090 in a clamped disk test fixture. The ideal test would be done at cryogenic temperatures with liquid hydrogen as the loading fluid.

Stress state studies on the SCC and hydrogen degradation of 7075 and 7090 have shown that Mode III (torsion) loading produced less embrittlement than Mode I (tension) loading. The degree of embrittlement decreased with aging for both alloys, being lowest for the overaged condition (85,99). These results demonstrate the need for correlation between the stress state in laboratory tests and actual design practice.

A disk rupture system for biaxial loading was designed at Virginia Tech (100). A schematic diagram of the system is shown in Figure 49. The working part of the system consists of a thick walled stainless steel plenum in which disks from 8.9 to 10 cm in diameter are clamped against an annulus. Pressurized gas is applied to one side of the disk, forcing it to bulge through the hole in the annulus. A convenient feature of the system is that it allows direct exposure to hydrogen (or any other gas) without the need for dynamic seals or elaborate test chambers.

Because the oxide film on aluminum alloys acts as a diffusion barrier, it may be necessary to cathodically charge the disks prior to loading. If this is the case, nitrogen will be used as the loading fluid for both charged and uncharged disks. These tests will be conducted at room temperature.

In order to facilitate hydrogen uptake, some disks will be abraded immediately prior to pressurizing with hydrogen. The abraded surface will not only remove the oxide layer, but will also tend to catalyze hydrogen uptake.

Some disks will be intentionally pitted prior to pressurizing. We will also attempt to preferentially pit grain boundary regions for comparison with pits within grains. This will allow us to evaluate the effect of grain boundary chemistry on the hydrogen embrittlement effect.

Disk rupture tests typically have failures which can be classified as bursts (ductile rupture) or leaks (brittle, early failure). In addition dome height position can be measured, via linear variable displacement transducers, as a function of gas pressure. This provides a means to evaluate deformation during the test.

Another method for evaluating disk rupture tests is the acoustic emission technique. A recent study using 1015 steel showed that cumulative acoustic emission counts, plotted as a function of gas pressure, gave significantly different results for testing in hydrogen compared with testing in nitrogen. Figure 50 shows the results, with a proposed mechanism to describe the difference. Alloy 2090 can be expected to provide different results. However, the disk rupture system, coupled with the acoustic emission technique, will help in assessing the effect of gaseous and/or cathodic hydrogen on the mechanical behavior of 2090, in the three tempers, in biaxial loading.

4. Material Needs

The material needs for this study are shown in the table below. The extensive Charpy impact testing will require the most material, due to the need for replicate testing for most conditions. The stress state study will use sheet material. ALCOA has already offered to supply 2090 and 2091 sheet material.

Table 3: Material Needs

<u>Test</u>	<u>Material</u>
Charpy Impact	1.3 cm plate, 25 cm by 250 cm
Stress State	0.6 mm sheet, 30 cm by 250 cm
Residual Stress	6.5 mm plate, 25 cm by 250 cm

D. Statement of Work

As part of a 24-month study, we will focus on microstructural aspects of hydrogen degradation in Al-Li alloys. This work will complement that done at the University of Virginia.

E. Key Personnel

The key personnel for the proposed research are Robert E. Swanson (Assistant Professor) and Robert W. Hendricks (Professor). Swanson is noted for his contributions in the area of stress state effects in metallic alloys and has considerable experience in the characterization and testing of rapidly solidified alloys, including atomized aluminum alloys such as 7090, twin-piston splat quenched magnesium alloys, and melt-spun aluminum-iron alloys. He is an expert in the fields of corrosion and fracture mechanics and has considerable experience in electron microscopy.

Mr. Swanson's resume is presented in Appendix II.

F. Equipment and Facilities

Virginia Polytechnic Institute and State University

1. Introduction

Located in the scenic mountains of southwestern Virginia, Virginia Tech is one of the nation's major institutions of higher learning. Sharing the distinctive character of both a land-grant and sea-grant university, Tech provides broad academic offerings, large

scale public service, and a wide spectrum of basic and applied research. With nearly 23,000 undergraduate and graduate students and a faculty of some 2,000, Tech is the largest university in the Commonwealth of Virginia.

Tech's fiscal 1986-87 research expenditures totaled \$75 million and are soon expected to reach the \$100 million mark. In total research expenditures, Tech ranks 49th, according to a recent National Science Foundation (NSF) Survey of 91 universities that spend more than \$30 million annually in support of research activities. And Tech continues to be within the top ten percent of universities in terms of research expenditures derived from industrial sources. A strong funding support base for research is shown by the fact that no one sponsor provides more than fifteen percent of the university's total sponsored research expenditures.

In addition to a strong research focus on engineering and agribusiness at Tech, university scientists are investigating a host of areas as diverse as cancer, geothermal energy, bacterial production of methane, robotics, social problems, power electronics, composites, absenteeism in business, air pollution, and quasars.

Virginia Tech has established a mutually beneficial relationship with business and industry in recognition of the need to engage in research dealing with the problems and opportunities of the private sector.

The close relationship between graduate programs and research ensures that problems, solutions, and techniques associated with specific research projects become a part of classroom curricula. Tech's broad and comprehensive research program provides excellent opportunities for graduate students to become involved in important research projects.

2. Academic Colleges

The University consists of eight academic colleges with over 70 separate departments.

College of Agriculture and Life Sciences
The College of Architecture and Urban Studies
College of Arts and Sciences
College of Business
College of Education
College of Engineering
College of Human Resources
Virginia-Maryland Regional College of Veterinary Medicine

College of Engineering. During the 1980s, Virginia Tech's College of Engineering has emerged as one of the nation's premier research institutions. In 1971, the College reported slightly less than \$1 million of funded research whereas, by 1987, the amount exceeded \$18 million. As a result, it now ranks in the top ten percent of the 220 accredited engineering colleges reporting their research expenditures to the American Society for Engineering Education.

At the same time, the College has maintained its reputation for offering an excellent education for the student who desires to obtain a baccalaureate degree. Today's entering freshman class has an average SAT score of 1200 out of a possible 1600. By graduating more than 1,000 students each year, the college consistently ranks in the top ten in the number of baccalaureate degrees granted.

The engineering graduate enrollment has climbed from 277 master's and doctoral students in 1970 to 1100 in the 1986-87 academic year. Graduate programs are offered in the following areas: aerospace, agricultural, biomedical, chemical, civil, electrical, engineering mechanics, environmental, industrial engineering and operations research, materials, mechanical, mining, and systems engineering.

It is the reputation of the faculty and their successes in securing contract research dollars that has allowed this phenomenal growth in the number of graduate students. During the past two decades, the College has attracted some truly exceptional individuals to the Blacksburg campus. Five of the six Virginian academics granted membership in the

prestigious National Academy of Engineering are on the Virginia Tech faculty. In less than a decade, the College has secured 24 named professorships, and it plans to establish 10 more in the near future. These endowed chairs are a means of recognizing eminent faculty for their effective teaching and extraordinary scholarship.

3. Academic Support Facilities

Indicative of Tech's commitment to research and undergraduate and graduate programs is the university library containing more than 1.7 million volumes and the the second largest microform collection in the world. The library is a member of the Association of Research Libraries and the Southeastern University Library Network. The University Library consists of The Carol M. Newman Library and four branches (or special Libraries): Architecture; Geology; Veterinary Medicine; and the Northern Virginia Center. All libraries use The Virginia Tech Library System (VTLS), an on-line system controlling circulation and the library catalog. This computerized program for accessing materials is widely acclaimed and has been purchased by numerous libraries across the country and abroad.

The implementation of sophisticated communication facilities has made the university a nationally recognized leader in communication technology, and has placed Tech in the forefront of high-tech communications management. A vast spider web of communication lines spans out across the nearly 3,000-acre campus, linking some 3,000 terminal and a significant number of the 8,000 personal computers to the computing center's mainframe. The university has installed more miles of cable and has more work stations, personal computers, and buildings served by its communications system than any other institution of higher learning in the country. The system will be further enhanced as a result of a recent \$7.6M contract with IBM for a new telecommunications system for the Blacksburg campus and the Graduate Center in Falls Church. The new system will integrate telephone and data communications by using the same switching equipment and cable distribution rather than two separate systems. This facility will add more than 5,000 data connections to the 6,000 already on campus.

The Computing Center at the University is built around an IBM 3084 system, an IBM 3090 and three VAX 11/780 systems. The IBM 3084 system operates under the control of VM and VMS and has 64 megabytes of memory. The IBM 390 and the Vector Facility operates under the control of VM and has the Vector Facility to support supercomputing. Two VAX 11/780 systems provide interactive computing under VMS. The IBM machine is used to support instructional, research, extension, and administrative activities. The VAX 11/780 systems are used primarily for interactive undergraduate instruction. A third VAX 11/780 and an IBM 4341 system are dedicated to CAD/CAM usage.

The computer facilities are available 24 hours a day (160 hours per week). The services provided by the Center include time-sharing, batch processing, remote printing, and personal computer facilities. For online and timesharing access, the system supports a variety of terminals (over 1,500) operating under different communication protocols and line speeds. There are a number of terminal laboratories and personal computer facilities housing over 300 units for student use. Remote printing stations are serviced from both on-campus and off-campus locations. The Computing Center is equipped with an array of printing devices, disk storage units, tape drives, and high quality plotters. The systems have more than 70-billion bytes of on-line storage.

The computing systems support a rather extensive array of compilers and interpreters, as well as statistical, mathematical, simulation, graphics, timesharing and other special purpose packages. In addition, the systems have data base management and text processing packages that are available for faculty, staff, and student use. High quality print devices are available for camera-ready copies of textual materials. An interface with the print shop provides for typesetting of computer-generated textual material.

Tech is developing a Corporate Research Center that is designed to attract corporate research and development operations. It is located adjacent to the main campus and the Virginia Tech airport which is

capable of handling corporate aircraft. Satellite antennas will enable communications (both up and down links) with fifteen to twenty satellites, thus providing two-way communications to virtually any place in the world.

4. Academic Departments and Programs

The College comprises ten degree-awarding departments and the Division of Engineering Fundamentals, which provides instruction to all engineering freshmen. Several programs of interdisciplinary study are also available at the graduate level.

Aerospace and Ocean Engineering Department
Agricultural Engineering Department
Chemical Engineering Department
Civil Engineering Department
Electrical Engineering Department
Engineering Science and Mechanics Department
Industrial Engineering and Operations Research Department
Materials Engineering Department
Mechanical Engineering Department
Mining and Minerals Engineering Department
Environmental Sciences and Engineering Group
Materials Engineering Science Group
Systems Engineering Group

Engineering Science and Mechanics Department. The department has 44 faculty, 132 undergraduates, and 163 graduate students. It offers a broad, fundamental curriculum in the physical sciences and applied mathematics and in their application to engineering. The program is interesting and challenging. A total of 22 credit hours of free electives, 12 credit hours of departmental electives and 6 credit hours of Project and Report give the student freedom to develop individually tailored programs of concentrated study. Undergraduate courses in engineering science and mechanics are taught on a service basis for all engineering curricula. A minor in mechanics is available for non-ESM students. The department also offers graduate programs leading to

M.Eng., M.S. (thesis and non-thesis options), and Ph.D. degrees. The Cooperative Education Program is available to qualified candidates at undergraduate and graduate levels. An honors program in engineering science and mechanics has been approved and is available for qualified students, successful completion of which is indicated on the diploma by the designation "in honors." Current research interests include stability of laminar flow control, laminar flow separation, finite-elements analyses, reliability and probability studies, nonlinear vibrations, nonlinear dynamics, nondestructive evaluation and testing, optical mechanics, composite materials and structures, adhesion science, acoustic emissions, stability and control of flexible spacecraft, spacecraft attitude determination, supersonic wind-generated waves, acoustic waves in ducts, fracture mechanics, stress intensity factors, boundary-layer separation, hydrodynamic stability, wave propagation, photoviscoelasticity, perturbation methods, weld defects, ductile fracture of polymers.

Materials Engineering Department. The department has 11 faculty, 101 undergraduates, and 30 graduate students. The undergraduate curriculum provides for specialized course work in the areas of phase equilibria, X-ray diffraction and spectroscopy, mechanical testing, optical microscopy, mathematical modeling of processes, atomic diffusion, hydrogen embrittlement effects, environmental degradation of materials, extractive metallurgy, and investigation of the electrical, optical, and thermal properties of metallic, ceramic, polymeric, and composite materials. Programs are available for graduate work leading to the M.S. degree. Students desiring the Ph.D. may participate in the materials engineering science degree program. The department participates in the Cooperative Education Program in which qualified students may alternate quarters of study with quarters of professional employment. Graduate study and research are concerned with ceramic, metallurgical, and polymeric systems including electrical and magnetic materials, powder processes, glasses, refractories, thin-films, high-temperature behavior, stress corrosion, quantitative microscopy, and extractive processes.

Materials Engineering Science Group. Research and graduate studies concerned with synthesis, characterization, understanding, and improvement of materials and materials response are coordinated through this group. Students from the physical sciences as well as engineering may pursue research and study in metals, ceramics, composites, and polymers. Research areas include mechanical behavior, physical chemistry of surfaces, X-ray analysis, corrosion, luminescence, adhesion science, and composites. The group administers a Ph.D. program in materials engineering science.

5. Major Research Groups

In a document of this size, it is impossible to summarize the many quality research programs conducted by individual faculty. However, the breadth of activity may be imparted by listing the various research groups, laboratories, and centers. Some groups include faculty drawn from more than one college.

- Center for Adhesion Science
- Center for Composite Materials and Structures
- Coal and Minerals Technology Group
- Composite Mechanics Group
- Construction Center
- The Energy Research Group
- Environmental Engineering Group
- Failure Analysis and Prevention Laboratory
- Fiber and Electro-Optics Research Center
- Generic Mineral Technology Center
- Geotechnical Engineering Project Center
- Human Factors Engineering Center
- Management Systems Laboratories
- Manufacturing, Automation and Robotics Center
- Materials Response Group
- Mining and Minerals Resources Research Institute
- Photoelastic and Fracture Laboratory

Polymer Materials and Interfaces Laboratory
Powell River Project
Satellite Communications Group
Turbomachinery and Propulsion Research Center
Virginia Power Electronics Center
Virginia Productivity Center
Relevant Non-College Centers
The University Center for Environmental Studies
Center for Coal and Energy Research
Virginia Water Resources Research Center

6. Academic Facilities

The main academic units of the College are housed in Norris, Patton, Randolph, and Whittemore Halls. Additional research facilities are located in nearby off-campus buildings within easy reach for faculty and graduate students. These units include the satellite station, fiber optics draw tower, geotechnical research building, and coal-cleaning laboratory. A more detailed description of the facilities is presented below.

Aerospace and Ocean Engineering facilities include a subsonic stability wind tunnel with a 6-foot by 6-foot test section, a 9-inch by 9-inch supersonic wind tunnel for Mach numbers 2 through 4, a towing tank, a cavitation testing, a structures laboratory, and analog, digital, and hybrid computers. Facilities for Agricultural Engineering include separate laboratories for research in soil and water conservation, water quality, forest engineering, soil-tillage tool interaction, precision seeding, conservation tillage and planting, energy herbaceous biomass, physical properties, electronics, and instrumentation. Recent equipment acquisitions include sophisticated signal analyzer equipment for data acquisition, an instrumented soil bin, a plant growth chamber, on-site fan-testing equipment, a field rainfall simulator, an auto analyzer, a particle size analyzer, an infiltrometer, a neutron probe, a conservation tillage seed planter, a

universal testing machine, a laboratory data acquisition unit, a concentric cylinder viscometer, and a wide range of equipment for watershed and water quality monitoring. Students have access to a departmental microcomputer laboratory and a micro-VAX II computer, in addition to the campus mainframe computer system. Chemical Engineering has laboratories in polymer characterization and polymer processing, catalysts, fluid particle systems, novel separation techniques, SPATE thermoelastic stress analysis system, environmental engineering, and biotechnology; equipment includes an FT-IR, GC mass spectrometer, an excimer laser, scanning electron microscopes, an X-ray diffraction unit, E beam, and other analytical tools. Civil Engineering laboratories for research in hydraulics, structural testing, soil mechanics and environmental sanitary engineering. Environmental Sciences and Engineering facilities include controlled-temperature rooms; instruments for the analysis of organic and halogenated compounds, heavy metals, and particle size; light incubators; a boat with motor; and other analytical equipment typically found in biological/chemical laboratories. Electrical Engineering facilities include a satellite-tracking station and laboratories for image processing, acoustooptics, fiber optics, computer aided design, hybrid microelectronics, power electronics, computer engineering, alternative energy, electronic materials, and power systems. The facilities in Engineering Science and Mechanics consist of an MTS axial-torsional loading system, modern materials testing equipment, a nondestructive evaluation lab, several composite materials labs, thermographic video cameras, a fluid-mechanics lab with a towing basin and carriage, a nonlinear vibrations lab, a biofluids lab, a fracture mechanics lab, minicomputers, and modern high-speed data-acquisition system. Industrial Engineering and Operations Research facilities include metal-casting, machining, CNC, automation, and robotics labs; telephotometric, microdensitometric, and microphotometric units; an auto simulator; an aircraft simulator; an ergonomics lab; PDP-11/10, PDP-11/55, and VAX-11/750 computers; and environmental and acoustical chambers. Research equipment and precision instrumentation

for mechanical engineering include hot-film and laser-doppler anemometer systems, calorimeter room, anechoic fatigue-testing machines, surface profile measuring equipment, gas chromatography equipment, a BAX-11/780 and a network of microvaxes for engineering design, and an IBM 4341 system for CAD/CAM. Materials Science facilities include lasers, hydrogen effects, electron microscopes, a hot-stage optical microscope, analog computers, a multitarget research sputtering system, and equipment for X-ray diffraction, electron beam microprobes, differential thermometric and gravimetric analysis, vacuum deposition, electrical properties measurement, and computer modeling. Mining and Mineral Engineering facilities include laboratories for rock mechanics, beneficiation, comminution,, sizing analyses, environmental control, mining systems, equipment evaluation, systems analysis, and health and safety. Mini and micro computers are located in departmental laboratories.

7. Materials Engineering Department

The Virginia Tech Materials Engineering Department laboratories and offices are housed in Holden Hall. The materials laboratory facilities of the department are outlined below.

Ceramic Processing Laboratory. A completely equipped laboratory is available for preparation, testing, and characterization of ceramics. Preparation facilities include: ball mills, hydraulic presses, hot press, and over 40 kilns of various designs. Testing and characterization facilities, all equipped with furnaces for high temperature and controlled atmospheres, include: creep machine, tensile testing machine, electrical conductivity apparatus, dielectric properties apparatus, dilatometer, differential thermal analyzer, and thermogravimetric apparatus. Equipment for the preparation of ceramic specimen and for examination by transmitted and reflected light microscopy, X-ray analysis, and electron beam microprobe analysis is also available on campus.

Environmental Degradation Lab. This facility includes potentiostats, automatic recording equipment, light microscope with

environmental test cell, biaxially-loaded disk rupture system, and other equipment for studying the various forms and effects of corrosion, liquid metal, and hydrogen in the behavior of materials. Newest addition is an EG&G model 332 corrosion measurement system with microcomputer control.

Electron Microscopy and Surface Characterization. Complete facilities are available for preparing and studying metallic, ceramic, and polymeric specimens. Facilities include a scanning transmission electron microscope (Philips 420), a scanning electron microscope, and an electron spectrometer for chemical analysis (KRATOS). Preparation facilities include electropolishing apparatus for metals, an ultra microtome with diamond knife for polymers, and will soon include an ion beam thinning apparatus for metals and ceramics. A separate complete electron metallography darkroom is also available.

Heat Treating. Various types of heat treating equipment are available, including muffle and recirculating air furnaces, a controlled atmosphere furnace, constant temperature oil baths, and a vacuum and inert atmosphere furnace with refractory metal and graphite heating elements.

Mechanical Testing. Testing laboratories are complete with hardness, tensile, fatigue, torsion, impact, and creep apparatus. Newest addition is an MTS model 810 mechanical test system with minicomputer.

Melting Facilities. Furnaces for melting alloys include an induction furnace with a 17-pound steel capacity and several small electrical resistance melting units.

Metalworking. Equipment is available for warm and cold rolling.

Light Microscopy. Complete facilities are available for the preparation and observation of metallic, ceramic, and polymeric materials. Preparation facilities include mounting and impregnation apparatus, grinding and polishing machines, electropolishing and etching devices, microtomes, and thin section machines. Observation facilities

include numerous microscopes and materialographs for examination and photography of specimens in black and white and in color by transmitted and reflected light, in bright field, dark field, and polarized light illumination and under differential and Normarsky interference contrast conditions, and for microhardness determinations.

Facilities for Atomic Arrangements in Near Surface Zone. Includes three X-ray systems especially designed for studies of diffusion-controlled reactions. Incorporates computer-controlled automation. A color graphics terminal is available for simulation studies. Three high-vacuum furnaces are used for ultra-clean specimen annealing. Thin films are prepared using a cryo-pumped Perkin-Elmer multitarget sputtering system. An RF power supply allows deposition of both ceramic and metallic films. In addition, access is available to two beamlines at the National Synchrotron Light Source (Brookhaven, NY) for very high intensity and selectable wavelengths for refined measurements.

Computers. Access is available to IBM 4341, IBM 3081, and DED VAX-11/780 time-sharing computers in addition to the University IBM 370 system. Various mini- and microcomputers are also available within the department for experimental control as well as computational needs.

High-Temperature Materials Laboratory. The equipment in this laboratory permits characterization of the mechanical, thermo-mechanical, and thermo-physical properties of structural materials for engineering application involving elevated and extreme temperatures. A closed-loop electro-hydraulic mechanical tester with environmental chamber permits evaluation of mechanical behavior such as creep, stress-strain behavior, strain-rate sensitivity, and fracture-mechanical response to temperatures as high as 2000oC. An electronically controlled thermo-mechanical tester allows measurement of thermal stress resistance and thermal fatigue under a variety of heat transfer conditions. A differential scanning calorimeter is used for measurement of specific heat and other thermo-physical property data. The thermal diffusivity of structural as well as other materials can be measured by the laser-flash diffusivity apparatus to temperatures in excess of

2000°C. Specimen preparation for the above measurements can be carried out with diamond tooling including diamond saw, core drills and polishing apparatus.

Applied Solid State Science Lab. Includes two vacuum evaporators and an RF sputtering system. Various equipment is also available for measurements related to thin films and junctions.

Environmental Degradation of Al-Li Alloys

Prepared for:
National Aeronautics and
Space Administration
Langley Research Center
Hampton, VA 23665

Attention: Mr. J.F. Royal, Jr.
Grants Officer, MS 126

For Consideration by: Mr. W. Barry Lisagor
M/S 188A
Metallic Materials Branch

Submitted by: Robert E. Swanson
Assistant Professor

Materials Engineering Department
Virginia Polytechnic Institute and State University
Blacksburg, VA 24061

VIRGINIA TECH

Office of
Sponsored Programs

301 Burruss Hall
Blacksburg, Virginia 24061
(703) 961-5281

February 29, 1988

Dr. Richard P. Gangloff
Department of Materials Science
University of Virginia
Charlottesville, Virginia 22901

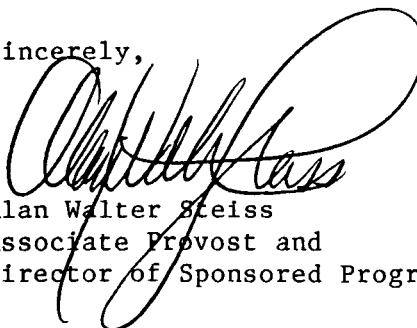
Dear Dr. Gangloff:

Enclosed are three (3) copies of a revised research proposal entitled "Environmental Degradation of Al-Li Alloys." This revision was prepared by Dr. R. E. Swanson of our Department of Materials Engineering and is to be included in your proposal to NASA Langley Research Center.

We appreciate the opportunity to submit this proposal to you. If questions of a fiscal or budgetary nature arise, please contact Mr. William Harris (703-961-5283). Questions of a technical nature should be addressed to Dr. Swanson or to me.

All correspondence related to this proposal should reference Proposal No. 88-0883-01.

Sincerely,



Alan Walter Steiss
Associate Provost and
Director of Sponsored Programs

AWS:pmh
Enclosures

cc: Dr. R. E. Swanson
Dr. C. W. Spencer
Mr. J. E. Osborne
Mr. W. G. Harris

SECTION VI

Program 4

NEW INITIATIVE ON ENVIRONMENTAL FRACTURE OF ADVANCED LIGHT METALS

William C. Porr, Jr. and Richard P. Gangloff

We propose to extend the scope of the original proposal (20) to include a fourth research program chosen from one of several topics which are critical to the damage tolerant application of advanced light metals in aggressive aerospace environments. Mr. William C. Porr, a PhD candidate who recently received his MS degree under M.R. Louthan at VPI, is currently enrolled in the Materials Science Department at UVa and is most interested in conducting research and graduate studies in this area.

Mr. Porr will formulate his research program, centered on a topic selected from one of the those described in an ensuing section. Selection will be based on the findings of the three parallel programs described previously and in consultation with metals and fracture mechanics researchers at the Langley Research Center. The product of this effort in year 2 will be a detailed literature review, the identification of fundamental questions and an approach, and initial experimentation. During year 3, the student will execute the planned research. We envision that year 2 funding will be limited to Mr. Porr's salary and modest experimental and support costs.

Research will examine one of the following areas:

- ✕ Elevated temperature crack growth in advanced PM aluminum alloys.
- ✕ Cryogenic crack growth in advanced PM aluminum alloys.

- ✕ Environmental fracture of aluminum alloy matrix-ceramic fiber composites.
- ✕ Fracture mechanics of surface flaw growth in thin sheet, advanced aerospace alloys.
- ✕ Hydrogen embrittlement of advanced light metals in high activity environments.

A brief proposal is provided for the first of these topics to illustrate the typical thrust of the new research program. A key element of each program is the emphasis on integrating advanced materials and fracture mechanics disciplines. It is envisioned that interactions with the Metallic Materials and Fatigue/Fracture Branches at NASA will greatly assist in this regard.

A. Elevated Temperature Crack Growth in Advanced PM Aluminum Alloys

1. Introduction

Advanced aluminum alloys are being produced by powder metallurgy processes, particularly involving rapid solidification and mechanical alloying, for aerospace and energy applications at here-to-fore unobtainable elevated temperatures (101-106). While excellent strengths have been developed, such materials are limited by low fracture resistance.

Aluminum-iron ternary and quaternary alloys containing either Ce, Ce+W, Ni, Mo, Mo+V, Mo+Cr or Si+V have been processed to develop acceptable 23°C tensile ductilities and long term elevated temperature strength at temperatures up to 325°C (107-113). Two problems are significant. These PM alloys exhibit reduced ductilities over the temperature range from about 125 to 275°C. (Tensile ductility increases monotonically with increasing temperature for wrought aluminum alloys (114)). Secondly, elevated temperature fracture resistance has been characterized by smooth specimen uniaxial tensile ductilities, with fracture mechanics measurements limited to ambient temperature, moist air environments. It is crucial to begin to consider the fracture

C-2

mechanics of the failure processes which are likely to control the durability of reusable tanks fabricated from the alloys.

The mechanisms for elevated temperature fracture of PM aluminum alloys are unclear. A variety of processes may contribute including processing factors (large defects, prior particle boundary oxides and hydroxides, dissolved hydrogen), environmental factors (external hydrogen or oxygen uptake), metallurgical factors (interface impurities, plastic strain localization) and mechanical factors (time dependent plasticity, dynamic environmental interactions).

2. Objective

The objective of the proposed research is to determine mechanisms for elevated temperature fracture to enable the development and damage tolerant application of advanced PM aluminum alloys.

The approach involves three short term goals: (1) To develop fracture mechanics measurement and analysis methods, (2) To characterize elevated temperature tensile fracture and subcritical crack growth, and (3) To develop micromechanical models of brittle cracking.

B. Technical Program

Research will emphasize powder metallurgy Al-Fe-X alloys, developed within the Light Metals Center at the University of Virginia and by collaborating companies, and model materials suggested by hypothesized mechanisms. Work will investigate elevated temperature tensile fracture during short term loading and subcritical crack propagation due to time dependent, creep-environment interactions.

1. Tensile Fracture

a. Background

Characterization of the fracture resistance of powder metallurgy alloys requires separate analyses of the extrinsic effect of large process defects (~ 5 to $10 \mu\text{m}$) and of the intrinsic fracture resistance of the microstructure. Smooth specimen tensile ductility

reflects the complex interaction of these factors. Such values exhibit scatter that obscures structure-properties relations; which, in turn, vary with specimen size/geometry and which are not applicable to design (115).

Fracture mechanics methods characterize the intrinsic toughness of the crack tip plastic zone for the initiation case, and of the two dimensional crack path and wake for propagation. This approach is well suited for studies of metallurgical and environmental effects, without the complication of varying defect populations. Data and models on defect tolerance may be combined with statistical information on defect distributions to predict smooth specimen or component life [116]. Plane strain fracture toughness measurements have been employed to study the room temperature fracture toughness of several Al-Fe-X alloys, for example (109). For aerospace applications, initiation toughness (K_{IC} or J_{IC}) should be supplemented by resistance curve concepts. Temperature effects on crack growth resistance have not been investigated.

b. Proposed Research

Suresh et al. recently demonstrated a combined initiation and propagation approach which employed J integral methods to characterize aging effects on the fracture resistance of Al-Li-Cu alloy plate (117). Such a resistance methodology will be developed for through-cracks and perhaps surface cracks in thin sheet (118). The intrinsic fracture toughness and tearing modulus of a selected microstructure will be established by monitoring the initiation and growth of an existing crack for rapid loading in moist air (119).

The effect of temperature (23 to 350/400°C) on fracture resistance will be measured and fracture surfaces will be characterized by electron metallography to survey operating cracking processes. Toughnesses will be compared to short bar results to further develop a method for fracture mechanics properties screening relevant to alloy and process development (120).

Presuming that fracture resistance declines over an intermediate temperature range, one or more experiments will be conducted to probe the mechanism. The effect of temperature on deformation and porosity/microcrack nucleation will be studied by interrupted and sectioned tensile specimens, coupled with analytical methods to measure gaseous hydrogen production (121). If implicated in the embrittlement, prior particle interface phases will be altered by processing or alloy composition changes. Heat treatment experiments, high purity or doped alloys and in situ Auger fracture experiments will be used if interfacial impurity effects are indicated. External environment effects will be investigated by elevated temperature fracture experiments in purified helium, oxygen and water vapor. Specimens will be preexposed to an electrochemical source of dissolved hydrogen, and to oxygen and water vapor at elevated temperatures and fractured (121,122).

The proposed study of tensile fracture could be readily expanded to investigate the effect of temperature from the cryogenic regime to the elevated levels described here for a single alloy.

2. Subcritical Creep Crack Propagation

a. Background

The chemical mechanisms for elevated temperature embrittlement are likely to be exacerbated by prolonged loading causing time dependent plasticity, environmental chemical reactions and bulk diffusion. Creep deformation may be sufficient to produce cracking in alloys which exhibit good time-independent tensile ductility. It is therefore important to examine subcritical "creep" crack propagation in PM aluminum alloys.

Creep crack growth has been observed in several commercial aluminum alloys (123-125), and more recently in experiments at UVa with complex alloy 2090. The contributions of crack tip creep deformation, environment, grain boundary weakness and microstructural instability have not been determined. Research on iron and nickel based alloys

indicates a dominant effect of oxidizing environments, for example (122,126). Fracture mechanics field parameters for elevated temperature, time dependent crack propagation have matured significantly over the past 10 years (127-129), however, these methods have not been applied to develop structurally reliable advanced aluminum alloys.

b. Proposed Research

Research will emphasize external environment and interfacial impurity effects on elevated temperature crack growth in PM aluminum alloys, and will build on the findings of the study of tensile fracture resistance.

Initial experiments will characterize crack propagation kinetics for constant or programmed slow loading in moist air, and in terms of small scale yielding (stress intensity, K) and steady state extensive creep (C^*) or transition (C_T) crack tip field parameters. Such parameters uniquely define the sizes of crack tip process zones and the stress, strain and strain rate distributions which govern crack propagation. K , C_T and C^* have been successfully employed in micromechanical modeling of crack growth and are applicable to time dependent damage tolerant design (128,129).

External environment and dissolved impurity effects will be separated by crack growth experiments conducted in purified helium, oxygen and water vapor environments. If fracture is enhanced by O_2 , then the dependence of the crack growth kinetics on partial pressure and temperature will be determined. Environmental crack growth response to rapid load and oxidizing gas pressure transients will be measured. If fracture occurs in the inert environment, then insitu Auger experiments will be conducted to identify the role of segregated solutes. Gas discharge and doping experiments, and the analyses described previously will be employed to examine the role of hydrogen. The aim of experimentation is to develop a micromechanical model of environmental embrittlement.

C. Closure

A research project is proposed with the goal of enabling the fracture resistant use of advanced powder metallurgy aluminum alloys in elevated temperature environments, through a foundation of fundamental understanding. Limited observations and the heterogeneity of PM products dictate that fracture mechanics measurements and analyses be employed to develop a physical basis for micromechanical modeling. Short term goals are proposed for problems of tensile fracture and subcritical creep crack propagation. The program requires a close collaboration with the developers of advanced PM alloys and researchers involved with advanced micromechanics and fracture mechanics studies.

SECTION VII

REFERENCES

1. W.E. Quist, G.H. Narayanan, and A.L. Wingert, "Aluminum- Lithium Alloys for Aircraft Structure-An Overview," pp. 313-334 in Ref. 4.
2. Aluminum Alloys - Physical and Mechanical Properties, Vols. I and II, E.A. Starke, Jr. and T.H. Sanders, Jr., eds., EMAS Ltd., Warley, West Midlands, UK (1986).
3. Aluminum-Lithium Alloys III, C. Baker, P.J. Gregson, S.J. Harris and C.J. Peel, eds., Institute of Metals, Oxford, UK, in press (1986).
4. Aluminum-Lithium Alloys II, T.H. Sanders, Jr. and E.A. Starke, Jr., eds., TMS-AIME, Warrendale, PA (1984).
5. Aluminum-Lithium Alloys, T.H. Sanders, Jr. and E.A. Starke, Jr., eds., TMS-AIME, Warrendale, PA (1981).
6. P.J. Gregson and H.M. Flower, "Microstructural Control of Toughness in Aluminum-Lithium Alloys," Acta Metall., Vol. 33. pp. 327-537 (1985).
7. A.K. Vasudevan, E.A. Ludwiczak, S.F. Baumann, R.D. Doherty and M.M. Kersker, "Fracture Behavior in Al-Li Alloys: Role of Grain Boundary δ ," Matls. Sci. and Engr., Vol. 72, pp. L25-L30 (1985).
8. T.H. Sanders, Jr., and E.A. Starke, Jr., "The Effect of Slip Distribution on the Monotonic and Cyclic Ductility of Al-Li Binary Alloys," Acta Metall., Vol. 30, pp. 927-939 (1982).
9. A.K. Vasudevan, A.C. Miller and M.M. Kersker, "Contribution of Na Segregation to Fracture Behavior of Al-11.4 At% Li Alloys," pp. 181-200 in Ref 4.
10. W. Yu and R.O. Ritchie, "Fatigue Crack Propagation in 2090 Aluminum-Lithium Alloy: Effect of Compression Overload Cycles," submitted to J. Engr. Matls. Tech., Trans. ASME, Ser. H. (1987).
11. N.J.H. Holroyd, A. Gray, G.M. Scamans and R. Hermann, "Environment Sensitive Fracture of Al-Li-Cu-Mg Alloys," pp. 310- 320 in Ref. 3.
12. E.I. Meletis, J.M. Sater and T.H. Sanders, Jr., "Environment Assisted Cracking in Al-Li Alloys," pp. 1157-1176 in Ref. 2.

13. E.L. Colvin, G.L. Cahen, Jr., G.E. Stoner and E.A. Starke, "Effect of Germanium Additions on the Corrosion Behavior of an Al-Li Alloy," Corrosion, Vol. 42, pp. 416-421 (1986).
14. D.O. Sprowls, "A Study of Environmental Characterization of Conventional and Advanced Aluminum Alloys for Selection and Design," NASA Contractor Report 172387, NASA-Langley Research Center (1984).
15. P.E. Bretz and R.R. Sawtell, "Alithalite Alloys: Progress, Products and Properties," pp. 47-56 in Ref. 3.
16. J. Glazer, S.L. Verzasconi, E.N.C. Dalder, W. Yu, R.A. Emigh, R.O. Ritchie and J.W. Morris, Jr., "Cryogenic Mechanical Properties of Al-Cu-Li-Zr Alloy 2090," in Advances in Cryogenic Engineering, ICMC 85, Vol. 32, in press (1985).
17. K.V. Jata and E.A. Starke, Jr., "Fatigue Crack Growth and Fracture Toughness Behavior of an Al-Li-Cu Alloy," Metall. Trans. A, Vol. 17A, pp. 1011-1026 (1986).
18. R.J. Bucci, "Selecting Aluminum Alloys to Resist Failure by Fracture Mechanisms," Engr. Frac. Mech., Vol. 12, pp. 407-441 (1979).
19. J. Glazer, S.L. Verzasconi, R.R. Sawtell and J.W. Morris, Jr., "Mechanical Behavior of Aluminum-Lithium Alloys at Cryogenic Temperatures," Metall. Trans. A, Vol. 18A, pp. 1695-1703 (1987).
20. R.P. Gangloff, G.E. Stoner and M.R. Louthan, Jr., "Environment Assisted Degradation Mechanisms in Aluminum-Lithium Alloys," NASA Proposal No. MS-NASA/LaRC-3545-87, University of Virginia (1986).
21. E.A. Colvin, Private Communication, Alcoa Laboratories (1987).
22. F. Lin and E.A. Starke, Jr., "Mechanisms of Corrosion Fatigue Crack Propagation of 7XXX Aluminum Alloys in Aqueous Environments," Hydrogen Effects in Metals, I.M. Bernstein and A.W. Thompson, eds., TMS-AIME, Warrendale, PA, pp. 485-492 (1981).
23. R.P. Gangloff, "Electrical Potential Monitoring of the Formation and Growth of Small Fatigue Cracks in Embrittling Environment," Advances in Crack Length Measurements, C.J. Beevers, ed., EMAS, United Kingdom, pp. 175-229 (1982).
24. "Standard Test Method for Measurement of Fatigue Crack Growth Rates," ASTM E647-86a, Annual Book of Standards, Vol. 03.01, ASTM, Philadelphia, PA, pp. 899-926 (1987).

25. R.P. Gangloff, "Electrical Potential Monitoring of Crack Formation and Subcritical Growth From Small Defects," Fatigue of Engineering and Structures, Vol.4, No.1, pp. 15-33 (1981).
26. H.H. Johnson, "Calibrating the Electric Potential Method for Studying Slow Crack Growth," Materials Research and Standards, Vol.5, No.9, pp. 442-445 (1965).
27. R.P. Gangloff, unpublished research (1987).
28. R.P. Gangloff, "Ethylene Inhibition of Gaseous Hydrogen Embrittlement in High Strength Steel," in Basic Questions in Fatigue, Vol. 2, ASTM STP, R.P. Wei and R.P. Gangloff, eds., ASTM, Philadelphia, in press (1987).
29. P.L. Andresen, R.P. Gangloff, L.F. Coffin and F.P. Ford, "Applications of Fatigue Analyses: Energy Systems," in Fatigue 87, R.O. Ritchie and E.A. Starke, Jr., eds., EMAS, West Midlands, UK, in press (1987).
30. K.T. Venkateswara Rao, Yu, W. and R.O. Ritchie, "Fatigue Crack Propagation in Aluminum - Lithium Alloy 2090: Part I Long Crack Behavior," Metall. Trans. A, in press (1987).
31. K.T. Venkateswara Rao, W. Yu, and R.O. Ritchie, "Fatigue Crack Propagation in Aluminum - Lithium Alloy 2090: Part II Small Crack Behavior," Metall. Trans. A, in press (1987).
32. W.A. Herman, R.W. Hertzberg and R. Jaccard, "A Simplified Laboratory Approach for the Prediction of Short Crack Behavior in Engineering Structures," Journal of Fatigue and Fracture of Engineering Materials and Structures, in press (1987).
33. R.O. Ritchie and J. Lankford, "Overview of the Small Crack Problem," Small Fatigue Cracks, R.O. Ritchie and J. Lankford, eds., TMS-AIME, Warrendale, Pa., pp. 1-5 (1986).
34. A. Saxena, S.J. Hudak, Jr., J.K. Donald and D.W. Schmidt, "Computer Controlled Decreasing Stress Intensity Technique for Low Rate Fatigue Crack Growth Testing," J. Testing Evaluation, Vol. 6, pp. 167-174 (1978).
35. S. Suresh, "Crack Deflection: Implications for the Growth of Long and Short Fatigue Cracks," Metall. Trans. A, Vol.14A, pp. 2375-2385 (1983).
36. D.L. Davidson and J. Lankford, in Fatigue '87, R.O. Ritchie and E.A. Starke, Jr., eds., Vol. IV, EMAS, West Midlands, UK, in press (1987).

37. M. Gao, P.S. Pao and R.P. Wei, "Role of Micromechanisms in Corrosion Fatigue Crack Growth in A 7075-T651 Aluminum Alloy," Proceedings of AIME Annual Meeting, Los Angeles, Cal., pp. 303-319 (1984).
38. R.E. Stoltz and P.M. Pelloux, "Mechanisms of Corrosion Fatigue Crack Propagation in Al-Zn-Mg Alloys," Metall. Trans., Vol.3, pp. 2433-2441 (1972).
39. J. Lankford, "The Growth of Small Fatigue Cracks in 7075-T6 Aluminum," Fatigue of Engineering Material and Structures, Vol.5, No.3, pp. 233-248 (1982).
40. P.L. Lane, J.A. Gray and C.J.E. Smith, "Comparison of Corrosion Behavior of Lithium-Containing Aluminium Alloys and Conventional Aerospace Alloys," Aluminum-Lithium Alloys III, C. Baker, P.J. Gregson, S.J. Harris and C.J. Peel, eds., Institute of Metals, Oxford, UK, pp. 273-281 (1986).
41. E.L. Colvin, S.J. Murtha and R.K. Wyss, "Stress Corrosion Cracking Susceptibility of Alloy 2090," Aluminum Alloys: Their Physical and Mechanical Properties, Vol. III, E.A. Starke, Jr. and T.H. Sanders, Jr., eds., EMAS Ltd., Warley, West Midlands, UK, pp. 1853-1867 (1986).
42. L. Christodoulou, L. Struble and J.R. Pickens, "Stress Corrosion Cracking of Al-Li Binary Alloys," Aluminum-Lithium Alloys II, T.H. Sanders, Jr. and E.A. Starke, Jr., eds., TMS- AIME, Warrendale, PA, pp. 561-579 (1984).
43. J.R. Galvele and S.M. de De Micheli, "Mechanism of Intergranular Corrosion of Al-Cu Alloys," Corrosion Science, Vol. 10, pp. 795-807 (1970).
44. I.L. Mueller and J.R. Galvele, "Pitting Potential of High Purity Binary Aluminium Alloys-I. Al-Cu Alloys-Pitting and Intergranular Corrosion," Corrosion Science, Vol. 17, pp. 179-193 (1977).
45. J.G. Rinker and M. Marek, "Microstructure, Toughness and Stress Corrosion Cracking Behavior of Aluminum Alloy 2090", Materials Science and Engineering, Vol. 64, pp. 203-221 (1984).
46. B.A. Baumbert and R.E. Ricker, "Effect of Heat Treatment on Corrosion Resistance of Al-Mg-Li Alloy," pp. 282-286, in reference 40.

47. C.T. Tsao and P.P. Pizzo, "A Potentiodynamic Study of Aluminum-Lithium Alloys in Aqueous Sodium Chloride Environment," Electrochemical Techniques for Corrosion Engineering, R. Baboian, ed., NACE, Houston, TX, pp. 133-150 (1986).
48. E.I. Meletis, J.M. Sater and T.H. Sanders, Jr., "Environment Assisted Cracking in Al-Li Alloys," Aluminum Alloys: Their Physical and Mechanical Properties, Vol. II, E.A. Starke, Jr. and T.H. Sanders, Jr., EMAS Ltd., Warley, West Midlands, UK, pp. 1157-1175 (1986).
49. N.J.H. Holroyd, A. Gray, G.M. Scamans and R. Hermann, "Environment Sensitive Fracture of Al-Li-Cu-Mg Alloys," pp. 310-320, in reference 40.
50. H. Kaesche, "Pitting Corrosion of Aluminum and Intergranular Corrosion of Aluminum Alloys," Localized Corrosion, B.F. Brown, J. Kruger, R.S. Staehle and A. Agrawal, eds., NACE, Houston, TX, pp. 516-525 (1972).
51. Private communication, J.P. Moran.
52. P.P. Pizzo, "Stress Corrosion Behavior of Aluminum-Lithium Alloys in Aqueous Salt Environments," pp. 627-656, in reference 42.
53. H.L. Craig, Jr., "Kinetic Studies of Aluminum Pitting Reactions," pp. 600-607, in reference 50.
54. J.R. Galvele, S.M. de De Micheli, I.L. Mueller, S.B. de Wexler and I.L. Alanis, "Critical Potentials for Localized Corrosion of Aluminum Alloys," pp. 590-599, in reference 50.
55. J.G. Craig, R.C. Newman, M.R. Jarrett and N.J.H. Holroyd, "Stress Corrosion Cracking and Pre-Exposure Effects in Al-Li-Cu-Mg Alloy 8090," Proc. 3rd Int. Conf. Environmental Degradation of Engineering Materials, Univ. Park, PA, (1987).
56. J.G. Craig, R.C. Newman, M.R. Jarrett and N.J.H. Holroyd, "Local Chemistry of Stress Corrosion Cracking in Al-Li-Cu-Mg Alloys," Conf. Proc. 4th International Conference on Aluminum-Lithium Alloys, to be published (1987).
57. T.J. Lennox Jr. and M.H. Peterson, "Potential and pH Relationships in Cathodically Polarized Metal Crevices," pp. 173-178, in reference 50.

58. N.J.H. Holroyd, G.M. Scamans and R. Hermann, "Environmental Interaction with the Crack Tip Region During Environment Sensitive Fracture of Aluminum Alloys," Embrittlement by the Localized Crack Environment, R.P. Gangloff, ed., TMS, Warrendale, Pa, pp. 327-347 (1984).
59. P.P. Pizzo, R.P. Galvin and H.G. Nelson, "Stress Corrosion Cracking behavior of Al-Li Alloys," pp. 627-652, in reference 42.
60. Private communication, J.P. Moran.
61. H.S. Issacs and B. Vyas, "Scanning Reference Electrode Techniques in Localized Corrosion," Electrochemical Corrosion Testing, ASTM STP 727, F. Mansfeld and U. Bertocci, eds., ASTM, pp. 3-33 (1981).
62. K.J. Bhansali and M.T. Hepworth, "the Corrodescope, Its Description and Application to the Study of Pitting Phenomena," Journal of Physics E:Scientific Instruments, Vol. 7, pp. 681-684 (1974).
63. P. Doig and J.W. Edington, "Use of Microelectrodes in the Study of Stress Corrosion in Aged Al-7.2wt-%Mg and Al-4.4wt%Cu Alloys," British Corrosion Journal, Vol. 2, pp. 88-90 (1974).
64. M. Marek and E.A. Starke Jr., "Potential Distributions Relating to Grain Boundaries on Corroding Aluminium Alloys," British Corrosion Journal, Vol. 11, 1, pp. 31-34 (1976).
65. H.S. Issacs, "Potential Scanning of Stainless Steel During Pitting Corrosion," pp. 158-167, in reference 50.
66. R.J. O'Halloran, L.F.G. Williams and C.P. Lloyd, "A Microprocessor Based Isopotential Contouring System for Monitoring Surface Corrosion," Corrosion, Vol. 40, 7, pp. 344-349 (1984).
67. H.S. Issacs and Y. Ishikawa, "Potential Determining Reactions During Pitting Corrosion of Aluminum," Metallic Corrosion, Vol. 4, National Research Council of Canada, Proceedings of the 9th ICMC, Toronto, pp. 150-154 (1984).
68. N.D. Kackley and R.M. Latanision, "A Study of Localized Corrosion in Aluminum Using The Scanning Potential Microprobe," pp. 191-197, in reference 67.
69. J.A. Davis, "Use of Microelectrodes for the Study of Stress Corrosion of Aluminum Alloys," pp. 168-172, in reference 50.

70. L.F. Jaffe and R. Nuccitelli, "An Ultrasensitive Vibrating Probe for Measuring Steady Extracellular Currents," Journal of Cell Biology, Vol. 63, pp. 614-628 (1974).
71. Y. Ishikawa and H.S. Issacs, "Study of Pitting Corrosion of Aluminum by Means of the Scanning Vibrating-Electrode Technique," Conf. Proc. on Corrosion and Exploitation of Aluminum Alloys, Cranfield, England (1983).
72. H.S. Issacs and M.W. Kendig, "Determination of Surface Inhomogeneities Using a Scanning Probe Impedance Technique," Corrosion, Vol. 36, pp. 269-274 (1980).
73. G. Buzzanca, C. Ronchetti and F. Ubert, "SCP (Scanning Current Probe) Technique for Measurements of EPR Degree of Sensitization of Stainless Steel Welds," p. 177-184, in reference 67.
74. H.S. Issacs and Y. Ishikawa, "Application of the Vibrating Probe to Localized Current Measurements," Electrochemical Techniques, NACE, Houston, TX, pp. 17-23 (1986).
75. D.J.G. Ives and G.J. Janz, eds., Reference Electrodes Theory and Practice, Academic Press, New York, Ch. 5 (1961).
76. C. Wagner, "Theoretical Analysis of Current Density Distribution in Electrolytic Cells," J. Electrochem. Soc., Vol. 98, pp. 116 (1952).
77. J.T. Waber, "Analysis of Size Effects in Corrosion Processes," p. 221-237, in reference 67.
78. M. Stern, "The Relation Between Pitting Corrosion and the Ferrous-Ferric Oxidation Reduction Kinetics on a Passive Surface," J. Electrochem. Soc., Vol. 104, pp. 600 (1957).
79. P.P. Pizzo, R.P. Galvin and H.G. Nelson, in Proc. 2nd Inter. Al-Li Conf., E.S. Starke, Jr. and T.H. Sanders, Jr., eds., TMS-AIME, Warrendale, PA, pp. 627-656 (1984).
80. P.P. Pizzo and D.L. Daeschner, in Aluminum Alloys - Their Physical and Mechanical Properties, E.A. Starke, Jr. and T.H. Sanders, Jr., eds., EMAS, West Midlands, U.K., pp. 1197-1219 (1986).
81. W.S. Miller, J. White and D.J. Lloyd, in Aluminum Alloys - Their Physical and Mechanical Properties, E.A. Starke, Jr. and T.H. Sanders, Jr., eds., EMAS, West Midlands, U.K., pp. 1799-1819 (1986).

82. E.C. Colvin, S.J. Murtha and R.K. Wyss, in Aluminum Alloys - Their Physical and Mechanical Properties, E.A. Starke, Jr. and T.H. Sanders, Jr., eds., EMAS, West Midlands, U.K., pp. 1853-1868 (1986).
83. R.E. Swanson, A.W. Thompson, I.M. Bernstein and J.L. Maloney, in Hydrogen Effects in Metals, A.W. Thompson and I.M. Bernstein, eds., TMS-AIME, Warrendale, PA, pp. 459-466 (1981).
84. J.R. Pickens and L. Christodoulou, in Metall.Trans. A., Vol. 18A, pp. 135-149 (1987).
85. R.E. Swanson, Ph.D. Thesis, Metallurgical Engineering and Materials Science Dept., Carnegie-Mellon University, Pittsburgh, PA (1983).
86. F.P. Ford, in Mechanisms of Environment Sensitive Cracking of Materials, P.R. Swann, F.P. Ford and A.R.C. Westwood, eds., The Metals Society, London, pp. 125-146 (1977).
87. A.W. Thompson and I.M. Bernstein, in Advances in Corrosion Science and Technology, Vol. 7, Plenum, New York,, pp. 53-175 (1979).
88. W.E. Wood and W.W. Gerberich, Metall. Trans., Vol. 5, pp. 1285-1294 (1974).
89. L. Montgrain and P.R. Swann, in Hydrogen in Metals, I.M. Bernstein and A.W. Thompson, eds., ASM, Metals Park, OH, pp. 575-584 (1974).
90. L. Christodoulou and H.M. Flower, in Acta. Met., Vol. 28, pp. 481-487 (1980).
91. H.W. Hayden and S. Floreen, in Corrosion, Vol. 27, pp. 429-34 (1971).
92. J.A.S. Green and W.G. Montague, Corrosion, Vol. 31, pp. 209-213 (1975).
93. J.R. Pickens, J.R. Gordon and L. Christodoulou, in High-Strength Powder Metallurgy Alloys, M.J. Koczak and G.J. Hildeman, eds., TMS-AIME, Warrendale, PA, pp. 177-192 (1982).
94. J.R. Pickens, J.R. Gordon and J.A.S. Green, Metall. Trans. A., Vol. 14A, pp. 925-930 (1983).
95. N.J.H. Holroyd, Alcan International Ltd., Banbury, U.K., personal communication (January 1986).

96. S.W. Ciaraldi, J.L. Nelson, R.A. Yeske and E.N. Pugh, in Hydrogen Effects in Metals, A.W. Thompson and I.M. Bernstein, eds., TMS-AIME, Warrendale, PA, pp. 437-447 (1981).
97. W.M. Mueller, J.P. Blackledge and G.G. Libowitz, in Metal Hydrides, Academic Press, New York, pp. 217-223 (1968).
98. D.A. Hardwick, M. Taheri, A.W. Thompson and I.M. Bernstein, Metall. Trans. A., Vol. 13A, pp. 235-239 (1982).
99. R.E. Swanson, A.W. Thompson and I.M. Bernstein, Metall. Trans. A., Vol. 17A, pp.1633-1637 (1986).
100. J. Masters, M.S. Thesis, Materials Engineering Dept., VPI & SU, Blacksburg, VA (1977).
101. Aluminum Alloys - Physical and Mechanical Properties, Vols. I and II, E.A. Starke, Jr. and T.H. Sanders, Jr., eds., EMAS Ltd., Warley, West Midlands, UK (1986).
102. Rapidly Solidified Powder Aluminum Alloys, ASTM STP 890, M.E. Fine and E.A. Starke, Jr., eds., ASTM, Philadelphia, PA (1986).
103. High Strength Powder Metallurgy Aluminum Alloys II, G.J. Hildeman and M.J. Koczak, eds., TMS-AIME, Warrendale, PA (1986).
104. High Strength Powder Metallurgy Aluminum Alloys, M.J. Koczak and G.J. Hildeman, eds., TMS-AIME, Warrendale, PA (1982).
105. F.H. Froes, Young-Won Kim and F. Hehmann, "Rapid Solidification of Al, Mg and Ti," J. Metals, August, pp. 14-21 (1987).
106. R. Sundaresan and F.H. Froes, "Mechanical Alloying," J. Metals, August, pp. 22-27 (1987).
107. Young-Won Kim, "Effect of Non-Uniform Microstructure and Hydrogen in High Temperature PM Aluminum Alloy Al-8.4Fe-7.2Ce," Progress in Powder Metallurgy, Vol. 43, in press (1987).
108. Young-Won Kim and F.H. Froes, "The Effect of Hydrogen in Rapidly Solidified Powder Aluminum Alloys," Aluminum, in press (1987).
109. D.J. Skinner, R.L. Bye, D. Raybould and A.M. Brown, "Dispersion Strengthened Al-Fe-V-Si Alloys," Scripta Metall., Vol. 20, pp. 867-872 (1986).
110. S.L. Langenbeck, W.M. Griffith, F.J. Hildeman and J.W. Simon, "Development of Dispersion-Strengthened Aluminum Alloys," pp. 410-422 in Ref. 102.

111. M.K. Premkumar, M.J. Koczak and A. Lawley, "Elevated Temperature Mechanical Behavior of P/M Dispersion Strengthened Al-Fe-Ni Alloys," pp. 265-284 in Ref. 103.
112. J.W. Simon, "Pratt-Whitney Materials Development," presented at NASA Workshop on Advanced Aluminum Alloy Technology for Cryogenic Tanks," Hampton, VA (1987).
113. W.M. Griffith, R.E. Sanders, Jr. and G.J. Hildeman, "Elevated Temperature Aluminum Alloys for Aerospace Applications," pp. 209-224 in Ref. 104.
114. B. Noble, S.J. Harris and K. Harlow, "Mechanical Properties of Al-Li-Mg Alloys at Elevated Temperatures," pp. 65-77 in Ref. 101.
115. W.M. Griffith and J.S. Santner, "Effect of Defects in Aluminum PM," pp. 125-145 in Ref 104.
116. R.L. Dreshfield, "Defects in Nickel-Base Superalloys," J. Metals, July, pp. 16-21 (1987).
117. S. Suresh, A.K. Vasudevan, M. Tosten and P.R. Howell, "Microscopic and Macroscopic Aspects of Fracture in Lithium- Containing Aluminum Alloys," Acta Metall., Vol. 35, pp. 25-46 (1987).
118. V. Kumar, M.D. German, W.W. Wilkening, W.R. Andrews, H.G. deLorenzi and D.F. Mowbray, "Advances in Elastic-Plastic Fracture Analysis," EPRI Report NP-3607, Palo Alto, CA (1984).
119. R.P. Gangloff, "Electrical Potential Monitoring of the Formation and Growth of Small Fatigue Cracks in Embrittling Environments," pp. 175-231 in Advances in Crack Length Measurement, C.J. Beevers, ed., EMAS, United Kingdom (1982).
120. S.B. Biner, J.T. Barnby and D.W.J. Elwell, "On the Use of Short Rod/Bar Test Specimens to Determine the Fracture Toughness of Metallic Materials," Intl. J. Fracture, Vol. 26, pp. 3-16 (1984).
121. C.D.S. Tuck, "The Embrittlement of Al-Zn-Mg and Al-Mg Alloys by Water Vapor," Metall. Trans. A, Vol. 16A, pp. 1503-1514 (1985).
122. R.H. Bricknell and D.A. Woodford, "The Embrittlement of Nickel following High Temperature Exposure," Metall. Trans. A, Vol. 12A, pp. 425-433 (1981).
123. V.M. Radhakrishnan and A.J. McEvily, "A Critical Analysis of Crack Growth in Creep," Trans. ASME, Vol. 102, pp. 200-206 (1980).

124. J.G. Kaufman and J.R. Low, Jr., "The Micromechanisms of Sustained Load Crack Growth in Al-Cu Alloys 2124 and 2219 at 300 F," Proc. 2nd Intl. Conf. on Mech. Behavior of Matls., Boston, MA, pp. 414-428 (1976)
125. K.M. Nibkin and G.A. Webster, "Temperature Dependence of Creep Crack Growth in Aluminum Alloy RR 58," Micro and Macro Mechanics of Crack Growth, K. Sadananda, B.B. Rath and D.J. Michel, eds., TMS-AIME, Warrendale, PA, pp. 137-152 (1982).
126. K. Sadananda and P. Shahinian, "Creep Crack Growth in Alloy 718," Metall. Trans. A, Vol. 8A, pp. 439-449 (1977).
127. J.L. Bassani, "Micro and Macro-Mechanics of High Temperature Fracture," Fracture: Interaction of Microstructure, Mechanisms and Mechanics, J.M. Wells and J.D. Landes, eds., TMS-AIME, Warrendale, PA, pp. 385-401 (1984).
128. H. Riedel, "Creep Deformation at Crack Tips in Elastic-Visco-Plastic Solids," J. Mech. Phys. Solids, Vol. 1, pp. 35-49 (1981).
129. A. Saxena, "Creep Crack Growth: Data and Models," Matls. Sci. and Engr., submitted (1987).

SECTION VIII

FIGURES

1987

1988

1989

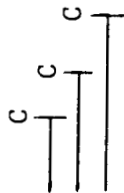
Mar May Jul Sept Nov Jan Mar May Jul Sept Nov Jan Mar May Jul

Literature Review and Research Proposal



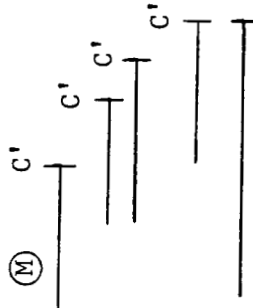
Phase I (Table 4)

- Microstructural characterization
- Electrochemical characterization
- Small crack fracture mechanics, automation and environmental cell methods development



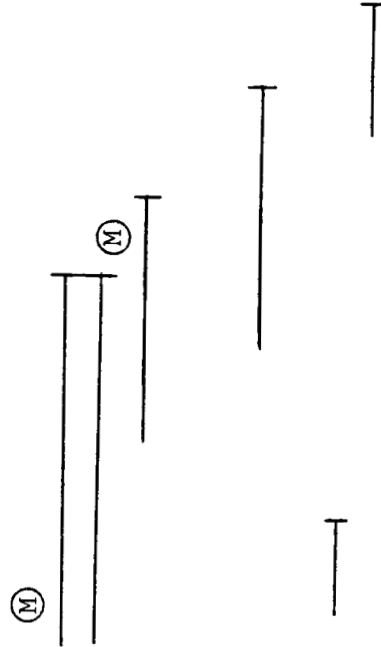
Phase II (Table 5)

- Characterization of intrinsic small crack propagation by constant K_{max}
- Effect of frequency
- Gaseous environment corrosion fatigue (He, H₂O, O₂)
- Aqueous environment corrosion fatigue (effect of potential)
- Fractographic studies



Phase III (Table 6)

- Mechanistic experiments from II
- Fracture toughness probe of corrosion fatigue damage
- Dissertation



Other

- Mechanistic follow-ups from Plascik with Wagner. Hydrogen emphasis.
- First annual report
- Final report

C - completed M - committee meeting

C' - completed with followup analyses in progress

Tables 4, 5, and 6 are presented in Appendix I

Figure 1

Program Schedule.

ORIGINAL PAGE IS
OF POOR QUALITY

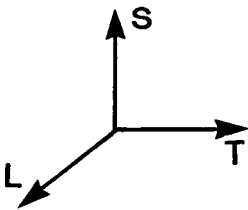
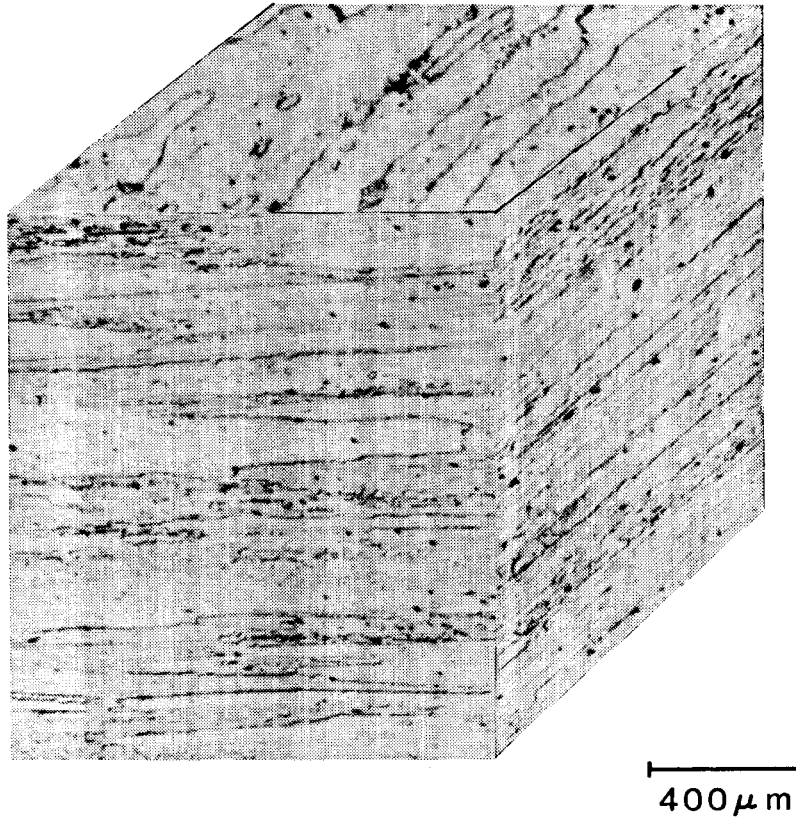


Figure 2

Microstructure of Alloy 2090 rolled plate (etched with Keller's reagent).

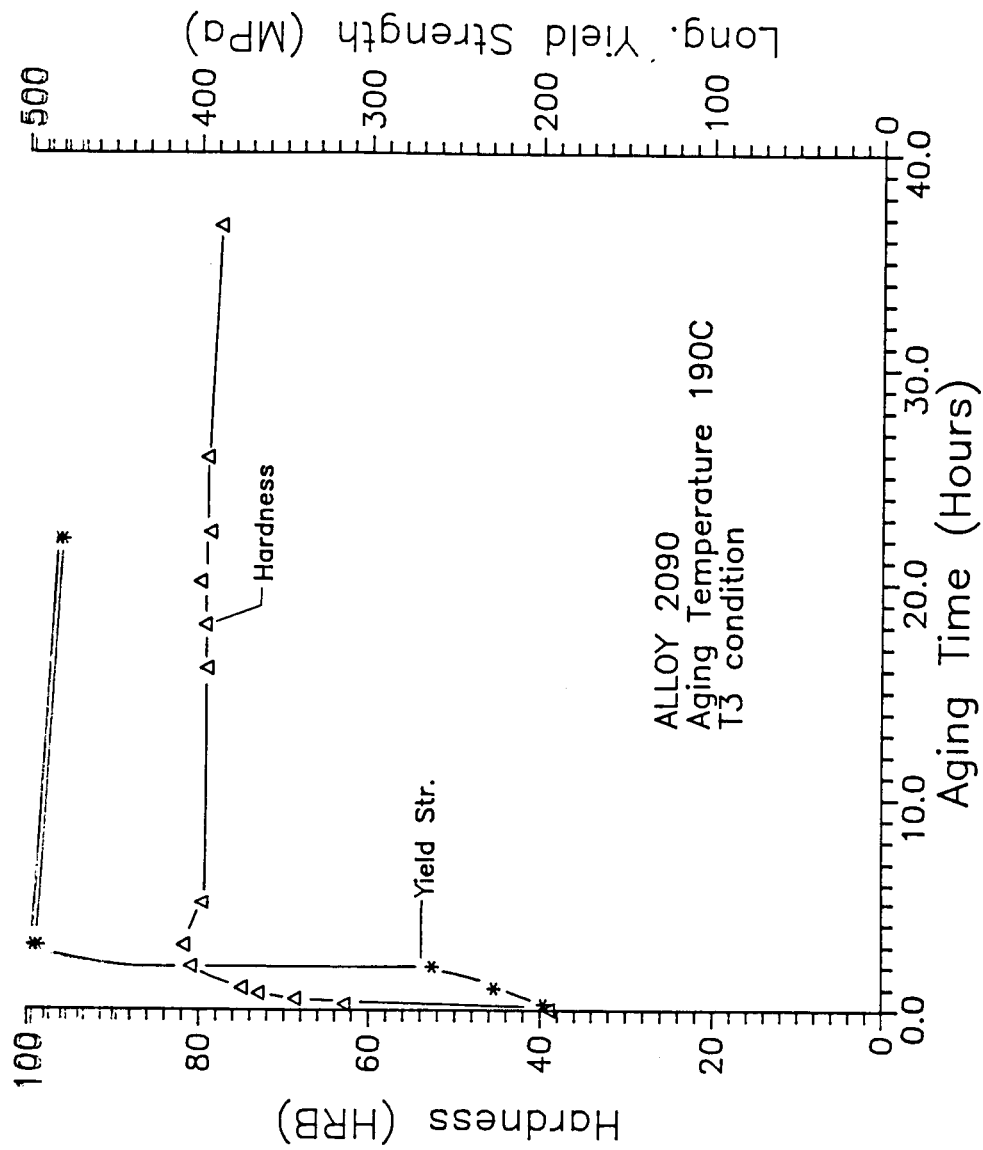


Figure 3

Precipitation strengthening characteristics of Alloy 2090 for aging at 190°C, and in terms of hardness and tensile yield strength change.

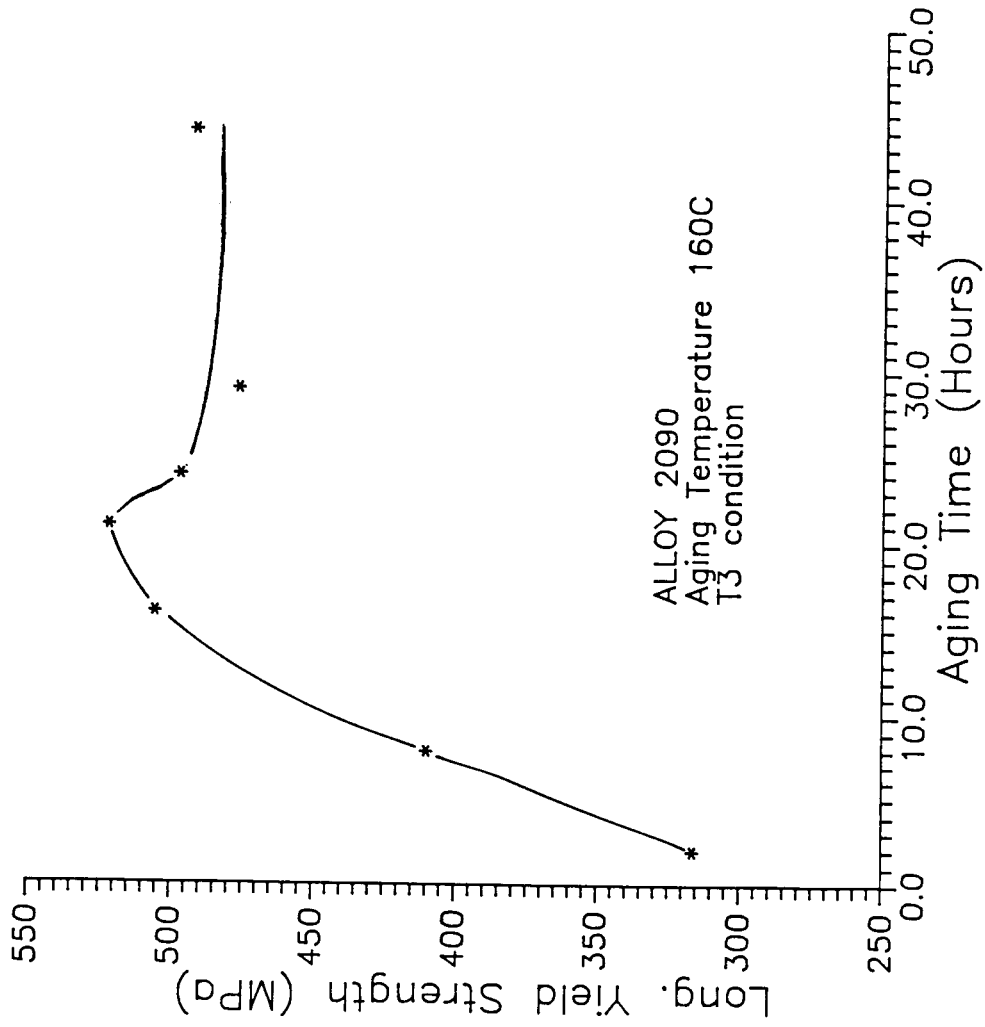


Figure 4

Precipitation strengthening characteristics of Alloy 2090 for aging at 160°C.

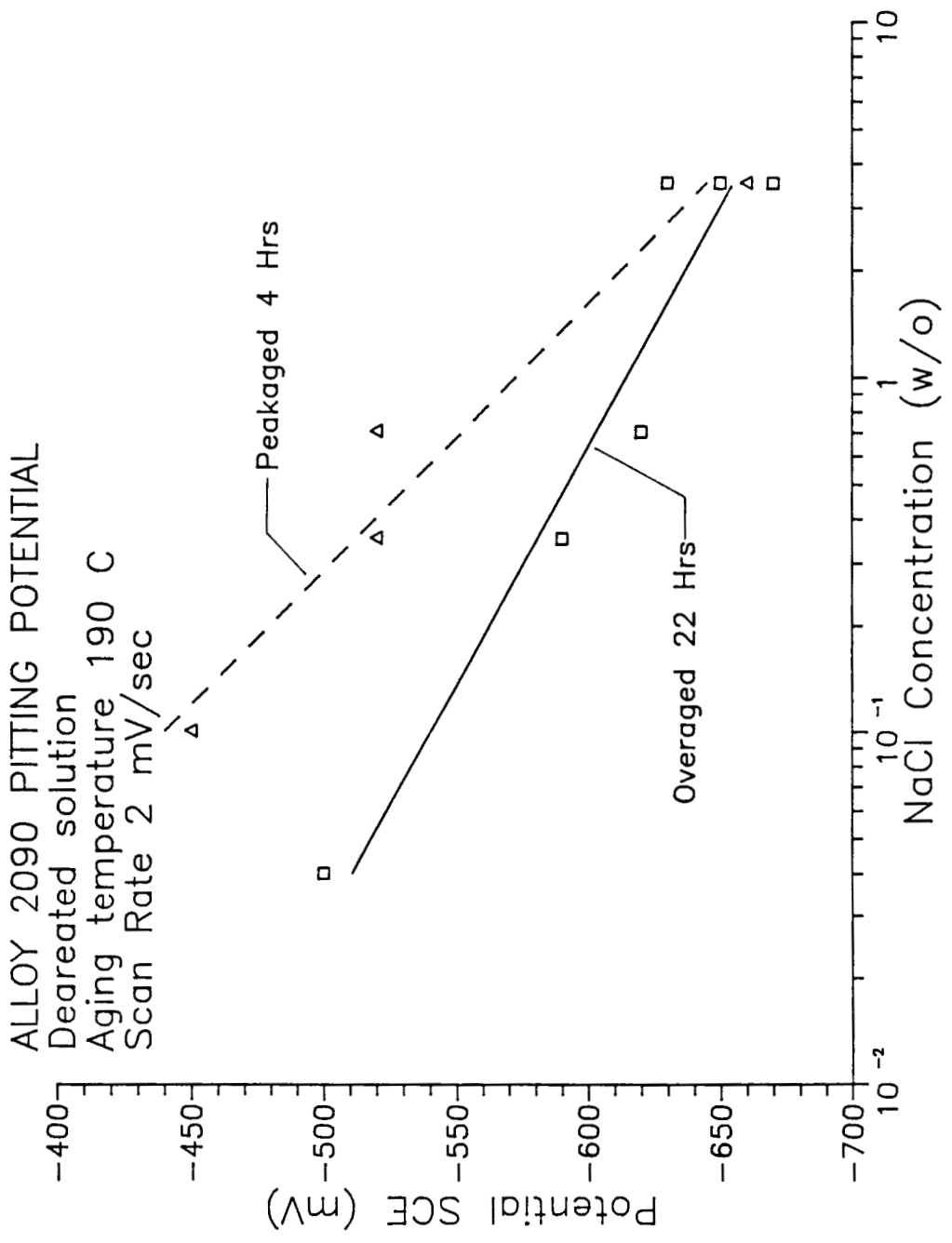


Figure 5

Variation of the pitting potential of peak aged and over aged Alloy 2090 as a function of NaCl concentration.

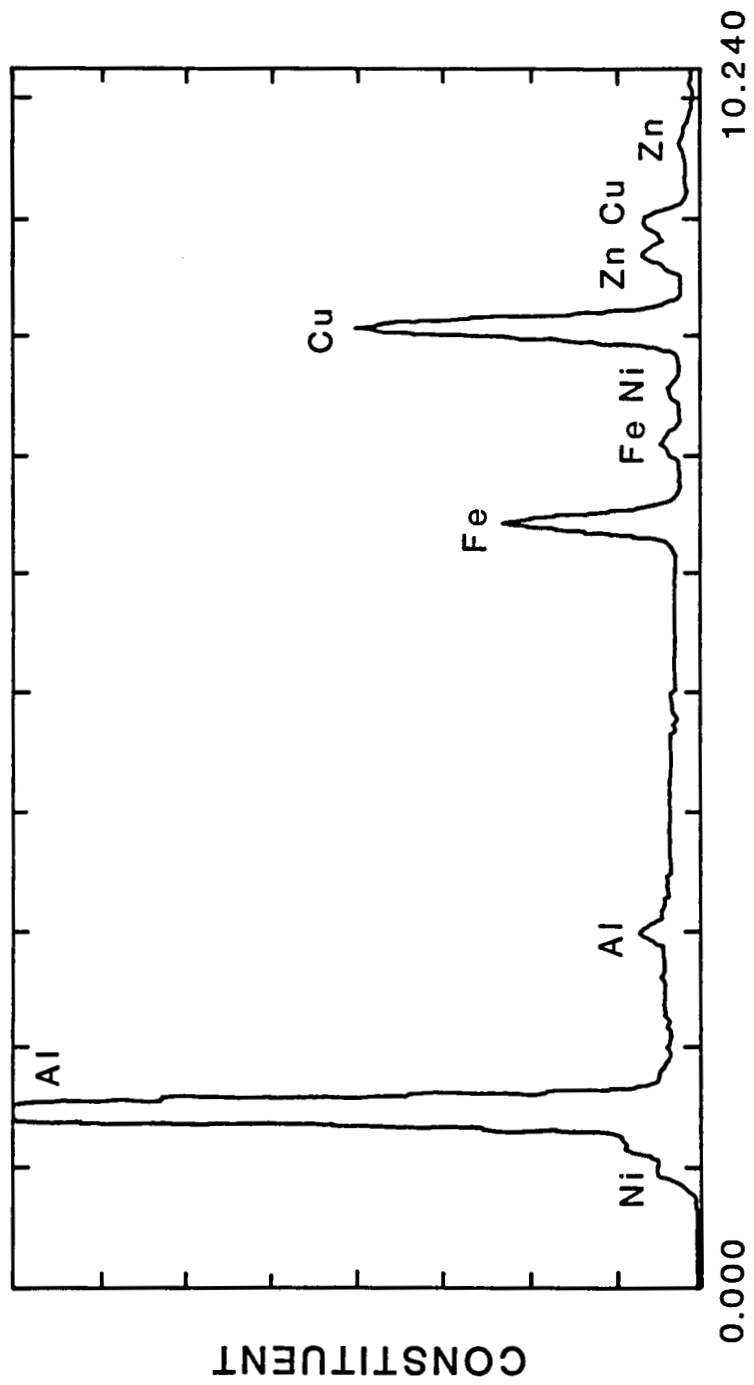


Figure 6a

Constituent particle composition by EDX analysis.

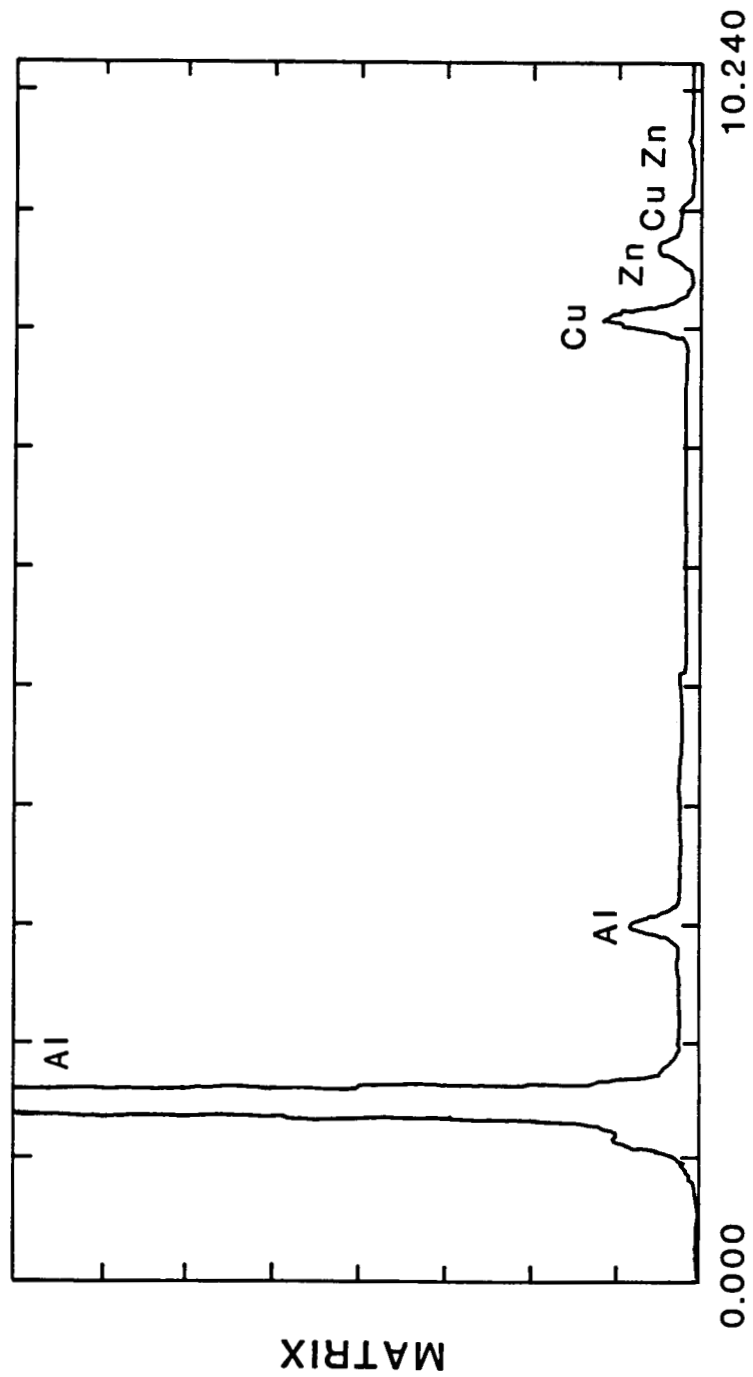
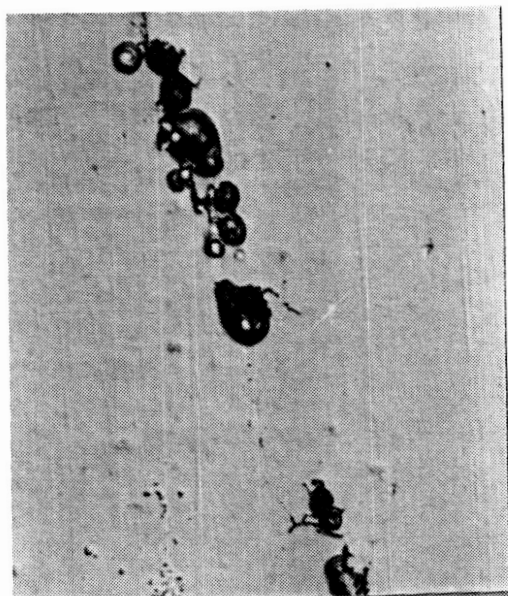


Figure 6b

Matrix composition by EDX analysis.



ORIGINAL PAGE IS
OF POOR QUALITY

10 μ m

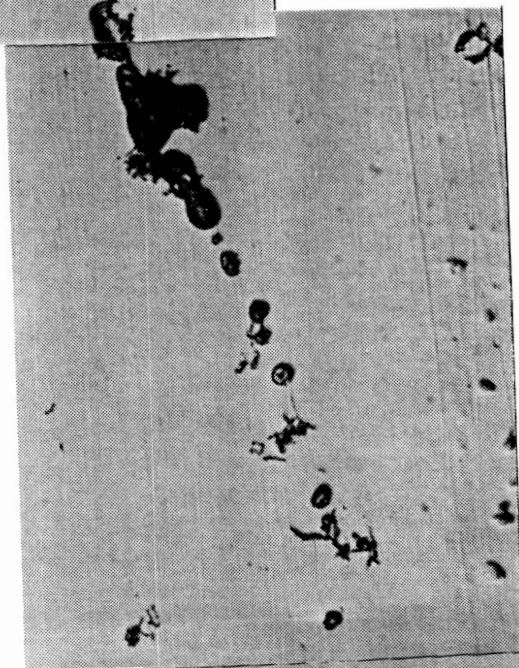


Figure 7

Stringer of constituent particle pits contained in peak aged Alloy 2090.
Test conditions; 0.1% NaCl, 5 days at -0.700 V (SCE).

ORIGINAL PAGE IS
OF POOR QUALITY

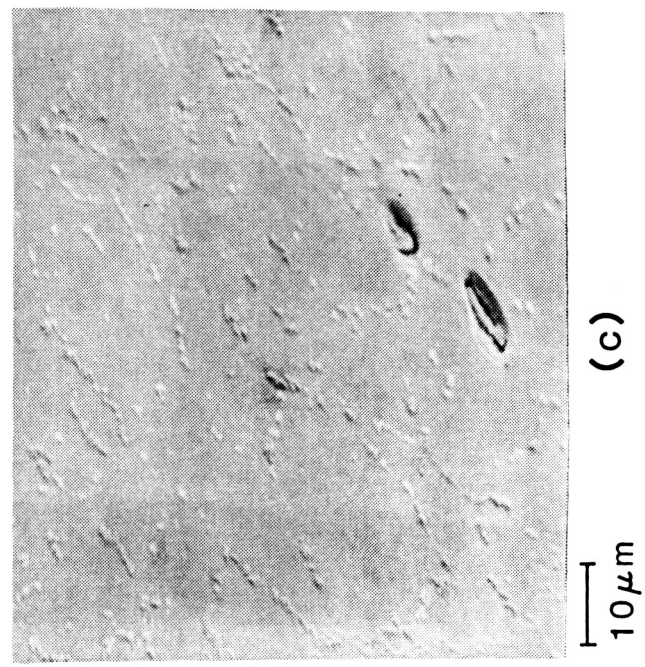
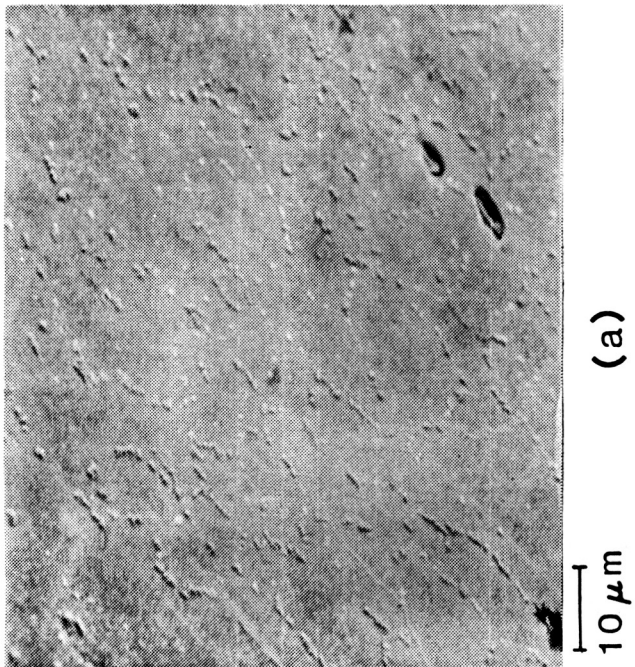
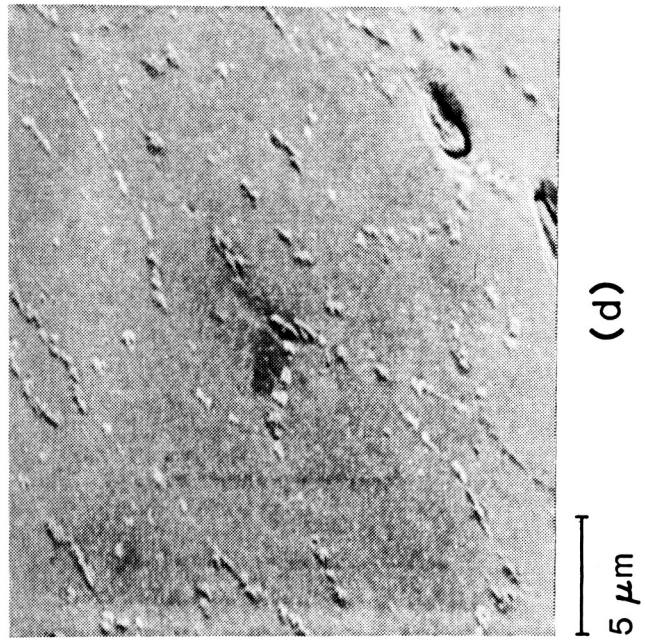
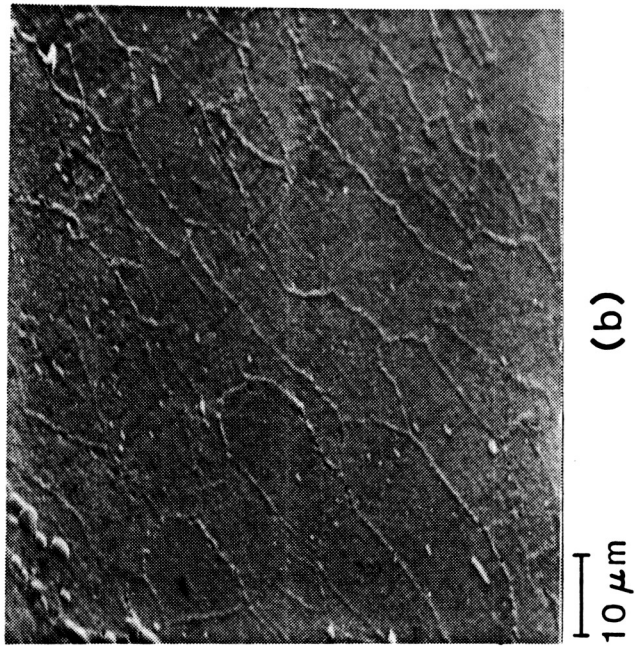
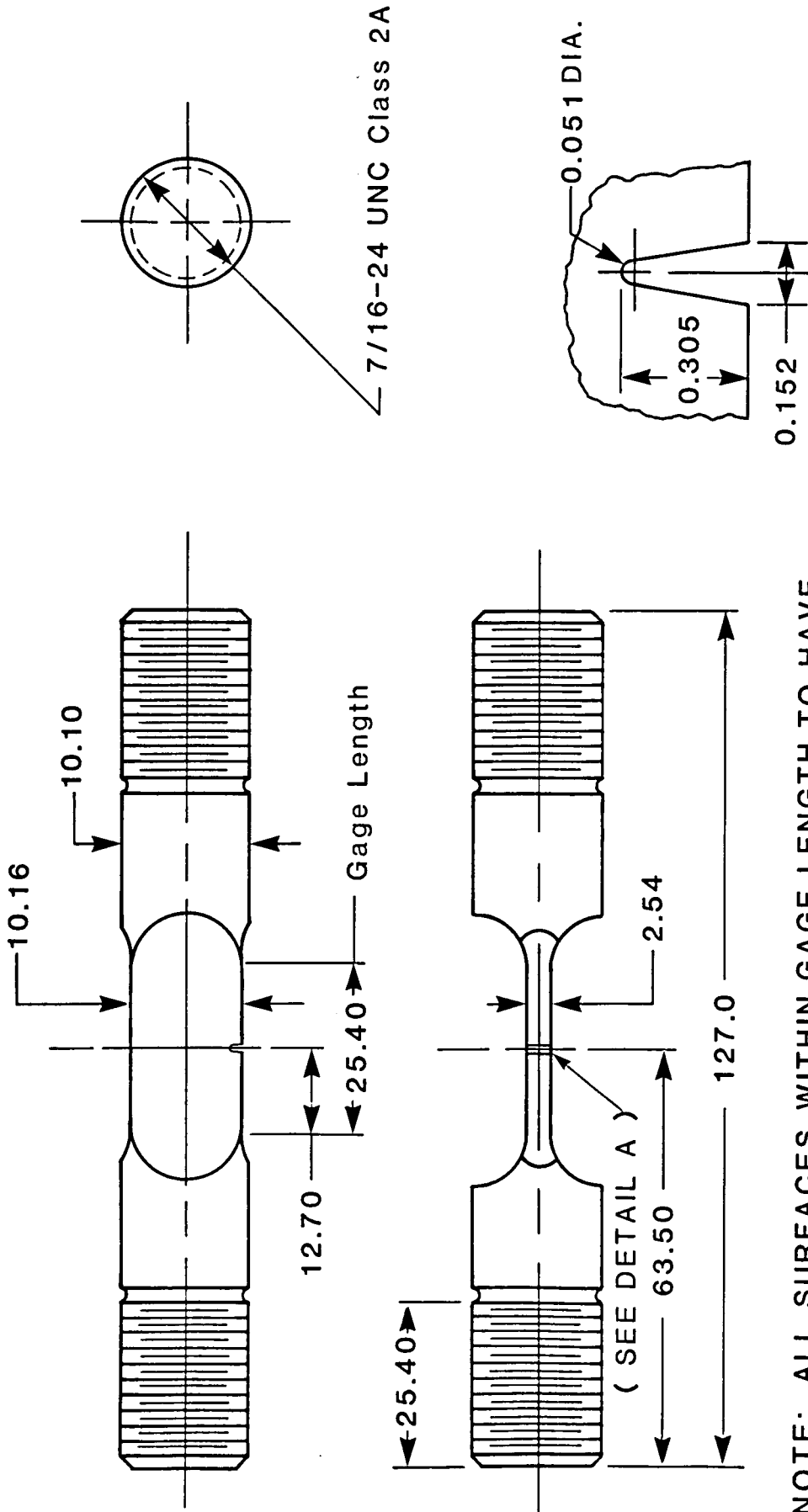


Figure 8

Sub-boundary pitting in peak aged Alloy 2090; (a) 1000X - exposed, (b) 1000X - etched sub-boundaries without chloride exposure, (c) 1500X - exposed, (d) 2000X - exposed. Test conditions; 0.1% NaCl, 3.5 days at

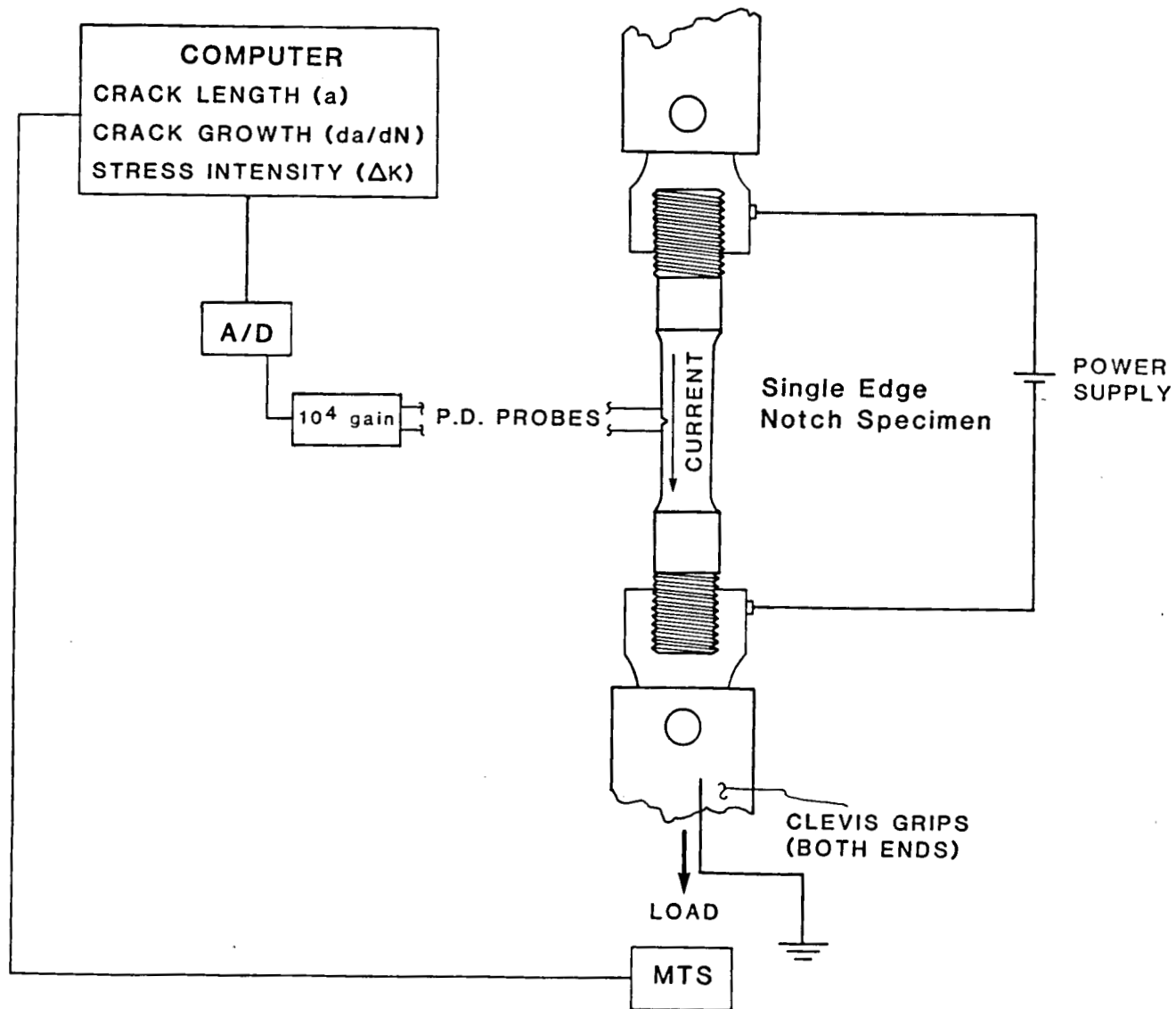


NOTE: ALL SURFACES WITHIN GAGE LENGTH TO HAVE SURFACES FINISH OF 0.2 μ m, BALANCE 0.8 μ m POLISH GAGE IN LONGITUDINAL TO SPECIMEN AXIS ONLY

ALL DIMENSIONS IN MILLIMETERS

Figure 9

Micronotched, short edge crack specimen design.



Potential Difference Testing

Figure 10

Computer automated electrical potential difference system for fatigue crack growth control and monitoring.

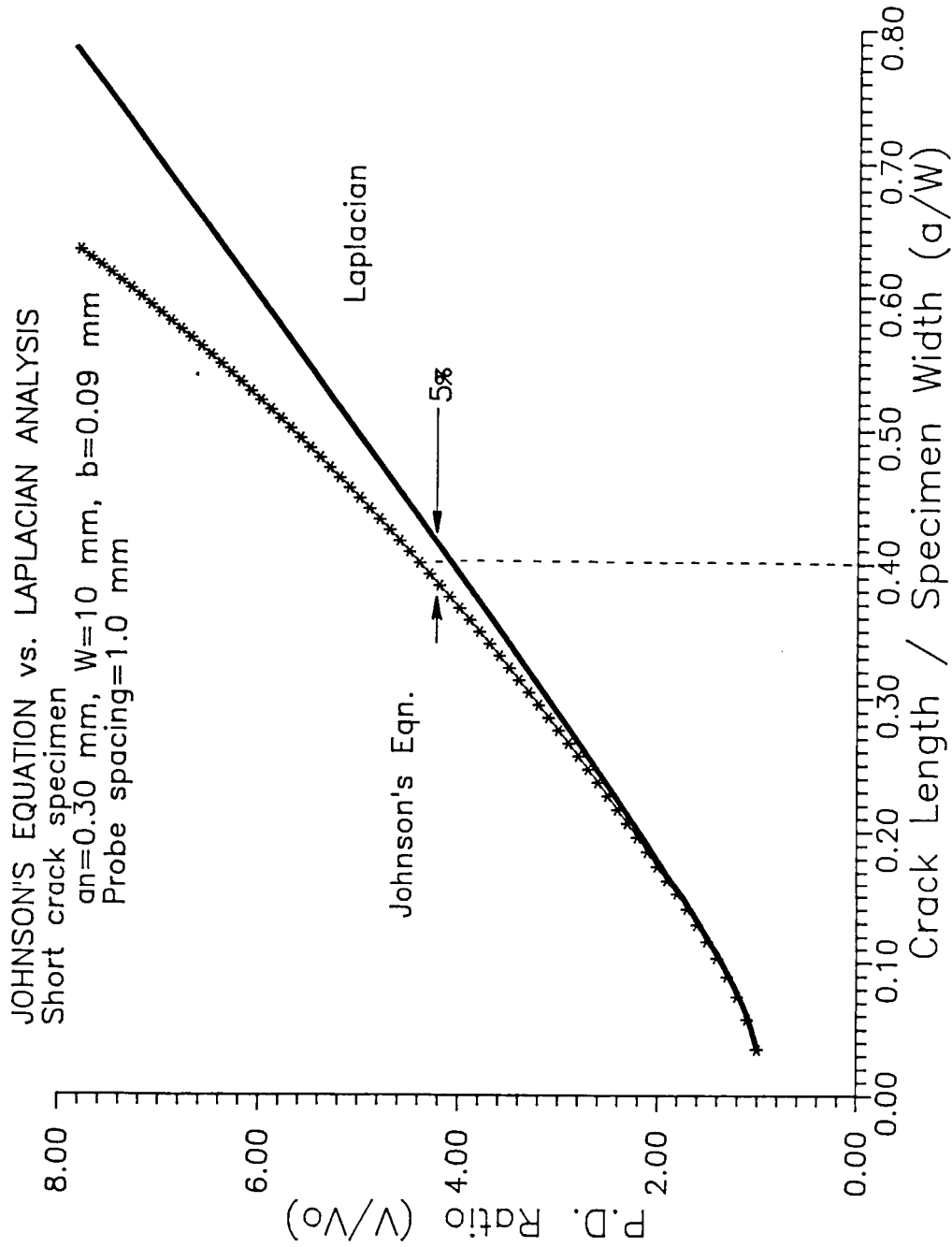


Figure 11

Comparison of the Laplacian analysis and Johnson's equation calibration procedures for relating measured electrical potential to crack length.

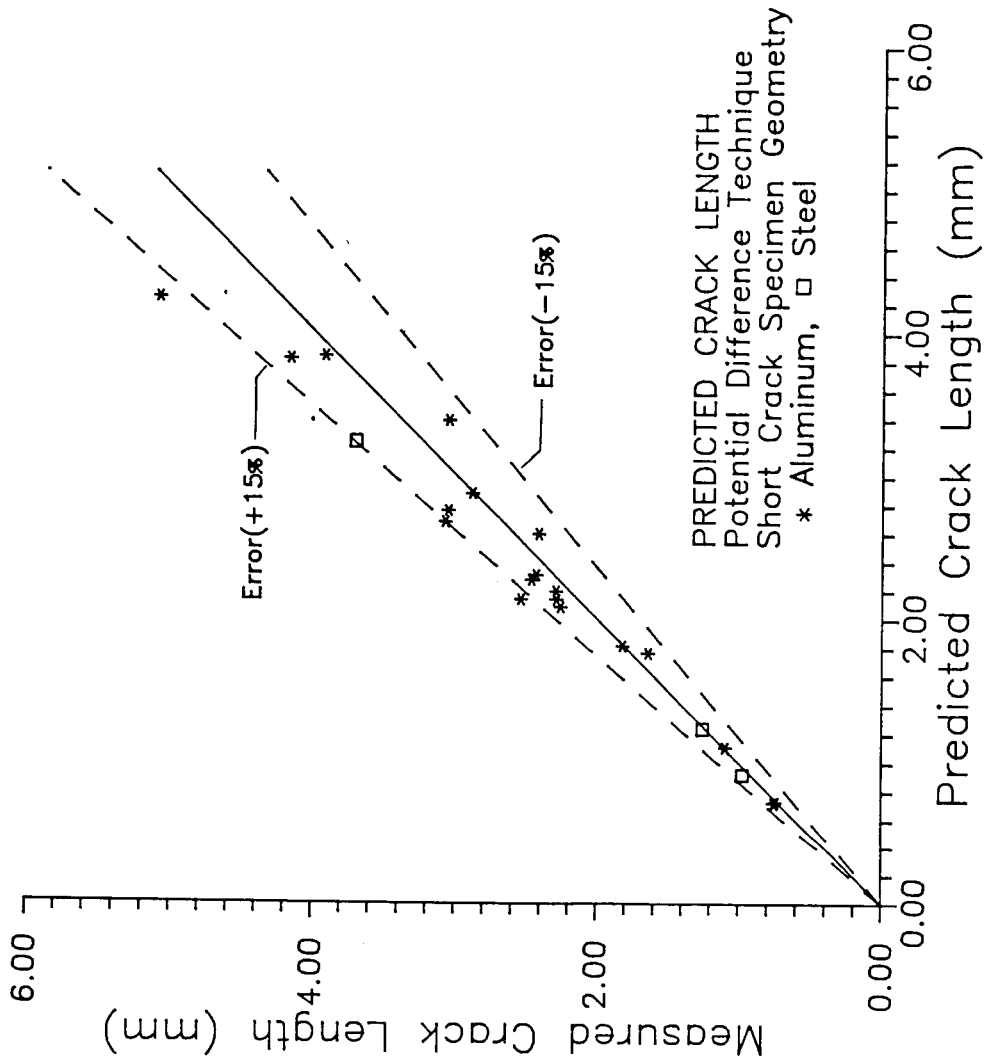


Figure 12

Crack length predicted by potential measurements and the Laplacian model versus crack length measured by SEM and optical fracture surface examination.

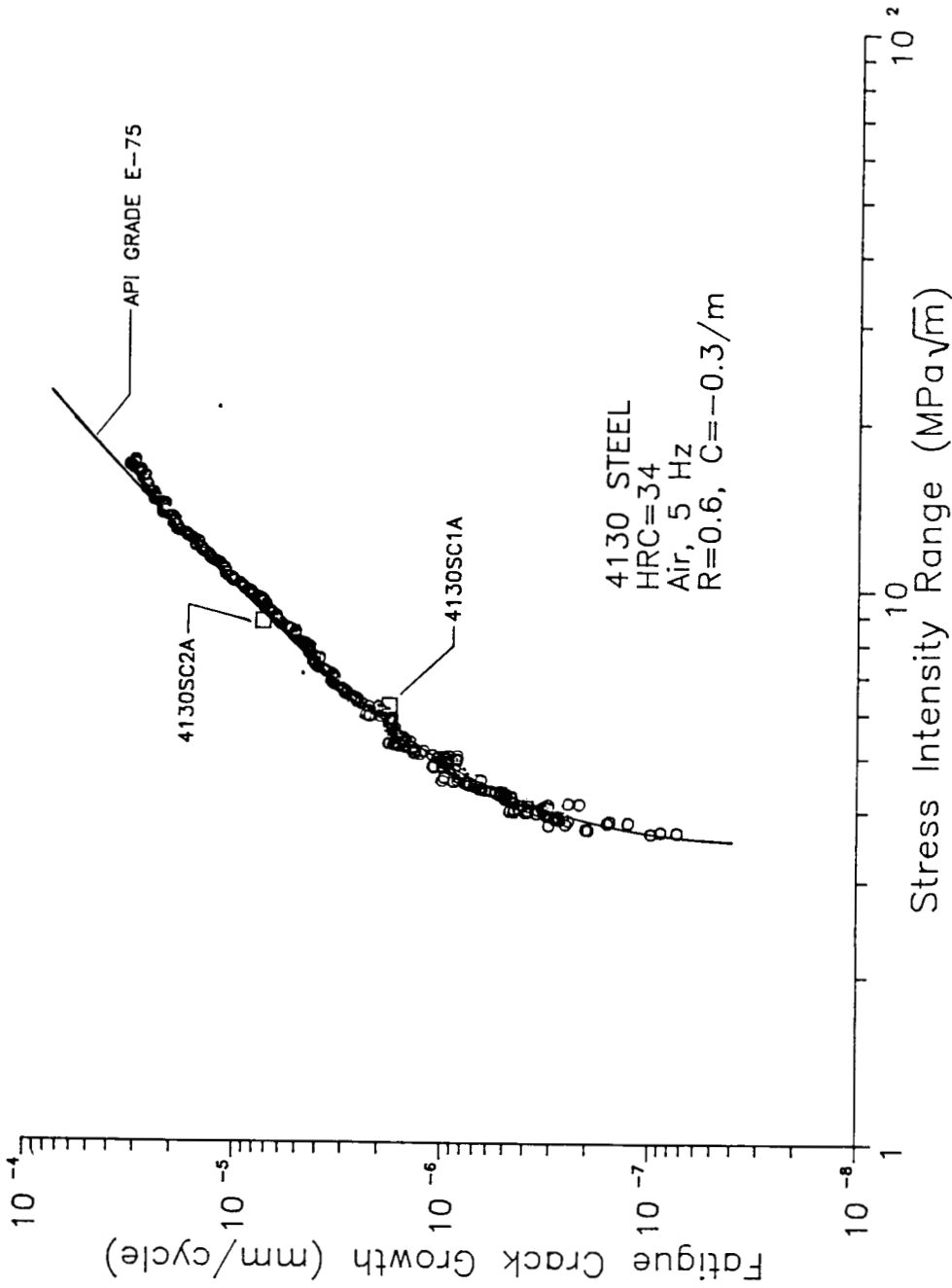


Figure 13

Comparison of 4130 steel constant ΔK and decreasing ΔK test results with the FCG characteristics of a comparable steel in moist air.

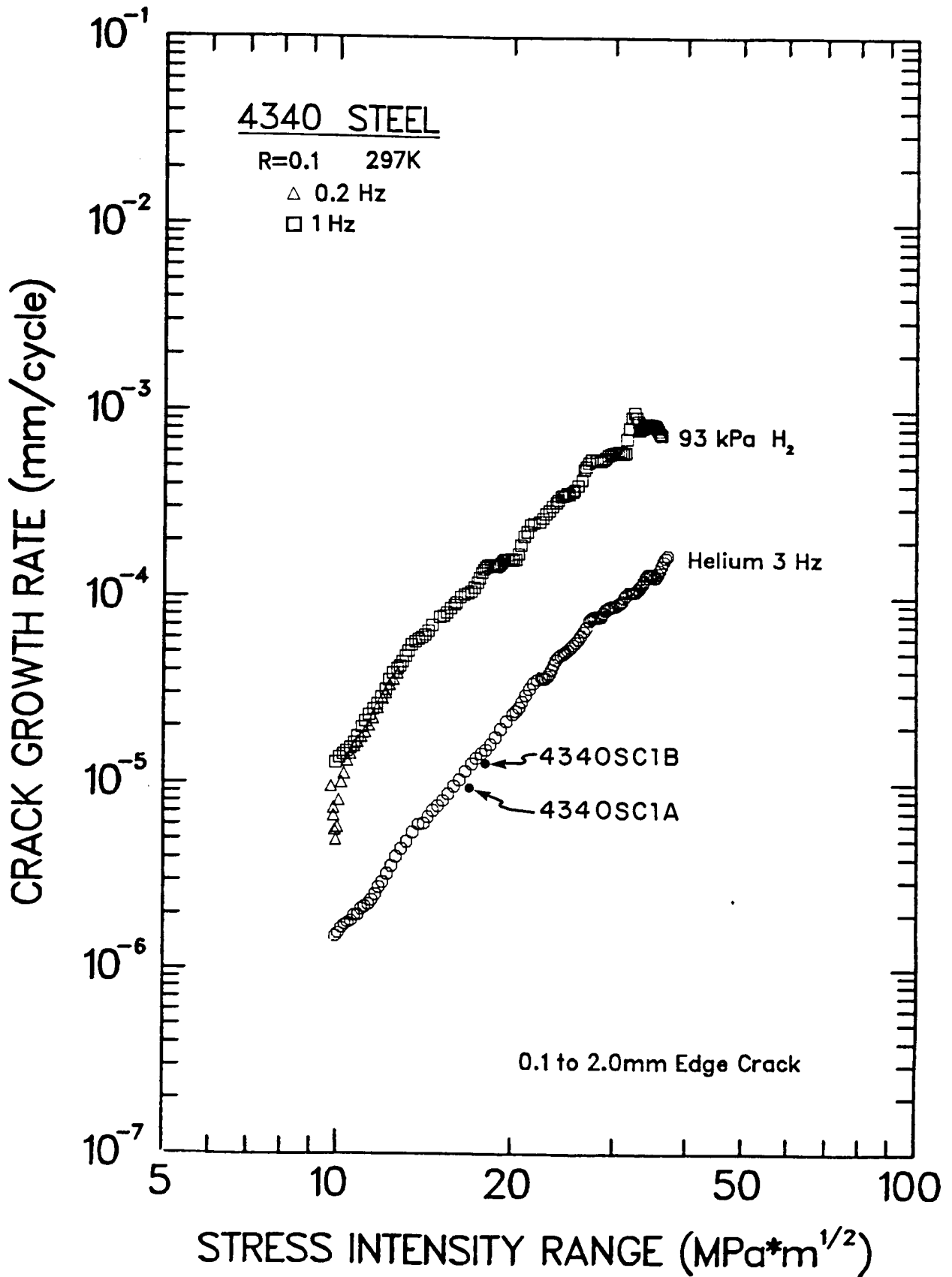


Figure 14

Comparison of two constant ΔK test results with the FCG characteristics of 4340 steel in the high purity helium environment.

AQUEOUS ENVIRONMENT TEST CELL

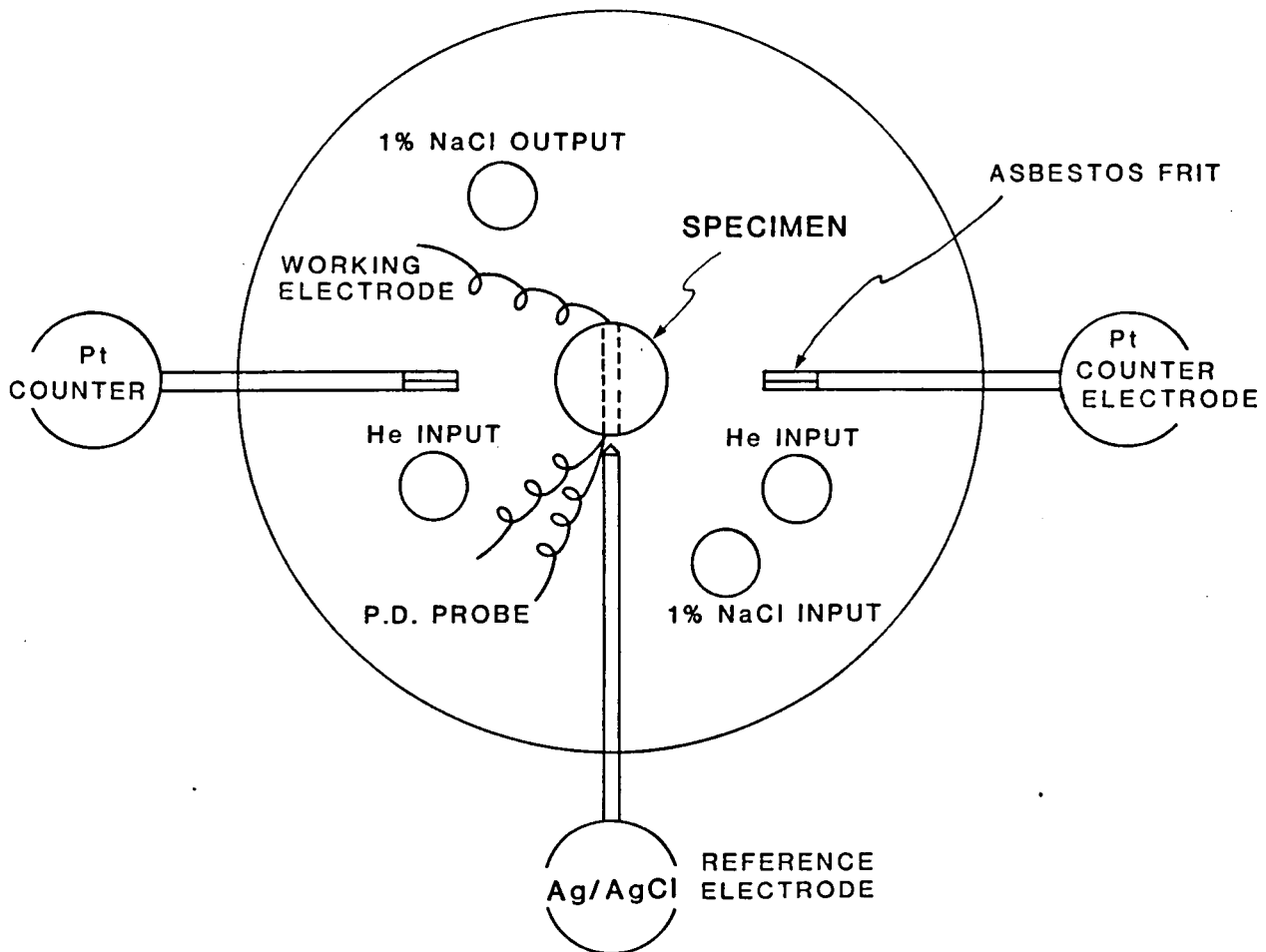


Figure 15

Test cell configuration for aqueous NaCl corrosion fatigue experiments.

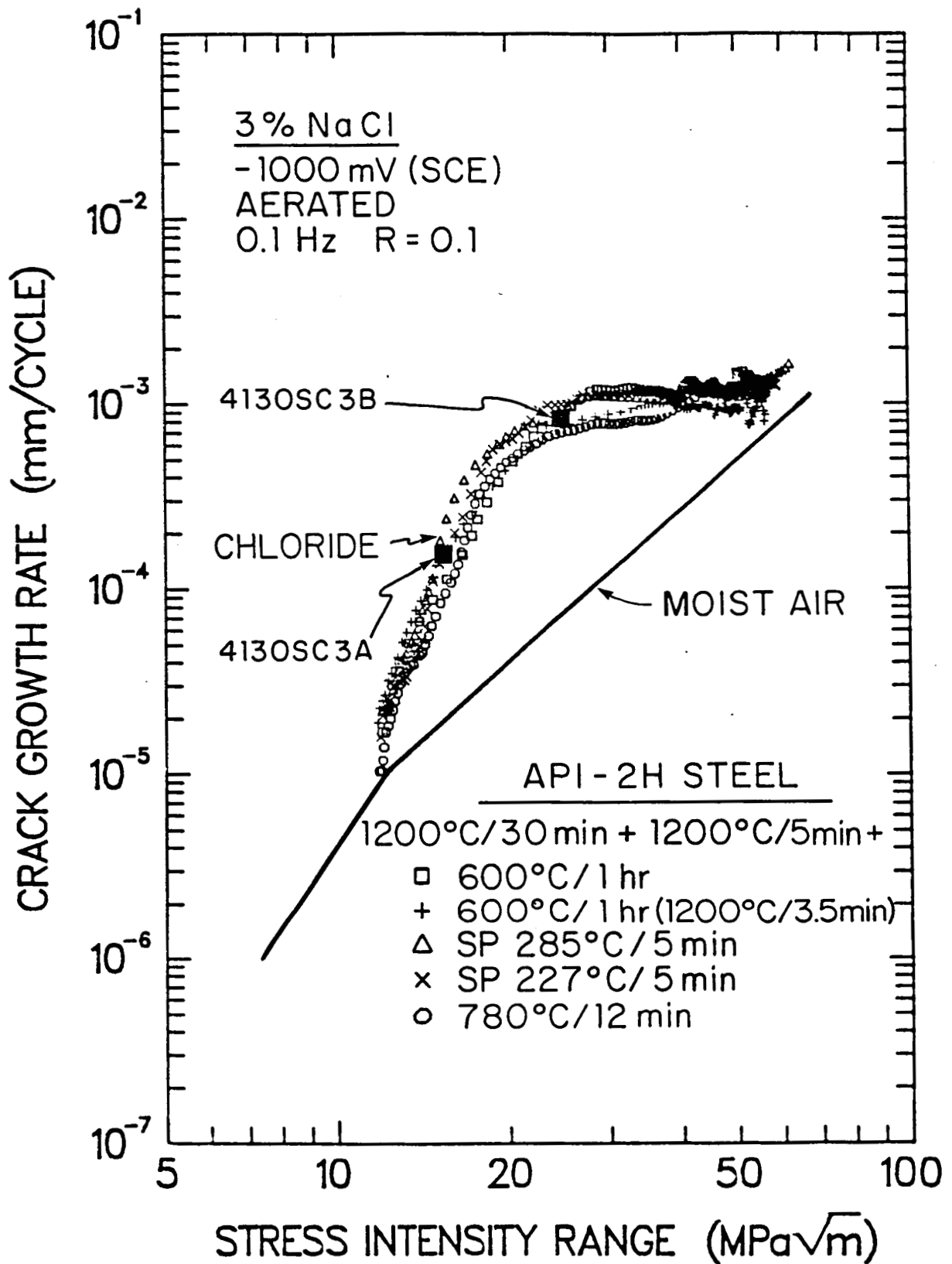


Figure 16

Comparison of two 4130 steel constant ΔK test results with the corrosion fatigue crack growth characteristics of API-2H steel in a deaerated NaCl environment with cathodic polarization.

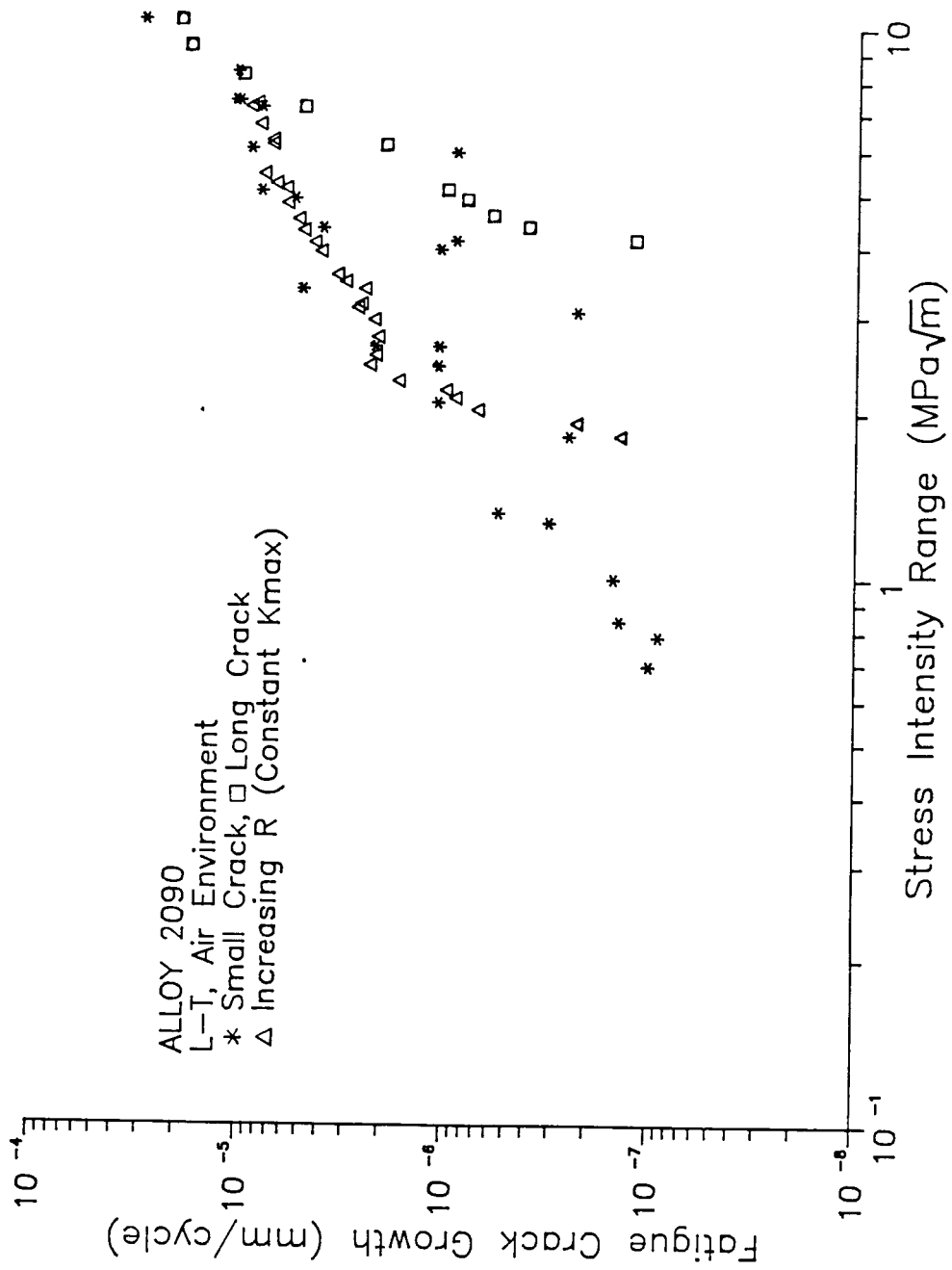


Figure 17

Comparison of the FCG characteristics of Alloy 2090 as measured by microstructurally small crack, long crack high R and long crack low R test techniques (after Ritchie et al. (30,31) and Hertzberg et al. (32).)

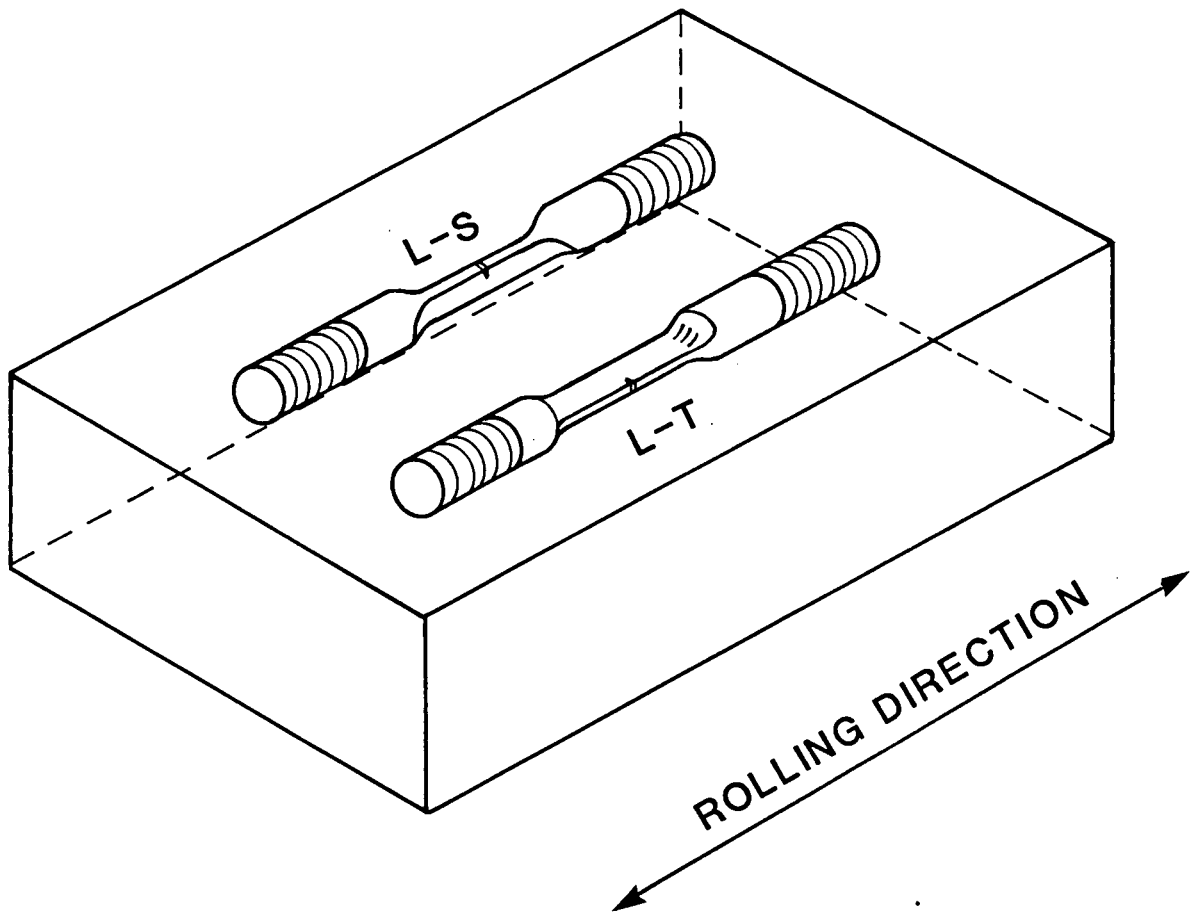


Figure 18

Short crack specimen orientation in rolled aluminum alloy plates.

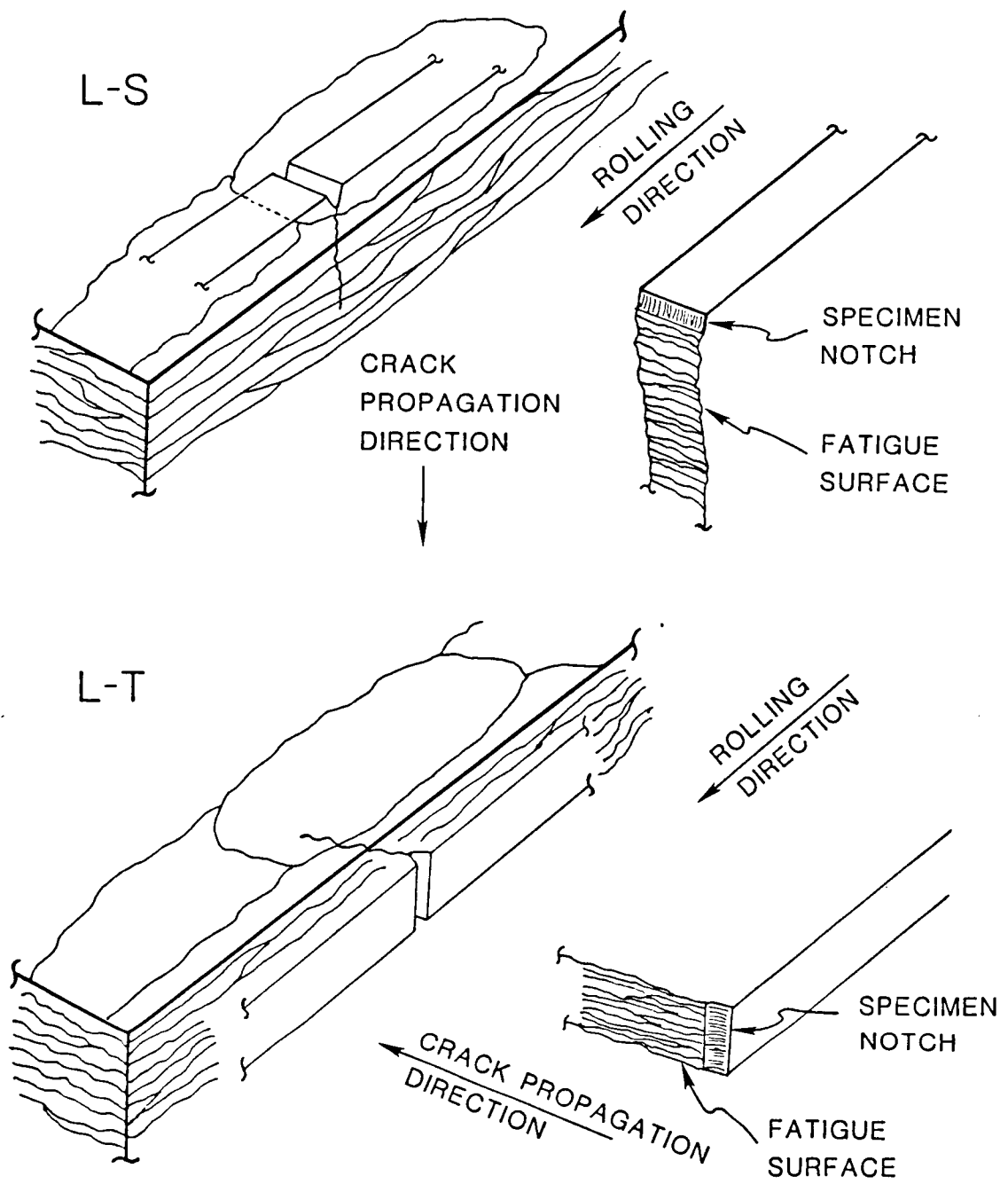
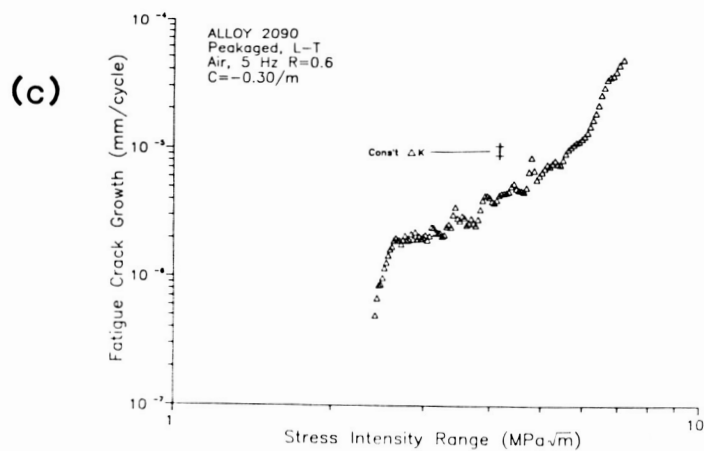
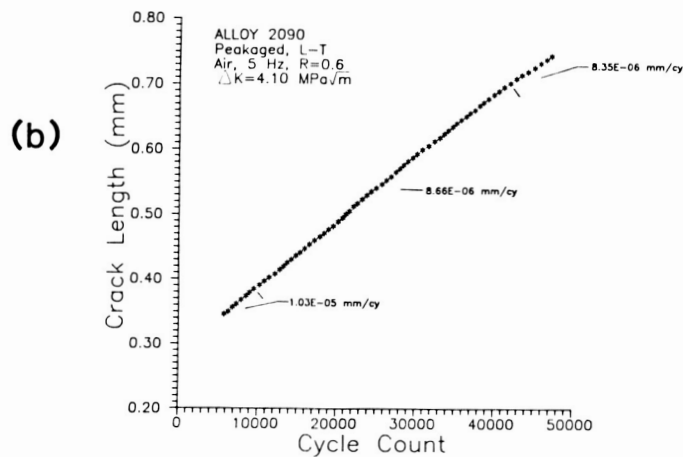
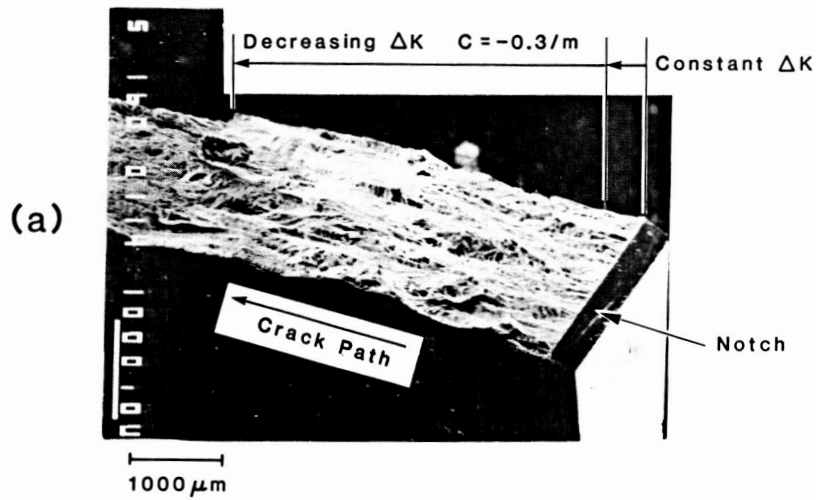


Figure 19

Illustration of short crack orientation for L-T and L-S microstructures.



ORIGINAL PAGE IS
OF POOR QUALITY

Figure 20

Fatigue crack growth in Alloy 2090 in the L-T direction; (a) short crack specimen fracture surface, (b) constant ΔK -constant R test results, (c) comparison of constant ΔK and decreasing ΔK -constant R test results.

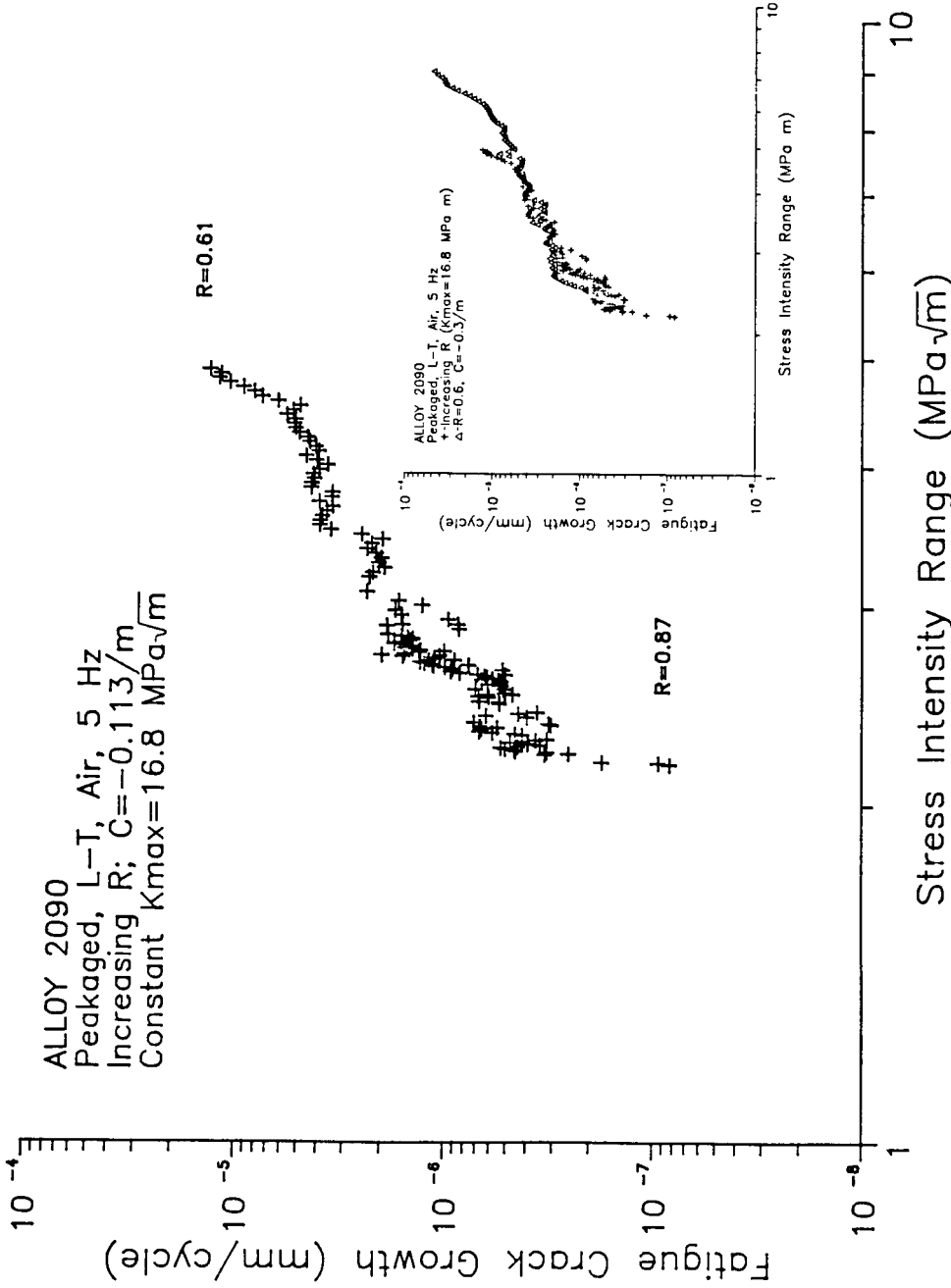


Figure 21

Short crack decreasing ΔK-increasing R/constant K_{max} test results for Alloy 2090 in the L-T orientation.

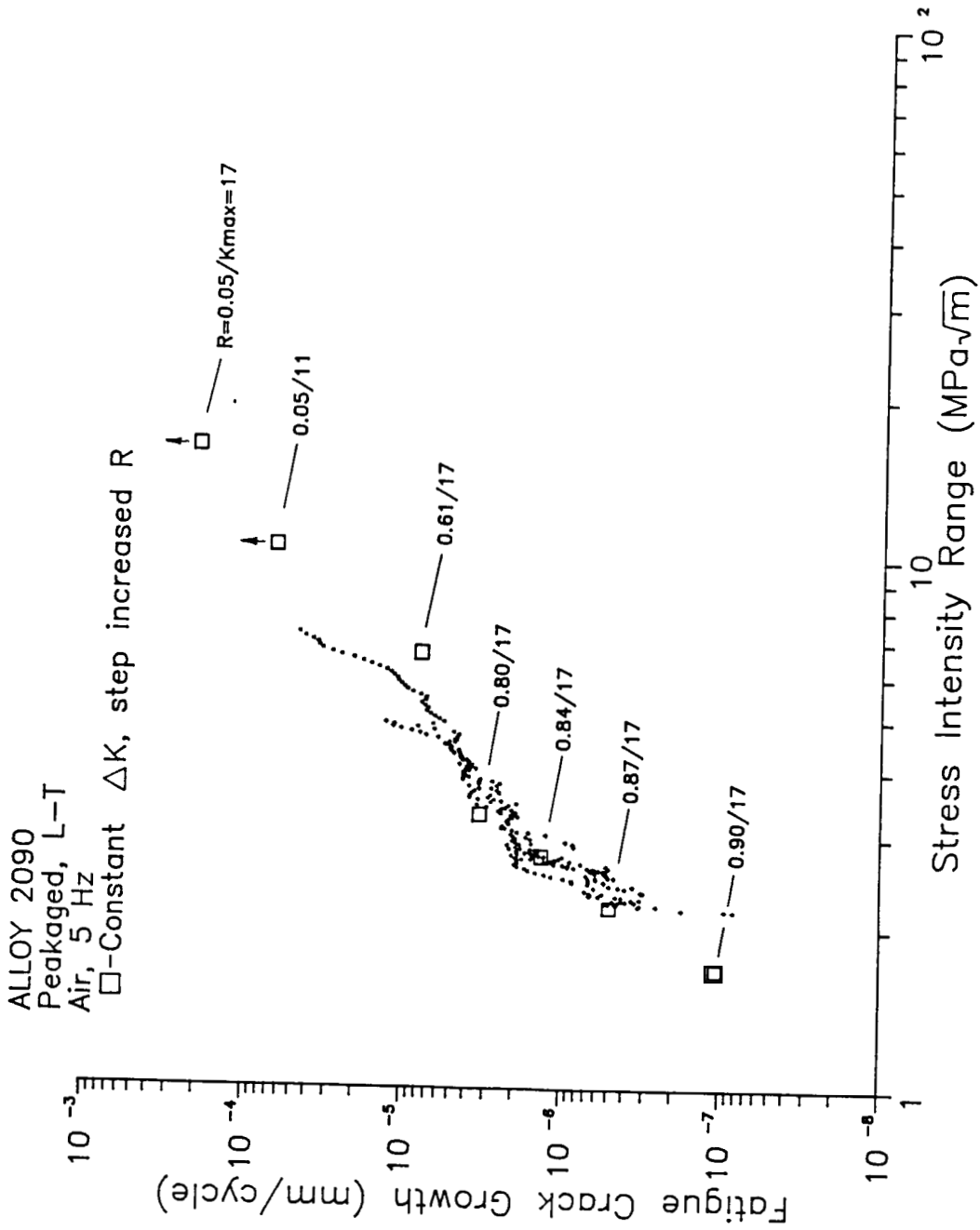


Figure 22

A comparison of the constant ΔK -step increased R/constant K_{max} test results with decreasing ΔK -constant R or constant K_{max} results for Alloy 2090 in the L-T orientation.

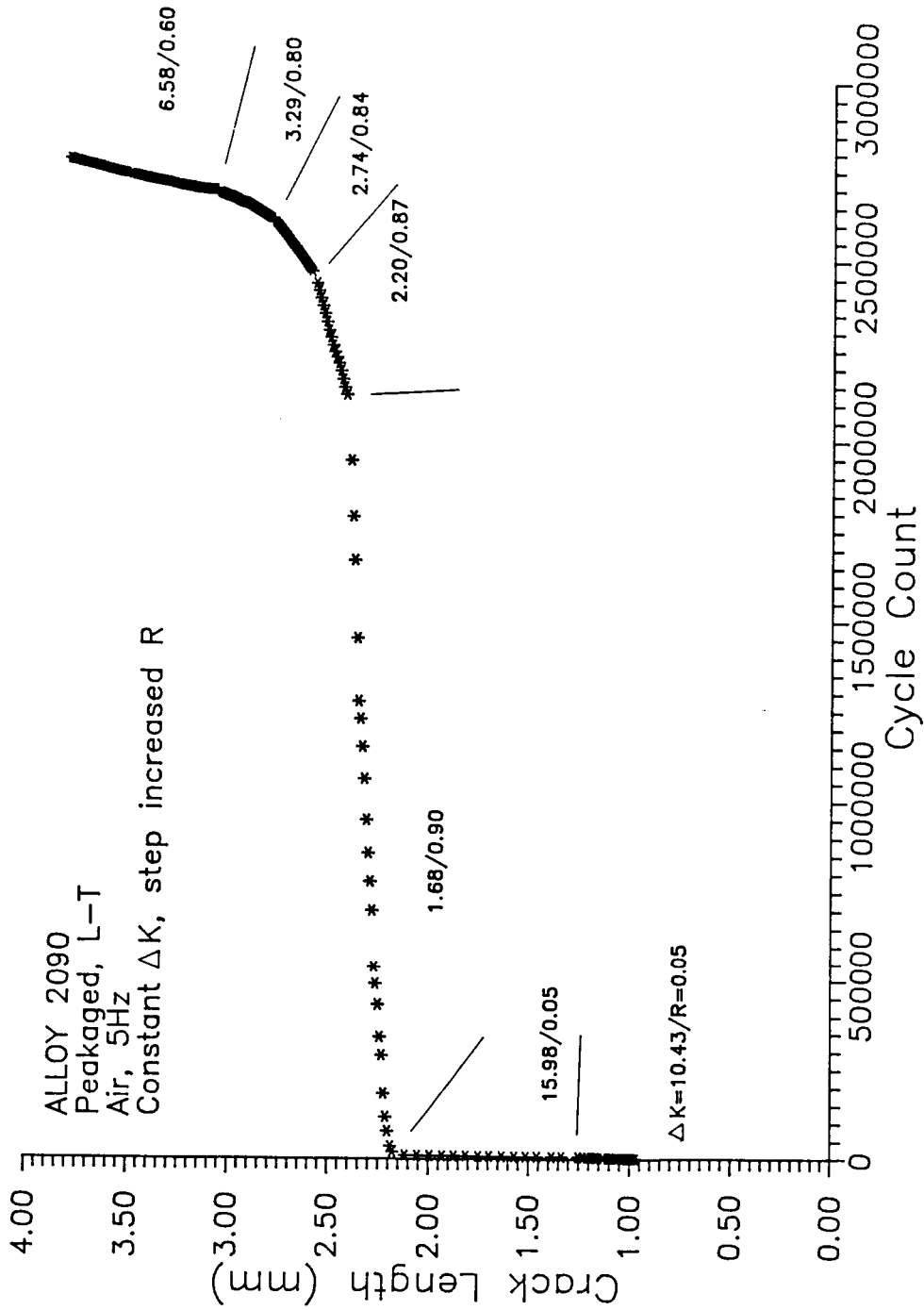


Figure 22a

Crack length versus loading cycles plot of the decreasing ΔK -increasing $R/\text{constant } K_{\text{max}}$ test results shown in Figure 22.

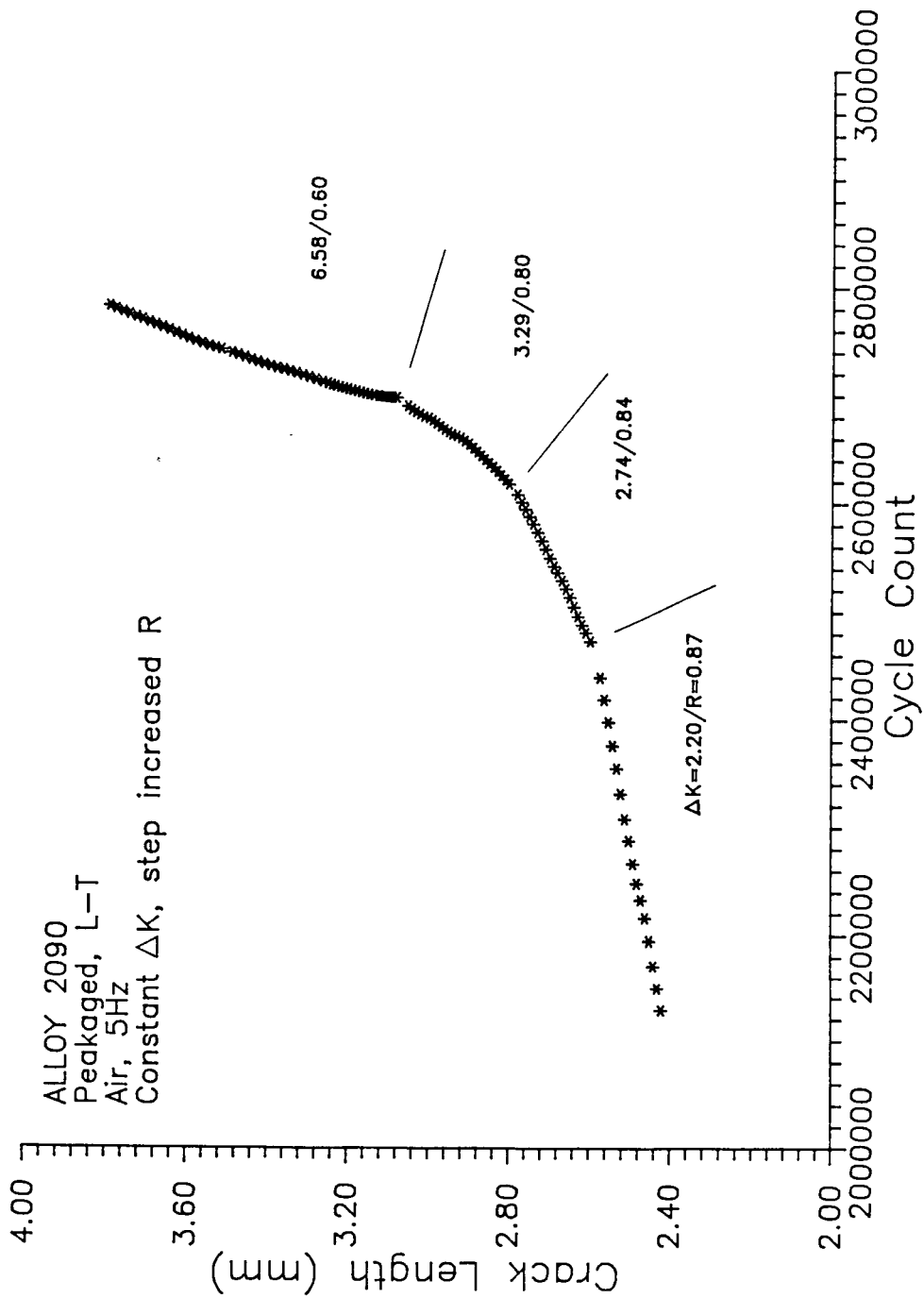


Figure 22b

A detailed crack length versus loading cycles plot of data shown in Figure 22a.

ORIGINAL PAGE IS
OF POOR QUALITY

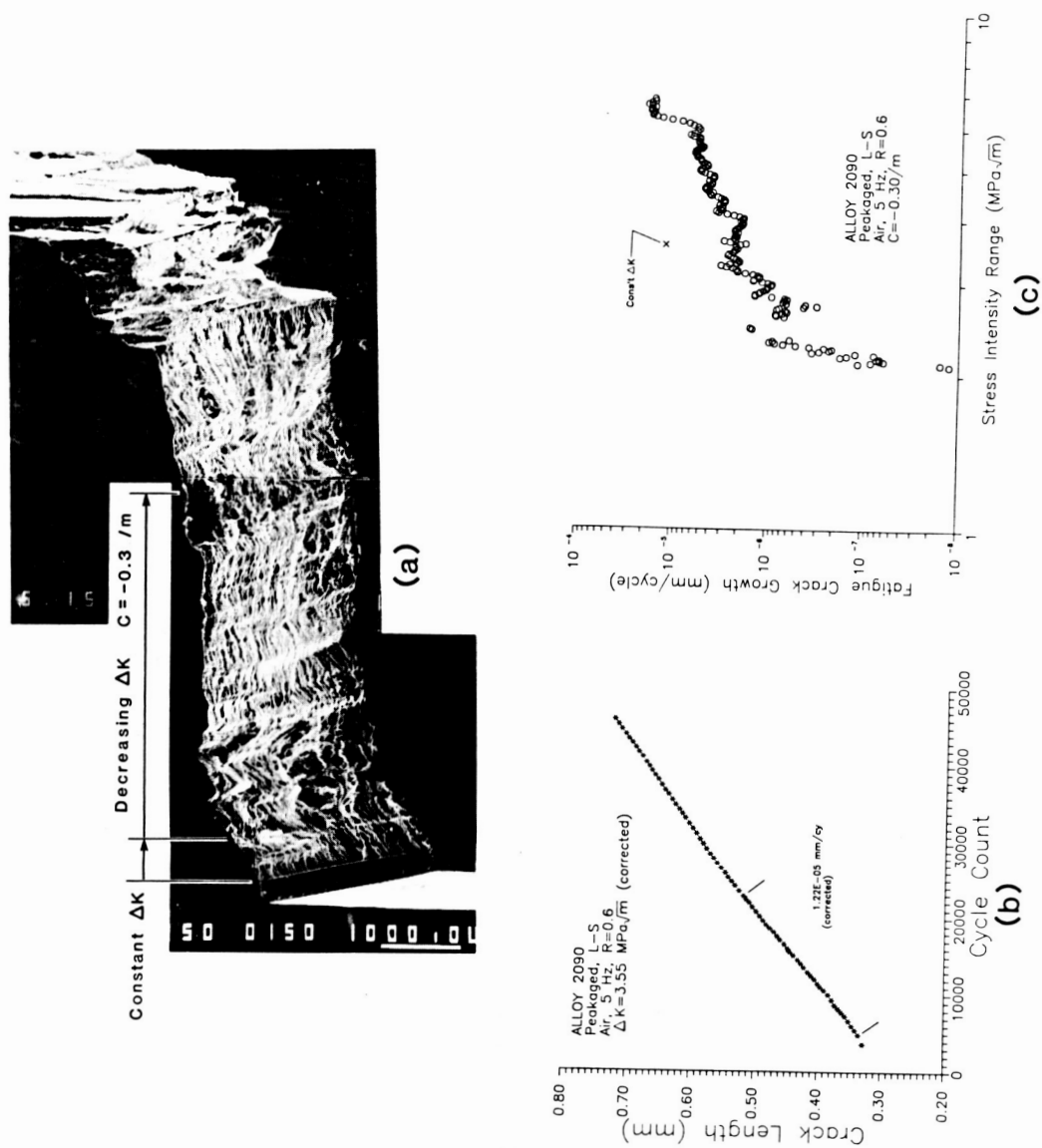


Figure 23

Fatigue crack growth in Alloy 2090 in the L-S direction; (a) short crack specimen fracture surface, (b) constant ΔK -constant R test results, (c) comparison of constant ΔK and decreasing ΔK -constant R test results.

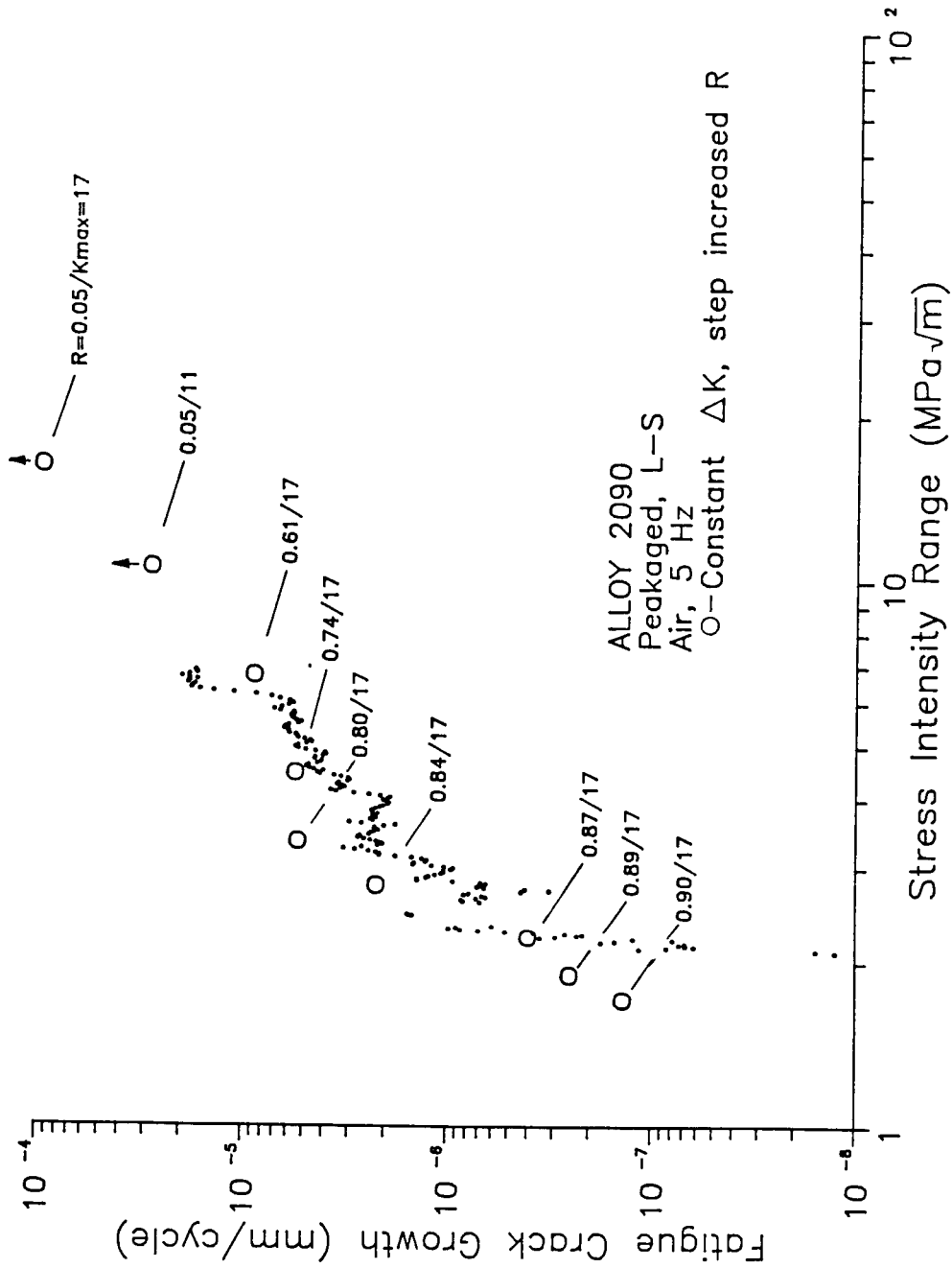


Figure 24

A comparison of the constant ΔK -step increased R/constant K_{max} test results with decreasing ΔK -constant R or constant K_{max} results for Alloy 2090 in the L-S orientation.

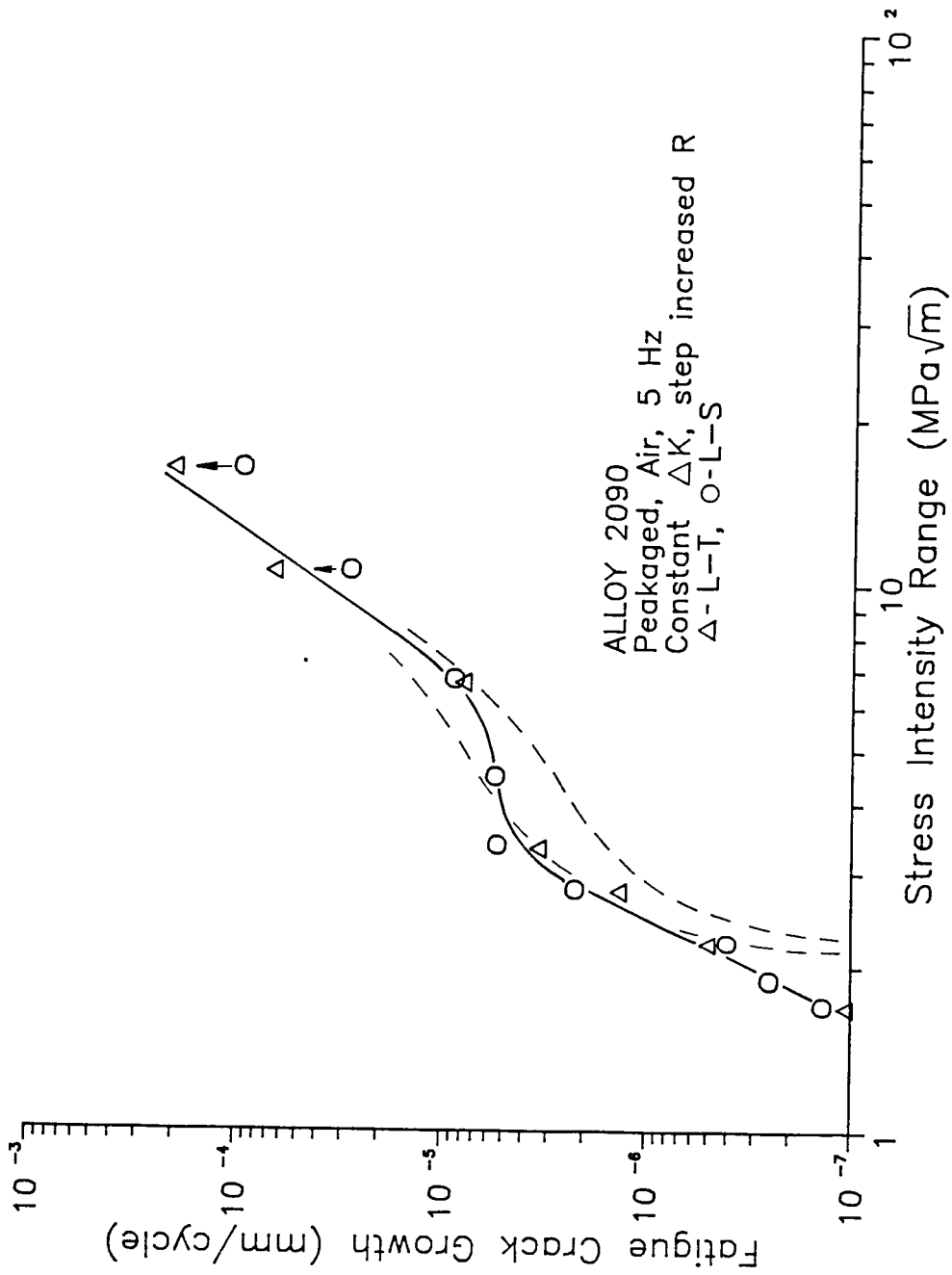


Figure 25

A summary of intrinsic fatigue crack growth in Alloy 2090 for two orientations.

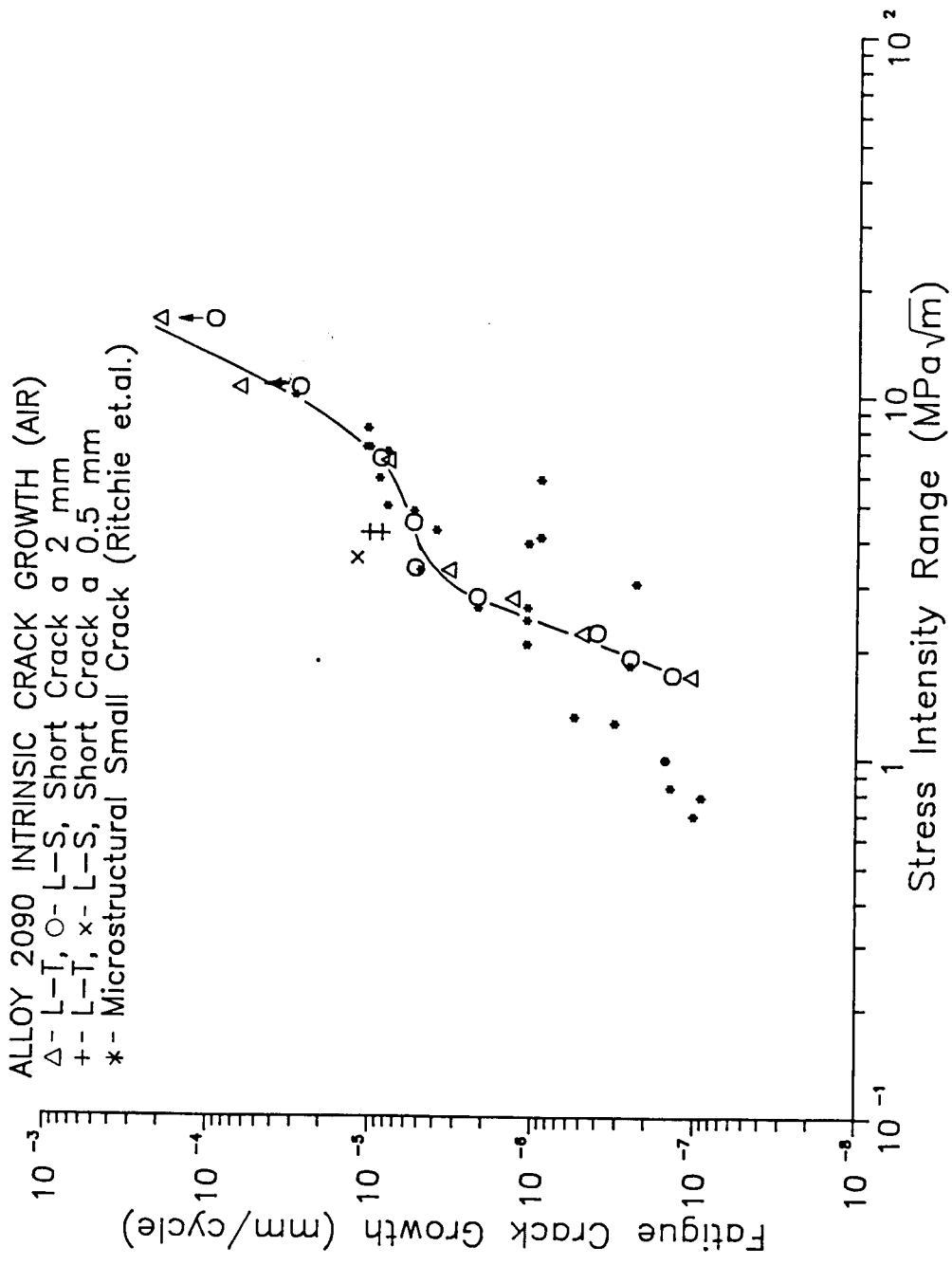


Figure 26

Intrinsic fatigue crack propagation in Alloy 2090, characterized by short crack constant stress intensity techniques and by microstructurally small crack replication procedures after Ritchie et al. (31).

ALLOY 7075, T651, L-S
 5 Hz, Constant ΔK , step increased R
 1% NaCl (-760 mV SCE), 2 kPa Helium
 2 kPa Water Vapor, 20 kPa Oxygen

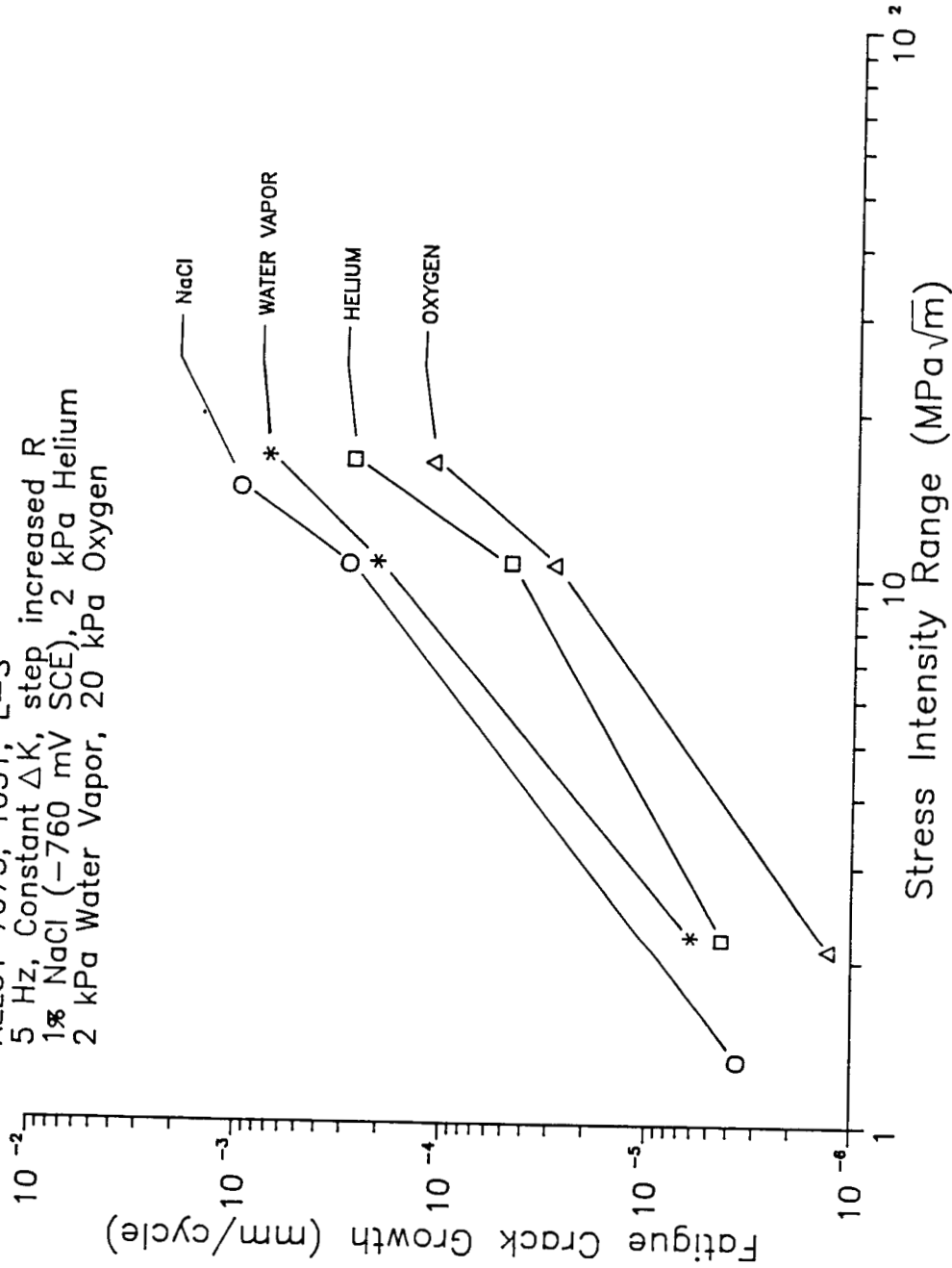


Figure 27

The effect of highly purified gaseous and aqueous environments on intrinsic corrosion fatigue crack growth in peak aged Alloy 7075 in the L-S orientation.

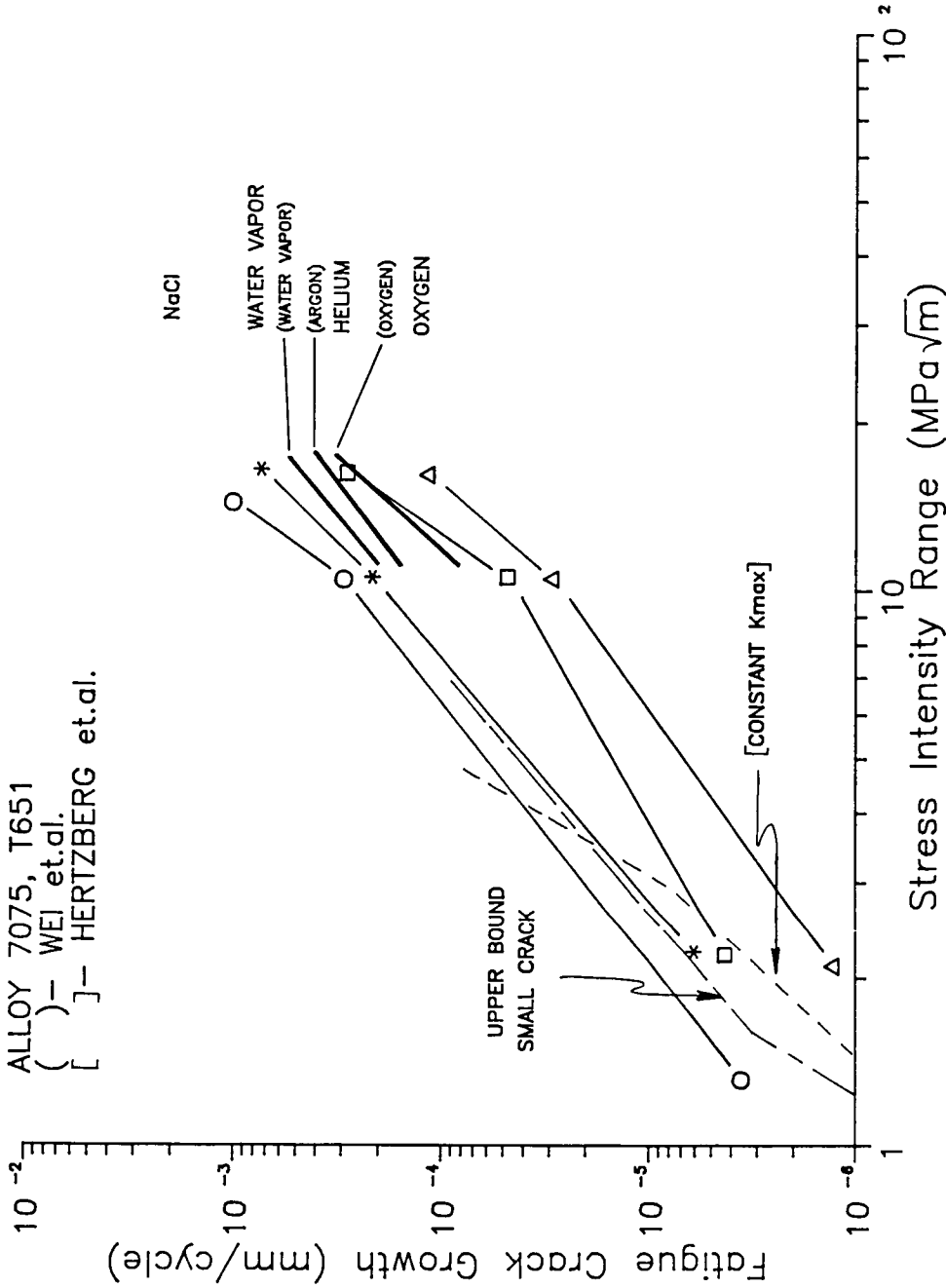


Figure 28

The results of current experiments from Figure 27 compared to literature data for corrosion fatigue at high ΔK (37) and to literature data for near threshold intrinsic fatigue crack growth (32).

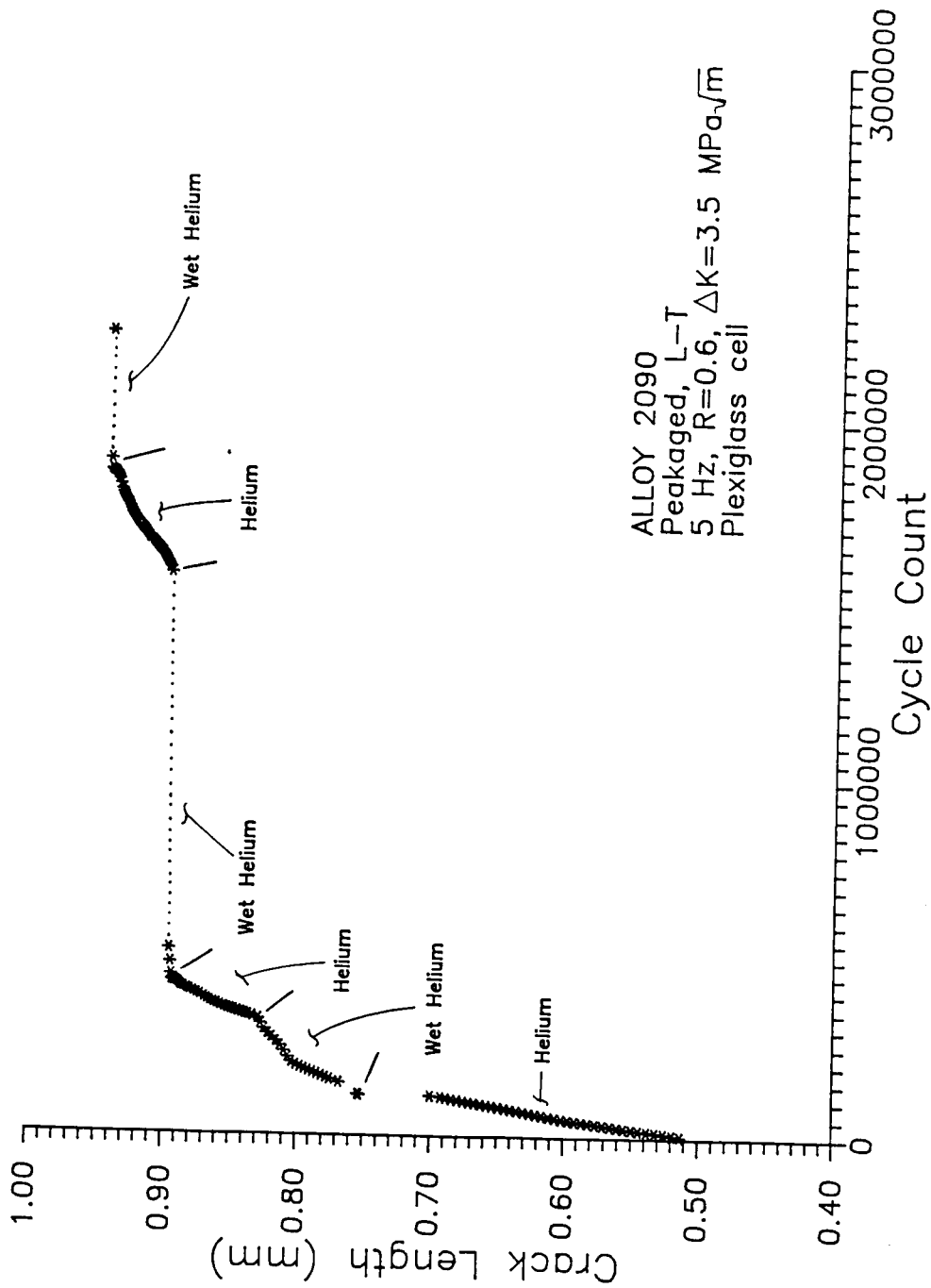


Figure 29

The effect of impure helium and water vapor + helium environments on fatigue crack growth in Alloy 2090 at constant stress intensity and constant R.

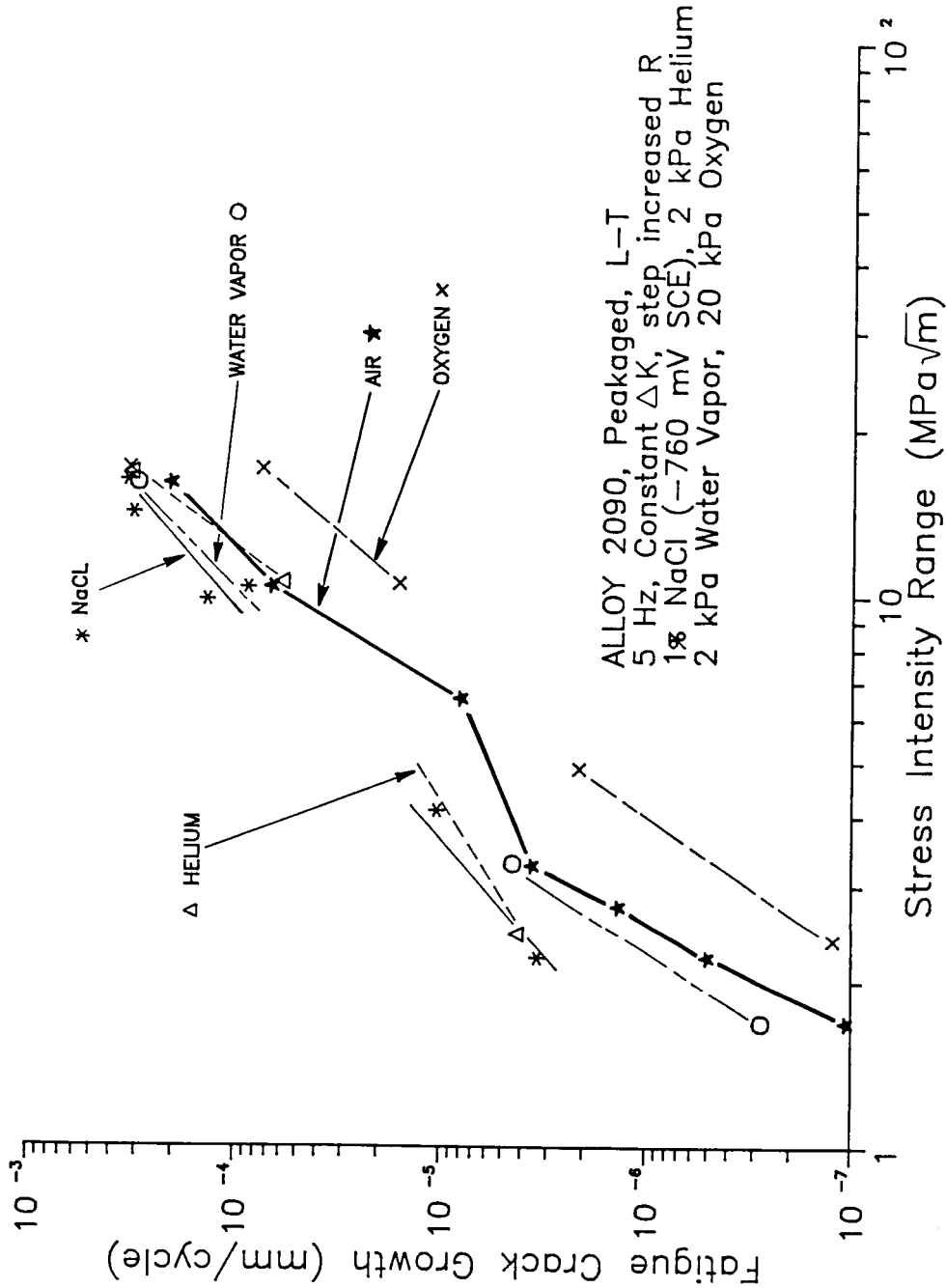


Figure 30

The effect of highly purified gaseous and aqueous environments on intrinsic corrosion fatigue crack growth in peak aged Alloy 2090 in the L-T orientation.

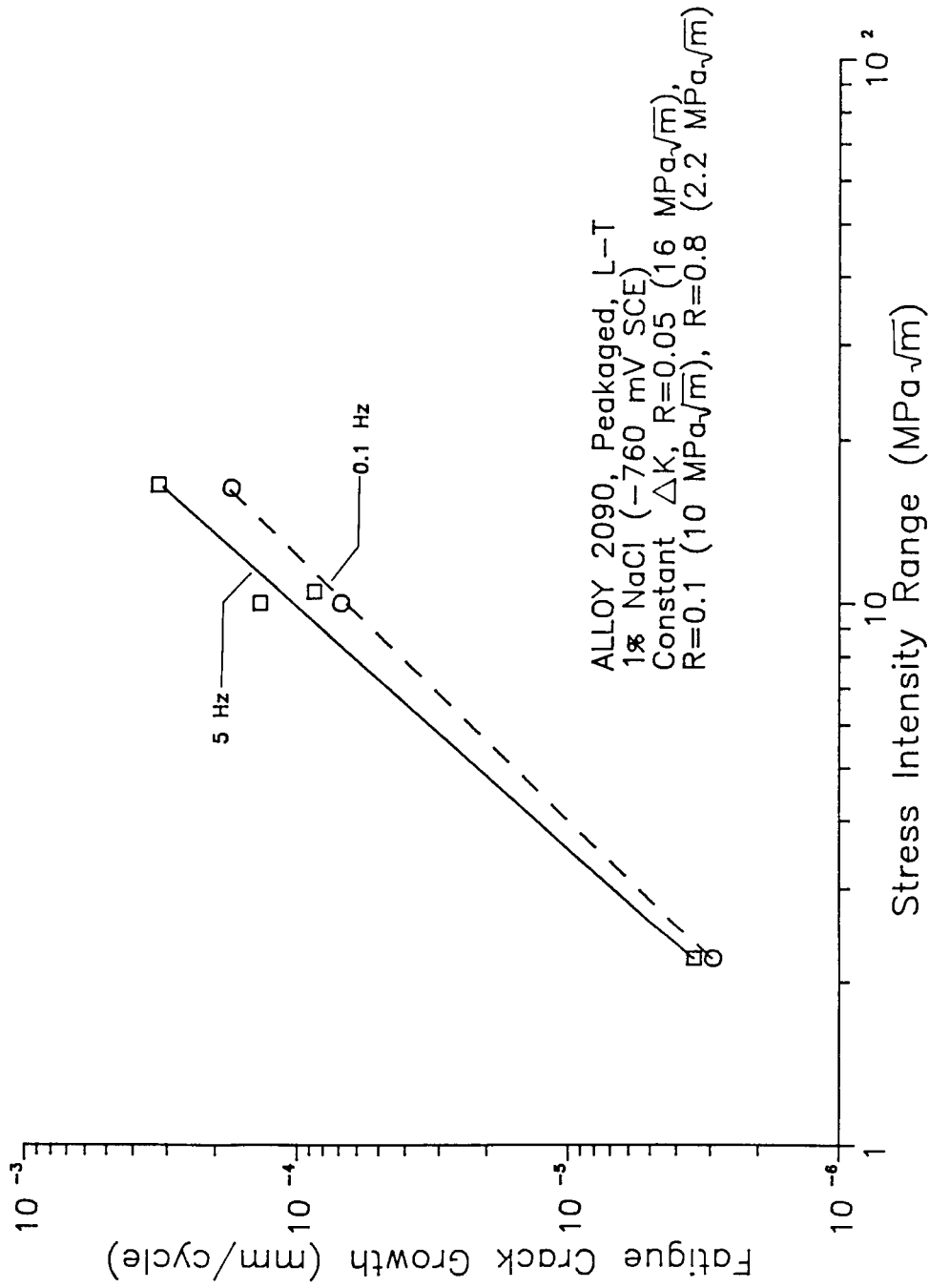


Figure 31

The effect of cyclic loading frequency on intrinsic corrosion fatigue crack propagation in L-T peak aged Alloy 2090 exposed to aqueous 1% NaCl at constant anodic potential.

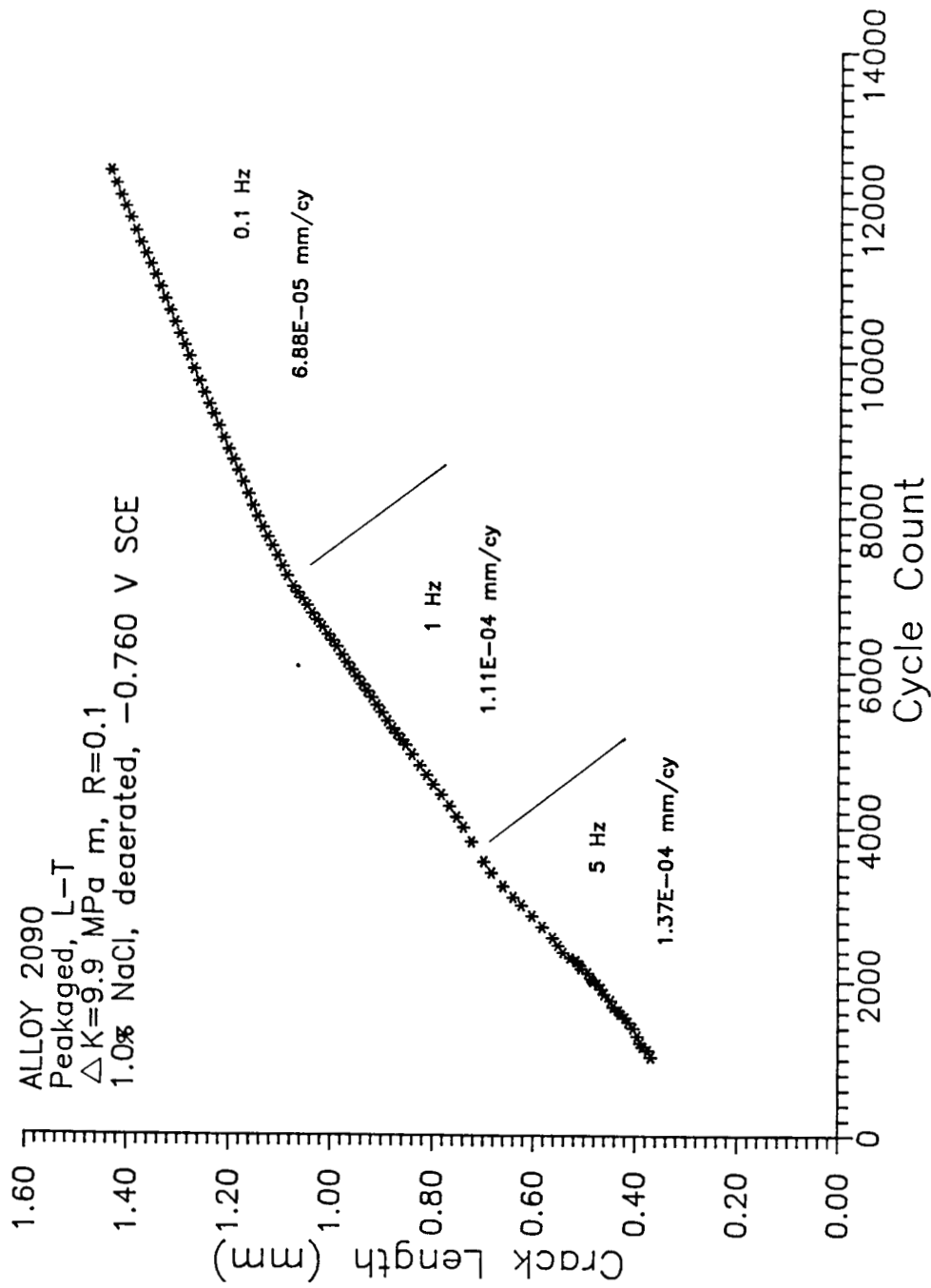


Figure 32

The effect of frequency on corrosion fatigue crack propagation in Alloy 2090 exposed to aqueous 1% NaCl at constant high applied stress intensity range and applied electrode potential.

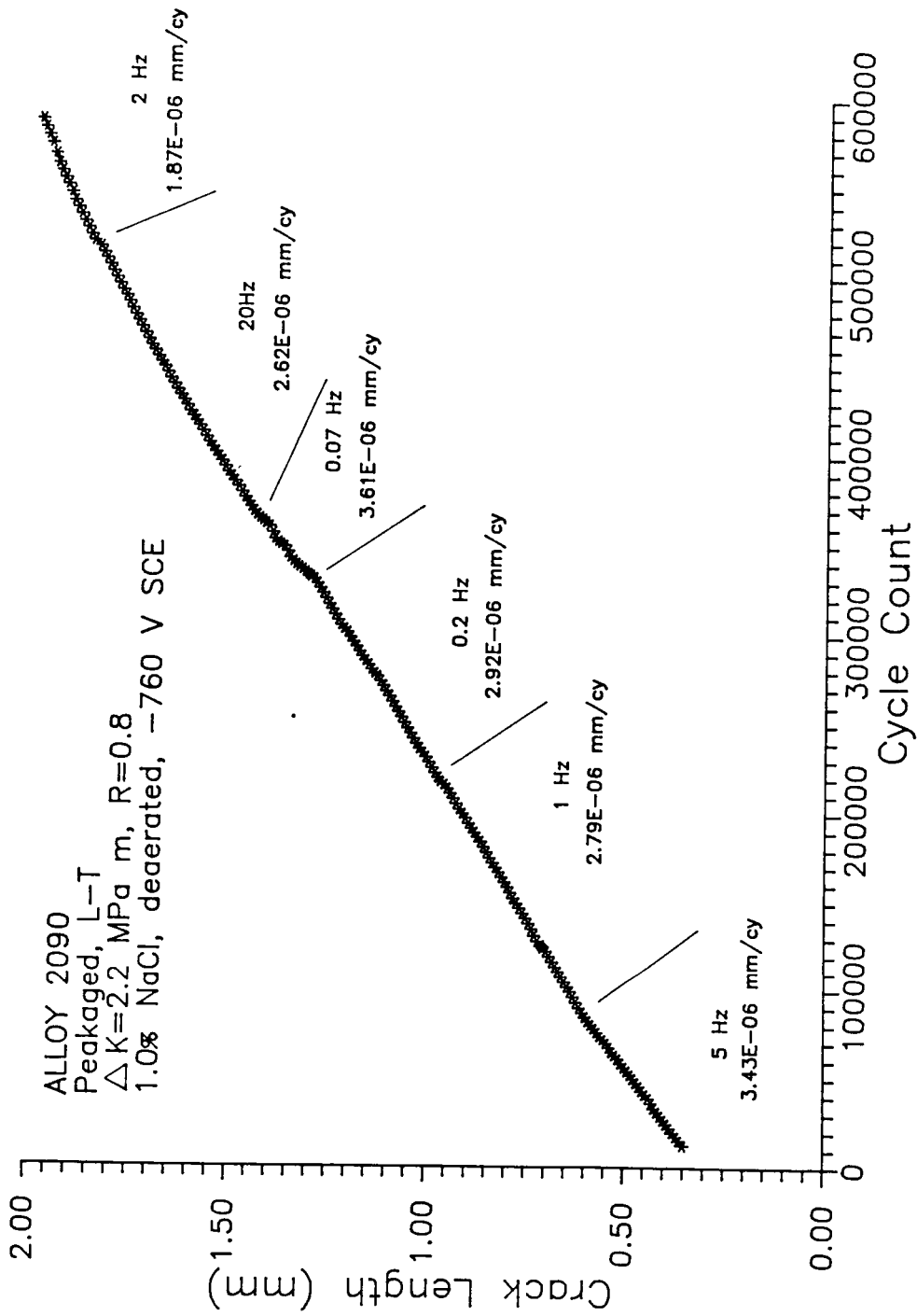


Figure 33

The effect of frequency on corrosion fatigue crack propagation in Alloy 2090 exposed to aqueous 1% NaCl at constant low applied stress intensity range and applied electrode potential.

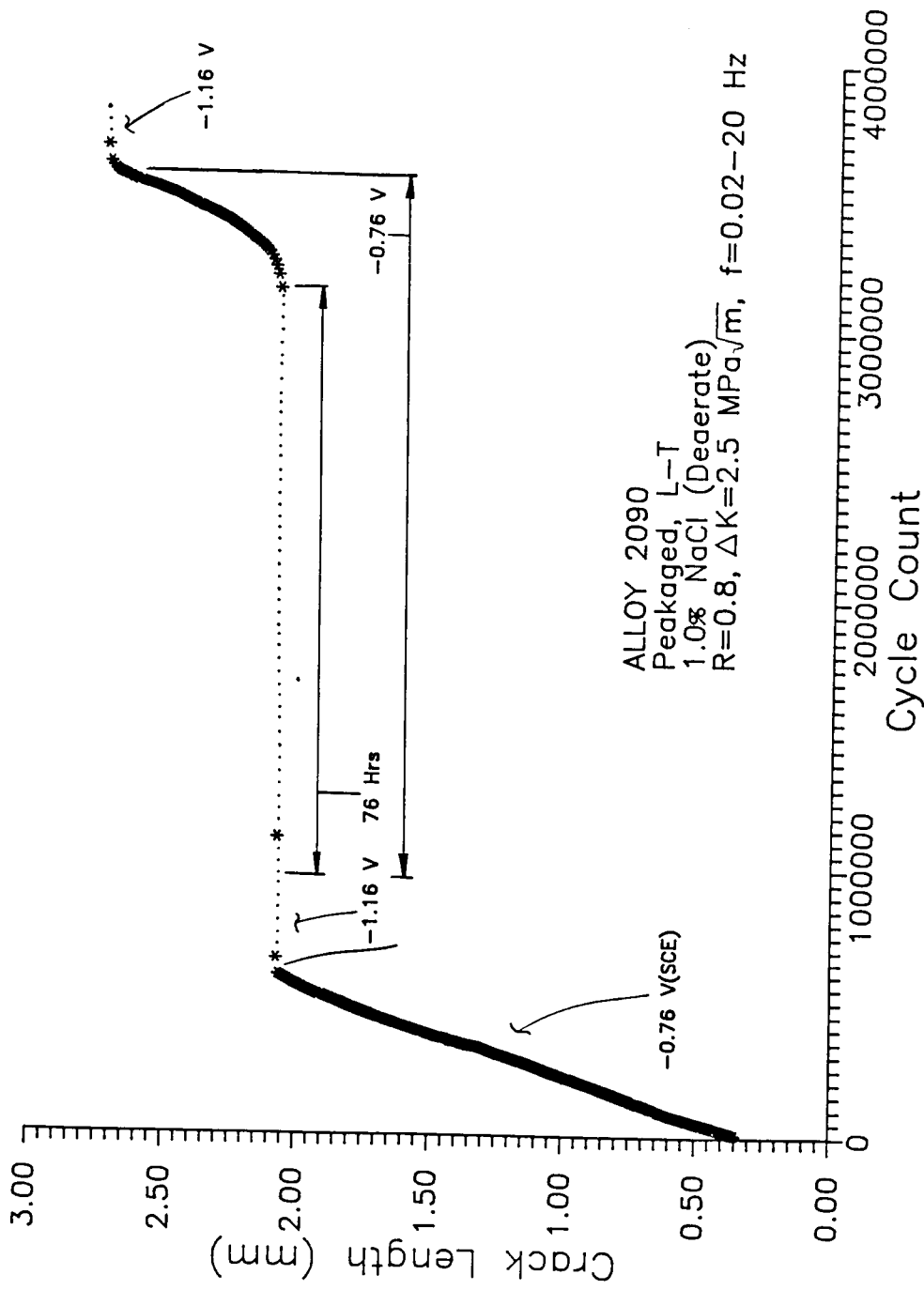


Figure 34

The effect of cathodic polarization on the intrinsic corrosion fatigue crack growth rate in L-T peak aged Alloy 2090 at a constant ΔK of 2.5 $\text{MPa}\sqrt{\text{m}}$ in deaerated 1% NaCl.

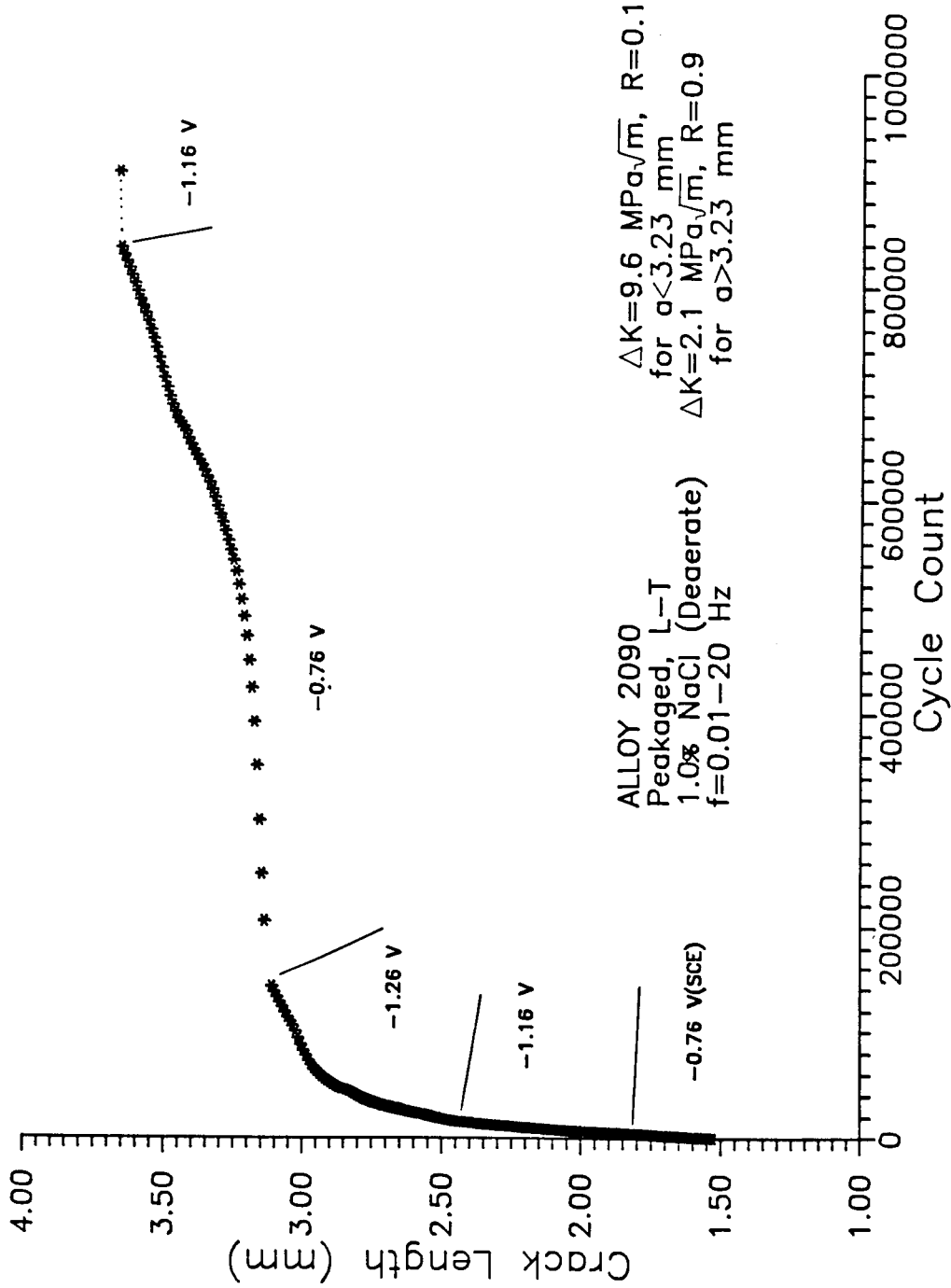


Figure 35

The effect of cathodic polarization on the intrinsic corrosion fatigue crack growth rate in L-T peak aged Alloy 2090 at constant ΔK levels of 2.1 and 9.6 $\text{MPa}\sqrt{\text{m}}$ for high and low R conditions, respectively and in deaerated 1% NaCl.

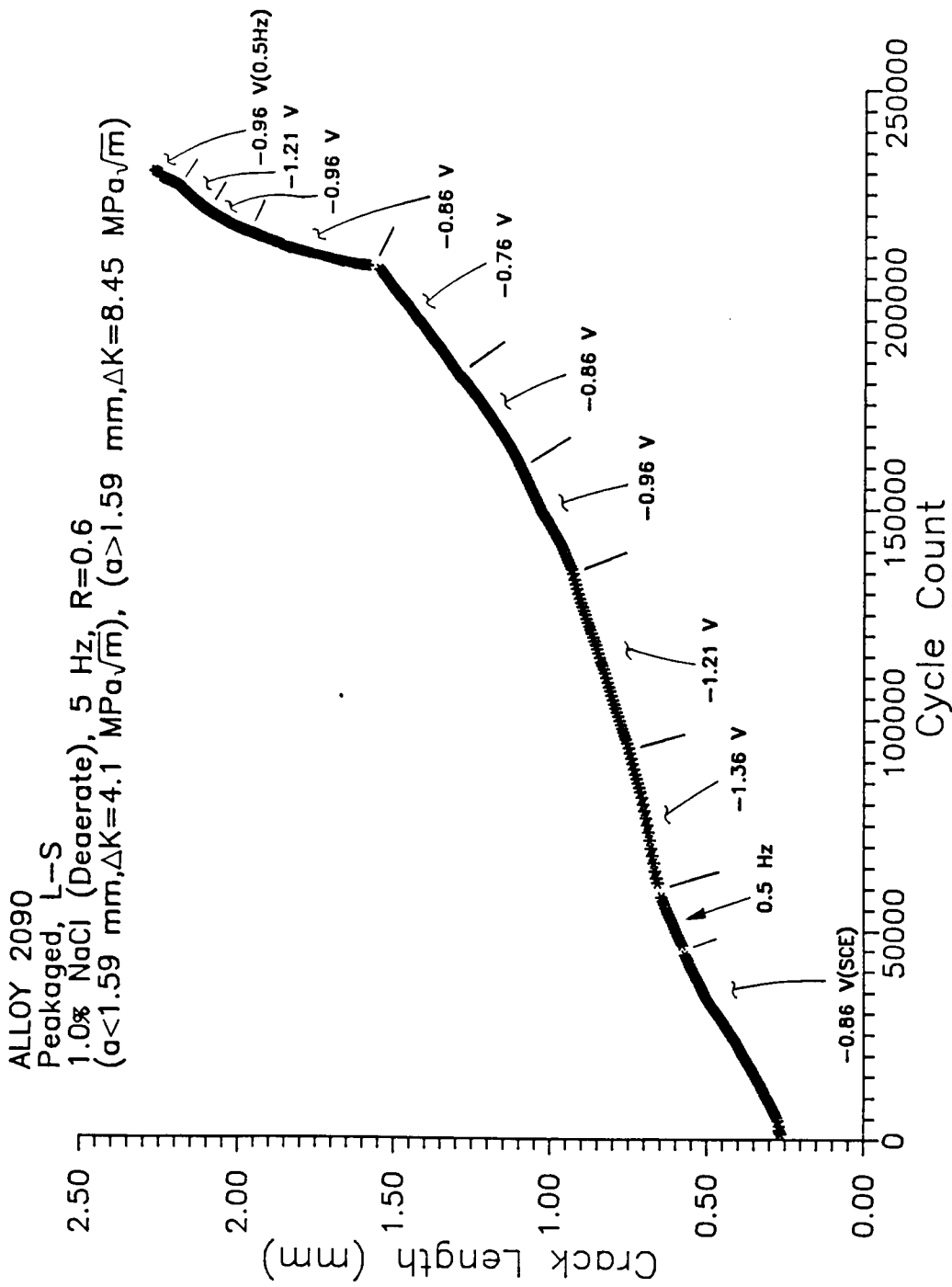


Figure 36

The effect of cathodic polarization on the intrinsic corrosion fatigue crack growth rate in L-S peak aged Alloy 2090 at constant ΔK levels of 4.1 and 8.5 MPa $\sqrt{m}^{\frac{1}{2}}$ at high low R = 0.6 and in deaerated 1% NaCl.

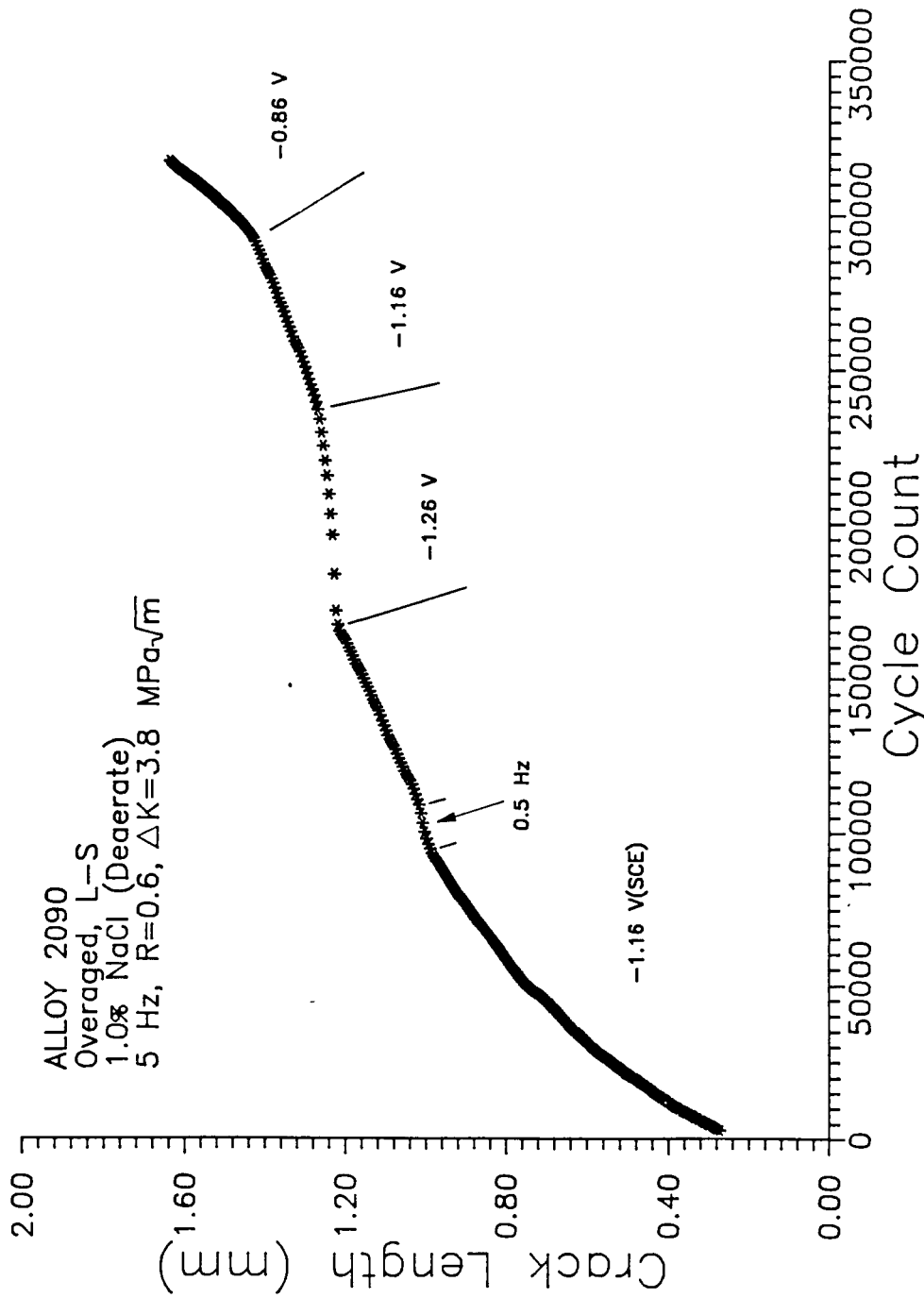


Figure 37

The effect of cathodic polarization on the intrinsic corrosion fatigue crack growth rate in L-S over aged Alloy 2090 at a constant ΔK level of $3.8 \text{ MPa}\sqrt{\text{m}}$ for high R = 0.6 and in deaerated 1% NaCl.

ORIGINAL PAGE IS
OF POOR QUALITY

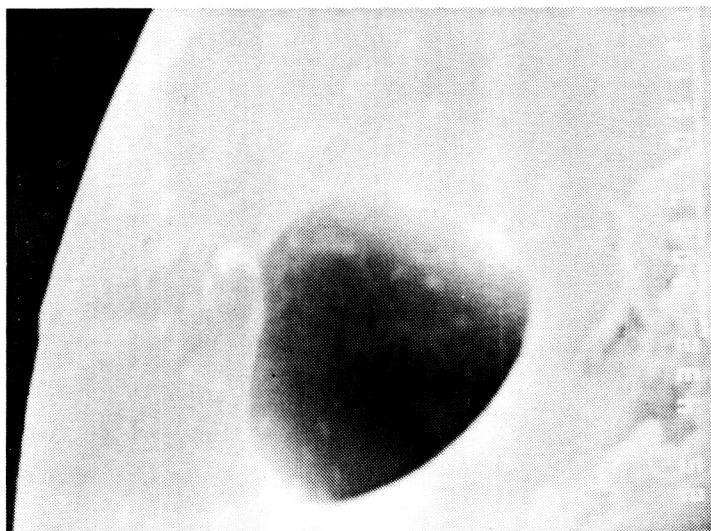
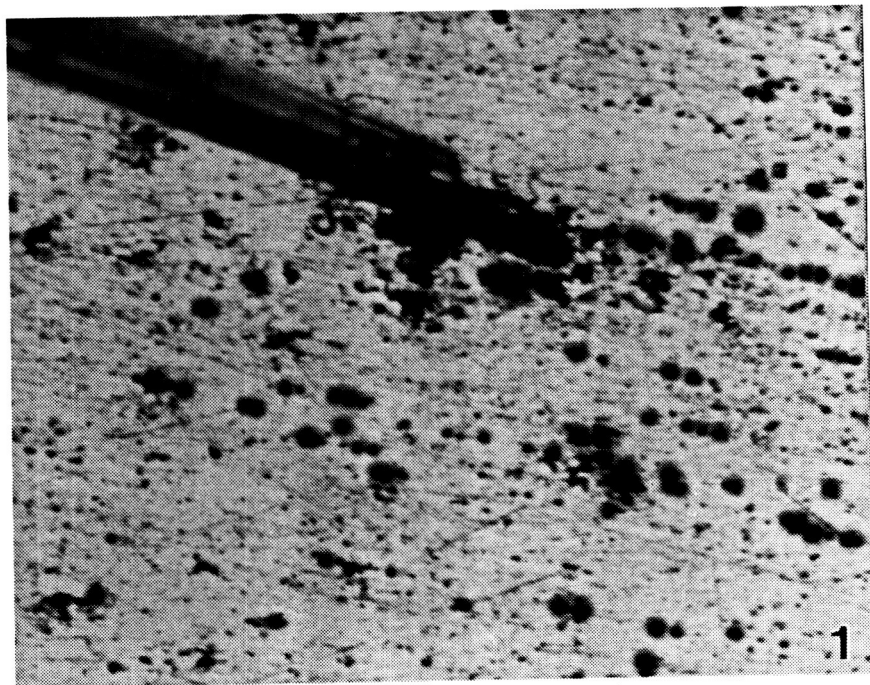


Figure 38

Scanning electron photomicrograph of the drawn tip of a glass pipette used in constructing a microreference electrode.

ORIGINAL PAGE IS
OF POOR QUALITY



50 μ m

Figure 39

Optical photomicrograph of a microreference electrode situated to measure the variation in potential due to the activity of the corroding pit on peak aged 2090 in 3.5 w/o NaCl solution.

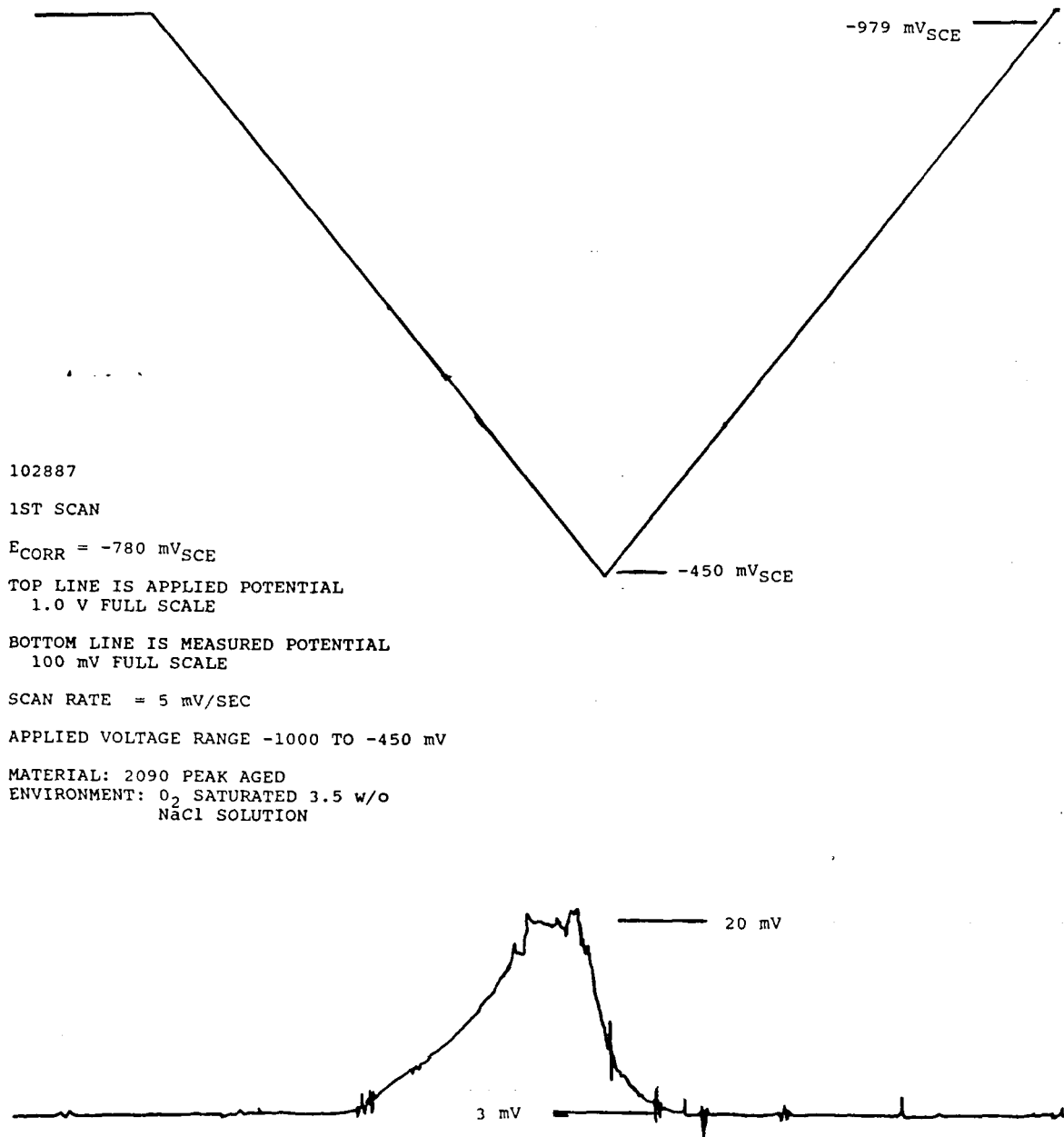


Figure 40

Plot of applied potential and potential variation measured by microreference electrode over a pit during a polarization scan vs. time. Peak aged 2090, 3.5 w/o NaCl solution.

ORIGINAL PAGE IS
OF POOR QUALITY

11987

1 ST SCAN

TOP LINE IS APPLIED POTENTIAL
2.0 V FULL SCALE

BOTTOM LINE IS MEASURED POTENTIAL
5 mV FULL SCALE

SCAN RATE = 5 mV/SEC

APPLIED VOLTAGE RANGE -1300 TO -450 mV

MATERIAL: 2090 PEAK AGED
ENVIRONMENT: O₂ SATURATED 3.5 w/o
NaCl SOLUTION

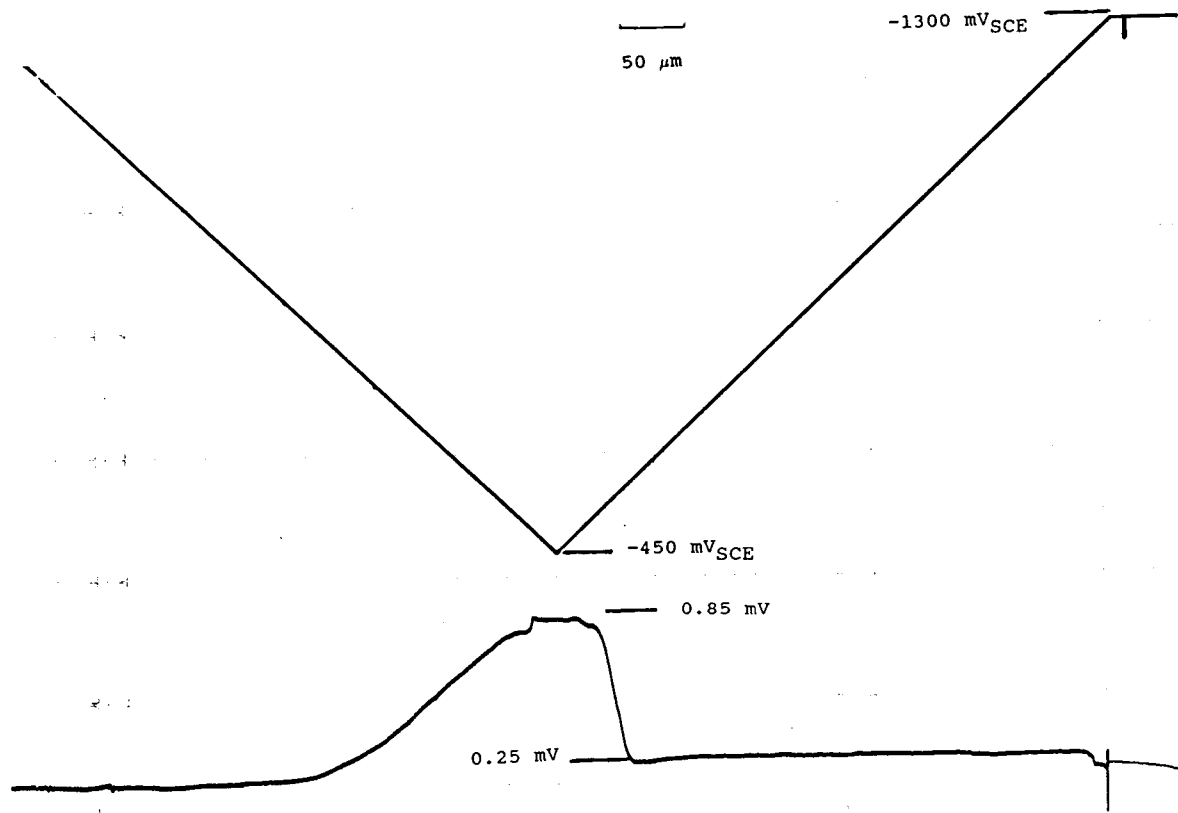


Figure 41

Same plot as in Figure 3. Measure potential represents the difference in potential between a microreference electrode near a pit and one removed from the pit by several hundred micrometers.

ORIGINAL PAGE IS
OF POOR QUALITY



50 μm

Figure 42

Optical photomicrograph of the evolution of gas bubbles during an in situ corrosion observation experiment.

ORIGINAL PAGE IS
OF POOR QUALITY

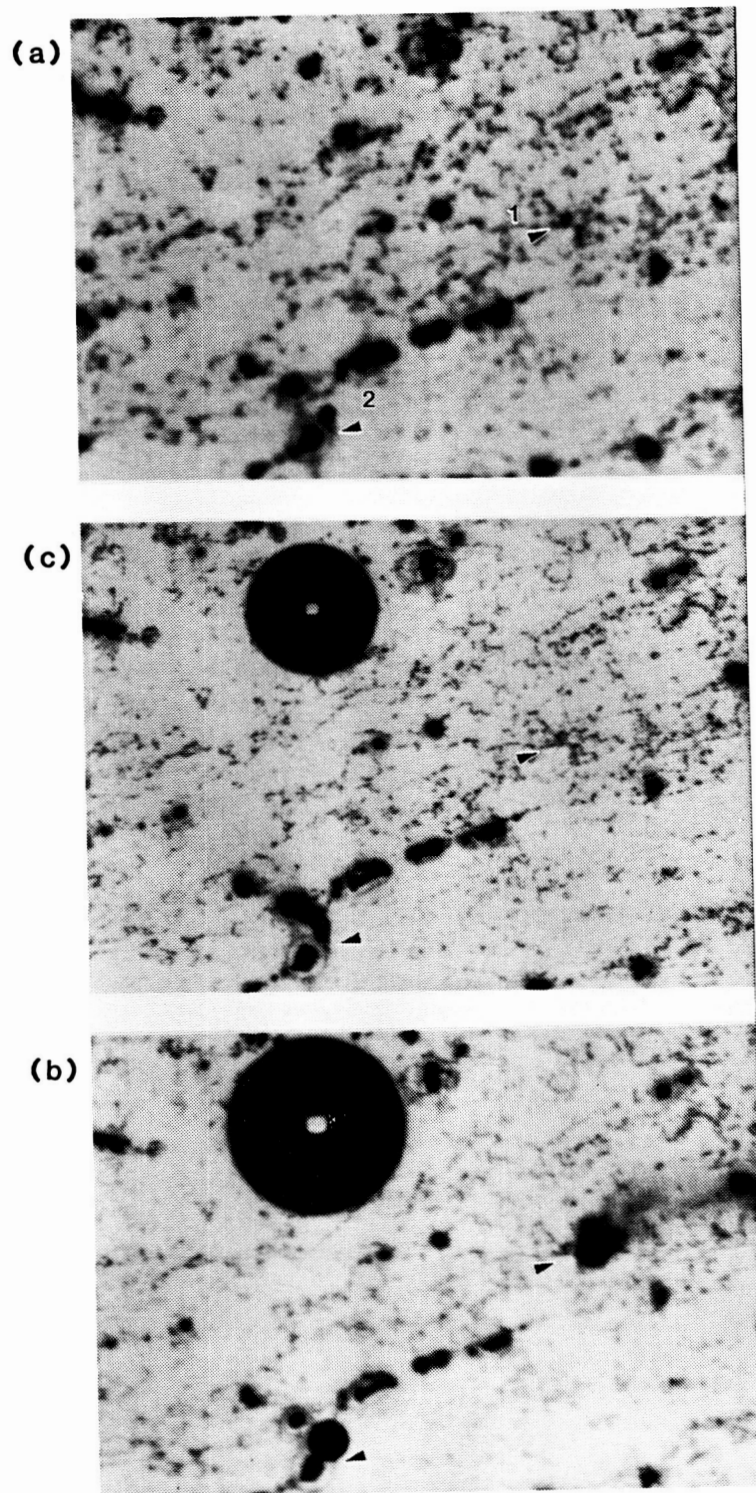


Figure 43 (a) No visible activity of E_{CORR} ($-1.0 V_{SCE}$).
(b) Site 1 inactive, site 2 active at $-1.3 V_{SCE}$.
(c) Site 1 active, site 2 inactive at $-0.7 V_{SCE}$.

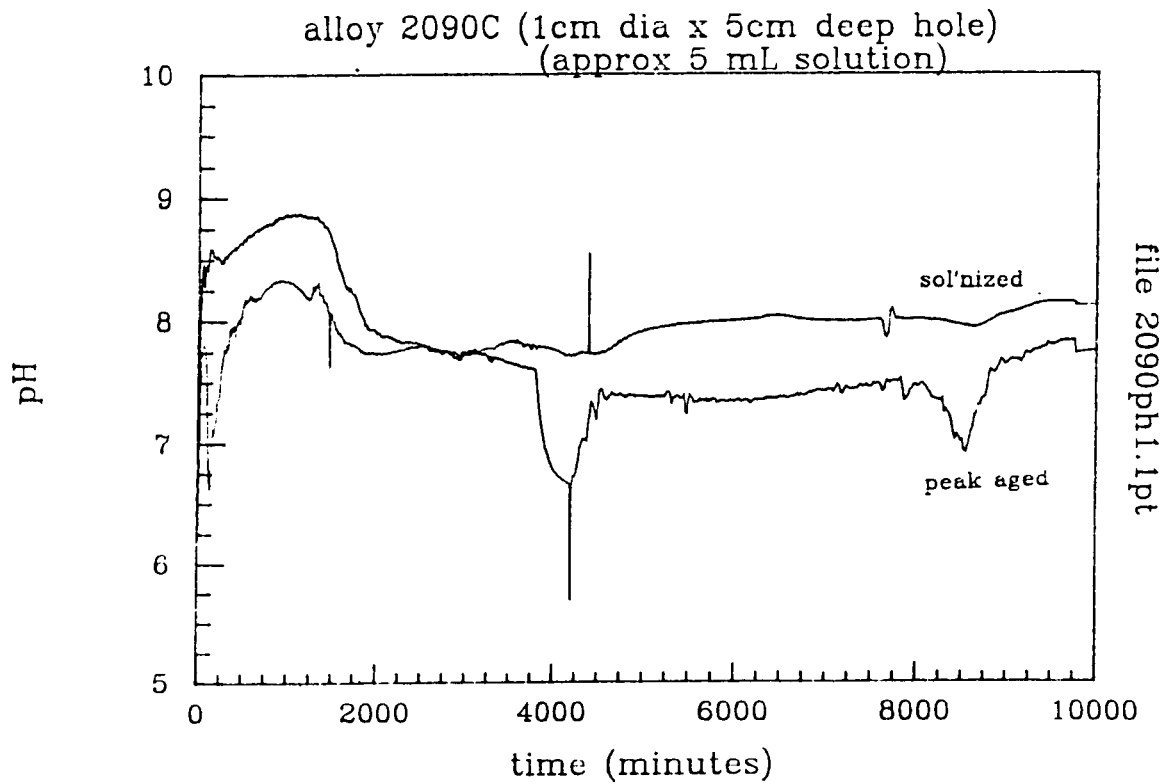


Figure 44

Plot of pH vs. time for 2090 in solutionized and peak aged conditions in an artificial crevice experiment.

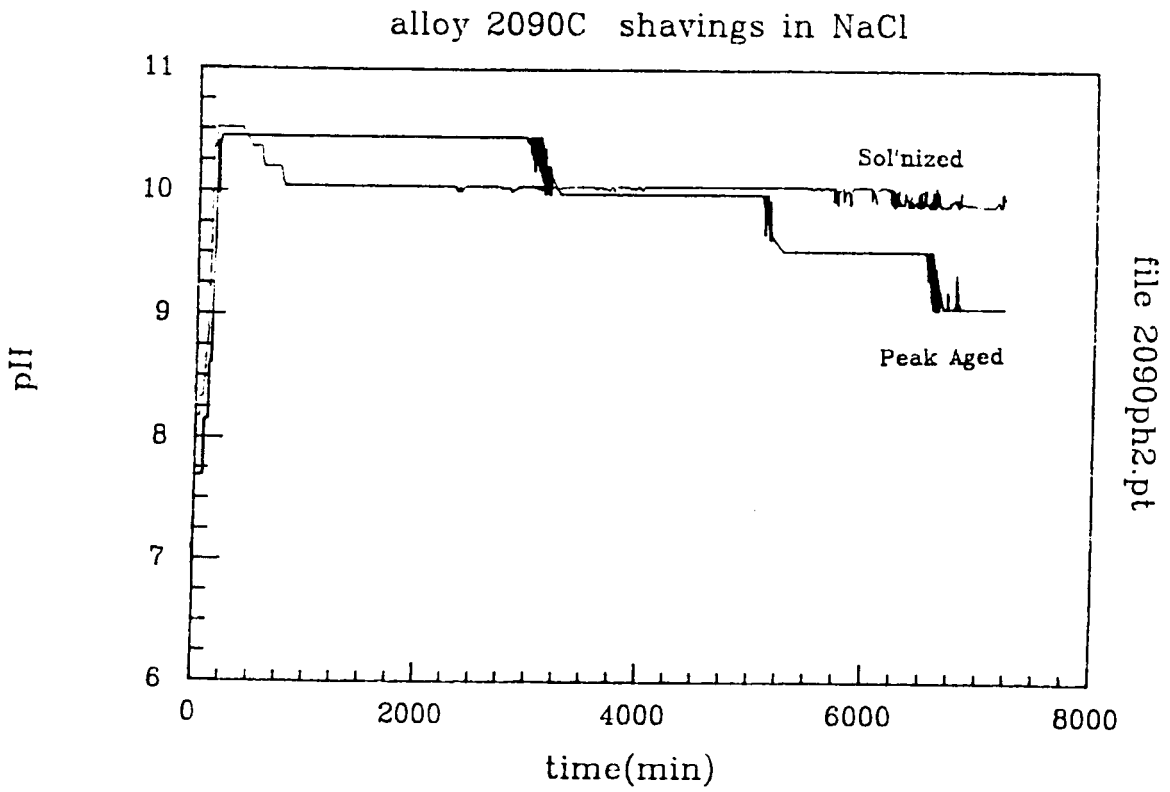


Figure 45

Plot of pH vs. time for solutionized and peak aged 2090 shavings immersed in 3.5 w/o NaCl solution.

ORIGINAL PAGE IS
OF POOR QUALITY

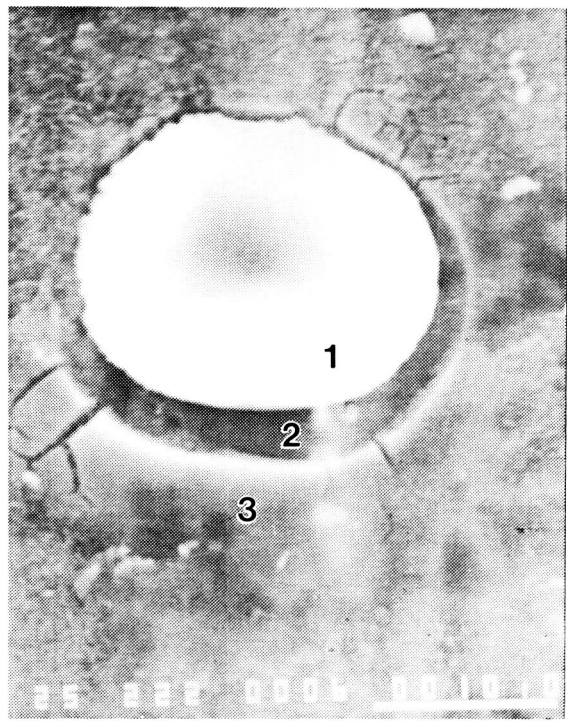
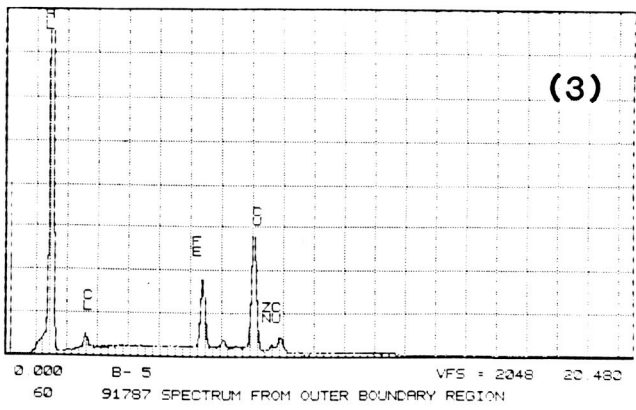
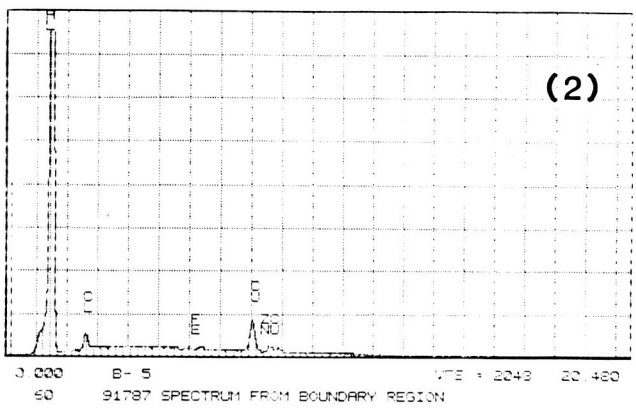
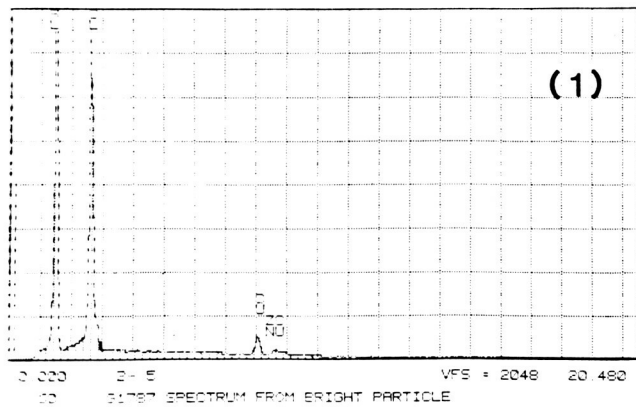


Figure 46

Scanning electron photomicrograph of a pitted region. EDS spectra show the signal obtained from the 3 different regions. Note variation in the chlorine and copper signals.

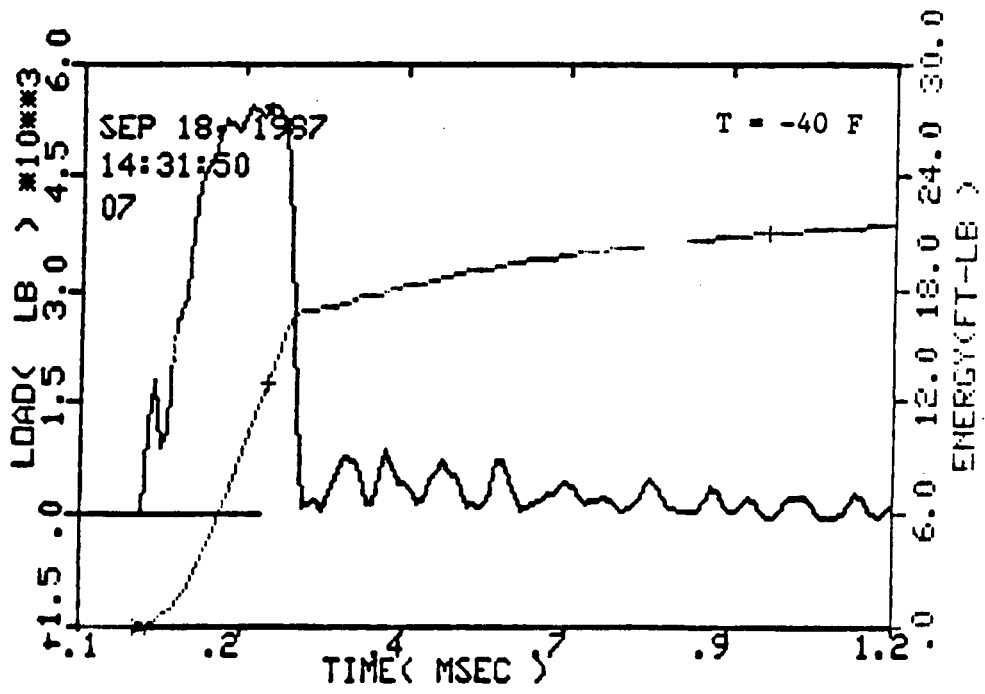
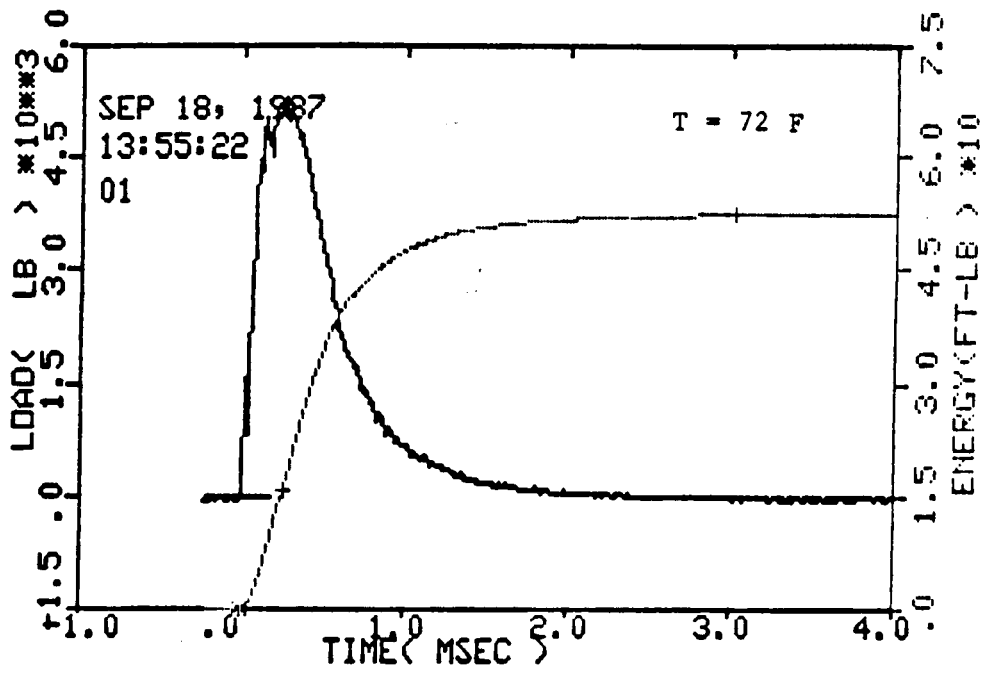


Figure 47

Typical time-history plots from Charpy V-notch tests.

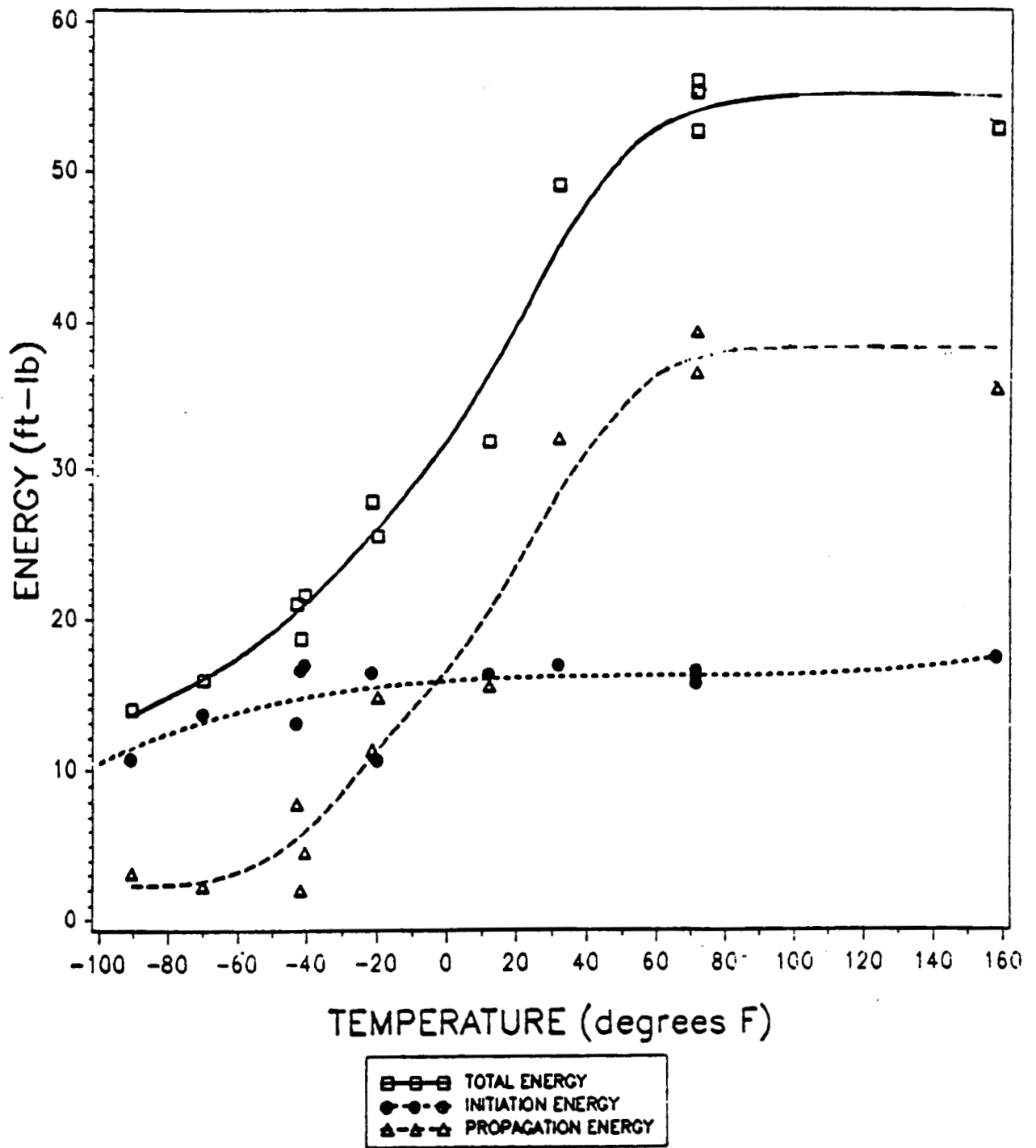


Figure 48

Charpy V-notch test results.

SCHEMATIC OF DISK PRESSURIZING ASSEMBLY

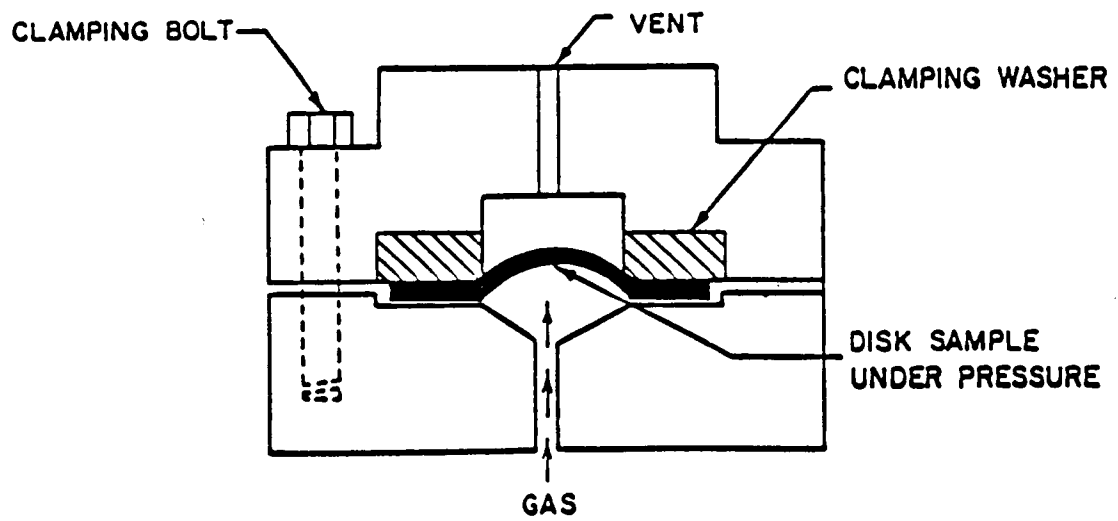


Figure 49

Schematic of disk pressurizing assembly.

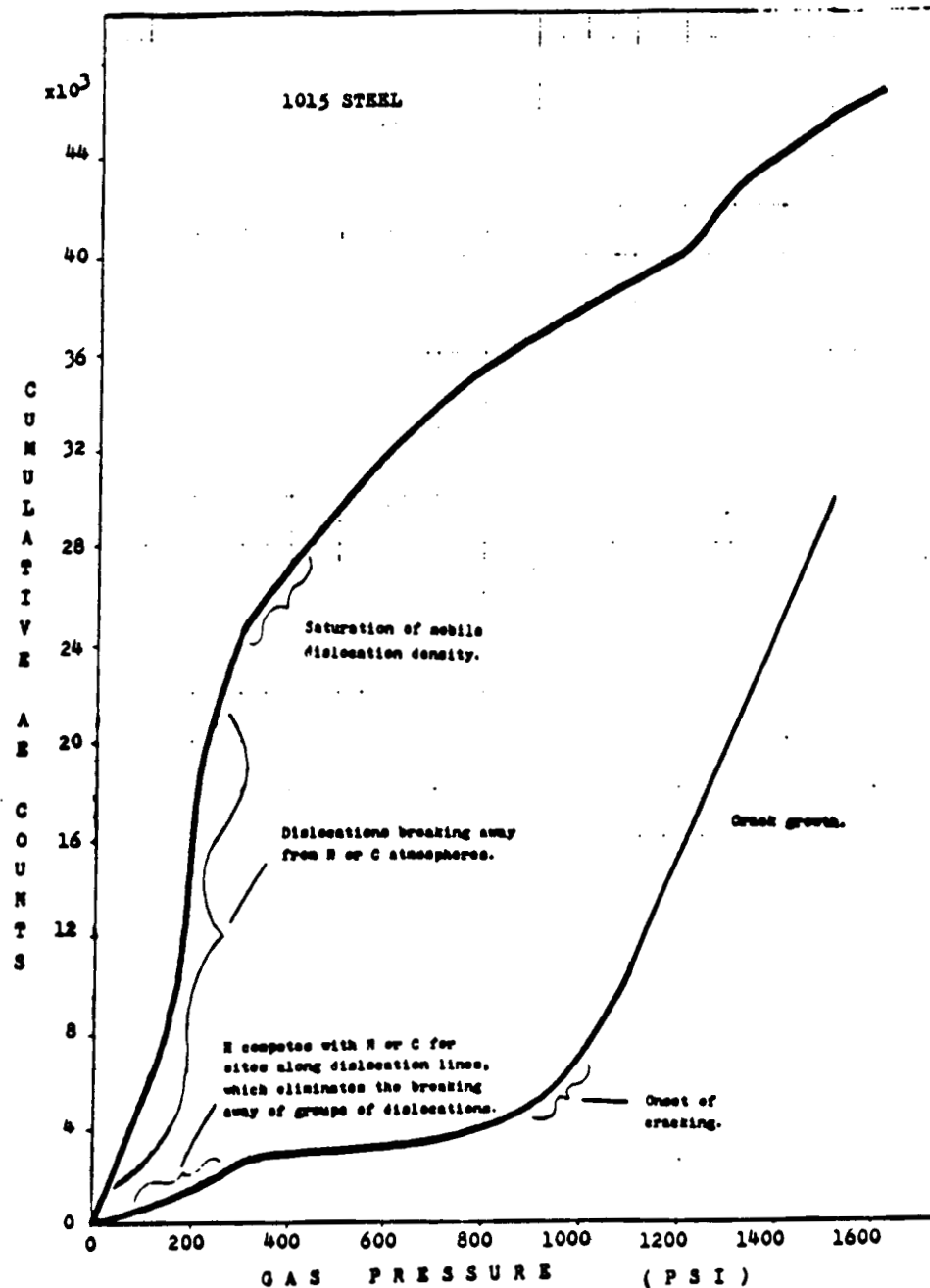


Figure 50

Graph of cumulative acoustic emission counts vs. gas pressure for mild steel disks tested in a disk pressurization system. Notes indicate the occurrence of various phenomena.

APPENDIX I

PROPOSAL OF RESEARCH

MECHANISMS OF INTRINSIC DAMAGE LOCALIZATION DURING CORROSION FATIGUE : Al-Li-Cu SYSTEM

R.S. Piascik

ABSTRACT

The objective of this research is to study mechanisms of crack tip damage fundamental to environmentally assisted fatigue crack growth in Al-Li-Cu alloys. Intrinsic mechanisms of fatigue crack growth in alloy 2090 are examined by fracture mechanics methods applied to small cracks. Two regimes of environmental effect, low mean stress-high stress intensity range hydrogen embrittlement and high R-near threshold cracking by hydrogen or film rupture/dissolution are studied by programmed constant stress intensity experimentation. The potential difference monitored crack growth studies are performed in purified helium, oxygen, water vapor and aqueous sodium chloride environments. Fatigue crack growth is first measured as a function of frequency and then for small crack-microstructure orientations giving single or multiple grains along the crack front. Experiments are designed to probe crack tip environmental damage for the two regimes. Crack interactions with grain boundaries will be resolved. Growth in gaseous environments will be compared to environmental effects produced by electrode potential controlled aqueous environments. Resulting crack growth transients will be continuously monitored and crack surface electrical conductivity will be characterized. Crack plastic zone corrosion and fatigue damage will be studied by fracture toughness

measurements of preexposed specimens. The goal of this research is to provide a mechanistic basis for the development of fatigue resistant alloys and a quantitative method of fatigue life prediction.

CONTENTS

	PAGE
1.0 Introduction	A-1
2.0 Background	A-2
2.1 Microstructure	A-2
2.2 Deformation and Fracture	A-4
2.3 Fatigue Crack Propagation	A-5
2.3.1 Extrinsic Effects	A-5
2.3.2 Short / Small Crack Behavior	A-6
2.4 Environmental Effects	A-8
2.4.1 Aluminum Lithium Alloy Corrosion and SCC in Aqueous Chloride	A-9
2.4.2 Corrosion Fatigue	A-12
2.4.2.1 Aluminum Alloys in Aqueous Chloride and Water Vapor	A-12
2.4.2.2 Aluminum Lithium Alloys in Aqueous Chloride and Distilled Water	A-14
2.4.3 Occluded Cell Chemistry	A-16
2.4.4 Mechanisms for Crack Tip Damage in Corrosion Fatigue	A-16
3.0 Proposed Experimental Approach	A-17
3.1 Experimental Methods	A-18
3.1.1 Short Crack Geometry	A-18
3.1.2 Potential Difference	A-19
3.1.3 Stress Intensity	A-20
3.2 Environment	A-21
3.2.1 Composition	A-21
3.2.2 Electrochemical Potential	A-22
3.2.3 Frequency	A-22
3.3 Material / Microstructure	A-23
3.3.1 Material	A-23
3.3.2 Crack Path	A-23
3.3.3 Precipitates / Boundaries	A-24
3.4 Experimental Program	A-25
3.4.1 Phases of Research	A-25
3.4.1.1 Phase 1 Experimentation	A-25
3.4.1.2 Phase 2 Experimentation	A-27
3.4.1.3 Phase 3 Experimentation	A-28
3.5 Summary of Expected Results	A-31
4.0 References	A-32

TABLES

1	Al-Li Alloy Microstructure	A-38
2	Mechanisms of Small Crack Growth	A-39
3	Effect of Cathodic Polarization on FCG	A-40
4	PHASE 1 Experiment Summary	A-41
5	PHASE 2 Experiment Summary	A-43
6	PHASE 3 Experiment Summary	A-44

FIGURES

1	Long Crack FCG Characteristics	A-45
2	Small Crack FCG Characteristics	A-45
3	Effect of Electrochemical Potential on SCC	A-46
4	FCG in 3.5% NaCl Solution and Dry Air	A-47
5	Effect of Frequency on FCG in Aqueous NaCl	A-48
6	Effect of Polarization on FCG in Aqueous Environment	A-49
7	Hypothesized FCG Regimes	A-50
8	Test Specimen Drawings	A-51
9	Potential Difference Testing Setup	A-52
10	Aqueous Environment Test Cell	A-53
11	Test Specimen Orientation	A-54
12	Fracture Surface Microstructure/Orientation	A-55

1.0 INTRODUCTION

The development of complex precipitation strengthened aluminum - lithium alloys with improved mechanical properties, lower density, and increased elastic modulus has been the objective of much research within recent years (A1-A4). Al-Li alloys containing Zr, Cu and/or Mg are becoming commercially available for aerospace application. Yet, potential problems of alloy degradation and failure currently impede reliable application of Al-Li alloys and require additional research. One such problem area that has gained considerable attention is alloy corrosion and environmental fracture.

Studies have shown that these high strength alloys are susceptible to intergranular failure which leads to the reduction of mechanical properties in the short-transverse (S-T) direction of rolled plate material. Intergranular failures, due to either mechanical fracture or environmental stress corrosion cracking, have been studied extensively. These studies have led to phenomenological understanding of Al-Li alloy fracture toughness and environmental degradation under monotonic loading. Although, little is currently known about the environmental mechanisms occurring at the crack tip, investigators have implicated both hydrogen embrittlement and anodic dissolution/film rupture as damage mechanisms.

Based on a review of current research in the area of environmental degradation of Al-Li alloys, it is apparent that other important areas of environmental fracture should be addressed. To date, the corrosion fatigue response of Al-Li alloys has not been systematically characterized or understood. Mechanisms of transgranular cracking in embrittling environments have not been identified.

The objective of the proposed research is to characterize corrosion fatigue crack propagation in Al-Li-Cu alloys exposed to aqueous electrolyte and gaseous environments, and to develop mechanisms of damage localization, with emphasis on crack tip - precipitate / boundary - environment interactions. Upon completion of preliminary work to

develop the necessary techniques, Phase 1, experiments will be performed to address the following questions:

PHASE 2: a) What are the growth kinetics and microstructural paths of corrosion fatigue cracks in Al-Li-Cu alloys, exclusive of extrinsic closure effects and relevant to two specific hypothesized regimes of environmental damage?

b) Is the short crack geometry uniquely sensitive to environmental embrittlement due to localized cell chemistry?

PHASE 3: a) What mechanisms of intrinsic damage localization occur within the identified regimes of environmental damage?
- high K regime embrittlement by hydrogen?
- low K regime surface film rupture/dissolution?

b) Do precipitates control intergranular and transgranular corrosion fatigue crack propagation due to enhanced galvanic dissolution, hydrogen production, imperfect passivation, strain localization or crack chemistry alteration?

Based on successful completion of this program; 1) Results will quantify the environmental effects on fatigue crack growth of short cracks which will lead to more precise component design life predictions, and 2) The identification of intrinsic crack tip damage mechanism(s) may assist in advanced alloy development.

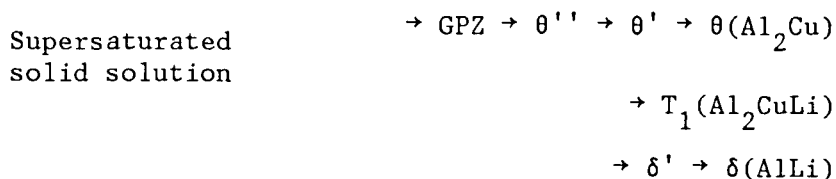
2.0 BACKGROUND

Environmentally assisted cracking of aluminum lithium alloys is dictated by damage mechanisms that are controlled by the interaction of environment, applied stress and microstructural features. The following paragraphs briefly describe Al-Li microstructures and summarize current understanding of the effect of stress and environment.

2.1 Microstructure

The addition of lithium to aluminum reduces density, significantly increases stiffness (A5), and results in homogeneous precipitation of a

coherent δ (Al_3Li) strengthening phase. Copper is added, as for example in commercial 2090 alloy ($\text{Al-2.9Li-1.1Cu-0.11Zr}$), to enhance solid solution and precipitate strengthening. The precipitation sequence for the Al-Cu-Li system is complex and summarized as follows (A6,A7,A8).



Zr is added to inhibit recrystallization and grain growth during thermo-mechanical processing. Table 1 is a list of matrix and grain boundary phases found in Al-Li binary and Al-Li-Cu-Zr alloys (A9-A11).

Upon aging, homogeneous precipitation of metastable δ occurs. Even though this precipitate is coherent with the matrix and can be sheared by moving dislocations, δ restricts dislocation motion and greatly enhances alloy strength. Partially incoherent T_1 and δ precipitate at high energy sites such as dislocations and subgrain boundaries. These copper bearing precipitates can reduce strain localization. Their effectiveness in homogenizing strain is dependent upon size and distribution which is controlled by deformation prior to aging. Controlled deformation prior to aging can produce a uniform distribution of nucleation sites (dislocations) for T_1 and δ precipitation. As aging times increase, T_2 and T_1 form and coarsen along high angle and sub grain boundaries, respectively, resulting in solute depleted precipitate free zones (PFZ's).

Rolling of plate produces an anisotropic grain structure, with flat elongated grains, oriented along the rolling direction. Those mechanical and corrosion properties which are affected by microstructure will be sensitive to plate orientation. Short transverse fracture and S-T stress corrosion cracking resistances are particularly poor.

Studies have linked these microstructural features to detrimental strain localization, grain boundary fracture and environmental degradation of Al-Li alloys.

2.2 Deformation and Fracture

Structural applications of Al-Li-Cu alloys require an understanding of how microstructure affects deformation and fracture under different loading conditions. Studies have shown that aging affects fatigue crack propagation by mechanisms dominated by slip behavior. Low fracture toughness properties have been linked to mechanisms of strain localization and precipitate nucleated microvoid formation at grain boundaries resulting in intergranular failure.

Studies of the effect of slip morphology on the monotonic and cyclic ductility of Al-Li binary alloys (A5,A12,A13) and Al-Li-Cu alloys (A14,A15) show that ductility is controlled by strain localization which depends on the extent of work softening on the glide plane. As aging is increased from underaged to peak strength, shearable precipitates localize monotonic strain in intense bands of deformation which produce stress concentrations. In overaged material, precipitates are not sheared, however, strain localization occurs in PFZ's formed by equilibrium grain boundary precipitates and results in increased intergranular fracture. Cracks nucleate at grain boundary ledges, formed by slip bands, during tensile tests and propagate either transgranularly or intergranularly along PFZ's dependent upon aging treatment. Cracks most often nucleate at slip bands during cyclic deformation and propagate either by a striated growth mechanism or by slip band decohesion; the path is contingent on the extent of strain localization. In overaged material, cracks nucleate at grain boundary precipitates and propagate intergranularly within the PFZ.

The effects of composition and aging treatment on the plane strain fracture initiation toughness (K_{IC}, J_{IC}) and crack growth resistance (T_r -tearing modulus) have been investigated for a high purity Al-Li-Cu-Zr alloy (A16). A major contribution to the fracture process in peakaged and overaged tempers arises from intergranular separation promoted by microvoid formation at grain boundary precipitates (possibly T_2). Microstructural "reversion" experiments (A17) have shown that a

decrease in fracture toughness is associated with increased amounts of equilibrium grain boundary precipitates for a constant fraction of strengthening phase and hence for constant slip band morphology.

The above results show that, in microstructures containing matrix precipitates and grain boundary precipitates, slip planarity, strain localization in PFZs, and grain boundary failure due to voids formed around T_2 particles control high angle grain boundary fracture and result in low fatigue crack initiation and fracture toughness properties. The relative contribution of each mechanism depends on microstructure. These microstructural factors can also influence fatigue and environmental crack propagation. Characterization of microstructure-property relations and precise mechanisms in this regard require separation of extrinsic and intrinsic factors.

2.3 Fatigue Crack Propagation

Most investigators have found that Al-Li alloys exhibit improved fatigue crack growth resistance compared to traditional 7000 and 2000 series aluminum alloys. Crack growth resistance is, however, linked to factors such as crack deflection and crack wake closure. Fatigue crack propagation paths tend to follow intense slip bands, producing an irregular and highly crystallographic fracture surface. Deflection and closure mechanisms are denoted as extrinsic because they depend on specimen/crack geometry, loading variables and crack-microstructure orientation. The fundamental or intrinsic fatigue crack growth characteristic of Al-Li alloys are masked by large extrinsic effects and are only recently the object of research. Critically, extrinsic effects on crack growth in standard laboratory specimens may be of little relevance to component application of Al-Li alloys.

2.3.1 Extrinsic Effects

The increased fatigue crack growth resistance of Al-Li alloys, at low stress intensity range, has been attributed to crack deflection and increased crack closure (A15,A18,A19).

Recent results (A18) have shown that threshold fatigue crack growth in Alloy 2090 was affected by varying degrees of closure associated with crack propagation direction (plate orientation). It was found that fatigue crack growth in air was highly anisotropic, with rates varying by up to four orders of magnitude between orientations, at constant applied ΔK . Typical results are shown in Figure 1. Crack growth parallel to the rolling plane (S-L and S-T orientation) was the fastest and exhibited the lowest threshold. The slowest growth rates were observed for cracks perpendicular to the rolling plane (L-T, T-L and T-S). It was concluded that the slower crack growth was due to crack tip shielding from crack deflection and resulting crack closure due to the wedging of fracture surface asperities. Crack extension in the rolling plane (i.e. S-L and S-T) occurred by an intergranular delamination mechanism, with little associated shielding. It is also apparent that changes in strain localization affect fracture surface roughness and thereby the level of closure (A15).

Results have shown that intrinsic (closure corrected) fatigue crack growth of Alloy 2090 occurs well below the extrinsic threshold. From these results, it is important to note that studies of fundamental crack tip damage in Al-Li alloys, as proposed herein will require that extrinsic effects be eliminated or accounted for.

2.3.2 Short / Small Crack Behavior

There is increasing evidence that the growth rates of small fatigue cracks generally exceed those of long cracks when subjected to the same applied ΔK (A20). This has been reported where cracks are small in length compared to microstructural dimensions, small relative to the scale of crack tip plasticity or when they are physically small (0.5 to 5 mm). Definitive mechanisms have been proposed to explain the breakdown in the fracture mechanics similitude concept at small crack sizes. Four mechanisms are relevant to small crack growth in aluminum lithium alloys, Table 2.

For physically short/small cracks (Items 1A and 1B, Table 2), closure forces are initially small. With increasing crack length, wake plasticity and roughness develop producing increased crack tip shielding resulting in reduced fatigue crack growth rates. Researchers (A21,A22) have recently characterized this behavior for alloy 2090. A comparison of long crack and short crack fatigue growth rates in terms of applied ΔK , Figure 2, shows that small crack growth continues at stress intensities below the long crack growth threshold. Also shown in Figure 2 is the good correlation of small fatigue crack growth compared to closure corrected ($\Delta K_{\text{eff}} = K_{\text{max}} - K_{\text{open}}$) long crack growth rates. These results illustrate that extrinsic closure effects play an important role in Al-Li alloy fatigue crack growth. Small fatigue cracks exhibit intrinsic (closure free) growth rates, thus providing a means for examining fundamental damage processes in fatigue and corrosion fatigue.

Mechanically short fatigue cracks (Item 2A, Table 2), with many grains along the crack front and with length comparable to the plastic zone, exhibit accelerated crack growth when compared to growth of long fatigue cracks. This anomalous behavior is due to large scale crack tip plasticity which violates the small scale yielding criteria of linear elastic fracture mechanics (LEFM). A more appropriate analysis for mechanically short crack growth is the J-integral or crack tip opening displacement (CTOD) techniques (A23).

Mechanically small fatigue cracks (Item 2B, Table 2) may exhibit no signs of an intrinsic threshold, but rather propagate at stress intensity levels below the closure corrected long crack threshold, as shown in Figure 2 for alloy 2090. Detailed studies have documented the small crack phenomena in 7000 and 2000 series alloys (A24,A25,A26,A27). Disturbingly high growth rates of small cracks embedded within a single grain are thought to be caused by crack tip opening strains that are unexpectedly high, based on applied ΔK . Small crack growth is influenced by microstructural features, i.e. high angle grain boundaries are known to arrest crack growth. The influence of microstructure on small crack growth during corrosion fatigue will be examined as part of this study.

Chemically short/small fatigue cracks (Items 3A and 3B, Table 2) exhibit increased growth rates due to environmental mechanisms, as observed for hydrogen environment embrittlement of steels (A28), and film rupture systems (A29). For such cases, the chemical driving force for environmental cracking increases in severity with decreasing crack length because of complex mechanisms involving mass transport by diffusion, ion migration and convection, and strain assisted chemical and electrochemical reactions. (A30). Complex models have been proposed to quantify these effects (A31), but predictions are specific to material - environment systems. These crack size - chemistry interactions have not been characterized or modeled for aluminum alloys in aqueous chloride environments. While accelerations of small corrosion fatigue cracks are suggested, retardations by novel transport/reaction mechanisms cannot be ruled out. Short/small crack corrosion fatigue experiments are required.

To summarize, short/small crack fatigue growth is not influenced by extrinsic closure effects that obscure crack tip driving forces. Crack tip damage mechanisms are more readily observed by short cracks experiments. Studies have also shown that the short crack geometry is uniquely sensitive to microstructural and environmental effects. These factors are relevant to applications of Al-Li alloys where high operating stresses and relatively low fracture toughness result in critical crack sizes on the order of 2 mm. Short/small cracks are also relevant to the fatigue and fracture behavior of thin sheet in aerospace tankage applications. Based on these observations, a short/small crack geometry will be used to study fatigue crack growth kinetics under varying environmental conditions.

2.4 Environmental Effects

Environmentally assisted fracture is likely to be controlled by chemical or electrochemical processes (hydrogen production, film rupture and active dissolution), combined with crack strain localization (slip

planarity and/or micro void formation). Microstructural features (PFZ's, large grain boundary precipitates, shearable matrix precipitates) play a critical role in the environmental processes. The goal of the proposed research is to isolate and identify those factors which control corrosion fatigue crack propagation in aluminum - lithium alloys.

2.4.1 Aluminum Lithium Alloy Corrosion and SCC in Aqueous Chloride

When compared to other high strength aluminum alloys, Li bearing alloys exhibit excellent resistance to intergranular stress corrosion cracking (IGSCC) in aqueous chloride solutions, but only for specific microstructure, electrochemical potential, immersion and loading conditions (A32,A33). Generalizations are suspect because many variables interact to influence embrittlement and mechanisms are not defined. Stress corrosion cracking studies of Al-Li alloys (under monotonic loading) have concentrated on the intergranular cracking and little is known about transgranular SCC.

Smooth specimens are embrittled at slow strain rates (10^{-6} to 10^{-7} sec⁻¹) and precracked specimens exhibit slow subcritical intergranular crack growth at low stress intensities ($\sqrt{10}$ MPa m^{1/2}) (A34-A36). Alternate immersion enhances intergranular corrosion and cracking when compared to continuous immersion in aqueous chloride (A32,A37). Preexposure to chloride solution results in subsequent embrittlement, possibly due to dissolved hydrogen, during tensile deformation in moist air (A32). A recent study of SCC in a Al-Li-Cu-Mg material has shown that CO₂ absorption on corroded surfaces pre-exposed to NaCl solution alters crack pH to a level (10.5 to 11.0) that favors brittle cracking (A38). These results suggest that alternate immersion crack initiation and small crack growth are caused by a complex environment containing chloride and bicarbonate ions. It was also concluded that these localized environmental considerations do not apply to long cracks, which are probably acidic.

Lithium in solid solution or as homogeneously distributed δ' does not promote stress corrosion cracking (A39). Rather, intergranular precipitates:

- δ , an AlLi grain boundary phase in binary Al-Li
- T_2 , an Al_6CuLi_3 grain boundary phase
- T_1 , an Al_2CuLi subgrain boundary phase

critically affect SCC properties (A39-42). Peak aged Al-Li alloys without copper, or alloys with a high Li to Cu ratio and aged for long times are embrittled. Reportedly, this is due to the presence of large grain boundary δ precipitates which may cause dissolution and/or strain localization at grain boundaries; the contribution of each is unclear. Overaged binary Al-Li alloys are more resistant to SCC than peak or underaged material, due possibly to crack blunting by dissolution of intergranular δ phase.

A recent study has shown that T_2 precipitates play a major role in the SCC susceptibility of Al-Li-Cu alloy (A43). The SCC crack growth studies showed that material containing large grain boundary T_2 precipitates exhibited reduced crack growth rates. It was concluded that enhanced localized dissolution, caused by the presence of grain boundary T_2 precipitates, reduced crack growth by blunting the crack tip. Alloys containing greater than approximately 1 wt. % copper (eg. 2020 [Al-1.2 Li-4.5 Cu] or 2090) are severely embrittled in the under and overaged conditions, with the T_1 phase implicated as degrading SCC resistance (A32,A33,A40,A42). Although, the mechanisms of environmental degradation associated with δ , T_2 and T_1 precipitates are unclear, the above studies have shown that precipitate morphology, resulting in strain localization and localized electrochemical reactions, plays an important role in the corrosion and stress corrosion cracking properties of aluminum lithium alloys.

Electrode potential strongly affects SCC in aqueous electrolytes. Polarization anodic to the open circuit potential in NaCl solutions increased surface preferential attack (pitting), thus promoting IGSCC nucleation and perhaps adversely affecting crack propagation by dissolution or hydrogen mechanisms (A35). Slight cathodic polarization (relative to open the circuit potential) decreased the propensity for IGSCC (A34-A36). These polarization results are similar to those observed for both 7000 and 2000 series alloys. For the former, the effect of electrochemical potential on stress corrosion crack growth and crack initiation (slow strain rate testing) is shown in Figure 3a and 3b, respectively (A44,A45). Investigations have been conducted to study the effect of small levels (0 to 300mV) of both anodic and cathodic polarization on the slow strain rate performance of 2000 series alloys (A45). These studies, as with 7000 series alloys, revealed reduced susceptibility under mild cathodic polarization and severe loss of tensile ductility under small anodic polarization. A correlation also exists between hydrogen permeability of 7000 series alloys in 0.5N NaCl as a function of applied electrochemical potential (A46). As shown in Figure 3a, cathodic polarization reduces hydrogen permeation and SCC susceptibility. Results suggest that hydrogen plays a critical role in the embrittlement of 7000 and 2000 series alloys when exposed to aqueous NaCl. The effect of slight cathodic polarization of aluminum alloys in aqueous NaCl may be a result of improving the quality of the protective oxide film (A47). The observation of similar electrochemically controlled SCC characteristics of AL-Li, 7000 series, and 2000 series alloys is important, suggesting that similar localized environmental effects are operative in these alloys. The demonstrated variation in Al alloy SCC susceptibility as a function of slight changes in anodic and cathodic polarization also reveals the importance of controlling crack tip electrochemical potential. The use of controlled electrochemical polarization experiments proposed herein will aid in determining the role of film formation, dissolution and hydrogen in crack tip mechanisms.

2.4.2 Corrosion Fatigue

Corrosion fatigue properties of aluminum alloys have been the subject of considerable research. Most of the studies performed to date have focused on conventional 7000 and 2000 series aluminum alloys. Few have investigated environmentally assisted fatigue in Al-Li alloys.

2.4.2.1 Aluminum Alloys in Aqueous Chloride and Water Vapor

Studies have shown that fatigue crack propagation in high strength aluminum alloys can be significantly enhanced by environment. The magnitude of the corrosion fatigue effect depends on a variety of material, environment and loading variables.

The fatigue crack growth characteristics of 2024-T3, 7075-T6, and 7178-T6, at low stress intensity levels ($\Delta K < 10 \text{ MPa m}^{\frac{1}{2}}$) in dry air ('10% R.H.) and 3.5% NaCl solution, are shown in Figure 4 (A48). A marked increase in fatigue crack growth was observed with exposure to 3.5% NaCl solution. These environmental effects have also been observed at higher levels of stress intensity (A49,A50). Studies have shown that increased fatigue crack growth, at moderate stress intensities ranging from 10 to 20 $\text{MPa m}^{\frac{1}{2}}$, is correlated to increased pure water vapor pressure (A51,A52). Investigators have also compared the near threshold crack growth rates of 2618 and 7075 alloys in vacuum and nitrogen containing 50 ppm water vapor (A53). A significant increase in fatigue crack growth was observed in both alloys when exposed to water vapor. The above investigators concluded that hydrogen ingress at and ahead of the crack tip plays an important role in the accelerated crack growth observed in 7000 and 2000 series alloys.

Corrosion fatigue crack growth rates at moderate to high ΔK are strongly influenced by cyclic loading frequency. Investigators have found that seawater markedly enhances fatigue crack growth (refer to Figure 5a) and that the cycle based enhancement is increased with decreasing frequency (A54). Other studies have shown that the fatigue

crack growth is dependent on the product of water vapor pressure and the reciprocal of load frequency (A51,A55). Based on these results, the observed frequency dependence is thought to be consistent with diffusion of atomic hydrogen ahead of the crack tip, a process which requires increased time for increased penetration. The opposite effect of frequency on fatigue crack growth rate has been observed at low stress intensity ranges (A56). The results, shown in Figure 5b, reveal increased growth rates at higher cyclic frequencies. This behavior was explained by a slip dissolution mechanism which involves film rupture, a process that is enhanced by increased crack tip strain rate at higher loading frequencies.

The crack growth data shown in Figure 5a and 5b converge at the same stress intensity range (10 to 15 MPa m^{1/2}), locating a point that separates two regions of frequency dependent crack growth. Crack closure and crack geometry-chemistry processes may have affected the fatigue crack growth correlations shown in Figure 5a. These history dependent effects may result in a high threshold stress intensity range, as seen in Figure 5a, masking crack growth frequency effects at low stress intensity ranges. The proposed short crack-constant ΔK tests will confirm the presence of the two frequency dependent crack growth regimes and investigate associated fatigue crack growth mechanisms.

As observed for stress corrosion cracking, corrosion fatigue is adversely affected by anodic polarization and more importantly the environmental effect is reduced by mild cathodic polarization. The effect of polarization on the fatigue crack growth of an Al-7%Mg alloy in 1N NaSO₄ solution is shown in Figure 6 (A56). Fatigue crack growth was increased by anodic polarization, but crack growth under mild cathodic polarization is decreased, approaching that observed for dry argon. Cathodic polarization fatigue studies of other aluminum alloys, shown in Table 3, have revealed the same increased corrosion fatigue resistance (A57-A61). Significantly, smooth bar fatigue life and slow strain rate SCC (discussed earlier) testing reveal increased environmental resistance under slight cathodic polarization. These

results suggest mild cathodic polarization alters surface film conditions resulting in improved environmental resistance.

Anodic and cathodic polarization will be used to alter crack tip environment to study possible cracking by dissolution/film rupture or hydrogen crack tip mechanisms.

2.4.2.2 Aluminum Lithium Alloys in Aqueous Chloride and Distilled Water

Most of the research performed to date has focused on general corrosion and stress corrosion cracking properties of Al-Li alloys. Few studies have emphasized the effect of environmentally assisted fatigue on these alloys. The limited number of studies performed to date have shown reduced smooth bar fatigue life in aqueous NaCl and little environmental effect in distilled water. Fatigue crack growth experimentation, using notched specimens, has revealed accelerated growth in both NaCl solution and distilled water.

The effect of environment on low cycle fatigue behavior of two alloys (Al-Li-Mn and Al-Cu-Li-Mn), and the high cycle fatigue behavior of Al-Cu-Li-Zr alloy 2090 have been investigated (A62). Smooth bar specimens (L-T orientation) were low cycle fatigue tested, in dry air ('2%R.H.), vacuum (' 10^{-6} Torr), laboratory air (50% R.H.), and distilled water. Results showed little difference in fatigue life when tested in these environments. High cycle fatigue testing in laboratory air and aqueous 3.5% NaCl (open circuit potential), using fully reversed loading at a frequency of 15 Hz, revealed a factor of two reduction in fatigue life when testing in the 3.5% NaCl solution. The fatigue strength of alloy 2090, in laboratory air and 3.5% NaCl solution, was also found to be comparable to alloy 7075. It was concluded that reduction in the fatigue resistance of alloy 2090, in aggressive sodium chloride environment, is due to a complex mechanism involving the interplay of microstructure and slip morphology with passive film breakdown by Cl^- , anodic dissolution and hydrogen embrittlement. Smooth bar Al-Li-Mn and Al-Li-Cu specimens were low cycle fatigue tested in dry air ('2%R.H) and

distilled water (A63). As observed above, no appreciable environmental affect on fatigue life was detected when testing in distilled water. Classically, fatigue life is reduced as chloride ions weaken the passive film, producing sites for crack initiation and advance by dissolution/film rupture or hydrogen embrittlement.

Fatigue crack growth studies, using notched specimens, have revealed increased crack growth in both NaCl solution and distilled water environment. A PM Al-Li-Cu alloy exhibited a five-fold increase in fatigue crack growth when tested ($f = 1$ Hz, $R = 0.1$) in 3.5% NaCl solution (open circuit potential) and compared to laboratory air environment (A64). The fatigue crack growth characteristics of a rapidly solidified Al-Li-Cu-Mn alloy was studied ($f = 10$ Hz, $R = 0.05$) in argon, air, distilled water, and 3.5% NaCl solution (open circuit potential) (A65). Fatigue crack growth rates in distilled water and 3.5% NaCl solution were found to be 2 to 3 times higher than in air or argon. Increased fatigue crack growth rates were also observed for an Al-Li-Mn and Al-Li-Cu alloys when tested ($f = 10$ Hz, $R = 0.1$) in distilled water and compared to dry air (‘ 2% R.H.) (A63).

Little is known about Al-Li alloy crack chemistry in aqueous environments. Distilled water environment test results suggest that occluded cell effects play an important role in producing an aggressive localized environment that results in increased corrosion fatigue crack growth. Possibly, the crack chemistry is altered by hydrogen production or elemental dissolution resulting in the aggressive environment.

As in conventional high strength aluminum alloys, Al-Li material exhibits retarded fatigue crack growth under mild cathodic polarization. The fatigue life of an Al-4.24Mg-2.13Li alloy was increased by mild cathodic potentials, but degraded by applied anodic and higher cathodic potentials (A66). Four point bend corrosion fatigue tests were performed at a frequency of 2.8 Hz in 0.5M NaSO₄ and 0.5M NaCl solution. It was suggested that higher cathodic polarization increases the pH of the solution at the surface and anodic polarization decreased pH,

resulting in an unstable passive film and decreased fatigue life. Little explanation was given for increased fatigue life under slight cathodic polarization. It is important to note that these electrochemical polarization effects parallel those observed for conventional high strength aluminum alloys, suggesting that similar mechanisms of environmental damage are operative.

2.4.3 Occluded Cell Chemistry

The localized electrochemistry within cracks, pits and crevices in Al-Li may be unique compared to conventional 7000 series aluminum alloys. For the latter, in 3% NaCl solution, the crack solution acidifies to pH 3 due to oxygen depletion, Al ion hydrolysis, and chloride ion enrichment (A67,A68). The cathodic potential where this process is eliminated is not defined. Alkaline (pH 10 to 11) conditions within occluded geometries in Al-Li have been reported. It was suggested that the environment is controlled by dissolution of Li ions which react with OH^- , from water reduction, to from LiOH^{++} at an equilibrium pH of 11 (A32,A69). Recently, NaCl pre-exposure studies of alloy 8090, an Al-Li-Cu-Mg material, showed that initiation and small crack propagation is favored by the attainment of a critical pH of 10.5 to 11 (A38). It was suggested that small crack pH is controlled by CO_2 absorption. As the crack grows, CO_2 plays less of a role in controlling pH and the crack tip environment acidifies by Al ion hydrolysis. The implications of crack chemistry differences on crack propagation are speculative, and the effects of applied potential and convective mixing during fatigue are undefined (A34,A70).

2.4.4 Mechanisms for Crack Tip Damage in Corrosion Fatigue

Film formation/rupture/dissolution and hydrogen embrittlement have been proposed as damage mechanisms during the corrosion fatigue of high strength aluminum alloys. Accelerated fatigue crack growth of high strength aluminum alloys after exposure to water vapor and aqueous environments and the dependence on frequency of environmental assisted FCG have led researchers to propose these crack

tip damage mechanisms. Little is known about these proposed crack tip mechanisms in aluminum lithium alloys and their specific roles during corrosion fatigue is speculative. The following is a brief discussion of two hypothesized regimes of environmentally induced damage.

Figure 7 is a plot of crack growth rate and stress intensity range identifying two regimes of aqueous environment fatigue crack growth; a low ΔK -REGION 1 and a higher ΔK -REGION 2. These two regions are characterized by opposite cyclic frequency responses. The low ΔK region exhibits increased fatigue crack growth with increased cyclic frequency and can be explained by a film formation/rupture mechanism (A56). The observed increased FCG at higher frequency is explained by the increased crack tip strain rate resulting in increased film rupture and enhanced slip step dissolution. Along with this mechanism, hydrogen ingress resulting in crack tip damage is plausible. In general many uncertainties remain concerning environmental effects on threshold fatigue crack growth. REGION 2 exhibits increased crack growth rate at low frequency, consistent with hydrogen formation and migration to the crack tip; a time dependent mechanism (A51). These hypothesized regimes of environmental damage form the basis of the proposed research. Much of the experimentation is directed at determining the mechanisms of damage localization in these two regimes.

3.0 Proposed Experimental Approach

The above review has shown that little is known about the corrosion fatigue properties of Al-Li alloys and even less about mechanisms of crack tip damage. Listed below are the major findings of the literature review:

- Limited Al-Li corrosion fatigue data
- Importance of extrinsic effects
- Importance of small crack size
- Fatigue crack growth frequency effect
- Cathodic/anodic potential effects
- Two regimes of environmental FCG - ΔK_{th} , Paris

The goal of the proposed research is to systematically explore these unknown areas by designing experiments to separate and quantify the critical factors which influence corrosion fatigue in the two regimes of stress intensity defined earlier.

3.1 Experimental Methods

3.1.1 Short Crack Geometry

Major emphasis will be placed on the study of short crack growth kinetics for Al-Li alloys. This crack geometry, in conjunction with controlled mean stress, should eliminate extrinsic crack tip effects, therefore producing crack growth characteristics which are a result of only intrinsic environmentally assisted fatigue mechanisms. Figure 8 is a detailed drawing showing the micronotched specimen that will be used for all fatigue testing. Specimen dimensions and fatigue test loading schemes have been chosen so that the following criterion are maintained.

In plane, small scale yielding criteria:

$$R_y \leq 0.1 (W-a)$$

$$P \leq P_{\text{limit}}$$

Out of Plane, plane strain criteria:

$$R_y \leq 0.15 B$$

where:

$$R_y = \text{monotonic plastic zone size (plane stress)}$$

$$= \left(\frac{1}{2}\pi\right) (K_{\text{max}}/\sigma_y)^2$$

$$P_{\text{limit}} = 1.072 (\beta\sigma_y(w-a))$$

$$\beta = [1 + (a/w-a)^2]^{1/2} - (a/(w-a))$$

$$\sigma_y = \text{yield stress}$$

W = specimen width
B = specimen thickness
a = crack length
P = applied load

Two notch depth designs have been chosen (0.305 mm and 0.889 mm) so that crack studies can be performed using a wide range of ΔK . To minimize residual stress and microstructural variations, specimens will be fabricated from material located away from the rolling surfaces and at the same plate elevation. Residual stresses will also be minimized by electrodischarge machining (EDM) of the notch.

3.1.2 Potential Difference

Most short crack measurement techniques, including replication, laser CMOD measurement, and optical, do not easily lend themselves to remotely monitored, aggressive environment crack growth studies; therefore, the potential difference method will be used for continuous crack length measurement. The potential difference method, which has been used for the study of environmental effects of short crack growth in steel (A73), has not been applied to aluminum alloy short crack research. Potential difference monitoring of short crack growth in remote contained environments is complex and further development of experimental techniques will be required before it can be applied to these short crack studies. Techniques needing development include: 1) A method of precision attachment of potential drop signal probes adjacent to the specimen micronotch; 2) The reliable detection of a small ($\sim 100 \mu V$ with $0.1 \mu V$ resolution) potential drop signal over extended periods of time (2 weeks); 3) The adaptation of this method, for Al alloys, to aggressive aqueous environments without interfering corrosion effects. Once developed, this method (as in steels) will have the unique ability to continuously monitor the growth and growth transients of short cracks in remote environments.

The experimental setup is shown in Figure 9. A constant current of approximately 12 amperes is applied to the specimen through the loading fixtures. Two 0.127 mm diameter copper potential drop probes are spot welded within a specified distance (0.3 to 0.5 mm) from the micronotch. The potential difference is monitored across these probes and converted from an analog to digital signal that is sent to a computer where all test functions are automatically controlled. Using an analytical calibration procedure (A73), crack depth is computed for each measured value of electrical potential. Based on previous studies (A73), crack growth resolution of less than 5 μm is expected. Crack growth rates are computed for each crack depth value using ASTM E647 methods. Associated crack tip stress intensities are calculated using methods described in the following section.

3.1.3 Stress Intensity

Fatigue crack growth rate testing will be performed at constant cyclic stress intensity. The use of constant ΔK experiments will ensure that the measurement of intrinsic fatigue crack growth is not masked by the introduction of extrinsic history effects and transient environment chemistry effects. The cyclic stress intensity for the single edge notch specimen is given as follows:

$$\Delta K = (\Delta P/BW) \sqrt{(\pi a)} F(a/W) \quad (74)$$

where ΔP = max load - min load

a = crack length

W = specimen width

B = specimen thickness

$$F(a/w) = \sqrt{[(2W/\pi a)\tan(\pi a/2W)] * \{0.752+2.02(a/W)+0.37[1-\sin(\pi a/2W)^3]\}}/\cos(\pi a/2W)$$

Specimen end rotation will be freely maintained by a clevised pull rod configuration. Constant crack tip ΔK is maintained by computer controlled load reduction. This is accomplished by using the SEN cyclic stress intensity equation and the following expression (A75).

$$\Delta K = \Delta K_0 \exp[C(a-a_0)] \quad (76)$$

where a_0 = initial crack length

a = current crack length

C = constant with dimension of 1/length

= 0 for constant ΔK test

Most studies of environmental effects on fatigue crack growth have been performed at relatively high stress intensities. The mechanisms of environmentally induced embrittlement identified at these stress levels may not be dominant at threshold levels. Therefore, experiments will be performed at both threshold and intermediate stress intensity ranges. By selecting appropriate stress ratio (R) values, all experiments will be performed at the same maximum stress intensity. This will allow changing to significantly different levels of ΔK without delays introduced by monotonic plastic zone crack growth retardation.

3.2 Environment

3.2.1 Composition

Fatigue testing will be performed in the following environments:

1. High purity helium
2. High purity helium and water vapor
3. High purity oxygen
4. Deaerated distilled water containing NaCl with constant potential polarization.

High purity helium will be used as an inert reference environment. Previous investigators have suggested that enhancement of fatigue crack growth by water vapor in 2000 and 7000 series aluminum alloys occurs by a hydrogen embrittlement mechanism (A51,A52). FCG testing of an Al-Li-Cu alloy will be performed in water vapor to investigate possible embrittlement by hydrogen. Crack tip oxide surface films and their effect on damage mechanisms will be studied in the pure oxygen environment. All high purity gaseous environmental testing will be performed in a vacuum system capable of a 3×10^{-9} torr atmosphere. Short crack effects will be studied in deaerated aqueous NaCl environment, under controlled anodic and cathodic electrochemical potential.

3.2.2 Electrochemical Potential

The open circuit potential of Al-Li alloys can vary significantly with time. Because of the dynamic corrosion behavior, specimen electrochemical potential will be controlled during aqueous environment FCG experiments. The specimens will be polarized to specific anodic and cathodic potentials to study mechanisms of crack tip damage under different crack tip environmental conditions.

The deaerated NaCl solution is continuously pumped through the test chamber at a controlled rate. Specimen electrochemical behavior is potentiostatically controlled using platinum counter electrodes and a Ag/AgCl reference electrode shown in Figure 10.

3.2.3 Frequency

Parametric studies will be performed in aqueous environments to determine the effect of frequency on corrosion fatigue crack growth rate at different stress intensity ranges. Based on these results, one test frequency will be chosen for all experiments. A test frequency will be chosen based on enhanced environmental crack growth and reasonable test duration. This will aid in the determination of the effects of various microstructural features on the corrosion fatigue behavior of Al-Li-Cu alloys.

3.3 Material / Microstructure

Mechanisms of corrosion fatigue, in Al-Li-Cu material, will be studied by monitoring the growth of short fatigue cracks along specific plate directions (L-T and L-S), as shown in Figure 11. These plate directions will allow the study of FCG characteristics along a path containing significantly differently microstructures.

3.3.1 Material

Corrosion fatigue testing will be conducted using commercial alloy 2090 (Al-2.4%Li-2.5%Cu-0.1%Zr) material obtained from Alcoa in the solution treated and stretched (T3) condition. Thermal treatments will be performed to obtain specific microstructures.

Limited FCG experiments will be conducted using a reference material, peakaged alloy 7075. The reference material was selected for the following reasons; 1) The occluded crack chemistry of alloy 2090 and alloy 7075 may be significantly different (high pH and low pH, respectively). Mechanistically, a comparison of the CF response of these alloys is of great interest; 2) The alloy 7075 short crack corrosion fatigue results will be compared to ample long crack literature data; 3) Alloy 2090 is designed to replace the commercial use of alloy 7075 and therefore it is of interest to compare their general CF response to aqueous environments.

3.3.2 Crack Path

By taking advantage of the anisotropic microstructure of Al-Li-Cu rolled plate, short crack testing can be used to study the effect of environment on different microstructural features. Fatigue crack growth experiments will be performed in the longitudinal-short (L-S) and longitudinal-transverse (L-T) directions, as shown in Figure 12. These two crack path directions have been selected to optimize the difference in crack front microstructural conditions. Figure 12 illustrates how the L-T and L-S directions will significantly change the high angle grain boundary microstructure sampled by the crack front. As

C-2

seen in Figure 12a, a flaw propagating normal to the pancake grain is completely embedded within one or two grains with the crack front sampling/impinging the subgrain microstructures. Based on small crack fatigue results (A21), the sampling of many subgrain boundaries (in Alloy 2090) by the crack front does not introduce an intrinsic threshold. The propagation of short cracks in the L-S direction may approach a microstructural small crack geometry and single crack-boundary interactions will be resolved.

Figure 12b shows a flaw oriented in the transverse or L-T direction. In this orientation, the microstructural morphology along the crack tip is significantly different than in the L-S direction. The L-T direction will allow many (10 to 30) high angle grain boundaries to be sampled by the crack front. If crack length is minimized, in the L-T and L-S directions, short crack geometry will be maintained and extrinsic effects (closure) eliminated. These crack paths will allow unique experiments to be performed by monitoring crack growth transients as significantly different microstructural features interact with the advancing crack front environment.

Recently micromechanical models have been proposed for fatigue crack deflection and fracture surface contact (A77). Fatigue crack growth changes are predicted based on crack deflection and associated closure processes. The crack path geometry shown in Figure 12a represents the microstructural path assumed for these models. Using this geometry, tests will be performed to confirm model predictions by accurately monitoring changes in crack growth as the advancing crack front changes direction.

3.3.3 Precipitates/Boundaries

Based on previous investigations, copper bearing precipitates and high angle grain boundaries have been identified as possible microstructural features involved in the environmental degradation of Al-Li-Cu alloys. Experiments will study crack tip interactions with these microstructural features under controlled

environmental conditions. The precipitate / boundary microstructures of particular interest are:

- High angle grain boundaries containing T_2 precipitates
- Subgrain boundaries containing T_1 precipitates
- High angle grain boundary precipitate free zones

A peakaged material (190°C for 3-4 hrs), exhibiting the above microstructural features, will be used for Phase 1 and 2 and most of Phase 3 experimentation. Reversion thermal treatments will be performed to isolate specific microstructural features for Phase 3 testing. Each microstructure will be characterized by optical and transmission electron microscopy.

3.4 Experimental Program

The proposed research is divided into three phases. Preliminary Phase 1 testing will be performed to develop experimental techniques and to determine test parameters. Phase 2 will address questions associated with characterization of corrosion fatigue crack propagation in Alloy 2090 regarding microstructural crack paths and environmental effects. Based on these data, Phase 3 experiments are designed to answer more specific questions directed at a mechanistic view of damage localization, with emphasis on crack tip-precipitate-environment interactions. The following is a summary of proposed work required to answer the questions posed in the introduction. An outline of Phases 1,2 and 3 is given Tables 4, 5, and 6, respectively.

3.4.1 Phases of Research

3.4.1.1 Phase 1: Preliminary Experiments

Electrochemical polarization experiments will be performed to determine the corrosion properties of Alloy 2090 as a function of NaCl concentration. A summary of these experiments is listed in Table 4. Underaged, peakaged and overaged material will be

anodically polarized while exposed to deaerated NaCl solution of varying salt content. These experiments will determine the open circuit potential, passive region characteristics and pitting (breakaway) potential for the different aging conditions and chloride concentrations. Detailed specimen surface microstructural examinations will characterize the relative susceptibility of precipitates and constituent particles.

The primary objective of the corrosion tests is to determine microstructural (heat treatment) and environmental conditions for corrosion fatigue testing. Specifically, a chloride concentration and material heat treatment will be selected to minimize localized pitting and crevice corrosion, and to limit fracture surface deterioration during corrosion fatigue testing. Fatigue specimen electrochemical potential will be selected based upon electrolyte IR-drop limits (cathodic potential) and pitting potential (anodic potential). The selected material microstructures will be characterized by transmission electron microscopy.

Because the proposed corrosion fatigue methods have not been applied to aluminum alloys, preliminary tests will be performed to develop and verify experimental techniques. Fatigue crack growth experiments summarized in Table 4 will be performed using well characterized 4130 steel and alloy 2090. Experimental results will be compared to literature data, generated by established techniques, thereby demonstrating the proposed short crack potential drop method.

A number of short crack fatigue experiments will be performed to demonstrate experimental techniques prior to final testing. Constant cyclic stress intensity testing of Alloy 2090 will be performed in helium and aqueous NaCl environments to verify that the methods proposed herein measure intrinsic crack growth. Aqueous chloride fatigue crack growth testing will be performed at near threshold and high levels of cyclic stress intensity. The crack growth rate will be monitored at various anodic and cathodic electrochemical potentials. Based on these

results, constant stress intensity ranges and electrochemical potential levels will be selected for testing in Phases 2 and 3.

3.4.1.2 Phase 2: Characterization of Intrinsic Corrosion Fatigue Crack Growth

Phase 2 experimentation has been designed to address those questions posed earlier:

- a) What are the growth kinetics and microstructural paths of corrosion fatigue cracks in Al-Li-Cu alloys, exclusive of extrinsic closure effects and relevant to two specific hypothesized regimes of environmental damage?
- b) Is the short crack geometry uniquely sensitive to environmental embrittlement due to localized cell chemistry?

Table 5 is a summary of the proposed Phase 2 testing. The experiments have been designed to investigate environmental damage within the two hypothesized regimes, near threshold and high ΔK . Levels of ΔK and corresponding R values, listed in Table 5, were chosen to eliminate crack tip extrinsic closure effects, and to maintain a constant maximum plastic zone size (monotonic or forward loading) to eliminate interfering FCG retardation effects when changing from high to near threshold ΔK levels.

Initial Phase 2 testing will be conducted at constant ΔK , in the aqueous NaCl environment, and at selected constant frequencies. The objective of these tests is to confirm the presence of the two frequency dependent regimes of environmental damage. An optimum frequency, based on environmental sensitivity and test duration, will be selected for the remainder of Phase 2 and Phase 3 experimentation.

The major portion of Phase 2 testing, will be directed at investigating the two regimes of environmental damage varying the key parameters of constant cyclic stress intensity, microstructure (L-T and L-S crack path direction), and environment (gaseous and aqueous). Based on the results of preliminary Phase 1 testing, aqueous experiments will

be conducted using specific environmental conditions (NaCl content and constant electrochemical potential). Alloy 2090 will be tested in the L-S and L-T directions to optimize microstructural differences at the crack tip. Results will be in the form of crack length (a) versus number of cycles (N) plots exhibiting linear characteristics at data acquisition intervals of a $5 \mu\text{m}$. Changes in slope (changes in crack growth da/dN) will be correlated with environment and detailed optical and SEM examinations of specimen fracture surfaces. Based on these results, the corrosion fatigue growth kinetics, microstructural paths and short crack geometry effects will be determined for an Al-Li-Cu material.

3.4.1.3 Phase 3: Definition of Localized Crack
Tip Damage

Phase 3 experiments are directed at specific questions pertaining to mechanisms of corrosion fatigue in Al-Li-Cu alloys. These questions are listed below:

- a) What mechanisms of intrinsic damage localization occur within the identified regimes of environmental cracking?
 - High ΔK regime: embrittlement by hydrogen?
 - Low ΔK regime: surface film rupture/dissolution?
- b) Do precipitates control intergranular and transgranular corrosion fatigue crack propagation due to enhanced galvanic dissolution, hydrogen production, imperfect passivation, strain localization or crack chemistry alteration?

A summary of Phase 3 testing is shown in Table 6. Experimentation is divided into three experimental areas; 1) embrittlement testing, 2) corrosion fatigue testing of selected microstructures, and 3) study of crack surface films by slow cycle potential difference measurements.

Embrittlement testing: K_{IC} or J_{IC} methods will be used to measure the fracture properties of corrosion fatigue specimens precracked in different environments and stress ranges. These CF specimens have a calculated, fatigue induced, embrittled, plastic zone ranging in size

from 80 μm to 175 μm , for a cyclic maximum stress intensity of 15 $\text{MPa m}^{\frac{1}{2}}$. It is hoped that fracture toughness test results and fracture surface examinations will yield information pertaining to fatigue induced embrittlement mechanism(s). By using resistance curve analysis, the extent of crack tip embrittlement will be quantified. The correlation of embrittlement zone size versus environment and microstructure may lead to mechanistic conclusions.

Corrosion fatigue testing of selected microstructures: The two major copper containing precipitates in Alloy 2090, T_1 (subgrain and matrix) and T_2 (high angle grain boundaries), have been implicated as environmentally sensitive in monotonic SCC experiments. The electrochemical potential of these precipitates is likely to control corrosion fatigue crack propagation in aqueous NaCl. Specifically, a small crack will be grown under constant stress intensity and in aqueous chloride environment to establish a steady state fatigue crack growth rate. The constant electrochemical potential will be changed anodically and cathodically (relative to open circuit potential) and the resultant transient crack growth rate measured by the potential difference method. A comparison of crack growth response will be monitored versus electrochemical potential for small cracks in the following microstructures:

- single grain with T_1 and θ'
- single grain without (minimal) T_1
- multiple grains along crack front with T_1 , θ' , and T_2
- multiple grains along crack front with T_2

Changes in aqueous NaCl fatigue crack growth will be monitored as cracks are grown through the above microstructures. Results will be compared to detailed fractographic examinations. These results will determine the effect of copper containing phases on environment assisted fatigue crack growth in Al-Li alloys. Based on these experimental results, other alloys (Al-Li binary or Al-Li-Cu-Mg alloy) may be considered for testing.

If results indicate that hydrogen embrittlement is a primary mechanism of Al-Li-Cu alloy corrosion fatigue crack growth, additional experiments will be performed to study mechanisms of hydrogen induced crack tip damage. The role of hydrogen will be investigated by performing inert and high purity water vapor fatigue experiments in large recrystallized grain Al-Li-Cu material. Water vapor affects fatigue crack growth and crack path in single crystals of Al-Zn-Mg alloy (A78). In dry air, Stage I cracking along {111} planes was observed, but exposure to moist air increased crack propagation rates and cracks grew in {111} planes. These effects were also found to be frequency dependent. Results suggest that lower frequencies allow increased bulk hydrogen diffusion to regions ahead of the crack tip where damage presumably evolves. Low frequency fatigue tests will be performed using Alloy 2090 plate material containing large recrystallized grains. A small corner crack will be grown into a single recrystallized grain. As the environment is changed from helium to high purity water vapor, the change in crack growth rate will be monitored and the corresponding change in crack path will be noted by fractographic examination. These studies will aid in the understanding of environmental effects on transgranular crack growth in the Al-Li-Cu system.

Surface film study: Small changes in crack surface contact and electrical conductivity will be studied for different cracking environments by examining the load or crack opening sensitivity or potential. These changes have mechanistic implications. Crack surface contact effects on electrical potential are amplified by increased surface conductivity. These effects have been observed for small cracks in 4130 steel tested in aqueous 3% NaCl solution and correlated to expected changes in crack chemistry and surface films (A73). Electrical potential contact effects will be monitored during Phase 2 and 3 experimentation. Precise measurement of contact electrical potential will be performed for Alloy 2090 and 7075, in inert and embrittling environments. These data will be correlated with fatigue crack growth results, fractographic observations and expected crack

chemistries, and used as a diagnostic tool to determine the role of surface films during corrosion fatigue.

As part of Phase 3 testing, detailed fracture surface examinations of gage length surfaces will characterize crack path and persistent slip band morphology. Fracture surface SEM examination will document crack path microstructural interactions. An attempt will also be made to fabricate TEM foils containing fracture surfaces. The foils will be prepared so that damage at or near the fracture surface can be characterized to identify fatigue and environmentally induced damage mechanisms.

3.5 Summary of Expected Results

Mechanisms of crack tip damage will be identified by analysis of corrosion fatigue and fracture toughness test results and correlations to detailed SEM and TEM fractographic analysis results. The following is a general summary of expected results.

<u>GENERAL TEST DESCRIPTION</u>	<u>EXPECTED RESULTS</u>
Phase 1: Preliminary Testing	<ul style="list-style-type: none"> - Qualify test techniques - Identify test environments - Determine test parameters - Determine FCG characteristics
Phase 2: Corrosion Fatigue Characterization	<ul style="list-style-type: none"> - Identify CF regimes - Determine effect of environment type and contribution of HE, dissolution, surface film - Identify possible susceptible microstructure - Compare CF in alloy 2090 and 7075
Phase 3: Damage Mechanisms	
Embrittlement Testing (K_{IC}/J_{IC})	<ul style="list-style-type: none"> - Confirm role of HE - Determine size of embrittlement zone versus exposure K and microstructure
Microstructure FCG Study	<ul style="list-style-type: none"> - Identify role of microstructure versus confirmed mechanism
Surface Film Study	<ul style="list-style-type: none"> - Identify role of surface films during CF for different environment types

4.0 References

- A1. Aluminum Alloys - Physical and Mechanical Properties, Vols I and II, E.A. Starke, Jr. and T.H. Sanders, Jr., eds., EMAS Ltd., Warley, West Midlands, UK (1986).
- A2. Aluminum - Lithium Alloys III, C. Barker, P.J. Gregson, S.J. Harris and C.J. Peel, eds., Institute of Metals, Oxford, UK, in press (1986).
- A3. Aluminum - Lithium Alloys II, T.H. Sanders, Jr. and E.A. Starke, Jr. eds., TMS-AIME, Warrendale, PA (1984).
- A4. Aluminum -Lithium Alloys, T.H. Sanders, Jr. and E.A. Starke, Jr. eds., TMS-AIME, Warrendale, PA (1981).
- A5. E.A. Starke, Jr. and T.H. Sanders, Jr., Journal of Metals, Vol. 33, p. 24 (1981).
- A6. H.K. Hardy and J.M. Silcock, Journal of the Institute of Metals, Vol. 84, p. 423 (1955-56).
- A7. J.M. Silcock, Journal of the Institute of Metals, Vol. 88, p. 357 (1959-60).
- A8. B. Noble and G.E. Thompson, Metal Science Journal, Vol. 6, p. 167 (1972).
- A9. W.A. Cassada, G.J. Shiflet and E.A. Starke, Jr., Scripta Metall., Vol.20, p.751 (1986).
- A10. J.C. Huang and A.J. Ardell, p. 455 in Aluminum-Lithium III, eds C. Baker et al., Institute of Metals, London, (1986).
- A11. M.H. Tosten, A.K. Vasudevan and P.R. Howell, p. 490 in Aluminum - Lithium Alloys III, eds. C.Baker et al., Institute of Metals, London, (1986).
- A12. T.H. Sanders, Jr. and E.A. Starke, Jr., Acta Metall., Vol. 30, p. 927 (1982).
- A13. T.H. Sanders, Jr., Material Science and Engineering, Vol. 43, p. 247 (1980).
- A14. T.S. Srivatsan and E.J. Coyne, Jr., International Journal Fatigue, Vol. 8, No. 4, p. 201 (1986).
- A15. K.V. Jata and E.A. Starke, Jr., Metall. Trans. A, Vol.17A, P. 1011 (1986).

- A16. S. Suresh, A.K. Vasudevan, M. Tosten and P.R. Howell, Acta Metall., Vol. 35, No 1, p. 25 (1987).
- A17. A.K. Vasudevan and R.D. Doherty, "Grain Boundary Ductile Fracture in Precipitation Hardened Aluminum Alloys," To be published Acta Metall., (1987).
- A18. K.T. Venkateswara Rao, W. Yu and R.O. Ritchie, "Fatigue Crack Propagation in Aluminum - Lithium Alloy 2090: Part I Long Crack Behavior," Submitted to Metall. Trans. A., (1986).
- A19. Wolfgang Ruch, Kumar Jata and E.A. Starke, Jr., p. 145 in Fatigue 84, ed., C.J. Beevers, West Midlands, UK (1984).
- A20. R.O. Ritchie and J. Lankford, p. 1 in Small Fatigue Cracks, R.O. Ritchie and J. Lankford, eds., TMS-AIME, Warrendale, PA. (1986).
- A21. K.T. Venkateswara Rao, W. Yu and R.O. Ritchie, "Fatigue Crack Propagation in Aluminum - Lithium Alloy 2090: Part II Small Crack Behavior," Submitted to Metall. Trans. A. (1987).
- A22. M.R. James, "Growth Behavior of Small Fatigue Cracks in Al-Li-Cu Alloys," Submitted to Scripta Metall. (1987).
- A23. S. Suresh and R.O. Ritchie, International Metals Review, Vol. 6, No. 6, p. 445 (1984).
- A24. J. Lankford, Fatigue in Engineering Materials and Structures, Vol.5, No.3, p.233 (1982).
- A25. D.L. Davidson and J. Lankford, Materials Science Engineering, Vol.74, p.189 (1985).
- A26. J. Lankford and D.L. Davidson, Small Fatigue Cracks, R.O. Ritchie and J. Lankford, eds., TMS-AIME, Warrendale, PA, p.51 (1986).
- A27. R.O. Ritchie, W. Yu, D.K. Holm and A.F. Blom, "Development of Fatigue Crack Closure with the Extension of Long and Short Crack in Aluminum Alloy 2124: A Comparison of Experimental and Numerical Results," Presented at ASTM International Symposium on Fatigue Crack Closure, Charleston, S.C., May 1986.
- A28. R.P. Gangloff, Metall. Trans. A., Vol. 16A, p.953 (1985).
- A29. F.P Ford and S.J. Hudak, Jr., Small Fatigue Cracks, R.O. Ritchie and J. Lankford, eds., TMS-AIME, Warrendale, PA, p.289 (1986).

- A30. R.P. Gangloff and R.O. Ritchie, p. 529 in Fundamentals of Deformation and Fracture, B.A. Bilby, K.J. Miller and J.R. Willis, eds., Cambridge University Press, Cambridge (1983).
- A31. A. Turnbull and R.C. Newman, p. 269 in Small Fatigue Cracks, R.O. Ritchie and J. Lankford, eds., TMS-AIME, Warrendale, PA (1986).
- A32. N.J.H. Holroyd, A. Gray, G.M. Scamans and R. Hermann, p. 310, in Ref. 2.
- A33. J.G. Rinker, M. Marek and T.H. Sanders, Jr., p. 597 in Ref. 4.
- A34. T. Magnin, C. Dubessy and P. Rieux, p. 1177 in Ref. 2.
- A35. P.P. Pizzo, R.P. Galvin and H.G. Nelson, p. 173 in Environment Sensitive Fracture: Evaluation and Comparison of Test Methods, ASTM STP 821, eds., S.W. Dean, E.N. Pugh and G.M. Ugiansky (1984).
- A36. J.B. Lumsden, "Effects of Electrochemical Potential on the Stress Corrosion Cracking of an Al-Li-Cu-Mg-Zr Alloy," presented at TMS-AIME Fall Meeting, Toronto (1985).
- A37. P.P. Pizzo and D.L. Daeschner, p. 1197 in Ref. 1.
- A38. J.R. Craig, R.C. Newman, M.R. Jarrett and N.J.H. Holroyd, p.313 in Environmental Degradation of Engineering Materials III, eds., M.R. Louthan, Jr., R.P. McNitt, and R.D. Sisson, Jr., Penn. State University (1987).
- A39. L. Christodoulou, L. Struble and J.R. Pickens, p. 561 in Ref 3.
- A40. E.I. Meletis, J.M. Sater and T.H. Sanders, Jr., p. 1157 in Ref. 1.
- A41. A.K. Vasudevan, P.R. Ziman, S.C. Jha and T.H. Sanders, Jr., p. 303 in Ref. 2.
- A42. E.I. Meletis, "Stress Corrosion Cracking Properties of 2090 Al-Li Alloy," p. 315 in Proc. Int. Conf. Fatigue, Corrosion Cracking, Fracture Mechanics and Failure Analysis, ed. V.S. Goel, ASM, Metals Park, Ohio (1986).
- A43. A.K. Vasudevan, J. Lin and R.E. Ricker, p.321 in Ref.38.
- A44. M.O. Speidel, Metall. Trans. A, Vol.6A, p.631 (1975).
- A45. N.J.H. Holroyd and G. M. Scamans, p. 202 in Proceedings of Environment-Sensitive Fracture: Evaluation and Comparison of Test Methods, Gaithersburg, Md. (1982).

- A46. R.J.Gest and A.R. Troiano, Corrosion, Vol.30, No.8, p.274 (1974).
- A47. M. Pourbaix, Atlas of Electrochemical Equilibria in Aqueous Solutions, NACE, Houston, Texas (1974).
- A48. J.A. Feeney, J.C. McMillan and R.P. Wei, Metall. Trans., Vol.1, p. 1741 (1970).
- A49. Fu-Shiong Lin and E.A. Starke, Jr., p. 485 in Hydrogen Effects in Metals, I.M. Bernstein and A.W. Thompson, eds., TMS-AIME, Warrendale, PA (1980).
- A50. A. Gysler, J. Lindigkeit and G. Lutjering, p.1113 in Proceedings of the 5th International Conf. on the Strength of Metals and Alloys, Aachen, Germany (1979).
- A51. R.P. Wei, P.S. Pao, R.G.Hart, T.W. Weir and G.W. Simmons, Metall. Trans. A, Vol 11A, p.151 (1980).
- A52. D.L. Dicus, p. 513 in Environment-Sensitive Fracture, Evaluation and Comparison of Test Methods, ASTM STP 821, S.W. Dean, E.N. Pugh and G.M. Ugiansky, eds., American Society for Testing and Materials, Philadelphia, PA (1984).
- A53. J. Petit, p.3 in Fatigue Crack Growth Threshold Concepts, D.L. Davidson and S. Suresh, eds., TMS-AIME, Warrendale, PA (1983).
- A54. H.J.H. Holroyd and D. Hardie, Corrosion Science, Vol.23, No.6, p.527 (1983).
- A55. F.J. Bradshaw and C. Wheeler, Int. J. Fract. Mech., Vol. 14, p. 255 (1969).
- A56. F.P. Ford, Corrosion, Vol.35, No.7, p.281 (1979).
- A57. E.F. Smith, R. Jacko and D.J. Duquette, p. 218 in Proceedings of Second International Congress of Hydrogen in Metals, eds., A.W. Thompson and I. M. Bernstein, ASM, Metals Park, Ohio (1977).
- A58. K. Endo, K. Komai and Y. Watanabe, p.71 in Proceedings of 19th Japan. Congress on Materials Research, Society of Materials Science, Kyoto (1976).
- A59. J.E. Dresty and O.F. Devereux, Metall. Trans., Vol.4, p. 2469 (1976).
- A60. S.P. Flodder and W.H. Hartt, p.41 in Proceedings of Fourth Annual Conference on Ocean Thermal Energy Conversion, Technical Information Center, Oak Ridge, Tenn., Section VII (1977).

- A61. F.D. Bogar and T.W. Crooker, NRL Report 8153, Naval Research Laboratory, Washington, D.C. (1977).
- A62. T.S. Srivatsan, E.I. Meletis, C.P. Dervenis and E.J. Coyne, Jr., p.543 in ref.38.
- A63. E.J. Coyne, Jr., T.H. Sanders, Jr. and E.A. Starke, Jr., p. 293, in ref. 4.
- A64. P.P. Pizzo, R.P. Galvin and H.G. Nelson, p. 627 in ref. 3.
- A65. P.S. Pao, K.K. Sankaran and J.E. O'Neal, p. 307 in ref. 3.
- A66. R.E. Ricker and D.J. Duquette, "The Use of Electrochemical Potential to Control and Monitor Corrosion Fatigue of Aluminum Alloys," Corrosion 85, Paper No. 354, NACE, Houston, TX (1985).
- A67. A.H. Le and R.T. Foley, Corrosion, Vol. 40, p. 195 (1984).
- A68. T.H. Nguyen, B.F. Brown and R.T. Foley, Corrosion, Vol. 38, p. 319 (1982)
- A69. N.J.H. Holroyd, G.M. Scamans and R. Hermann, p. 327 in Embrittlement by the Localized Crack Environment, R.P. Gangloff, ed., TMS-AIME, Warrendale (1984).
- A70. Embrittlement by the Localized Crack Environment, R.P. Gangloff, ed., TMS-AIME, Warrendale (1984).
- A71. D.J. Duquette, "Mechanisms of Corrosion Fatigue of Aluminum Alloys," AGARD Conference Proceedings No. 316, Cesme, Turkey, (April 1981).
- A72. A.W. Thompson, Matls. Sci and Engr., Vol. 43, p. 41 (1980).
- A73. R.P. Gangloff, p. 175 in Advances in Crack Length Measurements, C.J. Beevers, ed., EMAS, United Kingdom (1982).
- A74. H. Tada, P. Paris and G.I. Irwin, p. 2.10 in The Stress Analysis of Cracks Handbook, Del Research Corp., St. Louis, Missouri.
- A75. D.K Donald and D.W. Schmidt, J. of Testing and Evaluation, Vol.8, No.1, p.19 (1980).
- A76. Standard Test Method for Measurement of Fatigue Crack Growth Rates, ASTM E647-86a, Vol. 03.01, p. 899, ASTM, Philadelphia, PA (1987).

A77. S. Suresh, Metall. Trans.A, Vol.16A, p.249 (1985).

A78. M. Nageswararao and V. Gerald, Metall. Trans. A, Vol.7A, p.1847 (1976).

TABLE 1
Al-Li-Cu and Al-Li Microstructure

<u>Alloy</u>	<u>Matrix Phases</u>	<u>Sub Grain Boundary Phases</u>	<u>High Angle Grain Boundary Phases</u>	<u>Precipitate Composition</u>
Al-Li Binary	δ', δ	N/A	δ	δ' - Al_3Li δ - AlLi
Al-Li-Cu-Zr Alloy 2090 Stretched and Peakaged	$\delta', \text{T}_1, \theta', \beta'$	T_1	T_2, T_1	θ' - Al_2Cu T_1 - Al_2CuLi T_2 - Al_6CuLi_3 β' - Al_3Zr

TABLE 2

Mechanisms of Small Crack Fatigue Growth

	(A) <u>"Short"</u> Many grains @ front $R_y \gg \text{g.s.}$	(B) <u>"Small"</u> Microstructural Crack in 1 grain $R_y < 1 \text{ to } 2 \text{ g.s.}$
(1) Physical	$a < 1 \text{ mm}$ K effective Retarded Closure	
(2) Mechanical	$a \leq 1 \text{ to } 5 R_y$ SSY Violated Active Plasticity J Integral, CTOD	$a < \text{g.s.}, R_y < \text{g.s.}$ Enhanced crack opening Increased tip strain
(3) Chemical	$a < 5 \text{ mm}$ Crack geometry sensitive Mass transport and chemical reaction	

R_y - Crack tip reversed plastic zone size

g.s. - Grain size

a - Crack length

SSY - Small scale yielding (criterion of linear elastic fracture mechanics)

"Active plasticity" zone comparable in size to crack length

TABLE 3

Effect of Cathodic Polarization on FCG

Material	Observation	Reference
7075-T6 & T76	Smooth specimen - fatigue life in salt water increased by polarizing to -1.0v (SCE). At more negative potentials fatigue life reduced.	(57,59)
Al-Zn-Mn- Cu	Smooth specimen-cathodic potentials, to -1.3v, (SCE) lengthened fatigue life in 1% NaCl aerated solution. At potentials more cathodic, fractures become brittle in appearance.	(58)
5086-H34	Smooth specimen-cathodic polarization at -1.0v (SCE), in seawater @ 20Hz, produced a growth rate similar to that in air. A potential of -1.3 v (SCE) caused a more rapid growth rate.	(60)
5086-H116 -H117	In natural seawater, at low K, FCG decreased with decreasing potential.	(61)
5456-H116	No embrittling FCG effects were observed to a cathodic potential of -1.4v (Ag/AgCl).	(61)

TABLE 4

Phase 1 Experiment Summary

<u>Test Type</u>	<u>Material</u>	<u>Environment</u>	<u>Experimental Conditions</u>	<u>Objectives</u>
Potentiodynamic Polarization	Alloy 2090 Underaged Peaked Overaged	Deaerated NaCl - Water	Anodic Potential Scan from cathodic region to the breakaway potential. NaCl concentrations will be varied from 0.1 w/o to 3.5 w/o	<ul style="list-style-type: none"> - Determine general electrochemical characteristics of Alloy 2090 - Identify optimum environmental conditions for corrosion fatigue tests. - Observe microstructural localized corrosion for the different aging treatments.
Fatigue Crack Propagation	4130 Steel	Moist Air	Constant ΔK Decreasing ΔK ; C = $-0.30m^1$	<ul style="list-style-type: none"> - Demonstrate test techniques using small grain size material. Compare results with literature.
	4130 Steel	Aqueous NaCl	Constant ΔK Decreasing ΔK ; C = $-0.30m^1$	As above, demonstrate chemical crack size effect.
	Alloy 2090 Peaked L-S	Aqueous NaCl	Constant ΔK Decreasing ΔK ; C = $-1.07m^1$ Anodic electrode potential	<ul style="list-style-type: none"> - Establish test procedures under most aggressive environment to be studied.
	Alloy 2090 Peaked L-S	He	Constant ΔK Decreasing ΔK ; C = $-1.07m^1$	<ul style="list-style-type: none"> - Monitor growth under sustained anodic corrosion
		He + H ₂ O	Constant ΔK	<ul style="list-style-type: none"> - Monitor fatigue properties in He with water vapor.
	Alloy 2090 Peaked L-T	Moist Air	Constant ΔK Decreasing ΔK ; C = $-0.30m^1$	<ul style="list-style-type: none"> - Reproduce closure corrected literature data for Alloy 2090

TABLE 4 (continued)

<u>Test Type</u>	<u>Material</u>	<u>Environment</u>	<u>Experimental Conditions</u>	<u>Objectives</u>
	Alloy 2090 Peakaged L-S	Lab Air	Constant ΔK Decreasing ΔK ; C = $-0.30m^1$	- Compare FCG characteristic in L-S direction to L-T direction (above)
Fatigue Test	Alloy 2090 Peakaged L-T	Aqueous NaCl	Constant ΔK Decreasing ΔK ; C = $-0.30m^1$	- Characterize FCG in aqueous solution and compare to air environment; L-T direction
	Alloy 2090 Peakaged L-S	Aqueous NaCl	Constant ΔK Decreasing ΔK ; C = $-0.30m^1$	- Characterize FCG in aqueous solution and compare to air environment; L-S direction
	Alloy 2090 Peakaged and Overaged L-S	Aqueous NaCl	Constant ΔK Change specimen electrode potential during test (cathodic, open circuit anodic)	- Establish test techniques. - Monitor growth at various electrode potentials.

TABLE 5

Phase 2 Experiment Summary

Test No.	DK MPa m	R	f (Hz)	Crack Growth Increment (mm)	Material Type	Material Direction	Environment
2-1	2.2	0.8	20,5 2,1,0.2 0.07	2.5	2090	L-T	NaCl - Anodic - Cathodic
2-2	9.9 2.2	0.1 0.8	20,5 2,1,0.1, 0.01	3.8	2090	L-T	NaCl - Anodic - Cathodic
2-3	15.0 2.4	0.05 0.85	20,5 1,0.1, 0.01	2.5	2090	L-T	NaCl - Anodic
2-4	15.0 2.4	0.05 0.85	T.B.D.	2.0	2090	L-S	He
2-5	↓	↓	↓	↓	↓	↓	He+H ₂ O
2-6	↓	↓	↓	↓	↓	↓	O ₂
2-7	↓	↓	↓	↓	↓	↓	NaCl - Anodic
2-8	↓	↓	↓	↓	↓	↓	NaCl - Cathodic
2-9	↓	↓	↓	↓	↓	L-T	He
2-10	↓	↓	↓	↓	↓	↓	He+H ₂ O
2-11	↓	↓	↓	↓	↓	↓	O ₂
2-12	↓	↓	↓	↓	↓	↓	NaCl - Anodic
2-13	↓	↓	↓	↓	↓	↓	NaCl - Cathodic
2-14	↓	↓	↓	↓	7075	↓	He
2-15	↓	↓	↓	↓	↓	L-T	He+H ₂ O
2-16	↓	↓	↓	↓	↓	↓	O ₂
2-17	↓	↓	↓	↓	↓	↓	NaCl - Anodic
2-18	↓	↓	↓	↓	↓	↓	NaCl - Cathodic
2-19	ΔK ↓	R↑	↓	TBD	2090	L-S	NaCl - Cathodic
2-20	ΔK ↓	R↑	↓	TBD	2090	L-S	He

T.B.D. - To Be Determined

TABLE 6

Phase 3 Experiment Summary

<u>Test Type</u>	<u>Material</u>	<u>Environment</u>	<u>Experimental Conditions</u>	<u>Objectives</u>
J_{IC}/K_{IC} (Embrittlement)	Selected Specimens from Phase 2	Moist Air	Rising Load	- Determine the fatigue induced embrittlement characteristics of NaCl aqueous environment for two stress intensity ranges and two microstructural crack growth paths.
Fatigue (Microstructural)	Alloy 2090 with altered micro-structure: Low levels of T_1 and H_1 in the substructure and matrix with only T_2 on the high angle boundaries.	Aqueous NaCl	Constant ΔK Change specimen electrochemical potential during test LT	- Monitor crack growth kinetics versus environmental susceptibility and microstructure.
	As above	Aqueous NaCl	As above L-S	As above
	Large single recrystallized	Helium H_2O Vapor	Constant ΔK Single Grain Test	- Monitor crack growth kinetics and the change in crack path orientation versus environment.
(Surface Film)	Slow cycle crack surface potential measurement	Slow cycle crack surface contact electrical potential measurement		- Determine role of surface films during CF - Correlate results to expected crack chemistry

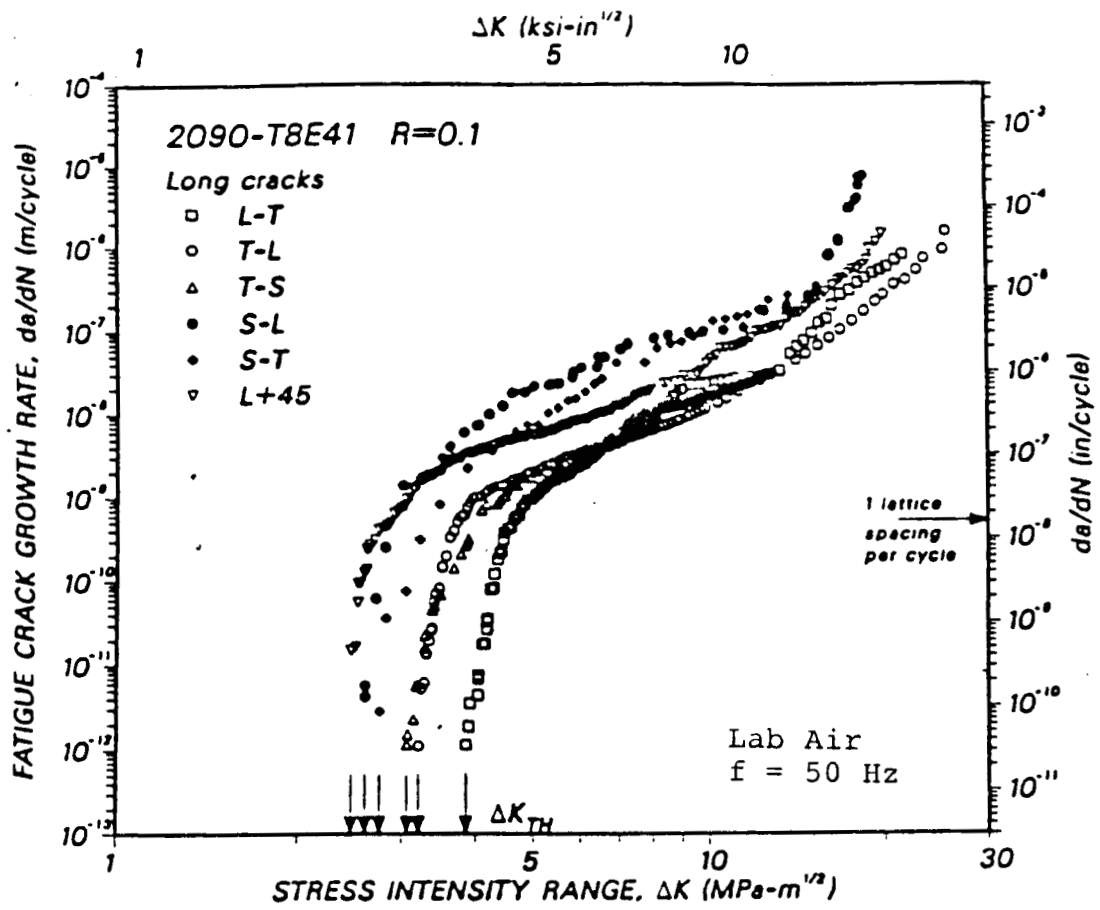


Figure 1 Fatigue Crack Growth for Different Plate Orientations (18)

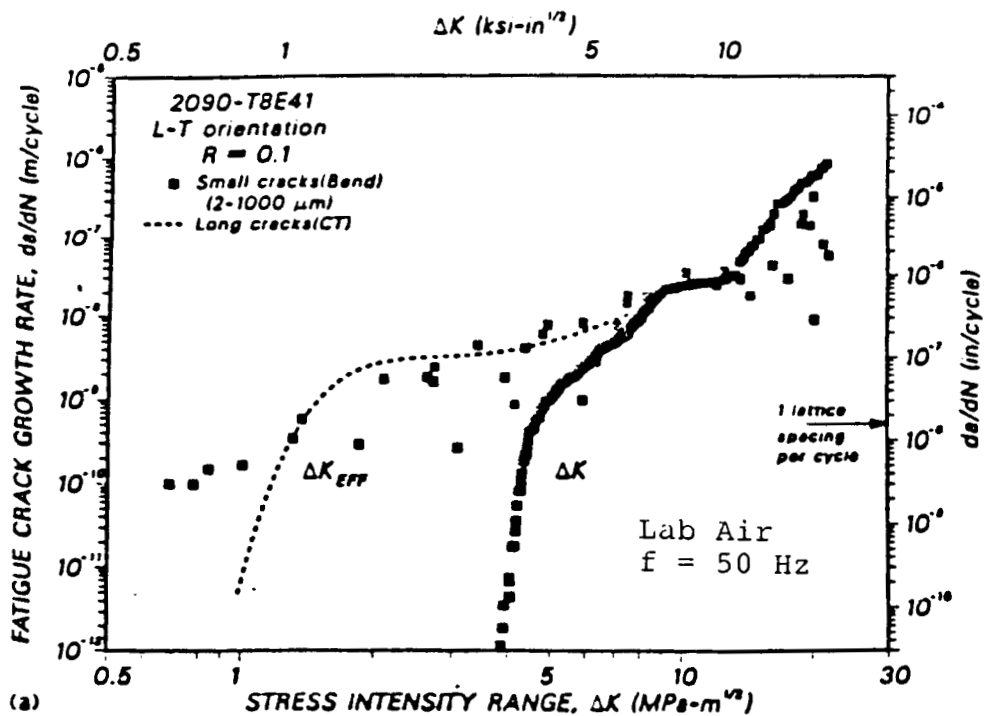
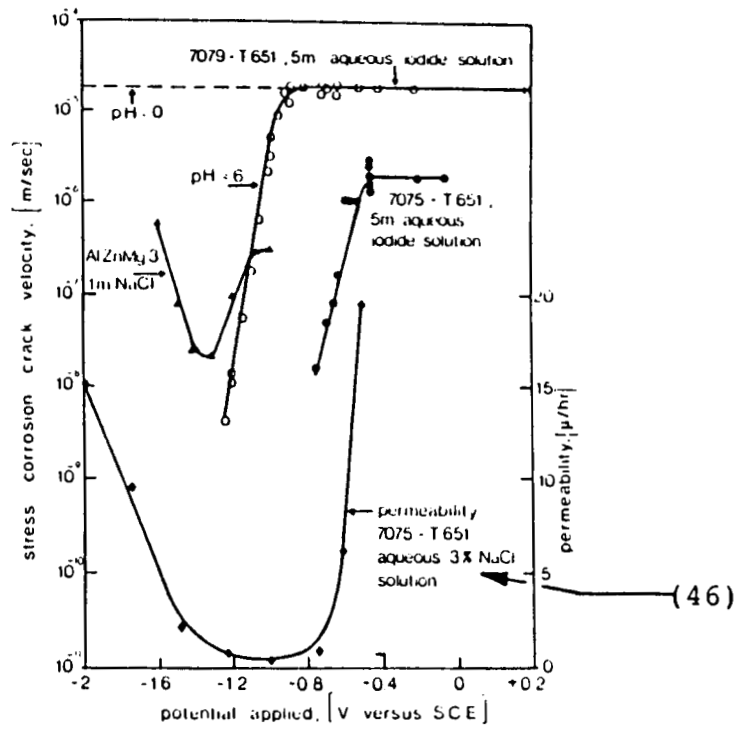
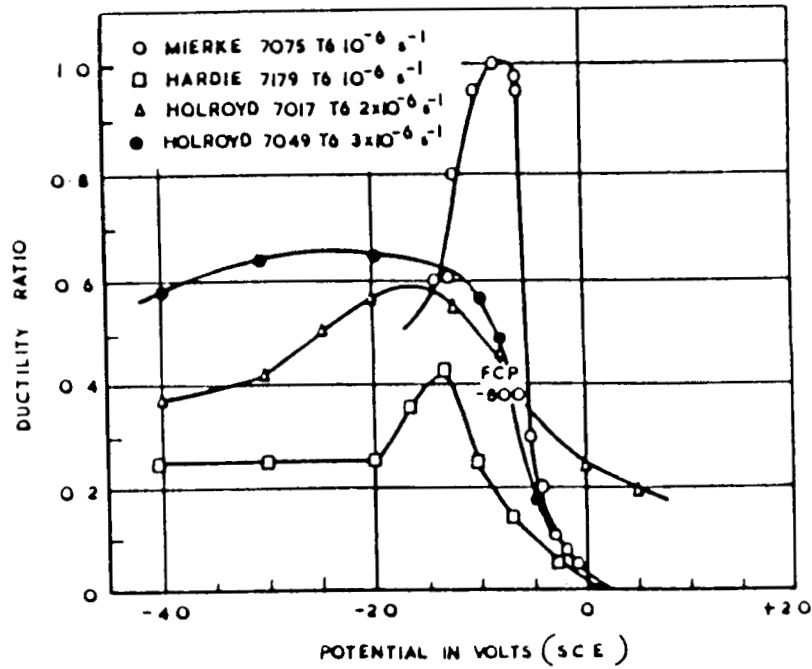


Figure 2 Comparison of the Growth Rates of Long and Microstructurally - Small Fatigue Cracks (21)



(a) SCC response (44)



(b) Slow strain rate response (45)

Figure 3 Effect of Electrochemical Potential on SCC

2024-T3

7075-T6

7178-T6

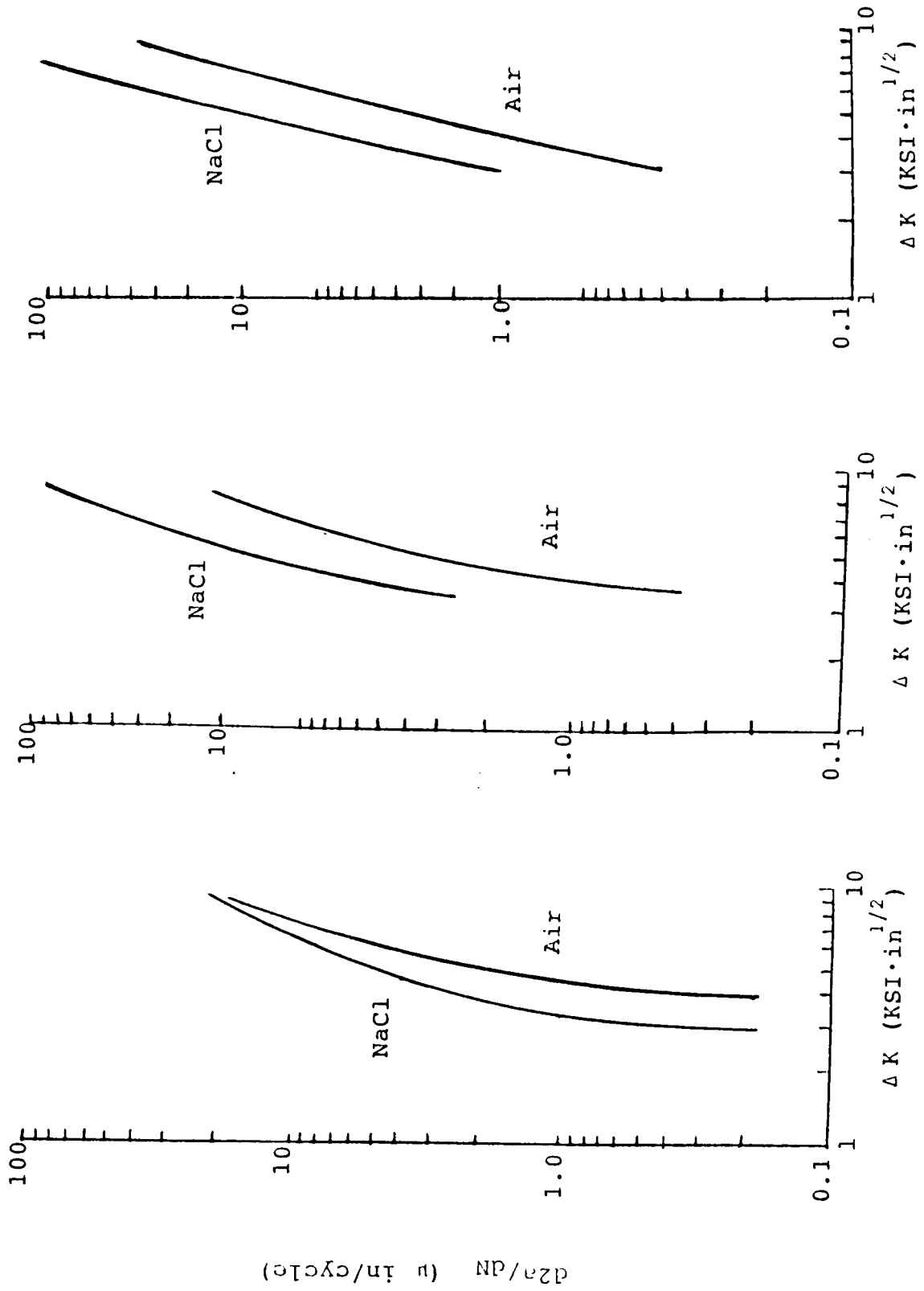
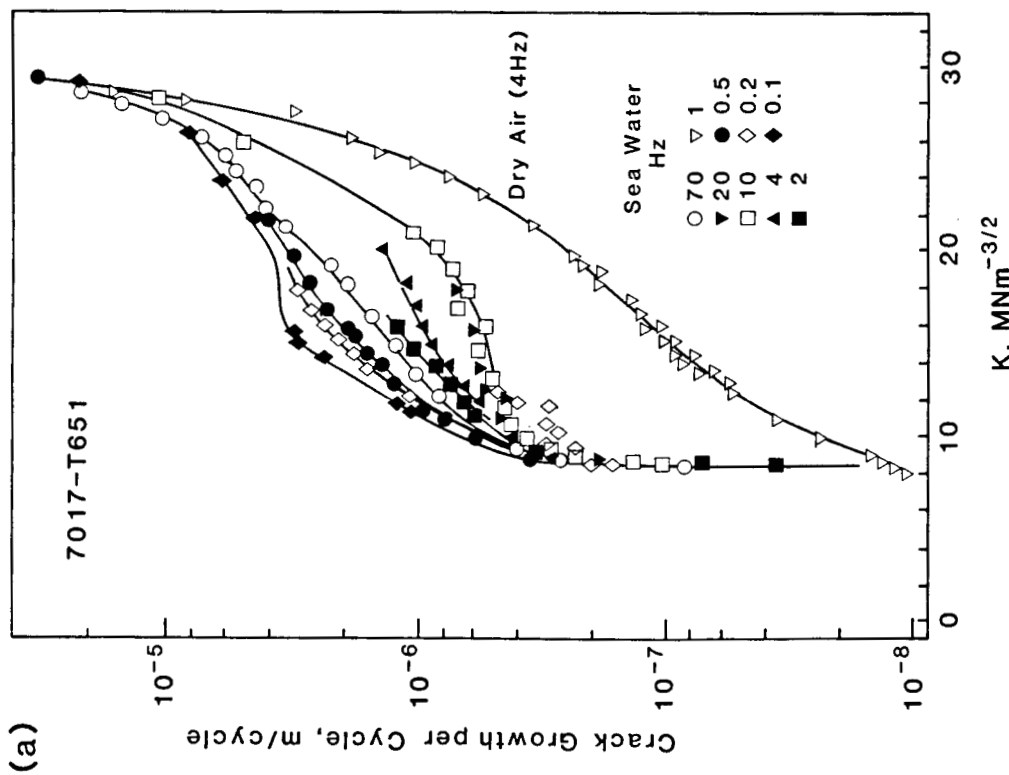
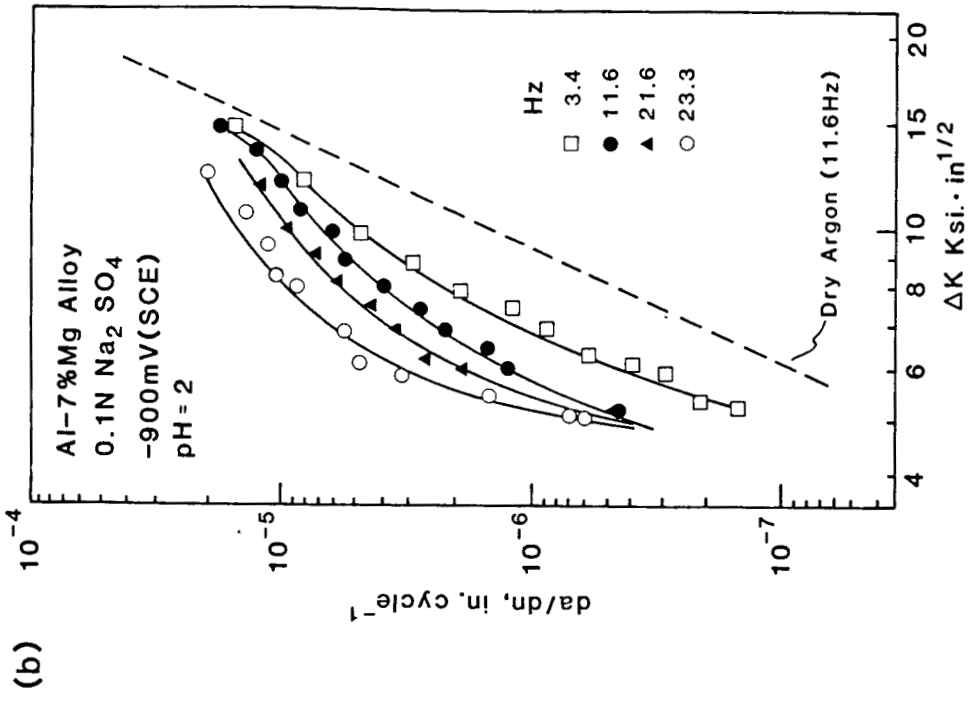


Figure 4 Fatigue crack growth in 3.5% NaCl solution and dry air (<10% R.H.), $f = 2 \text{ Hz}$, (48).



a) FCG at High ΔK (54)



b) FCG at Low ΔK (56)

Figure 5 Effect of Frequency on FCG in Aqueous Environments.

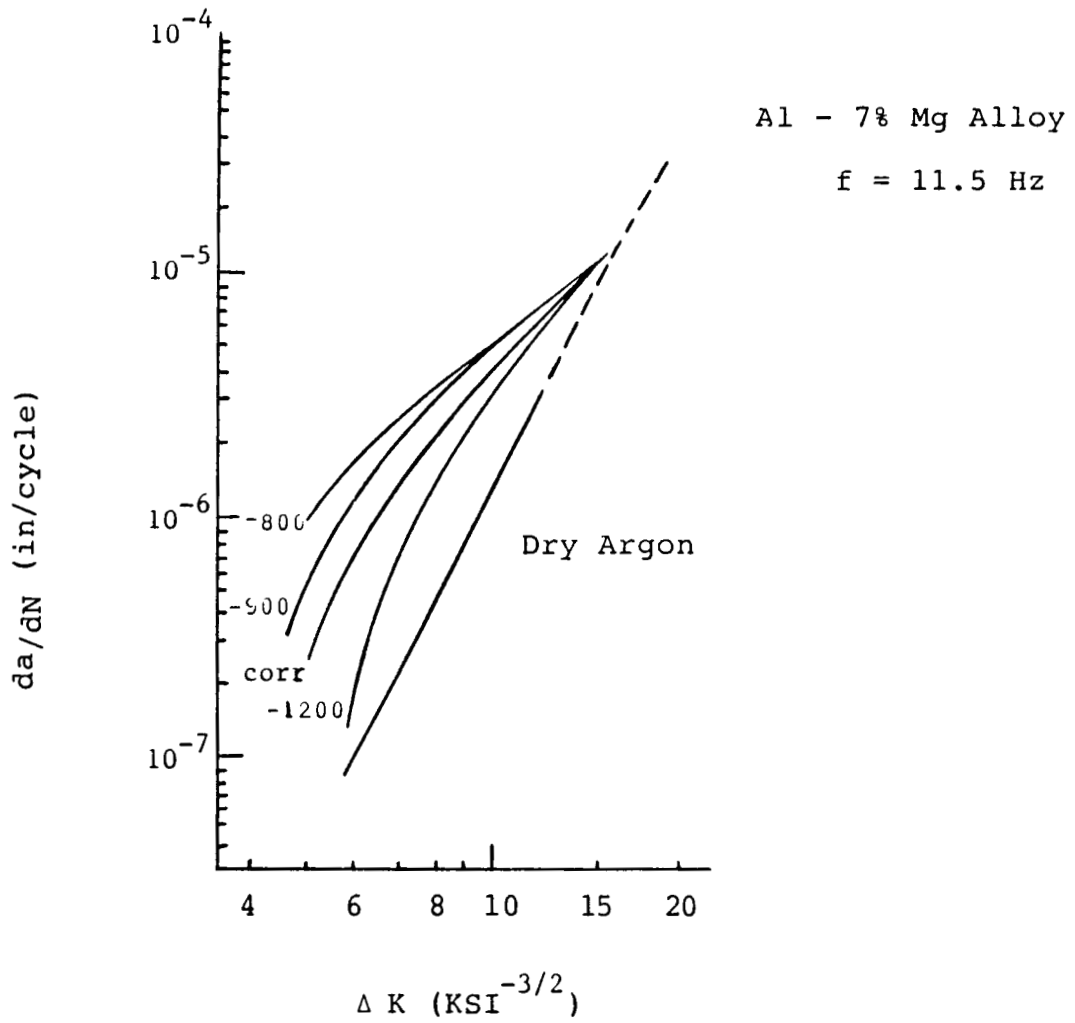


Figure 6 Effect of Polarization on FCG in 1N Na_2SO_4 Solution (56).

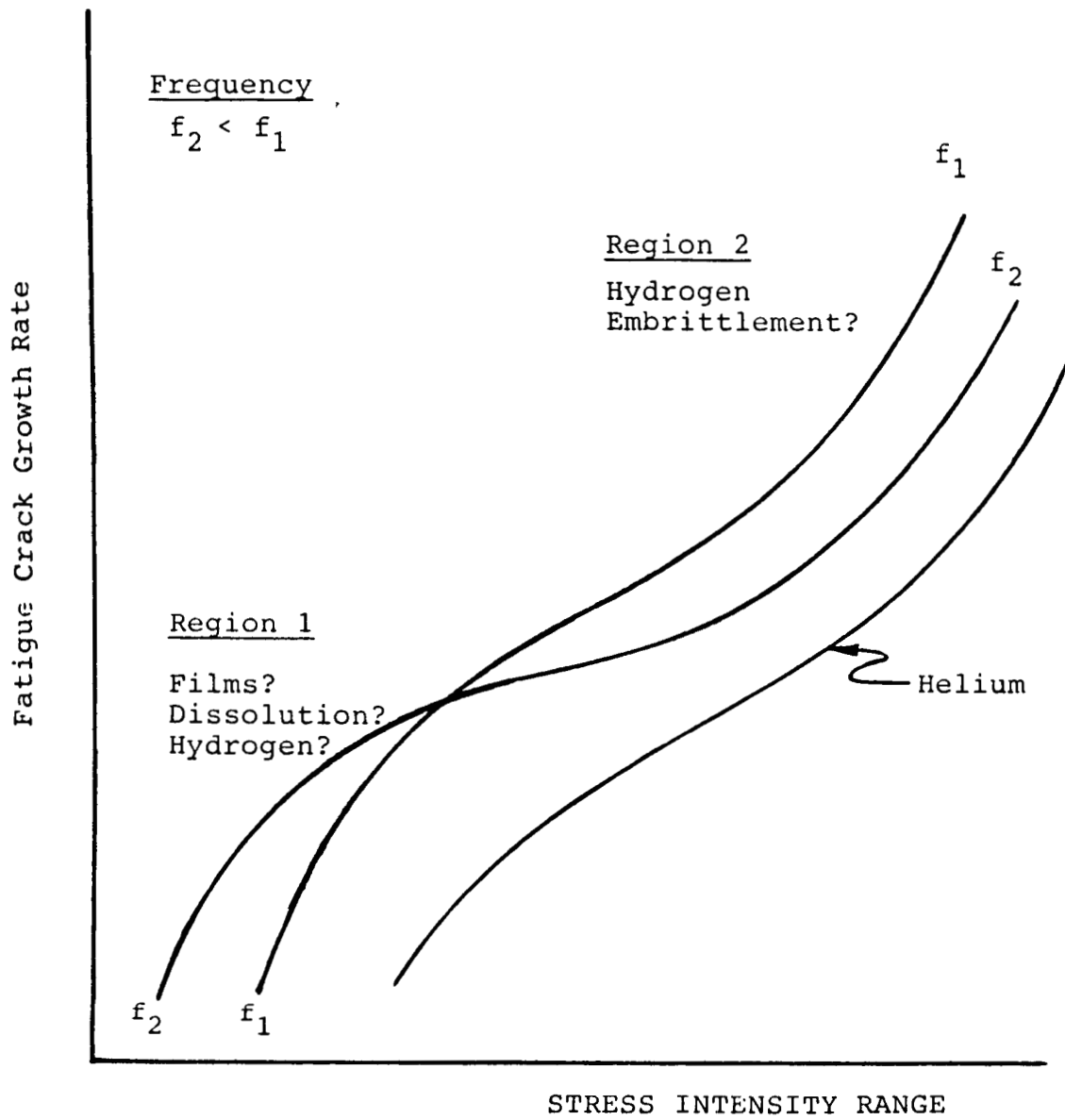
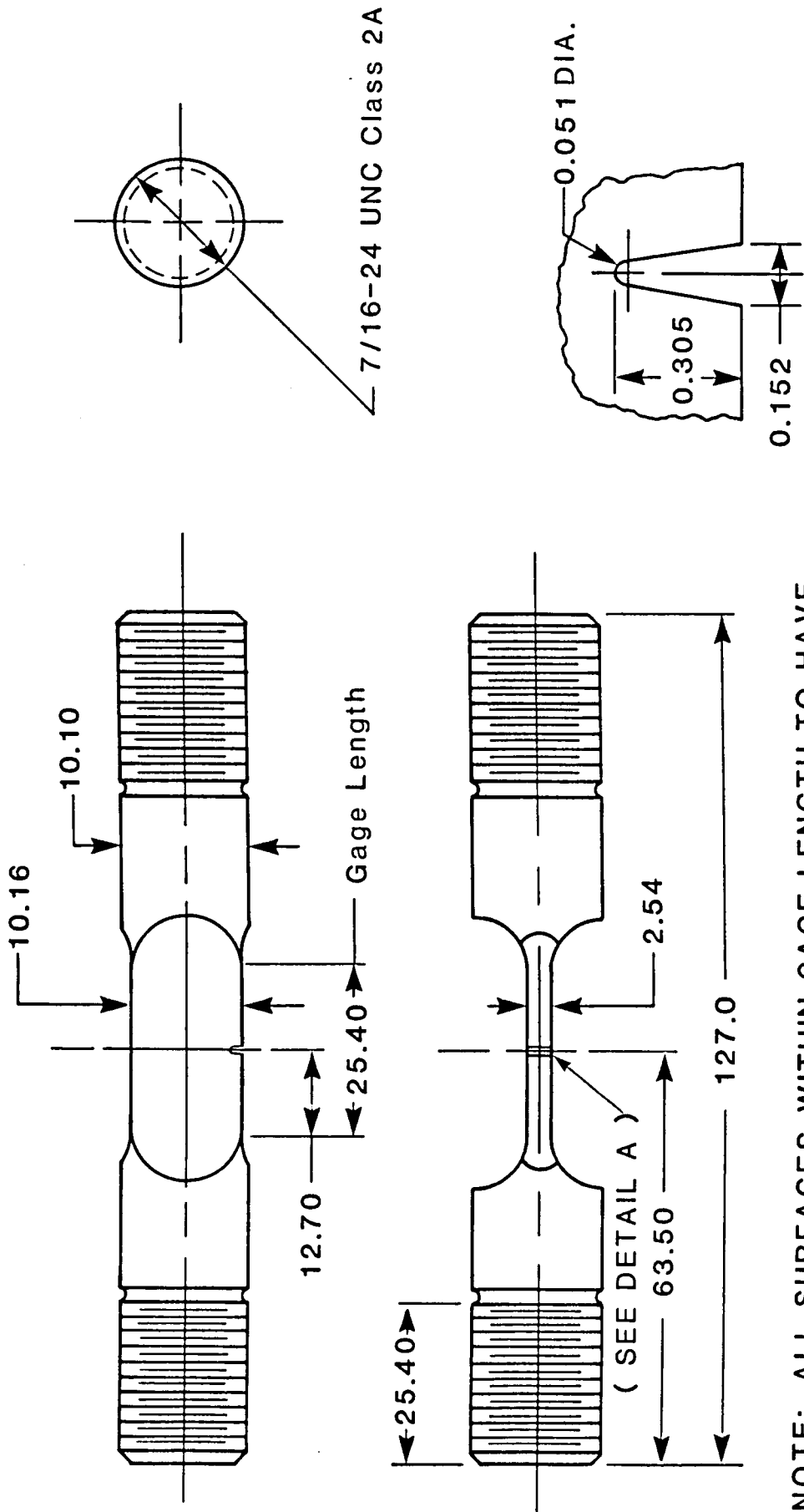


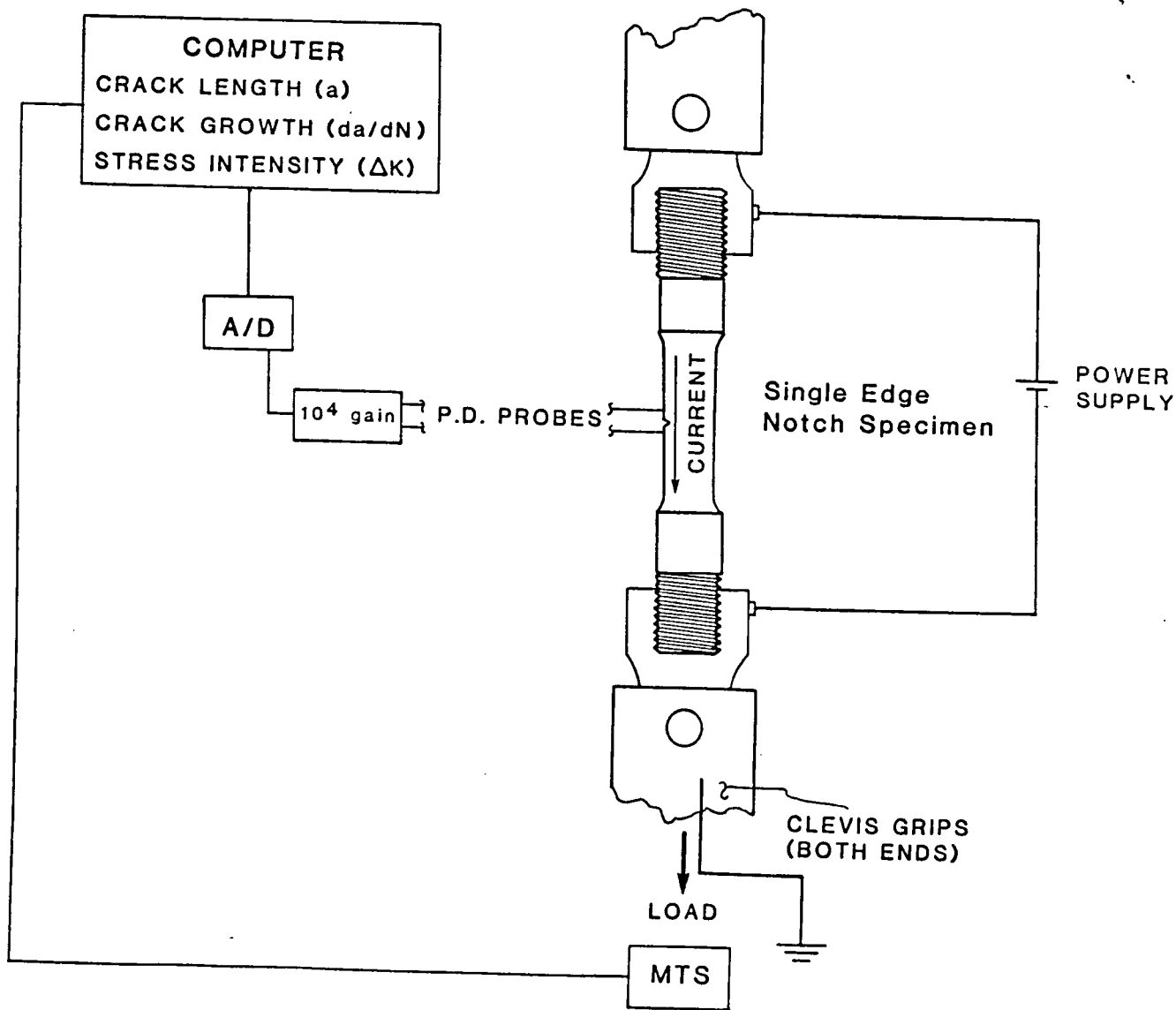
Figure 7 Hypothesized FCG Regime



NOTE: ALL SURFACES WITHIN GAGE LENGTH TO HAVE SURFACES FINISH OF 0.2 μ m, BALANCE 0.8 μ m POLISH GAGE IN LONGITUDINAL TO SPECIMEN AXIS ONLY

ALL DIMENSIONS IN MILLIMETERS

Figure 8 Test Specimen Drawings



Potential Difference Testing

Figure 9 Potential Difference Testing

AQUEOUS ENVIRONMENT TEST CELL

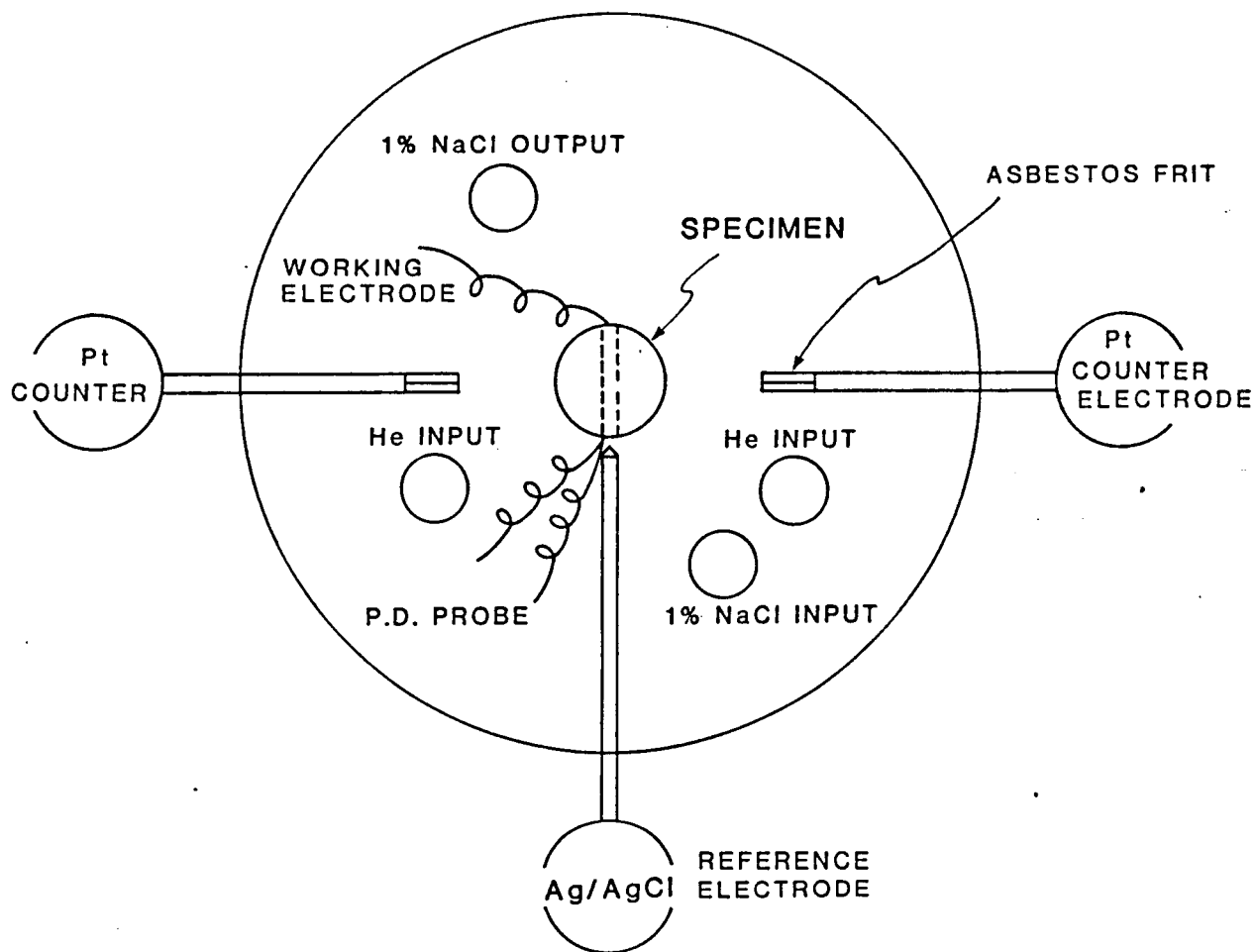


Figure 10 Aqueous Environment Test Cell

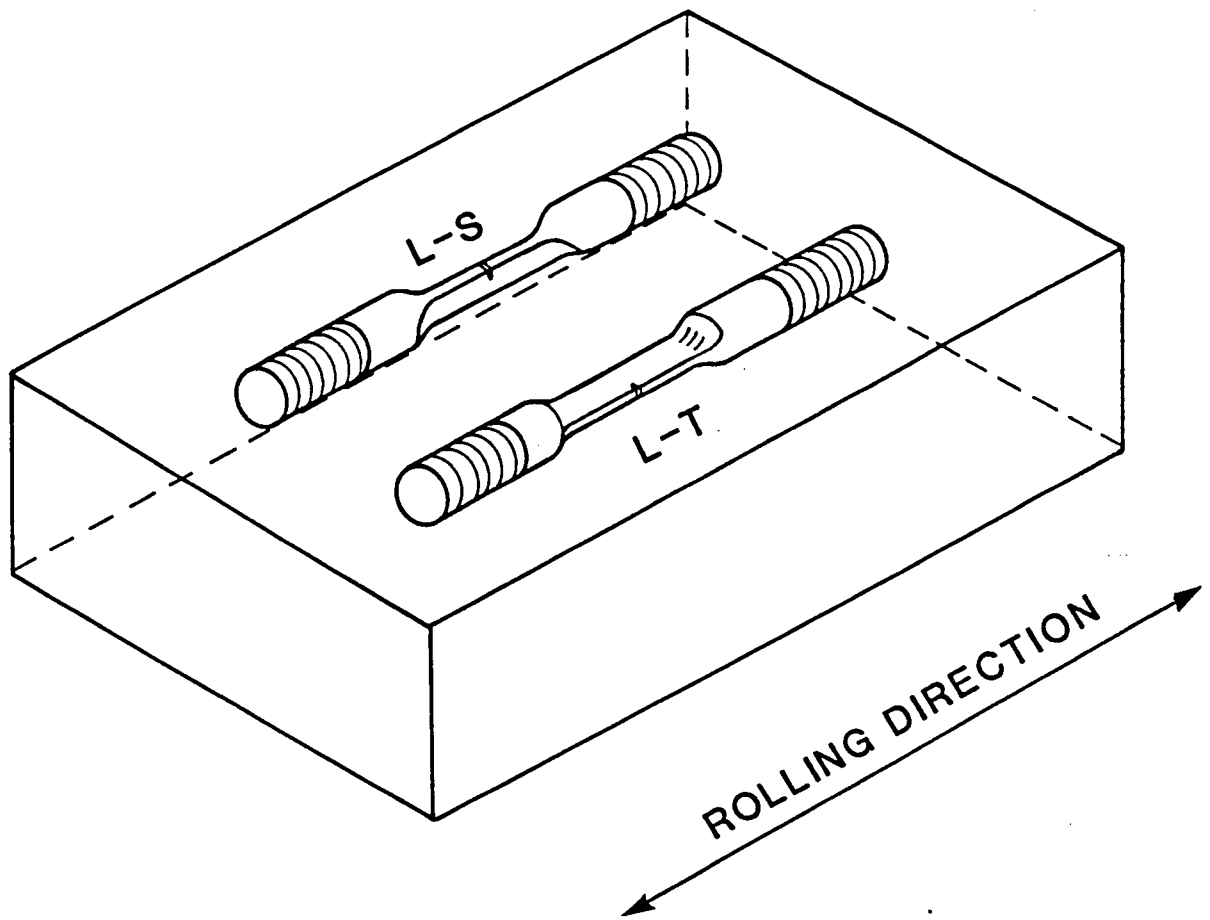


Figure 11 Test Specimen Orientation

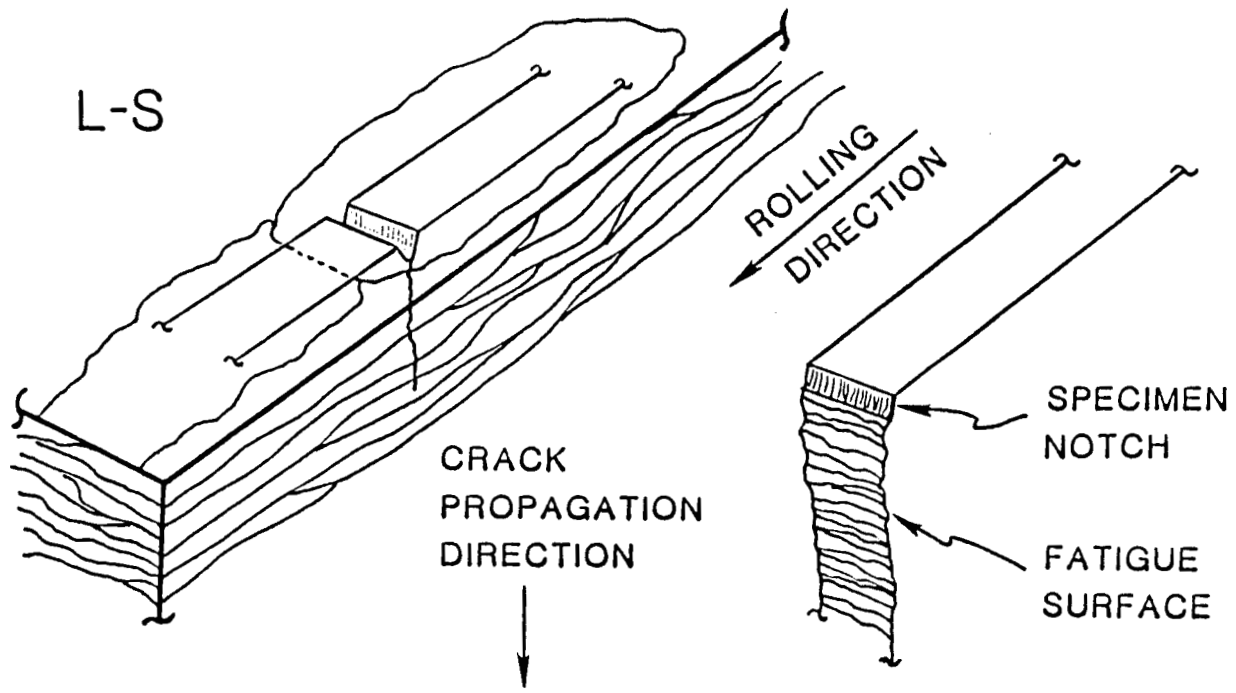


Figure 12a L-S Orientation

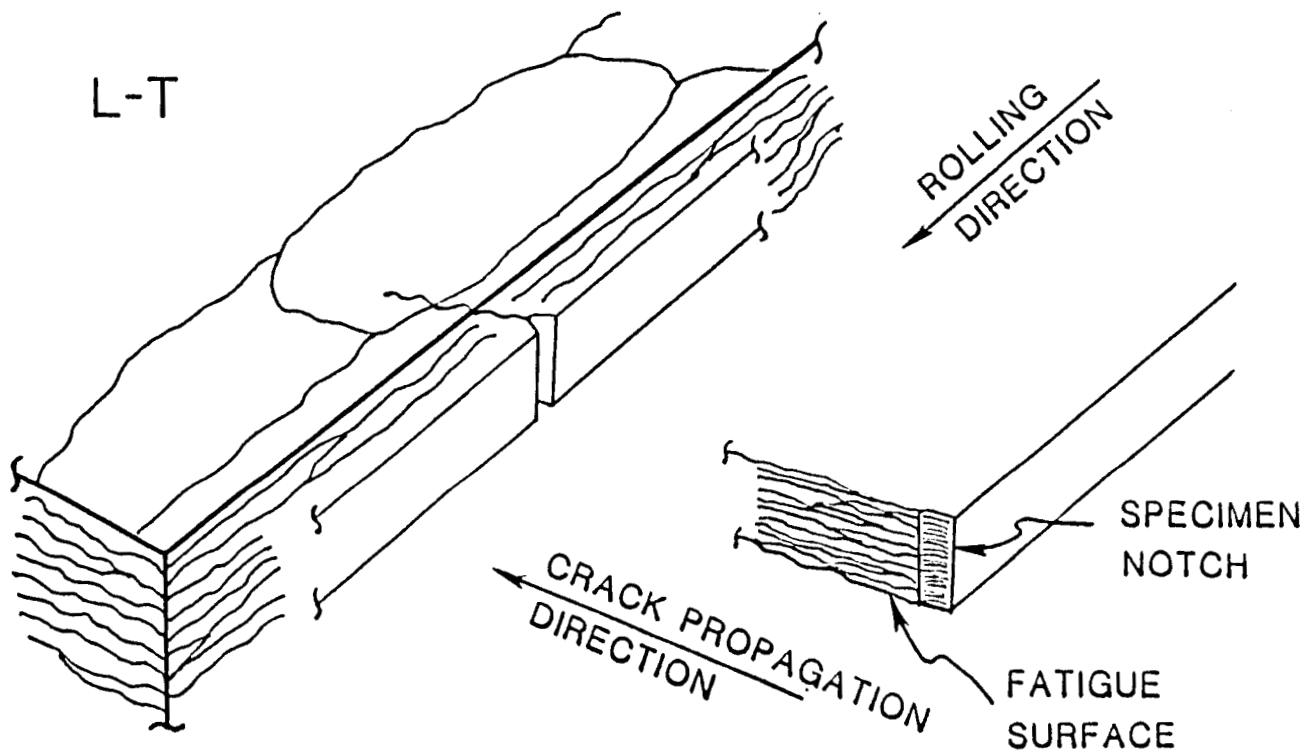


Figure 12b L-T Orientation

Figure 12 Fracture Surface Microstructure

APPENDIX II

CURRICULA VITAE

of

Richard P. Gangloff

Glenn E. Stoner

Robert E. Swanson

Richard P. Gangloff

Born:

Pittsburgh, Pennsylvania, August 4, 1948

Education:

B.S.	(metallurgy and materials science)	Lehigh University, 1970
M.S.	(metallurgy and materials science)	Lehigh University, 1972
Ph.D.	(metallurgy and materials science)	Lehigh University, 1974

Professional Experience:

Department of Metallurgy and Materials Science, Lehigh University, Bethlehem, PA
Instructor, 1970-1972
Research Assistant, 1972-1974

Corporate Research and Development Center, General Electric Co., Schenectady, New York
Metallurgist, 1974-1980

Corporate Research Science Laboratories, Exxon Research and Engineering Co., Annandale, New Jersey
Staff Metallurgist, 1980-1982
Senior Staff Metallurgist, 1982-1986

Department of Materials Science, School of Engineering and Applied Science, University of Virginia, Charlottesville, Virginia
Associate Professor, 1986 --

Honors and Awards:

BS with Highest Honors
Tau Beta Pi
Sigma Xi
Henry Marion Howe Medal, ASM

Richard P. Gangloff

Professional Societies and Committees:

American Society for Metals

Chairman, Metals Handbook Committee on Environmental Effects in Fatigue, 1984
Member, International Materials Review Committee

American Institute of Mining and Metallurgical Engineers

Chairman, Hudson-Mohawk Chapter, 1979
Member, Environmental Effects Committee
Member, Board of Review, Metallurgical Transactions

American Society for Testing and Materials

Chairman, Task Group on Elevated Temperature Cracking, 1982-83
Chairman, Task Group on Small Cracks, 1983-85
Chairman, Subcommittee E24.04 on Subcritical Crack Growth, 1985--
Member, Executive Committee E24 on Fracture Mechanics, 1985--

Research Interests:

The metallurgy, mechanics and chemistry of metal fatigue and fracture, with emphasis on mechanistic understanding for development of high performance materials and quantitative life prediction methods. Current research focuses on hydrogen embrittlement, corrosion fatigue, stress corrosion cracking and experimental fracture mechanics of ferrous, nickel based and aluminum alloys.

Richard P. Gangloff

Publications:

- Gangloff, R. P., Kraft, R. W., and Wood, J. D., "Fiberless Region Defects in Unidirectionally Solidified Al-Al₃Ni," Met. Trans., Vol. 3 (1972), pp. 348-350.
- Gangloff, R. P., and Hertzberg, R. W., "Elevated Temperature Tensile and Creep Rupture Behavior of the Unidirectionally Solidified Ni-Ni₃Nb Eutectic Composite," Proc. Conf. on In-Situ Composites, Vol. 2 (NMAB: Washington, 1972), pp. 83-103.
- Gangloff, R. P., and Wei, R. P., "Gaseous Hydrogen Assisted Crack Growth in 18Ni Maraging Steels," Scripta Met., Vol. 8 (1974), pp. 661-667.
- Coffin, L. F., and Gangloff, R. P., "Integrated Laboratory Methods for Evaluating PCI in Zircaloy-2 Fuel Cladding," Proc. Conference Water Reactor Fuel Performance (ANS: New York, 1977), pp. 346-355.
- Gangloff, R. P., and Wei, R. P., "Gaseous Hydrogen Embrittlement of High Strength Steels," Metall. Trans. A., Vol. 8A (1977), pp. 1043-1053.
- Gangloff, R. P., and Wei, R. P., "Fractographic Analysis of Gaseous Hydrogen Induced Cracking in 18Ni Maraging Steels," Fractography in Failure Analysis, ASTM STP 645 (ASTM: Philadelphia, PA, 1978), pp. 87-106.
- Tomalin, D. S., Adamson, R. B., and Gangloff, R. P., "The Performance of Irradiated Copper and Zirconium Barrier Modified Zircaloy Cladding Under Simulated PCI Conditions," Zirconium in the Nuclear Industry, ASTM STP 681 (ASTM: Philadelphia, PA, 1979), pp. 122-144.
- Gangloff, R. P., Graham, D. E., and Funkenbusch, A. W., "The Influence of Environment Purity on Gaseous Iodine Embrittlement of Zircaloy-2 and High Purity Zirconium," Corrosion, Vol. 35, No. 7 (1979), pp. 316-325.
- VanStone, R. H., and Gangloff, R. P., "The Effect of Processing Parameters on the Microstructure and Mechanical Properties of Rene 95 Consolidated from Gas Atomized Powders," in Rapid Solidification Processing, Principles and Technology II (Claitors Press: Baton Rouge, LA, 1980), pp. 317-330.

Richard P. Gangloff

Publications (continued):

- Gangloff, R. P., "Electrical Potential Monitoring of Crack Formation and Subcritical Growth from Small Defects," Fat. Engr. Matls. and Struct., Vol. 4, No. 1 (1981), pp. 15-33.
- Gangloff, R. P., "Quantitative Measurements of the Growth Kinetics of Small Fatigue Cracks in 10Ni Steel," Fatigue Crack Growth Measurement and Data Analysis, ASTM STP 738 (ASTM: Philadelphia, PA, 1981), pp. 120-138.
- Gangloff, R. P., "The Criticality of Crack Size in Aqueous Corrosion Fatigue," Res. Mech. Let., Vol. 1 (1981), pp. 299-306.
- Gangloff, R. P., "Electrical Potential Monitoring of the Formation and Growth of Small Fatigue Cracks in Embrittling Environments," in Beevers, C. J., ed., Advances in Crack Length Measurement (EMAS: United Kindom, 1982), pp. 175-231.
- Gangloff, R. P., "Solid Cadmium Embrittlement of Textured Zircaloy-2," in Kamdar, M. H., ed., Embrittlement by Liquid and Solid Metals (TMS-AIME: Warrendale, PA, 1984), pp. 485-505.
- Gangloff, R. P., "Oxygen Inhibition Model of the Chemical Crack Size Effect in Corrosion Fatigue," in Gangloff, R. P., ed., Embrittlement by the Localized Crack Environment (TMS-AIME: Warrendale, PA, 1984), pp. 265-290.
- Gangloff, R. P., and Ritchie, R. O., "Environmental Effects Novel to the Propagation of Short Fatigue Cracks," in Bilby, B. A., Miller, K. J., and Willis, J. R., eds., Fundamentals of Deformation and Fracture (Cambridge University Press: Cambridge, United Kindom, 1985), pp. 529-558.
- Gangloff, R. P., "Crack Size Effects on the Chemical Driving Force for Aqueous Corrosion Fatigue," Metall. Trans. A., Vol. 16A (1985), pp. 953-969.

Richard P. Gangloff

Publications (continued):

- Gangloff, R. P., "The Environmental Effect on Fatigue Crack Propagation," in Metals Handbook: Mechanical Testing, 9th edition, Vol. 9 (ASM: Metals Park, Ohio, 1985), pp. 403-410.
- Gangloff, R. P., "Inhibition of Aqueous Chloride Corrosion Fatigue by Control of Crack Hydrogen Production," in Critical Issues in Reducing the Corrosion of Steel (NSF/JSPS: Nikko, Japan, 1985), pp. 28-50.
- Gangloff, R. P., and Turnbull, A., "Crack Electrochemistry Modeling and Fracture Mechanics Measurement of the Hydrogen Embrittlement Threshold," in Jones, R. H., and Gerberich, W. W., eds., Modeling Environmental Effects on Crack Initiation and Propagation (TMS-AIME: Warrendale, PA, 1986), pp. 55-81.
- Gangloff, R. P., and Wei, R. P., "Small Crack-Environment Interactions: The Hydrogen Embrittlement Perspective," in Lankford, J., and Ritchie, R. O., eds., Small Fatigue Cracks (TMS-AIME: Warrendale, PA, 1986), pp. 239-264.
- Gangloff, R. P., "A Review and Analysis of the Threshold for Hydrogen Environment Embrittlement of Steel," Isserow, S. (ed.), in Corrosion Prevention and Control (U.S. Army Materials Technology Laboratory: Watertown, MA, 1986) in press.
- Gangloff, R. P., "Ethylene Inhibition of Gaseous Hydrogen Embrittlement in High Strength Steel," in Wei, R. P., and Gangloff, R. P., eds., Basic Questions in Fatigue, Vol. 2, ASTM STP (ASTM: Philadelphia, PA, 1987), in press.
- Gangloff, R. P., and Duquette, D. J., "Corrosion Fatigue of Metals: A Survey of Recent Advances and Issues," in Chemistry and Physics of Fracture, R. M. Latanision and R. H. Jones, eds. (Martinus Nijhoff Publishers BV, Netherlands, 1987), pp. 612-645.
- Wei, R. P., and Gangloff, R. P., "Environmentally Assisted Crack Growth in Structural Alloys: Perspectives and New Directions," in 20th National Symposium on Fracture Mechanics: Perspectives and Directions, ASTM STP, R. P. Wei and R. P. Gangloff, eds. (ASTM: Philadelphia, PA, 1987), in press.

Richard P. Gangloff

Publications (continued):

Andresen, P. L., Gangloff, R. P., Coffin, L. F., and Ford, F. P., "Applications of Fatigue Analyses: Energy Systems," in Fatigue 87, R. O. Ritchie and E. A. Starke, Jr., eds., (EMAS: West Midlands, UK, 1987), in press.

Gangloff, R. P., "Crack Tip Chemistry and Mechanics: Applications to Life Prediction," Matls. Sci. Engr. (1987), in press.

Books Edited:

Embrittlement by the Localized Crack Environment, eds., R. P. Gangloff, TMS-AIME, Warrendale, PA (1984).

Basic Questions in Fatigue, Vol. II, ASTM STP, eds., R. P. Wei and R. P. Gangloff, ASTM, Philadelphia, PA (1986), in press.

20th National Symposium on Fracture Mechanics: Perspectives and Directions, ASTM STP, eds, R. P. wei and R. P. Gangloff, ASTM, Philadelphia, PA (1987), in press.

Short Courses:

Modern View of Fatigue, Union College, 1975-present.

Aircraft Design and Development, NAVAIR, 1986-present.

Internal Reports:

General Electric - 12

Exxon - 14

Presentations (1980-1987):

Invited - 37

Contributed - 19

Intra-company Seminars - 14

Consulting:

Naval Research Laboratory

Exxon Research and Engineering Company

Crouse-Hinds

Infilco Degremont

Stephenson and Balthrop, Ltd.

Richard P. Gangloff

Invited Presentations:

<u>Title</u>	<u>Meeting</u>	<u>Place</u>	<u>Date</u>
"Environment Assisted Fracture of Metals: Damage Localization and Tolerance"	Washington, DC Chapter, ASM International	Washington, DC	May 1987
"Small Crack Fracture Mechanics"	Hudson-Mohawk Chapter, AIME	Albany, NY	Jan. 1987
"Damage Localization in Environment Assisted Cracking of Metals"	VAS	Harrisonburg, VA	May 1986
"Damage Localization Environment Assisted Cracking of Metals"	Brown University	Providence, RI	Apr. 1986
"Small Crack Effect in Environment Assisted Fracture of Steel"	Naval Research Laboratories	Washington, DC	Mar. 1986
"Small Crack Fracture Mechanics and the Development of High Performance Materials"	MIT-Dept. of Materials Sci.	Cambridge, MA	Apr. 1985
"The Growth of Small Fatigue Cracks in Embrittling Environments"	Kyoto University-Dept. of Materials Science	Kyoto, Japan	Mar. 1985
"Crack Geometry Effects on the Chemical Driving Force for Environmental Fracture"	General Electric Corp. Res. and Dev. Center	Schenectady, NY	Aug. 1984
"Crack Geometry Effects on the Chemical Driving Force for Environmental Fracture"	Battelle Laboratories	Columbus, OH	Jul. 1984
"Life Prediction by Crack Tip Modeling of Hydrogen Environment Embrittlement"	Mechanics and Physics of Crack Growth - DOE Workshop	Keystone, CO	Aug. 1987

Richard P. Gangloff

Invited Presentations (continued):

<u>Title</u>	<u>Meeting</u>	<u>Place</u>	<u>Date</u>
"Environmental Fracture of Metals"	Canadian Inst. Metallurgists International Symposium on Fracture	Winnipeg, Canada	Aug. 1987
"Environmentally Assisted Crack Growth in Structural Alloys: Perspectives and New Directions (By R.P. Wei)	20th National Symposium on Fracture Mechanics	Lehigh University	June 1987
"Applications of Fatigue Analyses: Energy Systems" (With P.A. Andresen, et al.)	Fatigue 87	University of Virginia	June 1987
"Corrosion Fatigue of HSLA Steels in Hydrogenous Electrolytes" (With R. Krishnamurthy)	Environmental Degradation of Engineering Materials	Penn State	Apr. 1987
"Corrosion Fatigue: Advances and Issues" (by D.J. Duquette)	NATO ARW on Chemistry and Physics of Fracture	Bad Reichenhall, West Germany	Sept. 1986
"Hydrogen Environment Embrittlement of Steel" (Contributed)	33 rd Sagamore Army Materials Research Conference	Burlington, VT	July 1986
"Microstructural Effects on Corrosion Fatigue of HSLA Steel in Aqueous Chloride" (By J.Y. Koo, Exxon) (Contributed)	Intl. Symp. on Off-Shore Mechanics and Arctic Engr.	Tokyo, Japan	Apr. 1986

Richard P. Gangloff

Invited Presentations (continued):

<u>Title</u>	<u>Meeting</u>	<u>Place</u>	<u>Date</u>
"Environmental Effects on the Propagation of Small Fatigue Cracks"	Engineering Foundation Conf. on Small Fatigue Cracks	Santa Barbara, CAL	Jan. 1986
"Crack Electro-chemistry Modeling and Fracture Mechanics Measurement of Sustained Load Cracking Thresholds" (With A. Turnbull)	AIME Symp. on Modeling Environmental Effects on Crack Initiation and Propagation	Toronto, Canada	Oct. 1985
"Inhibition of Aqueous Corrosion Fatigue by Control of Crack Hydrogen Production"	NSF-Japan Symp. on Reducing the Corrosion of Steel	Nikko, Japan	Mar. 1985
"Environmental Effects Novel to the Propagation of Short Fatigue Cracks" (With R.O. Ritchie)	Eshelby Memorial Symposium	Sheffield, England	Apr. 1984

Gangloff/CV5
Updated: 12/24/87

Glenn E. Stoner

Born:

Springfield, Missouri, 1940

Education:

B. S. (chemistry) University of Missouri, School of
Mines (MSM), 1962

M. S. (chemistry) University of Missouri, School of
Mines (MSM), 1963

Ph. D. (electrochemistry) University of Pennsylvania, 1968

Experience:

School of Engineering and Applied Science, University of Virginia,
Charlottesville, Virginia

Senior Scientist, 1968-1971 and 1972-1974

Department of Chemical Engineering:

Lecturer, 1971

Department of Materials Science:

Research Associate Professor, 1974-1977

Associate Professor, 1977-1983

Professor, 1983--

Visiting Appointments:

Visiting Associate Professor of Chemistry and Research Associate,
University of Missouri, Rolla, Missouri, 1970

Visiting Professor of Electrochemistry, Faculty, des Sciences, Uni-
versit, de Rouen, France, 1973-1974

Visiting Professor of Chemistry, University of Tel-Aviv, Ramat-
Aviv, Israel, May-August 1980

Glenn E. Stoner

Professional Societies and Appointed Committees:

Phi Kappa Phi

Sigma Xi

Tau Beta Pi

Kappa Mu Epsilon

American Heart Association Council on Thrombosis

Electrochemical Society

Editorial Board -- Biomaterials, Medical Devices and Artificial
Organs: An International Journal

Advisory Board: Wilkes College, Engineering Department, Wilkes
Barre, Pennsylvania

Member: National Association of Corrosion Engineers

Awards:

NASA Certificate of Recognition, May 1975

NASA Certificate of Recognition, December 1977

Professional Interests:

corrosion, energy conversion, biomaterials, electrocatalysis,
electrode kinetics, bioelectrochemistry

Consulting:

Consultant to ten companies and one national laboratory.

Patents:

"The Electrochemical Destruction of Pathogens," US Patent No.
3,725,226; Italian Patent No. 995,036; Great Britain Patent
No. 1,387,215 (other foreign patents pending)

"Method for Measuring Blood Clotting," US Patent No. 3,840,806
(with T. H. Boyd)

"Detecting the Presence of Microorganisms," US Patent No. 4,009,
078 (foreign patents pending)

Glenn E. Stoner

Patents (continued):

- "Detection of Microorganisms," US Patent No. 4,200,493 (with J. R. Wilkins)
- "Detection of Microorganisms," US Patent No. 4,246,343
- "Apparatus for Disinfection and Fluid Treatment," US Patent No. 4,384,943
- "Cavity Liner for Dental Restorations," US Patent No. 4,064,629 (with L. D. Zardiackas, foreign patents pending)
- "Apparatus and Method for Disinfecting Objects," US Patent No. 4,202,740 (with G. L. Cahen, Jr.)
- "Electrolysis Electrode," US Patent No. 4,285,796 (with G. L. Cahen, Jr.)
- "An Electrolysis Electrode," US Patent No. 4,337,138 (with G. L. Cahen, Jr.)

Publications:

- James, W. J., and Stoner, G. E., "Valence Exhibited by Zinc Amalgam Anodically Dissolving in Nitrate Solution," J. Am. Chem. Soc., Vol. 85 (1963), p. 1354.
- Bockris, J. O'M., Gileadi, E., and Stoner, G. E., "The Electrochemical Oxidation of Ethylene," J. Electrochem. Soc., Vol. 113 (1966), p. 585.
- Bockris, J. O'M., Stoner, G. E., and Cahan, B. D., "A Surface Conductivity Approach to Adsorption," Chemical Instrumentation, Vol. 1 (1969), p. 273.
- Bockris, J. O'M., Gileadi, E., and Stoner, G. E., "The Anodic Oxidation of Saturated Hydrocarbons: A Mechanistic Study," J. Phys. Chem., Vol. 73 (1969), p. 427.
- Stoner, G. E., "Electrosorption of Amino Acids, Peptides and Proteins in Relation to the Compatibility of Materials and the Human Body," J. Biomed. Mat. Res., Vol. 3 (1969), p. 655.
- Stoner, G. E., and Walker, L., "The Enzymatic and Electrochemical Polymerization of Fibrinogen," J. Biomed. Mat. Res., Vol. 3 (1969), p. 645.

Glenn E. Stoner

Publications (continued):

- Stoner, G. E., and Srinivasan, S., "Adsorption of Blood Proteins on Metals Using Capacitance Techniques," J. Phys. Chem., Vol. 74 (1970), p. 1088.
- Stoner, G. E., Catlin, A., and Gorman, R. R., "The Adsorption of Fibrinogen: An Electron Microscope Study," J. Phys. Chem., Vol. 75 (1971), p. 2103.
- Stoner, G. E., Srinivasan, S., and Gileadi, E., "Adsorption Inhibition as a Mechanism for the Antithrombogenic Activity of Some Drugs," J. Phys. Chem., Vol. 75 (1971), p. 2107.
- Stoner, G. E., Wawner, F., and Lawless, K., "A Corrosion Resistant Silver Tin Amalgam," J. Dent. Res., Vol. 50 (1971), p. 519.
- Stoner, G. E., Gileadi, E., and Senti, S., "The Effect of NaF and SnF₂ on the Rate of Corrosion of Dental Amalgams," J. Dent. Res., Vol. 50 (1971).
- Gileadi, E., and Stoner, G. E., "The Effect of Competition with Water on the Kinetic Parameters in Electrode Reactions," J. Electrochem. Soc., Vol. 118 (1971), p. 1316.
- Stoner, G. E., "A Rapid Method for Electron Microscopic Examination of Biological Specimens," Proc. 29th Meeting E.M.S.A (Baton Rouge, La.: Claitors Publishing Division, 1971), p. 486.
- Palaia, F., Catlin, A., Stoner, G. E., and Navarro, A., "An Improvement in the Vena-Cava Ring Implantation," J. Biomed. Mat. Res., Vol. 6 (1972), p. 143.
- Gileadi, E., and Stoner, G. E., "The Components of Electrode Potential," J. Electroanal. Chem., Vol. 36 (1972), p. 495.
- Chisolm, G. M., Gainer, J. L., Gainer, J. V., and Stoner, G. E., "Plasma Proteins, Oxygen Transport and Atherosclerosis," Atherosclerosis, Vol. 15 (1972), p. 327.
- Stoner, G. E., "Protein Interactions with Materials as Related to Thromboresistance," Biomaterials, Medical Devices and Artificial Organs: An International Journal, Vol. 1, No. 1 (1973), pp. 155-62.

Glenn E. Stoner

Publications (continued):

- Gainer, J. L., Chisolm, G. M., and Stoner, G. E., "Scanning Electron Microscope Studies of Aortic Structure," Angiologica, Vol. 10 (1973), pp. 10-14.
- Boyd, T. H., III, and Stoner, G. E., "Observations on Late Stages of Fibrinogen Polymerization in Human Plasma," Thrombosis Research, Vol. 3 (Pergamon Press, 1973), pp. 209-17.
- Srinivasan, S., Duic, L., Ramasamy, N., Sawyer, P. N., and Stoner, G. E., "Electrochemical Reactions of Blood Coagulation Factors--Their Role in Thrombosis," Berichte der Bunsen-Gesellschaft, Vol. 77 (1973), p. 799.
- Komp, D. M., Lyles, R. L., Jr., Boyd, T. H., III, Stoner, G. E., and Cox, B. J., "The Effect of Cancer Chemotherapeutic Agent on Fibrin Formation and Stabilization In Vitro," Pediat. Res., Vol. 8 (1974), p. 75.
- Wilkins, J. R., Stoner, G. E., and Boykin, E. H., "Microbial Detection Based on Sensing Molecular Hydrogen," App. Microbiol., Vol. 27 (May 1974), p. 949.
- Stoner, G. E., Sawyer, P. N., Srinivasan, S., Lucas, T., and Chisolm, G., "Vascular Injury and Thrombosis: A Scanning Electron Microscope Study," Thrombosis Research, Vol. 4 (1974), p. 699.
- Otani, H., Stoner, G. E., Johnson, L. B., and Wilsdorf, H. G. F., "Behavior of Dental Amalgam During Initial Stages of Setting," J. Gifu Dent. Soc., Vol. 1 (March 1974), pp. 25-30.
- Stoner, G. E., Gileadi, E., Kirwan, D. J., and Ludlow, J. C., "Immobilization of Trypsin on Carbon," Biotech. and Bioengineering, Vol. 17 (1975), p. 455.
- Zardiackas, L. D., Stoner, G. E., and Smith, F. K., "Dental Amalgam Stabilization by Selective Interfacial Amalgamation," J. Electrochem. Soc., Vol. 123 (November 1976) pp. 1596-98.
- Zardiackas, L. D., Stoner, G. E., and Smith, F. K., "Dental Amalgam Stabilization by Selective Interfacial Amalgamation," Biomat. Med. Dev., Art. Org., Vol. 4, No. 2 (1976) pp. 193-203.

Glenn E. Stoner

Publications (continued):

- Srinivasan, S., Cahen, G. L., and Stoner, G. E., "Electrochemistry in the Biomedical Sciences," Electrochemistry: The Past Thirty and the Next Thirty Years (Bloom, H., and Gutmann, F., eds., Plenum Press, 1977) pp. 57-87.
- Selegny, E., Vincent, J-C., Stoner, G. E., et Demarty, M., "Régulation et excitation de membranes d'enzymes in vitro," Biomimetique: C. R. Academie de Scienc, a Paris (Juillet 1977), pp. 117-20.
- Stoner, G. E., and Moran, P. J., "Energy Losses Occurring in Alkaline Electrolyzers," in Srinivasan, S., Salzano, F., and Landgrebe, A. R., eds., Industrial Water Electrolyzers, The Electrochemical Society, Inc., Vol. 78-4 (1978), pp. 169-75.
- Moran, P. J., Cahen, G. L., and Stoner, G. E., "Energy Losses Occurring in and New Electrode Concepts for Alkaline Electrolyzers," J. Electrochem. Soc., Vol. 126 (March 1979), p. 137.
- Stafford, G. R., Stoner, G. E., and Cahen, G. L., "An Investigation of the Electrochemical Behavior of Graphite Fiber-Polymer Composites," J. Electrochem. Soc., Vol. 126 (March 1979), p. 139.
- Zardiackas, L. D., and Stoner, G. E., "Electrochemical Characteristics of the S.I.A. Dental Amalgam Cavity Liner," Biomaterials, Vol. 1, No. 1 (January 1980), pp. 13-16.
- Cahen, G. L., Jr., Moran, P. J., Scribner, L. L. and Stoner, G. E., "Investigation of Nickel Whisker Networks as Electrodes for Hydrogen and Oxygen Evolution," J. Electrochem. Soc., Vol. 128, No. 9 (1981), pp. 1877-1880.
- Stoner, G. E., Cahen, G. L., Jr., Sachyani, M., and Gileadi, E., "The Mechanism of Low Frequency AC Electrochemical Disinfection," Bioelectrochem. and Bioenergetics, Vol. 9, No. 3 (1982), p. 229.
- Zardiackas, L. D., and Stoner, G. E., "Tensile and Shear Adhesion of the Amalgam to Tooth Structure Using SIA," Biomaterials, Vol. 4 (January 1983), pp. 9-12.
- Stoner, G. E., editor, "A Workshop Proceedings on the Principles and Applications of Electrochemistry," U.S. Army Research Office, January 19, 1984.

Glenn E. Stoner

Publications (continued):

- Taylor, S. R., Cahen, G. L., Jr., Stoner, G. E., Moran, P. J., and Ferralli, M. W., "Ionized Monomer Implantation Into Aluminum - A Seawater Immersion Study," in Fundamental Aspects of Corrosion Protection by Surface Modification, ed. E. McCafferty, C. R. Clayton, J. Oudar, The Electrochemical Society, Pennington, N.J., 1984. Also published in Proceedings, Vol. 84-3, pp. 62-67.
- Hansen, J. D., Cahen, Jr., G. L., and Stoner, G. E., "Determination of Electrocatalytic Activity of Nickel Whisker Electrodes," J. Electrochem. Soc., Vol. 132, No. 132 (1985).
- Paciej, R. C., Cahen, Jr., G. L., Gileadi, E., and Stoner, G. E., "Electrolytic Recovery of Gallium from Dilute Solutions Employing Microelectrodes," J. Electrochem. Soc., Vol. 132, No. 1307 (1985).
- Colvin, E. L., Cahen, G. L., Jr., Stoner, G. E., and Starke, E. A., Jr., "The Effect of Germanium Addition on the Corrosion of an Al-Li Alloy," Corrosion, Vol. 42, No. 7, p. 416-421 (1986).
- Moran, J. P., Starke, E. A., Jr., Stoner, G. E., and Cahen, G. L., Jr., "The Influence of Composition and Microstructure on the Corrosion Behavior of Two Al-Li Alloys," Corrosion 86, Paper no. 203, Corrosion, Vol. 43, No. 6, p. 374 (1987).
- Stoner, K. J., Cahen, G. L., Jr., and Stoner, G. E., "The Cathodic Polarization of Graphite Fiber-Polymer Matrix Composites in Natural Seawater as a Means of Slowing Their Rate of Mechanical Deterioration," Corrosion 86, Paper No. 289.
- Natishan, P. N., Stoner, G. E., and Cahen, G. L., Jr., "The Use of Graphite Fiber Polymer Matrix Composite Electrodes for the Electrochemical Disinfection of Latex," Ind. and Eng. Chem. Res., Vol. 26, No.1, pp. 125-128 (1987).
- Glass, J. T., Cahen, G. L., Jr., Stoner, G. E., and Taylor, E. J., "The Effect of Metallurgical Variables on the Electrocatalytic Properties of PtCr Alloys," J. Electrochem. Soc., Vol. 134, No. 1, p. 58-65 (1987).
- Scott, G. D., Stoner, G. E., and Cahen, G. L., Jr., "Thermal/Mechanical Alterations of SAE 1008 Steel and Fe-12ppmC Versus Hydrogen Overpotential in Alkaline Solution," (accepted for publication by J. Electrochem. Soc.).

Glenn E. Stoner

Invited Lectures:

"Interactions Between Materials and the Biological Environment,"
presented to the Facult, des Sciences, Universit, de Rouen,
France, November 1973.

"Electrochemical Disinfection of Water," presented to:

Department of Applied Physics and Engineering, Technische
Hogeschool Delft, Delft, The Netherlands, March 1974

The National Council for Research and Development, Jerusa-
lem, Israel, April 1974

Kibbutz Sde Boker, Israel, April 1974

The Weisman Institute of Science, Rehovot, Israel, April 1974

Department of Environmental Sciences, Technion-Israel Insti-
tute of Technology, Haifa, Israel, May 1974

Human and Environmental Science Laboratory, Hebrew Univer-
sity of Jerusalem, Jerusalem, Israel, May 1974

Laboratoire de Electrochimie (CNRS) et l'Universit, de Paris,
France, Juin 1974

Departments of Chemistry and Chemical Engineering, Univer-
sity of Missouri-Rolla, Rolla, Missouri, October 1974.

"A Short Course in Bioelectrochemistry," presented to Hooker
Chemical Corporation, Niagara Falls, New York, January 1976.

"Stabilization of Asbestos Separator Materials," presented to Hook-
er Chemical Corporation, Niagara Falls, New York, January
1976.

"Electrochemical Phenomena at Biological Interfaces," presented to
Northeast Regional ACS Meeting, Albany, New York, August
1976.

"Bioelectrochemistry and Biomaterials," presented to the Depart-
ment of Engineering, Wilkes College, Wilkes-Barre,
Pennsylvania, November 1977.

"Electrochemical Disinfection of Wastewater on Ships," presented to
Department of Chemistry, University of Tel Aviv, Ramat-
Aviv, Israel, April 1979.

"Composite Electrodes in Electrochemical Technology," presented to
Celanese Corporation, Linden, New Jersey, August 1979.

Glenn E. Stoner

Invited Lectures (continued):

- "Composite Electrodes in Electrochemistry," presented to PPG Corporation, Barbertown, Ohio, December 1979.
- "Electrochemical Disinfection of Wastewater on Ships," presented to Department of Applied Sciences, Brookhaven National Laboratories, January 1980.
- "Reactor Design and Electrochemical Waveform for Seawater Sewage Disinfection," Ben Gurion University and the Negev Institute, Beer Sheva, Israel, May 1980.
- "A Lecture Series in Corrosion Engineering and Industrial Electrolytic Industries," Department of Chemistry, University of Tel-Aviv, Ramat-Aviv, Israel, May-August 1980.
- "Corrosion and Mechanically Assisted Corrosion Failure of Materials Associated with Geothermal Energy Conversion," Los Alamos National Laboratory, Los Alamos, NM, July 1983.
- "The Effects of Polymer Ion Implantation into Aluminum: A Seawater Immersion Study," American Chemical Society Section Meeting, Raleigh, NC, November 1983.
- "The Electrochemical Oxidation of Saturated Hydrocarbons," Gas Research Institute Methane Activation Workshop, Houston, Texas, February 1985.
- "The Effect of Composition and Microstructure on the Electrode Kinetic Parameters for Hydrogen Evolution on Steel," University of Richmond, February 1987.

Glenn E. Stoner

Invited Lectures (continued):

"A Short Course in Corrosion Engineering":

- The Koppers Company, Baltimore MD, August 1980.
- U.S. Naval Surface Weapons Laboratory, Dahlgren, VA, October 1981.
- U.S. Naval Surface Weapons Laboratory, Silver Spring, MD, March 1982.
- U.S. Naval Ordnance Station, Indian Head, MD, October 1982.
- Virginia Electric Power Company, Richmond, VA, November 1982.
- Los Alamos National Laboratory, Los Alamos, NM, February 1983.
- Electric Power Generation Division, Babcock and Wilcox Corporation, Lynchburg, VA, March 1983.
- Los Alamos National Laboratory, Los Alamos, NM, July 1983.
- Lord Corporation, Erie, PA, April 1984.
- Los Alamos National Laboratory, Los Alamos, NM, July 1984.
- Virginia Electric Power Company, Yorktown Power Station, Yorktown, VA, August 1984.
- Newport News Shipbuilding Company, Newport News, VA, August 1984.
- Los Alamos National Laboratory, Los Alamos, NM, July 1985
- 3M Company, Saint Paul, MN, May 1987

Stoner/CV5
Updated: 09/04/87

ROBERT EDWARD SWANSON

2500 Gloucester Drive
Blacksburg, VA 24060
Telephone: (703) 961-5600 - work
(703) 961-0366 - home

Born: September 26, 1951
Marital Status: Married
Citizenship: U.S. (703)

PROFESSIONAL EXPERIENCE

November 1983 Present: VIRGINIA POLYTECHNIC INSTITUTE AND STATE UNIVERSITY
Blacksburg, VA 24061

Assistant Professor
Department of Materials Engineering

1980 - 1983 CARNEGIE-MELLON UNIVERSITY
Pittsburgh, PA 15213

Graduate Research Assistant - Department of
Metallurgical Engineering and Materials Science

Research in the area of structure/property relationships in high-strength aluminum alloys, especially rapidly-solidified P/M alloys. Specifically evaluated the role of microstructure in the hydrogen embrittlement and stress corrosion cracking susceptibility of 7xxx series alloys. Microstructures of these alloys were characterized using light microscopy, SEM, and STEM. Correlated SEM fractography with underlying microstructure. Cracking mechanisms proposed for the various microstructures.

1973-1979: WESTINGHOUSE-BETTIS ATOMIC POWER LABORATORY
West Mifflin, Pennsylvania.

Senior Engineer
Steam Generator Activity, Materials Performance

Performed and managed both in-house and contractual research efforts for development of alloys for use in as well as design of naval nuclear steam generator components. Developed test programs to simulate operating conditions, primarily for stress corrosion cracking of tubing and support plate materials. Conducted failure analyses which involved on-site inspection of nuclear plant steam generators.

Engineer - Light Water Breeder Reactor Project
Irradiation Test Activity

Performed in-pile irradiation tests to evaluate stress corrosion cracking performance of fuel sheath alloys.

Conducted major investigation of stress corrosion cracking performance of threaded fasteners used in LWBR. Designed fixtures to simulate actual loading conditions. Results were used directly in design and construction of LWBR.

Engineer - Light Water Breeder Reactor Project
Fuel Activity

Evaluated compaction processes to optimize parameters for fuel pellets of various sizes and compositions, especially with regard to crack and chip resistance. Followed program through manufacturing, including instrumentation of fuel rods as well as training of fuel technicians to minimize pellet damage. Various patent disclosures.

Associate Engineer - Advanced Naval Reactor Core
Core Performance

Evaluated corrosion and hydrogen-pickup behavior of fuel sheath materials to optimize thermomechanical treatments and develop new alloys. Various patent disclosures.

EDUCATION

- PhD. Carnegie-Mellon University (Metallurgical Engineering and Materials Science), December, 1983.
Thesis: Role of Hydrogen in the Stress Corrosion Cracking of 7xxx Series Aluminum Alloys; Advisors: I.M. Bernstein and A. W. Thompson
- MS University of Pittsburgh (Industrial Engineering), 1979. Advisor: D.E. Cleland
- MS University of Pittsburgh (Metallurgical and Materials Engineering), 1976.
Thesis: Effect of Isothermal Forging on Structure of Zirconium Alloys; Advisor: H.A. Kuhn
- BS Pennsylvania State University (Metallurgy) 1973.

TEACHING EXPERIENCE

- 1983 - Present VPI & SU, Assistant Professor.
Courses in Introduction to Materials Science and Engineering (MatE 2030), Principles of Metals and Ceramics (MatE 3020), Processing of Metals and Ceramics (MatE 3040), Structure-Property Relationships in Metals (MatE 3071), Structure-Property Relationships in Ceramics Lab (MatE 3072), Environmental Degradation of Engineering Materials (MatE 4140), Alloy Steels (MatE 5020), Metallic Corrosion (MatE 5121 and 5123).

RESEARCH AT VA TECH

"Development of Composite Surface Treatments for Wear and Corrosion Treatments," for \$19,872, Synertech, Inc., period 4 September 1984 to 2 November 1984. (PI and responsible for \$19,872).

"Hydrogen Embrittlement Testing of Inconel 600 and Beryllium," for \$7,063, Air Products and Chemicals, Inc., period 1 January 1985 to 1 April 1985. (Co-principal investigator with Professor M.R. Louthan. Louthan responsible for \$4,591, Swanson responsible for \$2,472).

"Corrosion-Resistant Magnesium Alloys via Rapid Solidification," for \$20,000, Universal Energy Systems, Inc./U.S. Air Force Wright Aeronautical Laboratory, period 1 January 1986 to 1 January 1987. (PI and responsible for \$20,000).

"Failure Analysis and Prevention Laboratory," for \$63,506, CIT/IMSE, period 1 June 1986 to 1 June 1987. (Co-principal investigator with Professor M.R. Louthan and visiting Professor T.A. Place. Louthan responsible for \$21,169, Place responsible for \$21,169, and Swanson responsible for \$21,168).

"Effect of Thermal Treatments on Mechanical Behavior of Tool Steels," for \$6,500, Windward International, Inc., period 1 January 1986 to 1 July 1986, (PI and responsible for \$6,500).

"Evaluation of Dry Process for Flue Gas Desulfurization," for \$10,000, ETS, Inc., period 1 March 1987 to 1 October 1987. (PI and responsible for \$10,000).

"Evaluation of Dry Process for Flue Gas Desulfurization," for \$10,000, CIT/IMSE, period 1 March 1987 to 1 October 1987. (PI and responsible for \$10,000).

"Development of Low-Expansion Ceramics for Diesel Engine Applications," for \$450,000, Martin Marietta Energy Systems, Inc. (Oak Ridge National Laboratories - DOE), period 1 March 1986 to 1 March 1989. (Co-principal investigator with Professor J.J. Brown. Brown responsible for \$292,500 and Swanson responsible for \$157,500).

"Determination of Residual Stresses in Railroad Car Wheels by X-Ray Diffraction," for \$93,968, CSX Transportation, Inc., period 1 June 1987 to 1 June 1988. (Co-principal investigator with Professor R.W. Hendricks. Hendricks responsible for \$61,079 and Swanson responsible for \$32,889).

"Determination of Residual Stresses in Railroad Car Wheels by X-Ray Diffraction," for \$49,719, CIT/IMSE, period 1 June 1987 to 1 June 1988. (Co-principal investigator with Professor R.W. Hendricks. Hendricks responsible for \$32,317 and Swanson responsible for \$17,402).

"Surface Treatments for Processing and Synthesis of Composites," for 85,370, Windward International, Inc., period 1 December 1987 to 1 December 1989. (Co-principal investigator with Professor N.S. Eiss, Mechanical Engineering. Swanson responsible for \$55,491 and Eiss responsible for \$29,879).

"Surface Treatments for Processing and Synthesis of Composites," for \$47,410, CIT/IMSE, period 1 December 1987 to 1 December 1989. (Co-principal investigator with Professor N.S. Eiss, Mechanical Engineering. Swanson responsible for \$30,817 and Eiss responsible for \$16,593).

HONORS AND RECOGNITIONS

1. Outstanding Young Men of America, 1985
2. Who's Who in Technology Today
3. Sigma Tau
4. Tau Beta Pi
5. Phi Kappa Phi
6. Sigma Xi

CURRENT FIELDS OF INTEREST

Fracture Mechanics
Environmental Cracking
Corrosion
Powder Metallurgy/Ceramics
Electron Microscopy
Computer Programming and Utilization

AFFILIATIONS

Member:	TMS-AIME	ASEE	IMS	ICTTE
	ASM	AES	IAHE	NSPE
	NACE	MRS	ACerS	SES
	ASTM	AAAS	FEF	

Summer Research Fellow (AFOSR) WPAFB, 1985

Registered Professional Engineer (Pennsylvania, Virginia)

Member: AIME Corrosion and Environmental Effects Committee

New Products Editor: METALLOGRAPHY, International Metallographic Society

HOBBIES

Photography, hiking, music, racquet sports.

REFEREED JOURNAL PUBLICATIONS

1. R.E. Swanson, A.W. Thompson, I.M. Bernstein and J.L. Maloney, Effect of Stress State on the Stress Corrosion Cracking of 7075 Aluminum, in Hydrogen Effects in Metals, TMS-AIME, Warrendale, PA, 1981, pp. 459-66.
2. R.E. Swanson, I.M. Bernstein and A.W. Thompson, Stress Corrosion Cracking of 7075 Aluminum in the T6-RR Temper, Scripta Met., 1982, Vol.16, pp. 321-24.
3. R.E. Swanson and M.R. Louthan, Material Defects, Gas Purity, and Hydrogen Embrittlement, International Journal of Hydrogen Energy, 1985, Vol. 10, No. 7/8, pp. 551-54.
4. D.P. Harvey, II, T.S. Sudarshan, M.R. Louthan, Jr., and R.E. Swanson, Corrosion Fatigue Behavior of 90/10 Copper - Nickel Cladding for Marine Structures, J. Materials for Energy Systems, 1985, Vol. 7, No. 3, pp. 269-75.
5. R.E. Swanson and Y-W Kim, Thermal Stability of Al-Fe-Ce Alloys in Aluminum Alloys - Their Physical and Mechanical Properties (E.A. Starke, Jr., and T.H. Sanders, Jr., eds.) EMAS, West Midlands, U.K., 1986, pp. 217-31.
6. R.E. Swanson, A.W. Thompson, and I.M. Bernstein, Effect of Notch Root Radius on Stress Intensity in Mode I and Mode III Loading, Metallurgical Transactions, 1986, Vol. 17A, pp. 1633-1637.
7. R.E. Swanson and R.C. Luken, Effects of Low Temperature Oxidation on the Mechanical Behaviour of ASTAR-811C, Refractory and Hard Materials, 1987, Vol. 6., No. 2, pp. 101-105.
8. R.E. Swanson and J. Kim, The Role of Re Additions on the Grain Size and Microstructure of Mo, accepted for publication by J. Heat Treating.

REFEREED PROCEEDINGS PAPERS

(* designates paper accepted on basis of abstract)

1. D.P. Harvey, II, T.S. Sudarshan, M.R. Louthan, Jr., and R.E. Swanson, Corrosion Fatigue Behavior of 90/10 Copper-Nickel Cladding for Marine Structures, in ASM Conference on Coatings and Bimetallics for Aggressive Environments (R.D. Sisson, ed.), ASM, Metals Park, Ohio, 1985.
2. R.E. Swanson, Hydrogen Effects on Ductile Fracture in Third International Conference - Environmental Degradation of Engineering Materials (M.R. Louthan, R.P. McNitt, and R.D. Sisson, eds.) Pennsylvania State University, University Park, PA, 1987, pp. 133-48.

- 3 R.E. Swanson, S.J. Lukezich, R. and R. Lewis, Metallographic Methods for RS Mg Alloys, to be published in Proceedings of the 20th Annual Convention of the International Metallographic Society.

CLASSIFIED REPORTS

- 1 Ten classified reports.

PRESENTATIONS

- 1 R. E. Swanson, A.W. Thompson, I.M. Bernstein and J.L. Maloney, Effect of Stress State on the Stress Corrosion Cracking of 7075 Aluminum, presented at the Third International Conference on Effect of Hydrogen on Behavior of Materials sponsored by TMS-AIME, National Science Foundation and Air Force Office of Scientific Research, Moran, WY, August, 1980.
- 2 R.E. Swanson, I.M. Bernstein and A.W. Thompson, Effect of Stress State on the Stress Corrosion Cracking of 7075 Aluminum in the T6-RR Temper, presented at TMS-AIME Fall Meeting, Pittsburgh, PA, October, 1980.
- 3 R.E. Swanson, Stress Corrosion Cracking of Brass in Tarnishing and Non-Tarnishing Solutions, Staff Seminar, National Bureau of Standards, Gaithersburg, MD, October, 1981.
- 4 A.W. Thompson, R.E. Swanson, and I.M. Bernstein, Environmental Embrittlement of a High-Strength P/M Al Alloy, presented at the TMS-AIME Annual Meeting, February, 1982.
- 5 R.E. Swanson, I.M. Bernstein and A.W. Thompson, The Role of Hydrogen in the Stress Corrosion Cracking of High-Strength Aluminum Alloys, presented at the International Congress on Technology and Technology Exchange, Pittsburgh, PA, May, 1982.
- 6 R.E. Swanson, I.M. Bernstein and A.W. Thompson, The Role of Hydrogen in the Stress Corrosion Cracking of P/M X7090 Aluminum, presented at the TMS-AIME Fall Meeting, October, 1982.
- 7 R.E. Swanson, I.M. Bernstein, and A.W. Thompson, The Role of Hydrogen in the Stress Corrosion Cracking of P/M 7090 Aluminum, presented at the TMS-AIME Fall Meeting, October, 1983.
- 8 R.E. Swanson and M.R. Louthan, Material Defects, Gas Purity, and Hydrogen Embrittlement, presented at the 5th World Hydrogen Energy Conference, Toronto, August, 1984.
- 9 R.E. Swanson, A.W. Thompson, and I.M. Bernstein, Effect of Notch Root Radius on Stress Intensity in Mode I and Mode III Loading, presented at Mechanics and Physics of Fracture, Cambridge, U.K., September, 1984.

10. R.E. Swanson, M.R. Louthan, R.C. Luken, and J.L. Lytton, The Effect of Environment on Mechanical Behavior of Refractory Alloys for Space Reactor Applications, presented at the TMS-AIME Fall Meeting, September, 1984.
11. R.E. Swanson, S.A. Blair, and R.D. Sisson, Corrosion Due to Acid Rain, 21st Meeting of Society of Engineering Sciences, VPI and SU, October, 1984.
12. R.E. Swanson, Fracture Mechanics of Environmentally-Induced Fracture in Precipitation-Strengthened Alloys, Staff Seminar, Cambridge University, England, July, 1985.
13. R.E. Swanson, Stress Corrosion Cracking Mechanisms in High-Strength Aluminum Alloys, Staff Seminar, ALCAN, Ltd., Oxon, England, July, 1985.
14. R.E. Swanson, Evaluation of Empirical Methods to Assess Role of Hydrogen in Stress Corrosion Cracking of Aluminum Alloys, Staff Seminar, University of Newcastle-upon-Tyne, England, July, 1985.
15. R.E. Swanson, Mechanics and Statistics of Microhardness Testing, Staff Seminar, Air Force Wright Aeronautical Laboratories, WPAFB, August, 1985.
16. M.R. Louthan, Jr. and R.E. Swanson, Crack-Induced Blunting - An Apparent Reduction in Crack Growth Rates, 22nd Meeting of Society of Engineering Sciences, Pennsylvania State University, October, 1985.
17. R.E. Swanson and Young-Won Kim, Thermal Stability of Al-Fe-Ce Alloys, International Conference on Aluminum Alloys, University of Virginia, June, 1986.
18. R.E. Swanson, Corrosion of RSP Magnesium Alloys, Staff Seminar, ALCAN, Ltd., Oxon, England, June, 1986.
19. R.E. Swanson, Ion Implantation of Chromium into Magnesium, Staff Seminar, TECVAC, Ltd., Stowe-cum-Quy, England, June, 1986.
20. R.E. Swanson, Novel Methods for Mechanical Testing of RSP Alloys, Staff Seminar, Sheffield University, July, 1986.
21. R.E. Swanson and R.C. Luken, The Influence of Microstructure upon Fracture Behavior of CPM-10V, TMS-AIME Fall Meeting, Orlando, Florida, October, 1986.
22. J. Kim and R.E. Swanson, The Role of Rare - Earth Additions in the Plastic Behavior of BCC Metals, TMS-AIME Fall Meeting, Orlando, Florida, October, 1986.

23. R. E. Swanson, Hydrogen Effects on Ductile Fracture, Third International Conference - Environmental Degradation of Engineering Materials, Pennsylvania State University, April, 1987.
24. R. E. Swanson, Galvanic Corrosion of Ceramics, Faculty-Staff Seminar Series, Department of Materials Engineering, Virginia Polytechnic Institute and State University, Blacksburg, Virginia, April, 1987.
25. R. E. Swanson, Galvanic Corrosion of Ceramic-Ceramic Composites, Fourth Annual Review of the Center for Composite Materials and Structures, Virginia Polytechnic Institute and State University, Blacksburg, Virginia, May, 1987.
26. R. E. Swanson, Alloy Design Considerations for Corrosion-Resistant Magnesium, U. S. Army Workshop on Viability of Magnesium in Military Hardware, Boston, Massachusetts, June, 1987.
27. R. E. Swanson, Ductile Fracture, Staff Seminar Series (for Sandia and Lawrence Livermore National Laboratories), Sandia National Laboratory, Livermore, CA, July, 1987.
28. R. E. Swanson, S. J. Lukezich, and R. Lewis, Metallographic Methods for RS Mg Alloys, 20th Annual Convention of the International Metallographic Society, Monterey, CA, July, 1987.

DISTRIBUTION LIST

Copy No.

1 - 3 National Aeronautics and Space Administration
Langley Research Center
Hampton, VA 23665
Attention: Mr. Dennis Dicus, MS 188A
Metallic Materials Branch

4 - 5* NASA Scientific and Technical Information Facility
Post Office Box 8757
Baltimore/Washington International Airport
Baltimore, MD 21240

6 Mr. J. F. Royall, Jr.
Grants Officer, MS 126
National Aeronautics and Space Administration
Langley Research Center
Hampton, VA 23665

7 - 8 Richard P. Gangloff, MS

9 Glenn E. Stoner, MS

10 Robert E. Swanson, Assistant Professor
Department of Materials Engineering
Virginia Polytechnic and State University
Blacksburg, VA 24061

11 R. S. Piascik, MS

12 R. G. Buchheit, Jr., MS

13 Thomas H. Courtney, Chairman, MS

14 E. H. Pancake, Clark Hall

15 SEAS Publications Files

*1 reproducible copy

JO# 0832:kmc

UNIVERSITY OF VIRGINIA
School of Engineering and Applied Science

The University of Virginia's School of Engineering and Applied Science has an undergraduate enrollment of approximately 1,500 students with a graduate enrollment of approximately 560. There are 150 faculty members, a majority of whom conduct research in addition to teaching.

Research is a vital part of the educational program and interests parallel academic specialties. These range from the classical engineering disciplines of Chemical, Civil, Electrical, and Mechanical and Aerospace to newer, more specialized fields of Biomedical Engineering, Systems Engineering, Materials Science, Nuclear Engineering and Engineering Physics, Applied Mathematics and Computer Science. Within these disciplines there are well equipped laboratories for conducting highly specialized research. All departments offer the doctorate; Biomedical and Materials Science grant only graduate degrees. In addition, courses in the humanities are offered within the School.

The University of Virginia (which includes approximately 2,000 faculty and a total of full-time student enrollment of about 16,400), also offers professional degrees under the schools of Architecture, Law, Medicine, Nursing, Commerce, Business Administration, and Education. In addition, the College of Arts and Sciences houses departments of Mathematics, Physics, Chemistry and others relevant to the engineering research program. The School of Engineering and Applied Science is an integral part of this University community which provides opportunities for interdisciplinary work in pursuit of the basic goals of education, research, and public service.